

**PHOTOCATALYTIC DEGRADATION OF
PESTICIDES USING TIO₂ NANOPARTICLES**

BY

MUTSEE TERMTANUN, BEng, MSc

**THESIS SUBMITTED TO UNIVERSITY
OF NOTTINGHAM OF DOCTOR OF
PHILOSOPHY**

NOVEMBER 2013

ABSTRACT

The problem of water pollution has been an environmental concern for many years. Numerous researchers are looking for an effective method to solve this issue.

Heterogeneous photocatalysis, using a semiconductor as a catalyst, is a promising method for the destruction of water polluting pesticides. This method has been called the Advanced Oxidation Process (AOP) which is one of the techniques for water treatment. Titanium dioxide (TiO_2) is the most widely accepted photocatalyst because it is non-toxic, stable to photocorrosion, low cost and can potentially work using sunlight rather than artificial sources of light. When titanium dioxide is illuminated by UV radiation, the absorption of photons of energy is then equal to or greater than its band gap width. This artefact leads to the formation of conduction-band electrons and valence-band holes on the surface of TiO_2 , which yield hydroxyl radicals, the primary oxidising species needed for the photocatalytic degradation of pollutants.

Supercritical water hydrothermal synthesis (ScWHS) is one of novel approaches for nanoparticle manufacture which involves the mixing of an aqueous metal salt stream with a supercritical water stream to produce nano-sized metal oxide particles. The engineering design for the mixing of these

two fluids is critical and a novel nozzle reactor has been developed at the University of Nottingham that can produce high quality particles with an excellent control over particle size and particle size distribution. By application of this technique, titanium dioxide (TiO_2), in nanoparticle form, was produced and used for the photocatalytic treatment of wastewater.

In this thesis, the photocatalytic degradation of the three pesticides - isoproturon, simazine and propazine - was measured using 3 different types of reactors: thin film fixed bed reactor (TFFBR), a stirred reactor, and a fluidised bed photoreactor. Various conditions were used: for example without UVC and UVA illumination, with commercial TiO_2 , with the synthesised TiO_2 , without any photocatalyst, low concentration, high concentration, and at different TiO_2 concentrations. The optimum TiO_2 concentration for the treatment of the three chosen pesticides was equal to 5 g litre^{-1} . The efficiency in decreasing the pesticides concentration of the synthesised TiO_2 (from ScWHS technique) with all three types of reactors was lower than that of the commercial titanium dioxide (P-25 TiO_2). The fluidised bed reactor appeared to give the highest performance amongst three reactors.

ACKNOWLEDGEMENT

I would like to express my profound gratitude to everyone who has been involved in my research. Firstly, I much appreciated the most valuable support, advice and comments from my supervisors, Prof. Edward Lester and Prof. Trevor Drage. Also, I feel really thankful to Prof. George Z. Chen, for his special encouragement that helped me to overcome many obstacles.

Secondly, many thanks are due to my colleagues: Miquel Gimeno Fabra, Thomas Huddle, Christopher Straykey, Haiping Shen, Sherif Elbasuney and Selina Tang, who always gave me their kindness and help throughout the period of my research. Also, I would like to take this opportunity to say thank you to the many co-workers, staff, technicians in the School of Chemistry and School of Chemical and Environmental Engineering for their assistance and friendship.

Finally, my wholeheartly thanks is given to the love from my family and my friends in university and outside university, who were always there when I needed their warmness and a shoulder to lean on.

CONTENTS

ABSTRACT	i
ACKNOWLEDGEMENTS	iii
CONTENTS	iv
LIST OF FIGURES	xvi
LIST OF TABLES	xxxvii
Chapter 1 INTRODUCTION	1
1.1 Introduction	1
1.1.1 Examples of common water pollutants	1
1.1.2 Definition of pesticides (in general view)	2
1.1.3 Group of pesticides (categorised by Ministry of Environment, Ontario, Canada)	3
1.1.4 Water pollution from pesticides: the pesticides usually found in wastewater	8
1.1.5 Selected pesticides used in this thesis	10
1.1.6 Legislation of pesticides in respect to human consumption	14
1.2 Research objectives	15
1.3 Thesis structure	16
Chapter 2 BACKGROUND AND REVIEW OF LITERATURE	19
2.1 Introduction to background and review of literature	19

2.2 The photolysis or photodissociation process	19
2.3 The principle of photocatalysis	20
2.3.1 Homogeneous photocatalytic reactions	20
2.3.2 Heterogeneous photocatalytic reactions	20
2.4 The photo-Fenton reaction	22
2.5 Advanced Oxidation Processing (AOP)	23
2.6 Photocatalytic materials	24
2.7 Mechanism/reactions of TiO ₂ photocatalyst	24
2.8 Photocatalytic degradation pathways and intermediates	27
2.9 Degradation pathways of isoproturon, simazine and propazine	30
2.10 The toxicity assessment of isoproturon, simazine and propazine using % inhibition of bacteria	36
2.11 Factors affecting the photocatalytic kinetics	37
2.11.1 Crystal phase of photocatalyst	38
2.11.2 Organic pollutant concentration	42
2.11.3 TiO ₂ concentration	46
2.11.4 O ₂ initial concentration	50
2.11.5 pH	53
2.11.6 Reaction temperature	56
2.11.7 Irradiation wavelength	57
2.11.8 Light intensity	59

2.11.9 Additional oxidants	60
2.11.10 Mode of the catalyst application: the suspended or immobilized system	62
2.12 Photocatalytic reactor	63
2.12.1. Reactors using suspended solid photocatalysts	63
2.12.1.1 Annular reactors with horizontal flow	63
2.12.1.2 Thin-film slurry photocatalytic reactor (TFS)	64
2.12.2 Fixed catalyst systems	65
2.12.2.1 Thin Film Fixed Bed Reactor (TFFBR)	65
2.12.2.2 Packed Bed Reactor (PBR), fixed bed reactor and fluidised bed reactor	66
2.12.2.3 Fibre Photoreactor (FP) and Optical Fibre Photoreactor (OFP)	67
2.12.2.4 Rotating Disc Reactor (RDR)	69
2.12.2.5 Photocatalytic Membrane Reactors (PMRs)	69
2.13 Key elements of reactor design for photocatalytic reaction	71
2.13.1 Mass transfer and contact between chemical compounds and photocatalyst	72
2.13.2 Photocatalyst activation	72
2.13.3 Oxygen content in two phases? systems	72
2.14 Supercritical water hydrothermal synthesis (ScWHS)	73

2.15 The ScWHS process	74
2.16 Conclusions from review of literature	75
Chapter 3 EXPERIMENTAL	78
3.1 Introduction to experimental	78
3.2 Chemicals and materials	78
3.3 Procedure for supercritical water synthesis of TiO ₂	79
3.4 Thin Film Fixed Bed Reactor System (TFFBR)	82
3.4.1 Surface coating method	84
3.4.2 Experimental procedures for the TFFBR	86
3.4.3 Operating conditions	87
3.5 Stirred photoreactor	87
3.5.1 Operating conditions	88
3.6 Fluidised bed photoreactor system	89
3.6.1 Experimental procedure for fluidised bed photoreactor	91
3.7 Analytical Techniques	92
3.7.1 High Performance Liquid Chromatography (HPLC)	92
3.7.2 Ultraviolet-visible Spectroscopy (UV-Vis)	94
3.7.3 Scanning Electron Microscopy (SEM) and Energy Dispersive X-ray Spectroscopy (EDAX)	95
3.7.4 Transmission Electron Microscope (TEM)	96
3.7.5 X-Ray Diffraction (XRD)	97

3.8 Calibration curves for pesticides quantification	99
3.9 Conclusions of the Experimental Chapter	106
Chapter 4 PHOTOCATALYTIC DEGRADATION OF PESTICIDES USING THIN FILM FIXED BED REACTOR	107
4.1 Introduction to TFFBR results	107
4.2 Aims and objectives for TFFBR experiments	108
4.3 Characterisation of the TiO ₂ photocatalysts: Scanning Electron Microscope (SEM) image and Energy Dispersive X-ray Spectroscopy (EDAX) data	109
4.4 Control experiments to determine the difference between photolysis and photocatalytic reaction	111
4.4.1 Determination of the pesticides degradation rate in the absence of UV excitation but the presence of TiO ₂	112
4.4.2 Determination of the rate of loss of pesticides in the presence of UV irradiation without a TiO ₂ catalyst.	113
4.5 Photocatalytic degradation, effect of TiO ₂ and the feed flow rate	120
4.6 Influence of initial pesticides concentration	129
4.7 Influence of photocatalyst type (the commercial VS the synthesised)	132
4.8 Conclusions of TFFBR experiments	140

Chapter 5 PHOTOCATALYTIC DEGRADATION OF 142

PESTICIDES USING STIRRED PHOTOREACTOR

5.1 Introduction to a stirred photoreactor results 142

5.2 Aims and objectives 143

5.3 Control experiments to determination the rate of pesticide loss 144

in the absence of UV but the presence of TiO_2

5.4 Determination of the effect of P-25 TiO_2 concentration on 147

photocatalytic degradation

5.5 Influence of catalyst type on the photocatalytic degradation 155

(P-25 TiO_2 VS synthesised TiO_2)

5.6 X-ray Diffraction (XRD) results at different sintering temperature 163

5.7 Conclusions of stirred photoreactor experiments 168

Chapter 6 PHOTOCATALYTIC DEGRADATION OF 169

PESTICIDES USING FLUIDISED BED

PHOTOREACTOR

6.1 Introduction to fluidised bed photoreactor results 169

6.2 Aims and objectives 170

6.3 Control experiments, determination of the rate of loss of pesticides 172

degradation rate in the absence of UV but in the presence of TiO_2

6.4 UVA and UVC photolysis	173
6.5 Photocatalytic degradation of pesticides	175
6.6 Effect of P-25 TiO ₂ concentration on the photocatalytic degradation	184
6.7 Influence of catalyst type (P-25 TiO ₂ VS synthesised TiO ₂)	192
6.8 Transmission Electron Microscopy (TEM) results	197
6.9 X-Ray Diffraction (XRD) results	200
6.10 Conclusion of fluidised bed photoreactor experiments	202
Chapter 7 CONCLUSION AND RECOMMENDATIONS	205
7.1 Overview of results and experimental work	205
7.2 Conclusions	206
7.3 Recommendations for future work	208
APPENDICES	210
APPENDIX I: Student T-test for TFFBR results	211
I.1 UVA/UVC photolysis of isoproturon	211
I.2 UVA/UVC photolysis of simazine	211
I. 3 UVA/UVC photolysis of propazine	211
I.4 UVC photolysis of isoproturon VS simazine	212
I.5 UVC photolysis of simazine VS propazine	212
I.6 UVC photolysis of isoproturon VS propazine	212

I.7 UVA photolysis of isoproturon VS simazine	212
I.8 UVA photolysis of simazine VS propazine	213
I.9 UVA photolysis of isoproturon VS propazine	213
I.10 UVA photocatalytic of isoproturon at high flow rate (100 ml min ⁻¹)	213
VS low flow rate (20 ml min ⁻¹)	
I.11 UVA photocatalytic of simazine at high flow rate (100 ml min ⁻¹)	213
VS low flow rate (20 ml min ⁻¹)	
I.12 UVA photocatalytic of propazine at high flow rate (100 ml min ⁻¹)	214
VS low flow rate (20 ml min ⁻¹)	
I.13 UVC photocatalytic of isoproturon at high flow rate (100 ml min ⁻¹)	214
VS low flow rate (20 ml min ⁻¹)	
I.14 UVC photocatalytic of simazine at high flow rate (100 ml min ⁻¹)	214
VS low flow rate (20 ml min ⁻¹)	
I.15 UVC photocatalytic of propazine at high flow rate (100 ml min ⁻¹)	214
VS low flow rate (20 ml min ⁻¹)	
I.16 UVC photocatalytic of isoproturon at low initial concentration	215
(2.5 ppm) VS high initial concentration (20 ppm)	
I.17 UVC photocatalytic of propazine at low initial concentration	215
(2.5 ppm) VS high initial concentration (20 ppm)	

APPENDIX II: Student T-test for stirred photoreactor results	216
II.1 Adsorption concentration of isoproturon VS simazine in the absence of UV	216
II.2 Adsorption concentration of simazine VS propazine in the absence of UV	216
II.3 Adsorption concentration of isoproturon VS propazine in the absence of UV	217
APPENDIX III: Student T-test for fluidised bed photoreactor results	218
III.1 Adsorption concentration of isoproturon VS simazine in the absence of UV	218
III.2 Adsorption concentration of simazine VS propazine in the absence of UV	218
III.3 Adsorption concentration of isoproturon VS propazine in the absence of UV	219
III.4 UVA photolysis of isoproturon VS simazine	219
III.5 UVA photolysis of simazine VS propazine	219
III.6 UVA photolysis of isoproturon VS propazine	219
III.7 UVC photolysis of isoproturon VS simazine	220
III.8 UVC photolysis of simazine VS propazine	220

III.9 UVC photolysis of isoproturon VS propazine	220
III.10 UVA photolysis of isoproturon using fluidised bed VS stirred photoreactor	220
III.11 UVA photolysis of isoproturon using fluidised bed VS TFFBR	221
III.12 UVA photolysis of simazine using fluidised bed VS stirred photoreactor	221
III.13 UVA photolysis of simazine using fluidised bed VS TFFBR	221
III.14 UVA photolysis of propazine using fluidised bed VS stirred photoreactor	221
III.15 UVA photolysis of propazine using fluidised bed VS TFFBR	222
III.16 UVC photolysis of isoproturon using fluidised bed VS stirred photoreactor	222
III.17 UVC photolysis of isoproturon using fluidised bed VS TFFBR	222
III.18 UVC photolysis of simazine using fluidised bed VS stirred photoreactor	222
III.19 UVC photolysis of simazine using fluidised bed VS TFFBR	223
III.20 UVC photolysis of propazine using fluidised bed VS stirred photoreactor	223
III.21 UVC photolysis of propazine using fluidised bed VS TFFBR	223

III.22 UVA photocatalytic of isoproturon using fluidised bed VS stirred photoreactor	223
III.23 UVA photocatalytic of simazine using fluidised bed VS stirred photoreactor	224
III. 24 UVA photocatalytic of propazine using fluidised bed VS stirred photoreactor	224
BIBIOLOGRAPHY	225

LIST OF FIGURES

Figure 1.1 Triazine isomers: (1) 1,2,3 triazine, (2) 1,2,4 triazine, (3) 1,3,5 triazine	4
Figure 1.2 Chemical structure of carbamic acid group	4
Figure 1.3 Structure of DDT, an example of pesticides in OCs group	4
Figure 1.4 Chemical structure of phenoxy acid	5
Figure 1.5 Paraquat structure	6
Figure 1.6 Phenylurea structure	6
Figure 1.7 Two isomeric forms of thiocarbamate	6
Figure 1.8 Statistical data of used pesticides in 2006 in UK	9
Figure 1.9 Use of isoproturon (kg/hr) with crops in UK	11
Figure 1.10 Rate of use (kg/ha) for simazine with crops in UK	13
Figure 1.11 Structure of three pesticides	14
Figure 2.1 Mechanism of photocatalytic reaction in TiO ₂	26
Figure 2.2 Degradation pathway of isoproturon in the water	30
Figure 2.3 Degradation pathway of simazine, cyanazine, atrazine and propazine in water	31

Figure 2.4	Scheme of proposed pathway for simazine photocatalytic degradation	33
Figure 2.5	Proposed degradation pathway of simazine in UV/TiO ₂ system	34
Figure 2.6	Tentative photodegradation pathway of propazine	35
Figure 2.7	Results of toxicity in the triazine samples at condition simazine pH = 5.5, TiO ₂ concentration = 0.25g/l, atrazine pH = 6, TiO ₂ concentration = 1.8 g/l, immersion well photoreactor	36
Figure 2.8	Crystalline structures of titanium dioxide (a) anatase, (b) rutile	38
Figure 2.9	Photocatalytic oxidation of acetaldehyde with Degussa P-25 TiO ₂ , nanostructured anatase and rutile	41
Figure 2.10	Possible mechanisms for enhancement of photocatalytic activity caused by contact between (a) anatase TiO ₂ (b) rutile TiO ₂ and (C) coexistence of anatase and rutile TiO ₂	42
Figure 2.11	Initial rate of reaction calculated by L-H kinetics as a function of the initial concentration of isoproturon,	45

simazine, and propazine

- Figure 2.12** Influence of catalyst concentration on the photocatalytic degradation rate of isoproturon at UV=238 nm, 0.5 mM isoproturon, 250 ml, and P-25 (0.5, 1, 2 and 3 g litre⁻¹) 47
- Figure 2.13** Effect of catalyst loading at pH = 7, radiation intensity = 185.2 W m⁻², C_{TiO₂} = TiO₂ concentration (kg m⁻³), τ = optical thickness, dimensionless, N_{Re} = Reynolds number, Q = volumetric flowrate (m³ s⁻¹) 48
- Figure 2.14** Effect of TiO₂ concentration on the photodegradation efficiency of glyphosate, t = 1.0 hr 49
- Figure 2.15** Effect of the amount of TiO₂ on the photodegradation efficiency of methamidophos, annular photoreactor, 375 W medium pressure mercury lamp, reaction temperature =30 °C, illumination time = 30min 49
- Figure 2.16** Effect of added molecular oxygen on the degradation rate of vanillin in the presence of Degussa P-25, UV-100 and ZnO. Experimental conditions: substrate concentration (0.5 mM), V = 250 mL, pH = 2 for TiO₂ samples and 52

pH = 6 for ZnO, Degussa P-25, UV-100 and
ZnO = 1 g litre⁻¹, immersion well photoreactor,
125 W medium pressure Hg lamp, irradiation time = 45 min

Figure 2.17 Effect of initial pH value on the photodegradation 55

efficiency of trichlorfon using TiO₂, annular photoreactor,
375 W medium pressure mercury lamp, illumination
time = 30 min

Figure 2.18 Influence of pH on the degradation rate of vanillin 55

using Degussa P-25, UV-100 and ZnO = 1 g litre⁻¹
experimental conditions: substrate concentration (0.5 mM),
V = 250 mL, immersion well photo-reactor, 125 W medium
pressure Hg lamp, pH range (2, 4, 6, 8, 10 and 12), continuous
O₂ purging and stirring, irradiation time = 45 min

Figure 2.19 Effect of anions on the photocatalytic degradation rate 56

constants of Butachlor

Figure 2.20 Comparison of the photocatalytic degradation of 57

chlorfenapyr at 300 nm of UV at different temperature.

The initial concentrations of chlorfenapyr and

TiO₂ = 800 mg litre⁻¹, pH = 6

Figure 2.21 Geometry of annular photoreactor	63
Figure 2.22 Geometry of TFS (Thin-film slurry photoreactor)	64
Figure 2.23 Geometry of water fountain photoreactor	65
Figure 2.24 Flowchart of TFFBR (Thin Flim Fixed Bed Reactor)	66
Figure 2.25 Illustration of FP (Fibre Photoreactor)	68
Figure 2.26 Layout for OFP (Optical Fibre Photoreactor)	68
Figure 2.27 Horizontal RDR (Rotating Disc Reactor)	69
Figure 2.28 Schematic of submerged membrane photocatalytic reactor	70
Figure 2.29 Influence of the different physical parameters which govern the reaction rate r (r is generally comprised between 1 and 0.1 mmol hr ⁻¹): (A) mass of catalyst; (B) wavelength; (C) initial concentration of reactant; (D) temperature; (E) radiant flux	76
Figure 3.1 Supercritical hydrothermal synthesis rig	80
Figure 3.2 Schematic of TFFBR photocatalytic reactor	82
Figure 3.3 Photograph of the TFFBR photocatalytic reactor	83
Figure 3.4 Photograph of the reactive area and the water source	84
Figure 3.5 (a) Photograph of a P-25 TiO ₂ coated surface on the stainless steel plate (b) SEM image of P-25 TiO ₂	84

coated surface at a magnification 200 μm

Figure 3.6 SEM image of synthesised TiO_2 coated surface	85
Figure 3.7 The set-up of stirring batch reactor	88
Figure 3.8 Schematic diagram of the fluidised bed photoreactor	90
Figure 3.9 Photograph of the fluidised bed photoreactor	90
Figure 3.10 Schematic diagram of HPLC	93
Figure 3.11 Double beam UV-Vis spectrophotometer	95
Figure 3.12 Geometry of SEM	96
Figure 3.13 Geometry of TEM	97
Figure 3.14 Schematic diagram of XRD	99
Figure 3.15 Overall chromatograph peak at concentration 5 ppm of isoproturon, simazine, and propazine	101
Figure 3.16 Structure of triazines	102
Figure 3.17 HPLC chromatogram of a mixture of isoproturon, simazine and propazine (1 mg litre^{-1} each)	103
Figure 3.18 Isoproturon calibration curve	105
Figure 3.19 Simazine calibration curve	105
Figure 3.20 Propazine calibration curve	106
Figure 4.1 EDAX data of surface structure of 40 % wt of P-25 TiO_2 on TFFBR	110
Figure 4.2 EDAX data of surface structure of 14 % wt of synthesised	110

- Figure 4.3** Remaining concentration (as a function of initial concentration), versus time plot for isoproturon, simazine and propazine over P-25 TiO₂ plate in the absence of UV irradiation (initial pesticide concentration = 20 ppm, flow rate = 20 ml min⁻¹) 113
- Figure 4.4** Remaining percentage after loss of isoproturon versus time: effect of light wavelength on the photolysis reaction (without catalyst), Initial concentration 20 ppm, flow rate = 20 ml min⁻¹ 115
- Figure 4.5** Remaining percentage after loss of simazine versus time: effect of light wavelength the photolysis reaction of simazine (without catalyst). Initial concentration 20 ppm, flow rate = 20 ml min⁻¹ 116
- Figure 4.6** Remaining percentage after loss of propazine versus time: effect of light wavelength on the photolysis reaction of propazine (without catalyst). Initial concentration 20 ppm, flow rate = 20 ml min⁻¹ 116
- Figure 4.7** UVC photolysis on isoproturon, simazine, and propazine 118

without any photocatalyst, initial concentration = 20 ppm,

flow rate = 20 ml min⁻¹

Figure 4.8 Simazine degradation by direct photolysis and photocatalysis. 118

8 UV lamps, initial simazine concentration was 2.5×10^{-5} M,

TiO₂ dosage = 0.1 g litre⁻¹, and initial pH = 5.6.

Figure 4.9 General degradation pathways of simazine (A) 119

where (B) is deisopropyl atrazine and (C) is diamino

chlorotriazine produced by photolytic loss of alkyl groups

Figure 4.10 Remaining percentage after loss of isoproturon versus 121

time (initial concentration =20 ppm) using P-25 TiO₂

under UVA with high and low flow rate

Figure 4.11 Remaining percentage after loss of simazine versus time 122

(initial concentration = 20 ppm) using P-25 TiO₂ under

UVA with high and low flow rate

Figure 4.12 Remaining percentage after loss of propazine versus time 122

(initial concentration = 20 ppm) using P-25 TiO₂ under

UVA with high and low flow rate

Figure 4.13 Remaining percentage after loss of isoproturon versus time 123

(initial concentration = 20 ppm) using P-25 TiO₂ under

UVC with high and low flow rate (100 ml min^{-1} and 20 ml min^{-1} , respectively)

Figure 4.14 Remaining percentage after loss of simazine versus time 124

(initial concentration = 20 ppm) using P-25 TiO_2 under

UVC with high and low flow rate (100 ml min^{-1} and 20 ml min^{-1} , respectively)

Figure 4.15 Remaining percentage after loss of propazine versus time 124

(initial concentration = 20 ppm) using P-25 TiO_2 under

UVC with high and low flow rate (100 ml min^{-1} and 20 ml min^{-1} , respectively)

Figure 4.16 Different flow structure (a) FFLF is falling film 127

laminar flow, (b)PF is plug flow, and (c) SF is slit flow

Figure 4.17 The difference between laminar flow and turbulent flow 127

Figure 4.18 Comparison of photocatalytic degradation of three 128

pesticides at high flow rate (initial concentration = 20 ppm)

using P-25 TiO_2 under UVC

Figure 4.19 Comparison of photocatalytic degradation of three 129

pesticides at low flowrate (initial concentration = 20 ppm)

using P-25 TiO_2 under UVC

- Figure 4.20** Remaining percentage after loss of isoproturon versus time 131
(initial concentration =2.5 ppm) using P-25 TiO₂ under UVC
with low flow rate
- Figure 4.21** Remaining percentage after loss of propazine versus time 131
(initial ncentration = 2.5 ppm) using P-25 TiO₂ under
UVC with low flow rate
- Figure 4.22** Remaining percentage (per gram of photocatalyst) after 133
loss of isoproturon versus time (initial concentration =
20 ppm) under UVA using P-25 TiO₂ comparing to
synthesised TiO₂
- Figure 4.23** Remaining percentage (per gram of photocatalyst) after 134
loss of isoproturon versus time (initial concentration =
2.5 ppm) under UVA using P-25 TiO₂ comparing to
synthesised TiO₂
- Figure 4.24** Remaining percentage (per gram of photocatalyst) after 134
loss of isoproturon versus time (initial concentration =
20 ppm) under UVC using P-25 TiO₂ comparing to
synthesised TiO₂
- Figure 4.25** Remaining percentage (per gram of photocatalyst) after 135

loss of isoproturon versus time (initial concentration = 2.5 ppm) under UVC using P-25 TiO₂ comparing to synthesised TiO₂

Figure 4.26 Remaining percentage (per gram of photocatalyst) after 136

loss of simazine versus time (initial concentration = 20 ppm) under UVC using P-25 TiO₂ comparing to synthesised TiO₂

Figure 4.27 Remaining percentage (per gram of photocatalyst) after 136

loss of simazine versus time (initial concentration = 2.5 ppm) under UVC using P-25 TiO₂ comparing to synthesised TiO₂

Figure 4.28 Remaining percentage (per gram of photocatalyst) after 138

loss of propazine versus time (initial concentration = 20 ppm) under UVA using P-25 TiO₂ comparing to synthesised TiO₂

Figure 4.29 Remaining percentage (per gram of photocatalyst) after 138

loss of propazine versus time (initial concentration = 2.5 ppm) under UVA using P-25 TiO₂ comparing to synthesised TiO₂

Figure 4.30	Remaining percentage (per gram of photocatlyst) after loss of propazine versus time (initial concentration = 20 ppm) under UVC using P-25 TiO ₂ comparing to synthesised TiO ₂	139
Figure 4.31	Remaining percentage (per gram of photocatalyst) after loss of propazine versus time (initial concentration = 2.5 ppm) under UVC using P-25 TiO ₂ comparing to synthesised TiO ₂	139
Figure 4.32	Structure of dodecenyl succinic anhydride (DDSA)	140
Figure 5.1	Degradation rate of pesticides in the absence of UV but the presence of P-25 TiO ₂ = 5 g litre ⁻¹	146
Figure 5.2	Adsorbed concentration of isoproturon in the absence of UV onto TiO ₂ at different isoproturon concentration. TiO ₂ concentration = 0.4 g litre ⁻¹ and isoproturon concentration = 1-8 ppm	147
Figure 5.3	Effect of P-25 TiO ₂ loadings on the degradation of isoproturon versus time under UVA irradiation	148
Figure 5.4	Effect of P-25 TiO ₂ loadings on the degradation of simazine versus time under UVA irradiation	149

Figure 5.5 Effect of P-25 TiO ₂ loadings on the degradation of propazine versus time under UVA irradiation	149
Figure 5.6 $\ln [C_R]/[C_0]$ (Remaining concentration divided by initial concentration of isoproturon when using 10 g litre ⁻¹ of P-25 TiO ₂) versus time	151
Figure 5.7 Optimum P-25 TiO ₂ loading of the stirred reactor under UVA, k value was calculated from Figure 5.1, Figure 5.2, and Figure 5.3	152
Figure 5.8 The six principal directions of photons scattering in the six-flux model (SFM) and the scattering probabilities	154
Figure 5.9 Degradation of propazine (initial concentration = 2.5ppm) using P-25 TiO ₂ and synthesised TiO ₂ under UVA	156
Figure 5.10 Photograph of synthesised TiO ₂ after sintering at 900 °C for an hour	158
Figure 5.11 Degradation of isoproturon (initial concentration = 2.5ppm) using the synthesised TiO ₂ under UVA, [TiO ₂] = 5 g litre ⁻¹ after drying at 80 °C and sintering at 900 °C	159
Figure 5.12 Degradation of simazine (initial concentration = 2.5ppm)	159

using the synthesised TiO₂ under UVA,

[TiO₂] = 5 g litre⁻¹ after drying at 80 °C

and sintering at 900 °C

Figure 5.13 Degradation of propazine (initial concentration = 2.5ppm) 160

using the synthesised TiO₂ under UVA,

[TiO₂] = 5 g litre⁻¹ after drying at 80 °C

and sintering at 900 °C

Figure 5.14 Degradation of isoproturon (initial concentration = 2.5ppm) 161

using the synthesised TiO₂ under UVC, [TiO₂] = 5 g litre⁻¹

after drying at 80 °C and sintering at 900 °C

Figure 5.15 Degradation of simazine (initial concentration = 2.5ppm) 161

using the synthesised TiO₂ under UVC, [TiO₂] = 5 g litre⁻¹

after drying at 80 °C and sintering at 900 °C

Figure 5.16 Degradation of propazine (initial concentration = 2.5ppm) 162

using the synthesised TiO₂ under UVC, [TiO₂] = 5 g litre⁻¹

after drying at 80 °C and sintering at 900 °C

Figure 5.17 Degradation of propazine using the synthesised TiO₂ 163

under UVA [TiO₂] = 5 g litre⁻¹ after drying at 80 °C

and sintering at 900 °C compared with the non-sintering

synthesised TiO₂

Figure 5.18 Results of XRD analysis of synthesised TiO₂ at different 165

temperatures

Figure 5.19 XRD of pure titanium when oxidation in the temperature 167

range 400 – 800 °C

Figure 6.1 Decrease in the concentration of pesticides in the absence of 173

UV irradiation but in the presence of P-25 TiO₂ (5 g litre⁻¹)

Figure 6.2 UVA photolysis of isoproturon, simazine, and propazine 174

without any catalyst

Figure 6.3 UVC photolysis of isoproturon, simazine, and propazine 175

without any catalyst

Figure 6.4 Effect of light wavelength on the photocatalytic 179

oxidation rate of isoproturon, [TiO₂] = 5 g litre⁻¹,

initial concentration of isoproturon = 2.5 ppm,

P-25 TiO₂ sintered at 900 °C for an hour

Figure 6.5 Effect of light wavelength on the photocatalytic 179

oxidation rate of simazine, [TiO₂] = 5 g litre⁻¹,

initial concentration of simazine = 2.5 ppm,

P-25 TiO₂ sintered at 900 °C for an hour

Figure 6.6 Effect of light wavelength on the photocatalytic 180

oxidation rate of propazine, UVA [TiO₂] = 5 g litre⁻¹,

UVC [TiO₂] = 5 g litre⁻¹, initial concentration of simazine

= 2.5 ppm, P-25 TiO₂ sintered at 900 °C for an hour

Figure 6.7 Effect of air flow rate on liquid phase phenol 183

degradation fraction

Figure 6.8 Photocatalytic degradation of isoproturon using 185

fluidised bed reactor under UVA with P-25

TiO₂ concentration 2.5, 5 and 7.5 g litre⁻¹

Figure 6.9 Photocatalytic degradation of simazine using 185

fluidised bed reactor under UVA with P-25 TiO₂

concentration 5 and 7.5 g litre⁻¹

Figure 6.10 Photocatalytic degradation of isoproturon, simazine 188

and propazine using fluidised bed reactor under UVA

with P-25 TiO₂ concentration 5 g litre⁻¹

Figure 6.11 Photocatalytic degradation of isoproturon using 189

fluidised bed reactor under UVC with P-25 TiO₂

concentration 2.5, 5 and 7.5 g litre⁻¹

Figure 6.12	Photocatalytic degradation of isoproturon, simazine and propazine using fluidised bed reactor under UVC with P-25 TiO ₂ concentration 5 g litre ⁻¹	190
Figure 6.13	The linear relationship between ln [C _R]/[C ₀] (remaining concentration divided by the initial concentration of isoproturon using P-25 7.5 g litre ⁻¹ under UVA) and time	191
Figure 6.14	Optimum P-25 TiO ₂ loading of the fluidised bed photoreactor under UVA (a), and UVC (b) irradiation for photocatalytic degradation of isoproturon, k value was calculated from Figure 6.8, and Figure 6.12 of isoproturon degradation	192
Figure 6.15	Photocatalytic degradation of isoproturon under UVA using synthesised TiO ₂ 5 g litre ⁻¹ compared with using P-25 TiO ₂ 5 g litre ⁻¹	193
Figure 6.16	Photocatalytic degradation of isoproturon under UVC using synthesised TiO ₂ 5g litre ⁻¹ compared with using P-25 TiO ₂ 5 g litre ⁻¹	194
Figure 6.17	Photocatalytic degradation of simazine under UVA	195

using synthesised TiO_2 5 g litre^{-1} compared with

using P-25 TiO_2 5 g litre^{-1}

Figure 6.18 Photocatalytic degradation of simazine under UVC 195

using synthesised TiO_2 5 g litre^{-1} compared with

using P-25 TiO_2 5 g litre^{-1}

Figure 6.19 Photocatalytic degradation of propazine under UVA 196

using synthesised TiO_2 5 g litre^{-1} compared with

using P-25 TiO_2 5 g litre^{-1}

Figure 6.20 Photocatalytic degradation of propazine under UVC 197

using synthesised TiO_2 5 g litre^{-1} compared with

using P-25 TiO_2 5 g litre^{-1}

Figure 6.21 TEM photograph of P-25 TiO_2 in aqueous suspension 198

Figure 6.22 TEM photograph of synthesised TiO_2 in aqueous 199

suspension (a) fine particles with the size of 10-15 nm

(b) start to agglomerate due to high surface area

Figure 6.23 UV-Vis spectroscopy of the P-25 TiO_2 comparing 202

with the synthesised TiO_2

LIST OF TABLES

Table 1.1 Three examples of pesticides in OPs group	5
with molecular formula and chemical structures:	
Parathion methyl, fenitrothion, parathion	
Table 1.2 Common pesticides in each group categorized	7
by chemical structure	
Table 1.3 The 12 pesticides most often found in UK drinking water	9
Table 1.4 The total usage of pesticides in the UK	10
Table 1.5 Structure refinement and crystal data of isoproturon	12
Table 1.6 Maximum acceptable values (MAVs) for the pesticide	15
residues in the drinking water in New Zealand	
Table 2.1 List of herbicides degradation by the TiO ₂	29
photocatalysis, the main reaction pathways,	
the transformation products (TPs)	
Table 2.2 Main intermediates produced in the photocatalytic	32
reaction of simazine	
Table 2.3 Photocatalytic degradation of bromacil in an aqueous	40
suspensions under the different types of TiO ₂	

Table 2.4 Degradation rate of indole-3-acetic acid (IAA) in Degussa P-25 TiO ₂ suspension at different indole-3-acetic acid (IAA) concentrations	46
Table 2.5 Photocatalytic degradation of tebuthiuron at different Degussa P-25 TiO ₂ concentration	50
Table 2.6 Influence of pH on the photocatalytic degradation of various pollutants	54
Table 2.7 Comparing % removal of pesticides by photocatalytic treatments before adding H ₂ O ₂ and after adding H ₂ O ₂	61
Table 2.8 Comparing the advantages and drawbacks of suspended and immobilized photocatalytic system	71
Table 3.1 Comparing molecular weight of three chosen pesticides	102
Table 6.1 Photocatalytic reaction rate of isoproturon, simazine, and propazine using P-25 TiO ₂ under UVA and UVC (reaction rate constant at the first 10 minutes)	186

Chapter 1

INTRODUCTION

1.1 Introduction

The increase in the worldwide contamination of freshwater systems with industrial and natural chemicals is a major environmental problem. Since drinking water is becoming increasingly scarce, investigation into the decontamination of the impure water has risen substantially because of an increased presence of pollutants, such as surfactants, pesticides, dyes, persistent organic chemicals and heavy metals. Although the pesticides are usually present in low concentrations, many of them raise considerable toxicological concerns, particularly when present as complex mixtures. The three pesticides investigated in this thesis - isoproturon, simazine and propazine - are three of the most frequently detected pesticides in groundwater.

1.1.1 Examples of common water pollutants

1. Industrial chemicals (solvents, intermediates, petrochemicals) :
tetrachloromethane, methyl-t-butylether, BTEX (benzene, toluene, xylene)
2. Industrial products (additives, lubricants, flame retardants):
phthalates, PCBs (Polychlorinated biphenyls), polybrominated diphenylethers

3. Consumer products (detergents, pharmaceuticals, hormones, personal-care products): nonylphenol ethoxylates, antibiotics, ethinyl estradiol, ultraviolet filters
4. Biocides (pesticides, nonagricultural biocides): DDT, atrazine, tributyltin, triclosan
5. Geogenic/natural chemicals (heavy metals, inorganic, taste and odor, cyanotoxines, human hormones): lead, cadmium, mercury, arsenic, selenium, fluoride, uranium, geosmin, methylisobornol, microcystins, estradiol
6. Disinfection/oxidation (disinfection by-products): trihalomethanes, haloacetic acids, bromate
7. Transformation products (metabolites from above chemicals): metabolites of perfluorinated compounds, chloroacetanilide herbicide metabolites

1.1.2 Definition of pesticides (in general view)

'Pesticide' is a broad term, covering a range of products that are used to control pests. Slug pellets, ant powder, weed killers, and rat and mouse baits are examples of pesticides which are encountered in daily life.

1. Insect killers (insecticides)
2. Mould and fungi killers (fungicides)
3. Weedkillers (herbicides)

4. Slug pellets (molluscicides)
5. Plant growth regulators
6. Bird and animal repellents
7. Rats and mouse killers (rodenticides)

Pesticides are widely used for the control of plant disease and weeds. Many pesticides, including herbicides and fungicides are highly toxic to terraneous and aquatic life; this is a particular problem in agricultural areas. They can enter into the environment by several routes such as spraying, soil and storage, as well as wastewater discharge. Moreover, these compounds can contaminate surface and groundwater, posing a risk to wildlife and human health, due to the potential toxicity of these compounds. Environmental contamination occurs when these pesticides drift from application site via air and rain water, into groundwater by leaching through soil, running off the treated land via storm or irrigation water, or migrating from application sites (Zhou et al., 2007).

1.1.3 Groups of pesticides

Pesticides can be categorised into 9 major groups, based on their by chemical structures (Ministry of Environment, Ontario, Canada, 2010).

1. Triazine (N-Containing pesticides): a group of compounds whose molecules contain an unsaturated ring of three carbon and three nitrogen atoms.

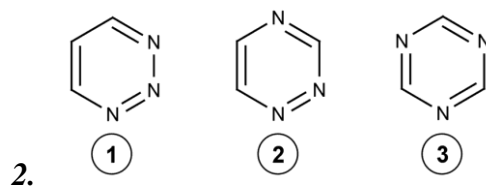


Figure 1.1 Triazine isomers: (1) 1,2,3 triazine ,(2) 1,2,4 triazine ,(3) 1,3,5 triazine

2. Carbamates (Cbs): a salt or ester containing the anion NH_2COO^- , derived from compound carbamic acid.

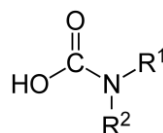


Figure 1.2 Chemical structure of carbamic acid group

3. Organochloride (OCs): pesticides containing chloride.

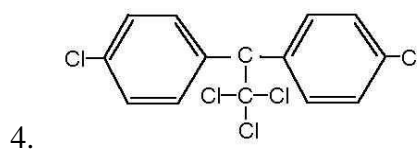


Figure 1.3 Structure of DDT, an example of pesticides in OCs group

4. Organophosphorous (OPs): pesticides containing phosphorus.

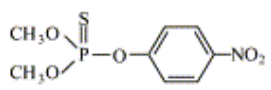
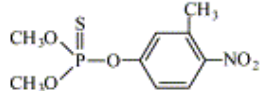
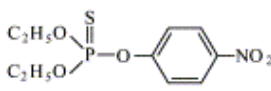
Pesticides	Molecular formula	Structure
Parathion methyl (PTM)	C ₉ H ₁₀ O ₃ NS	
Fenitrothion (FT)	C ₁₀ H ₁₄ O ₃ NS	
Parathion (PT)	C ₉ H ₁₂ O ₃ NS	

Table 1.1 Three examples of pesticides in OPs group with molecular formula and chemical structures: Parathion methyl, fenitrothion, parathion

- Chlorophenols (CPs): for example; trichlorophenol, pentachlorophenol, dichlorophenol, 2-chlorophenol
- Phenoxy acids (PAs): a family of chemicals related to the growth hormone indoleacetic acid (IAA).

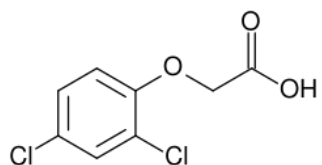


Figure 1.4 Chemical structure of Phenoxy acid

- Quaternary ammonium compounds (Q) are positively charged polyatomic ions of the structure NR₄⁺ with R being alkyl or aryl groups. Examples of the pesticides in this group are Diquat and Paraquat.

8. Phenylurea (PhUrs): a chemical compound on which relatively nontoxic herbicides are based.

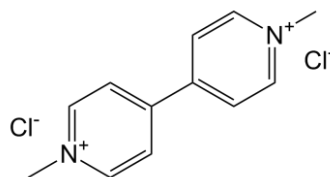


Figure 1.5 Paraquat structure

9. Thiocarbamate (ThCbs): a family of organosulfur compounds.

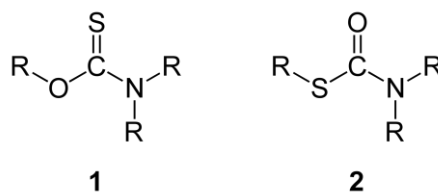


Figure 1.7 Two isomeric forms of Thiocarbamate

Table 1.2 presents 9 different groups of pesticides, as described above.

The pesticides in each group are given.

N	Cbs	Ocs	Ops	CPs	Pas	Q	PhUrs	ThCbs
Alachlor	Aldicarb	Aldrin	Dimethoate	2-,3-,4-Chlorophenols	MCPA	Diquat	Chlortoluron	Butylate
Atrazine	Bendiocarb	Chlordan	Malathion	2,3-2,4-Dichlorophenols	Propoxur	Paraquat	Diuron	Cydoate
Cyanazine	Carbaryl	Heptachlor	Parathion	2,5-2,6-Dichlorophenols			Isoproturon	EPTC
Metolachlor	Carbofuran	DDT	Diazinon	3,4-3,5-Dichlorophenols			Fenuron	Eptam
Prometryne	Triallate	lindane	Chlorpyrifos	2,3,5-Trichlorophenols			Monuron	Molinat
Simazine		Methoxychlor	Fenthion	2,4,6-Trichlorophenols			Metobromuron	Thiocarbazil
Propazine		PCB	Monocotophos	Pentachlorophenol				Thiobencarb
		Trifluralin	Terbufos					Vapam
			Temephos					Vernolate
			Phorate					

Table 1.2 Common pesticides in each group categorized by chemical structure

1.1.4 Water pollution from pesticides

Atrazine, simazine, isoproturon, chlortoluron and mecoprop represent the most widespread contaminants in drinking water, as shown in Table 1.3 (Ward et al., 1993). Simazine and atrazine are so widely used that they are found in nearly all the water sources in Europe (Croll, 1991). They are slowly broken down in the soil where it has a low mobility, although they are still commonly detected in low concentrations in both the ground and surface water. Simazine is shown to display chronic toxicity in laboratory animals (Turner, 2003). The World Health Organization (WHO) set the guideline value for simazine in the drinking water at 0.002 mg/l (Mohapatra and Michell, 2003). Atrazine is relatively persistent and more mobile in soil than simazine. It is slowly degraded by photolysis and microbial action in soil, although it can remain in water for many years and cause long-term adverse effects in the aquatic environment (simazine MSDS, propazine MSDS from Sigma-Aldrich). The health effects of atrazine are evidence of a highly toxic, carcinogenic substance. WHO has now set guideline values for atrazine in drinking water at 0.002 mg/l (Hamilton *et al.*, 2003).

Frequently occurring	Commonly occurring
Atrazine ($C_8H_{14}ClN_5$)	2,4-D ($C_8H_6Cl_2O_3$)
Chlortoluron ($C_{10}H_{13}ClN_2O$)	Dicamba ($C_8H_6Cl_2O_3$)
Isoproturon ($C_{12}H_{18}N_2O$)	Dichlorprop ($C_9H_8Cl_2O_3$)
MCPA ($C_9H_9ClO_3$)	Dimethoate ($C_5H_{12}NO_3PS_2$)
Mecocrop ($C_{10}H_{11}ClO_3$)	Linuron ($C_9H_{10}Cl_2N_2O_2$)
Simazine ($C_7H_{12}ClN_5$)	2,4,5-T ($C_8H_5Cl_3O_3$)

Table 1.3 The 12 pesticides most often found in UK drinking water. All are herbicides except for dimethoate, which is an insecticide (Ward et al., 1993).

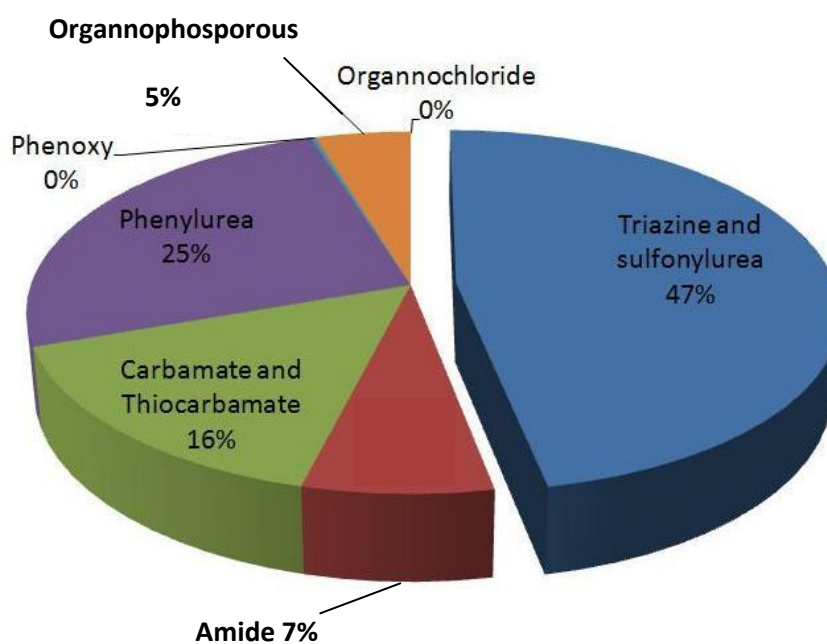


Figure 1.8 Statistical data of used pesticides in 2006 in UK (from Food and Environmental Research Agency, 2006)

Pesticides	Area Treated (ha)	Percentage (%)
Triazine and sulfonylurea	4050000	47
Amide	600000	7

Carbamate and thiocarbamate	1350000	15.7
Phenylurea	2200000	25.6
Phenoxy	20000	0.2
Organnophosphorus	400000	4.5
Organnochloride	0	0
Total	8620000	100

Table 1.4 *The total usage of pesticides in the UK (from Food and Environmental Research Agency, 2006)*

From Figure 1.8 and Table 1.4, most agricultural areas in 2006 are treated with triazine, which is equal to 47% of all the agricultural areas in the United Kingdom.

1.1.5 Selected pesticides used in this thesis

1. Isoproturon (3-(4-isopropylphenyl)-1,1-dimethylurea) is a phenylurea herbicide, which consists of an aromatic ring with an alkylic chain and a ureic group (diamide), acting to inhibit the photosynthesis (Gora et al., 2006). It has been used for pre- and post- emergence of annual grass, wild oats, annual meadow grass and many broad leaf weeds in winter wheat, spring and winter barley and winter rye.

Figure 1.9 shows the use of isoproturon in UK agriculture during 1990-2009. Isoproturon seems to have been used in lower amounts after 1996 and constantly applied until 2009.

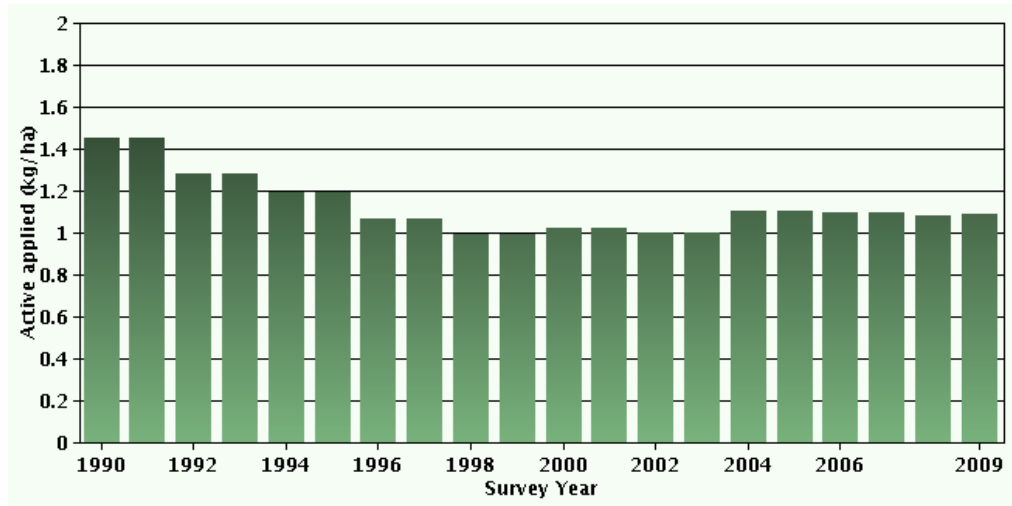


Figure 1.9 Use of isoproturon (kg/hr) with crops in UK (from The Food and Environmental Research Agency, 2006)

Identification code	Isoproturon
Empirical formula	C ₁₂ H ₁₈ N ₂ O
Formula weight	206.28
Temperature	293(2) K
Wavelength	0.71073 Å
Crystal system	Orthorhombic
Space group	<i>Pbca</i>
Unit cell dimensions	$a = 10.1862(17)$ Å, $\alpha = 90^\circ$ $b = 11.0301(19)$ Å, $\beta = 90^\circ$ $c = 20.981(4)$ Å, $\gamma = 90^\circ$
Volume	2357.4(7) Å ³
Z	8
Density (calculated)	1.162 mg/m ³
Absorption coefficient	0.075 mm ⁻¹
<i>F</i> (000)	896
Crystal size	0.30 × 0.25 × 0.04 mm ³
Theta range for data collection	1.94–31.29°.
Index ranges	–14 ≤ <i>h</i> ≤ 14, –15 ≤ <i>k</i> ≤ 15, –29 ≤ <i>l</i> ≤ 30
Reflections collected	12,860
Independent reflections	3056 [<i>R</i> (int) = 0.0803]
Completeness to theta = 31.29°	79.4%
Refinement method	Full-matrix least-squares on <i>F</i> ²
Data/restraints/parameters	3056/0/191
Goodness-of-fit on <i>F</i> ²	0.805
Final <i>R</i> indices [<i>I</i> > 2σ(<i>I</i>)]	<i>R</i> 1 = 0.0508, ω <i>R</i> 2 = 0.1247
<i>R</i> indices (all data)	<i>R</i> 1 = 0.2779, ω <i>R</i> 2 = 0.1619
Extinction coefficient	0.0011(6)
Largest diff. peak and hole	0.155 and –0.146 e Å ⁻³

Table 1.5 Structure refinement and crystal data of isoproturon (Vrielynck et al., 2006)

Table 1.5 shows the properties of isoproturon; for example the calculated density, crystal size, structure refinement, unit cell dimensions, etc.

2. Simazine (6-chloro-*N,N'*-diethyl-1,3,5-triazine-2,4-diamine) is a s-triazine herbicide. Figure 1.11 indicates that simazine consists of an alkylic chain bound to the N-exocyclic. It is used in various herbicide

formulations, in agriculture, for controlling plant production, and in orchards, with Christmas trees and in recreational areas.

Figure 1.10 shows the use of simazine in UK agriculture during 1990-2009. There was a decrease in the use of simazine from 1996 to 2005. However, since 2006, the use of simazine has significantly increased.

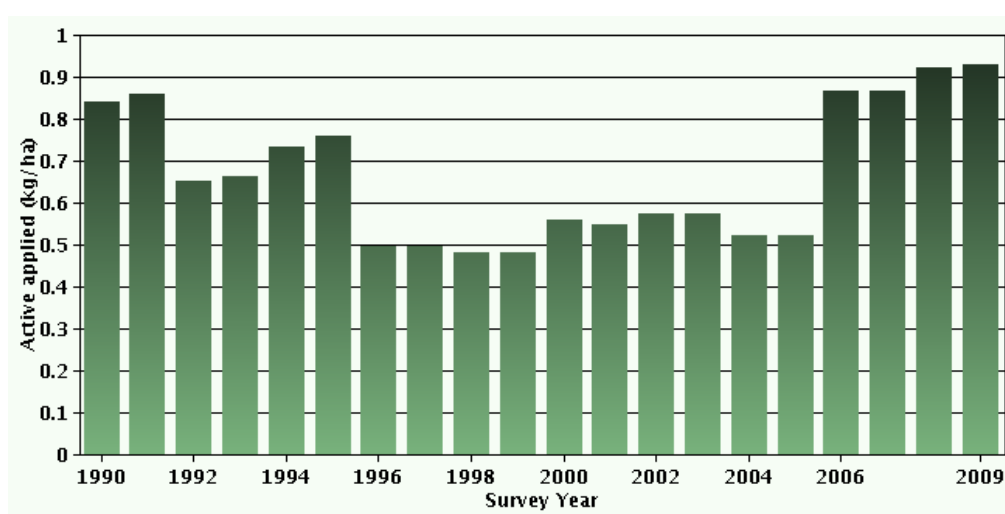


Figure 1.10 Rate of use (kg/ha) for simazine with crops in UK (from *The Food and Environmental Research Agency, 2006*)

3. Propazine (6-Chloro-N, N'-bis(1-methylethyl)-1,3,5-triazine-2,4-diamine) is a selective s-triazine herbicide used for the control of most annual broadleaf weeds and annual grasses. Its structure consists of the alkylic chain bound to the exocyclic N-amino group, as shown in Figure 1.12. Its principal mode of action is to selectively inhibit plant photosynthesis.

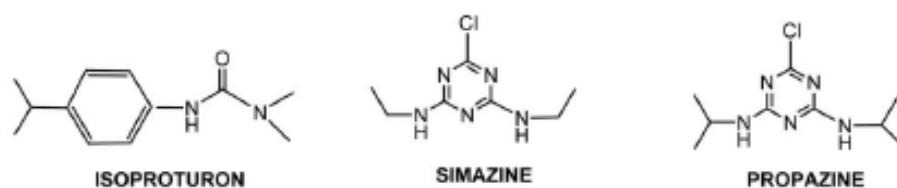


Figure 1.11 Structure of three pesticides

1.1.6 Legislation of pesticides in respect to human consumption

In the European Union, there is a maximum admissible concentration (MAC) which, in turn, defines that the minimum specified requirements of potable water. Each pesticide is limited to 0.1 $\mu\text{g/l}$ up to a maximum of 0.5 $\mu\text{g/l}$ for the total pesticides (Ward *et al.*, 1993). Table 1.6, the ‘maximum acceptable value’ (MAV) of pesticides in drinking water, was defined by the New Zealand Ministry of Health. Pesticide regulations relating to the drinking water of New Zealand are presented to show MAVs of three chosen pesticides (isoproturon, simazine and propazine). The MAV for isoproturon is 10 $\mu\text{g/l}$, for simazine 2 $\mu\text{g/l}$ and for propazine 70 $\mu\text{g/l}$. From the definition, MAV values are designed to take into account consumption of a lifetime. However, the quality of drinking water should not be degraded by the MAV level. The removal of excess pesticides in the water may therefore be necessary and there are different approaches to reducing their total concentration, including air stripping, granular activated carbon adsorption (GAC) and advanced oxidation processing (AOP).

Pesticide	µg/l	Pesticide	µg/l	Pesticide	µg/l
Alachlor	20 ^a	1,3-Dichloropropene	20 ^a	Oxadiazon	200 ^b
Aldicarb	10	Dichlorprop	100	Pendimethalin	20
Aldrin/dieldrin	0.03	Diquat	10	Pentachlorophenol	10 ^b
Atrazine	2 ^b	Diuron	20 ^b	Permethrin	20
Azinphos methyl	4 ^b	Fenoprop	10	Picloram	20 ^b
Bentazone	400 ^b	Heptachlor and heptachlor epoxide	0.04	Pirimiphos methyl	100
Bromacil	400 ^b	Hexachlorobenzene	1 ^a	Pirimisulfuron methyl	900
Carbofuran	8	Hexazinone	400 ^b	Procyimidone	700
Chlordane	0.2	Isoproturon	10	Propanil	20
Chlorpyrifos	70	Lindane	2	Propazine	70 ^b
Chlortoluron	40	MCPA	2	Pyridate	100
Cyanazine	0.7	Mecoprop	10	Simazine	2 ^b
2,4-D	40	Metalaxyl	100 ^b	2,4,5-T	10
2,4-DB	100	Methoxychlor	20	Terbutylazine	8
DDT + isomers	2	Metolachlor	10	Thiabendazole	400 ^b
Diazinon	10	Metribuzin	70 ^b	Triclopyr	100 ^b
1,2-Dibromo-3-chloropropane	1 ^a	Molinate	7	Trifluralin	30
1,2-Dichloropropene	2 ^b	Oryzalin	400 ^b	1080	3.5 ^b

^aFor excess lifetime cancer risk of 10⁻⁵.

^bProvisional maximum acceptable value.

Table 1.6 Maximum acceptable values (MAVs) for the pesticide residues in the drinking water in New Zealand (Hamilton et al., 2003, Ministry of Health, NZ. Drinking-water standards for New Zealand, 2000)

1.2 Research objectives

The main objectives of this study are:

- (i) To use TiO₂ nanoparticles synthesised by the supercritical water in the waste water treatment
- (ii) To characterise TiO₂ produced via hydrothermal synthesis using Scanning Electron Microscopy (SEM), Transmission Electron Microscopy (TEM), Ultraviolet-Visible absorption spectroscopy (UV-Vis) and X-Ray Diffraction (XRD)
- (iii) To design, construct and develop three different types of reactors (thin film fixed bed reactor, stirred reactor and fluidised bed

photoreactor) for the treatment of the water polluted by the three named pesticides

(iv) To evaluate the effectiveness of commercial P-25 TiO₂ compared with ScWHS synthesised TiO₂ when applied to the photocatalytic degradation of the aqueous solutions of selected pesticides (isoproturon, simazine and propazine)

(v) To study the effect of the operating parameters such as catalyst concentration, pesticide concentration, and the wavelength of light on the photocatalytic degradation of the pesticides

1.3 Thesis structure

This thesis is composed of 7 chapters. Each chapter addresses different research issues.

Chapter 1: An outline of the global water pollution problem, particularly water polluted by pesticides, and the use of pesticides in agriculture. Pesticides are categorised into different categories, and the impacts of each category are identified. The structures of the three pesticides related to this research are provided. The objectives of this research and outlines of the thesis structure are also included.

Chapter 2: The basic concepts of photolysis, the homogeneous photocatalysis, the heterogeneous photocatalysis, and also 'Photo-Fenton reaction' are reviewed. This chapter mainly discusses the fundamental knowledge of photocatalysis, the choice of photocatalysts, the mechanism, and the effecting

factors in the reaction. An up-to-date review of the literature of all the above topics is also addressed. The TiO₂ nanoparticles synthesis is also reviewed.

Chapter 3: This chapter explains the experimental part of the photocatalysis, which comprises of the reagents and materials, the photocatalysis reactor including, the thin film fixed bed reactor (TFFBR), the stirred reactor, and the fluidised bed photoreactor. Standard operating procedures are also included in this chapter. The experimental set-up of the reactor used to synthesise the nanoparticles is also presented. The schematic diagram and the photograph of the system are offered. All the technical and analytical methods used in this research are addressed.

Chapter 4: The results from the TFFBR are presented. The efficiency of this reactor with a synthesised TiO₂ surface is compared with a commercial TiO₂. The results of the photocatalytic degradation under the different conditions are presented.

Chapter 5: The results from the stirred reactor are presented. The impact of the photocatalyst loadings is presented in this chapter. The optimum TiO₂ concentrations for the photocatalytic degradation of isoproturon, simazine and propazine are evaluated. The photocatalytic performance of the synthesised TiO₂ is compared with the commercial one. The promising explanations are addressed. X-ray diffraction (XRD) results are proposed to support the explanation.

Chapter 6: The results from the fluidised bed photoreactor are presented. The influence of UV wavelength and photocatalyst concentration is discussed.

The efficiency of ScWHS synthesised TiO_2 is compared to the commercial TiO_2 in term of the photocatalytic activity.

Chapter 7: Overall conclusions of the research. Recommendations are made for improving the efficiency of a UV based photo-oxidation system. Potential future work is also addressed in this chapter.

Chapter 2

BACKGROUND AND REVIEW OF LITERATURE

2.1 Introduction

The purpose of this chapter is to give an overview of the fundamental principles of heterogeneous photocatalysis. The mechanisms, the kinetics and the effect of the different parameters on the photocatalytic rate are outlined. A variety of reactor designs are presented and an introduction to the synthesis of the nanocatalysts, using supercritical water, is also given. This synthesis method was used to prepare nanoparticles titanium dioxide which was used in experiments to compare the photocatalytic efficiency with the commercial P-25 TiO₂.

2.2 Photolysis or Photodissociation process

Photolysis is a chemical process by which molecules are broken down through the absorption of light. Photons, with their energy being inversely proportional to their wavelength, can affect the chemical bonds of a chemical compound by the cleavage of one or more covalent bonds in a molecular entity (Muller, 1994). The general photolysis reaction can be given as



2.3 The principle of photocatalysis

2.3.1 Homogeneous photocatalytic reactions

In homogeneous photocatalysis, the reactants and the photocatalysts are in the same phase. The most commonly used homogeneous photocatalysts are the ozone, the transition metal oxide and the photo-Fenton systems. The mechanism of the hydroxyl radical production by the ozone is as follows,



2.3.2 Heterogeneous photocatalytic reactions

Heterogeneous photocatalysis is defined as the acceleration of the photoreaction in the presence of a catalyst in the difference phase (Radwan, 2005). In the context of pesticide and contaminant removal, it has also been referred to as advanced oxidation processing (AOP) or photocatalytic oxidation (PCO). The initial interest in heterogeneous photocatalysis began in 1972, when the photochemical splitting of the water into hydrogen and oxygen, using TiO_2 , was shown to be possible (Fujishima and Honda, 1972). From that date, extensive work has been carried out to produce hydrogen from the water by this novel oxidation reduction reaction using a variety of semiconductors (Mill and Hunte, 1997; Mill *et al.*, 1993; Hoffmann *et al.*, 1995).

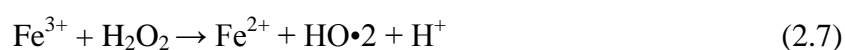
Ten years ago, a number of researchers focused on using semiconductor materials as photocatalysts for the removal of organic and inorganic species from the aqueous or gas phase. This method has been put forward as a means of environmental protection, due to its ability to oxidise the organic and inorganic substrates (Fox and Dulay, 1993).

Heterogeneous photocatalysis is a complex sequence of the reactions. Its mechanism composes of five steps (Hermann, 1999, Pirkanniemi and Sillanpaa, 2002), which are:

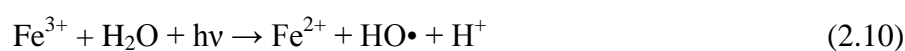
- (i) Mass transfer of the organic contaminant in the liquid phase to the TiO_2 surface
- (ii) Adsorption of the organic contaminant onto the photon activated TiO_2 surface
- (iii) Photocatalysis reaction for the adsorbed phase on the TiO_2 surface
- (iv) Desorption of the intermediate from the TiO_2 surface
- (v) Mass transfer of the intermediate from the interface region to the bulk fluid

2.4 The Photo-Fenton reaction

The Fenton reaction is a homogeneous photocatalytic process which does not involve light illumination. Conversely, in the Photo-Fenton system, an iron catalyst is used in the presence of hydrogen peroxide under an irradiation source of the visible wavelength (approximately 450-600 nanometre). It was originally recognised in the 1960s and still remains one of the most applied AOPs for its ability to degrade high loadings of organic compounds in highly saline conditions (Chong *et al.*, 2010). The advantages of this method are an environmentally-friendly reagent; using the sunlight; the relatively cost-effective process, and the replenishing of the hydroxyl radical which is the key for oxidation. These Fenton and photo-Fenton reactions might occur simultaneously with TiO₂ photocatalysis during the UV irradiation period, post-TiO₂ photocatalysis period or as a stand-alone photo-Fenton process. The photo-Fenton mechanism is shown below (Pirkanniemi and Sillanpaa, 2002),



The additional sources of OH radicals should be considered: through the photolysis of H₂O₂, and through the reduction of Fe³⁺ ions under the UV light:



The efficiency of Fenton type processes, which will influence its feasibility for the larger scale application, is largely dependent on several parameters, such as the concentration of hydrogen peroxide, pH and the intensity of the UV (Bigda, 1995). These reactions have been proven more efficient than the heterogeneous photocatalysis but the disadvantage is that the process requires the optimum pH of 4 (since iron precipitates at the higher pH and additional processing is necessary to remove the iron).

2.5 Advanced Oxidation Processing (AOP)

AOP covers a suite of chemical treatment procedures designed to remove the organic and inorganic materials in the waste water by oxidation. It is attractive as a means for removing pesticides from water because it can destroy the hazardous contaminants, rather than simply transfer them to another phase, as with other techniques, such as the air stripping and granular activated carbon adsorption (GAC). Overall the TiO₂/UV photocatalysis process is known to have many important advantages. For the heterogeneous photocatalysis, the liquid phase organic compounds are degraded to their corresponding intermediates and further mineralised to carbon dioxide, water and mineral salts, if the irradiation time is extended. (Garcia *et al.*, 2006; Vora *et al.*, 2009; Ahmed *et al.*, 2011).

2.6 Photocatalytic materials

Various noble metals (Ru, Pt, Rh, Ir, and Pd) and some metal oxides (Cu, Mn, Co, Cr, V, Ti, Bi, and Zn) have traditionally been used as heterogeneous catalysts (Pirkanniemi and Sillanpaa, 2002). Ideal photocatalysts should have the following properties (Bhatkhande *et al.*, 2001; Radwan *et al.*, 2005):

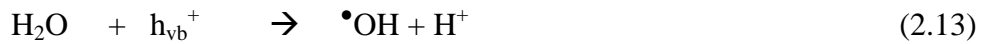
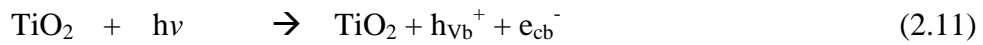
- (i) photoactivity
- (ii) biological and chemical inertness
- (iii) stability towards photocorrosion
- (iv) suitability towards visible or near UV light
- (v) low cost
- (vi) lack of toxicity

TiO₂ is known as an excellent photocatalyst due to its properties. It has been used in a variety of applications, for example, electroceramics, glass and degradation of chemicals in the water and in the air. It has been used in the form of a suspension, or an immobilised water treatment.

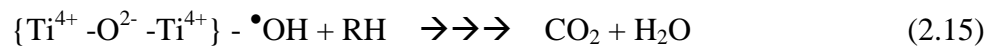
2.7 Mechanism/reactions of TiO₂ photocatalyst

When titanium dioxide is illuminated by UV radiation, it usually corresponds to wavelength < 380 nm (Pirkanniemi and Sillanpaa, 2002). Photons that have an energy equal to or greater than the band gap width, usually 3.2 eV for anatase or 3.0 eV for rutile (Chong *et al.*, 2010), leads to the formation of conduction-band electrons and valence-band holes, which subsequently diffuse to the particle surface in competition with the bulk recombination

(Linsebigler *et al.*, 1995). At the surface, these carriers are trapped by defective sites, surface states or oxidising or reducing agents. They are then able to initiate the redox reactions with other substrates. The trapped electron reduces the pre-adsorbed acceptor A to A⁻, and the trapped hole oxidises the pre-adsorbed electron donor D to D⁺ (Serpone and Emeline, 2004, Pirkanniemi and Sillanpaa, 2002).



To prevent electron-hole recombination, it is necessary for illumination to take place in the presence of an electron acceptor. For this purpose, illumination is generally carried out in an oxygen rich environment:



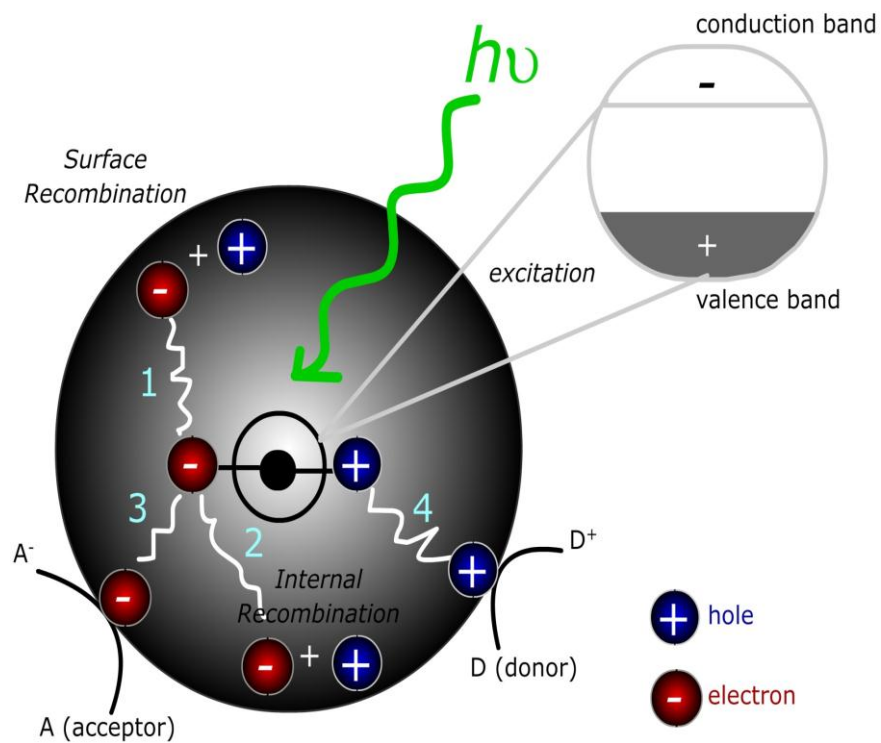


Figure 2.1 Mechanism of photocatalytic reaction in TiO_2 (Linsebigler *et al.*, 1995)

The reaction of photogenerated holes with water molecules and hydroxyl ions adsorbed on the surface of the TiO_2 in Equation (2.12 and 2.13) results in the formation of hydroxyl radicals in Equation (2.15) (Abramovic *et al.*, 2004), whereas the electron in the conduction band reduces the oxygen adsorbed on the photocatalyst. It has been suggested that these hydroxyl radicals and superoxide radical anions are the primary oxidising species in the photocatalytic oxidation processes. The hydroxyl radicals attack organic compounds, which results in various reaction intermediates and produces the final products, which are CO_2 and H_2O . The efficiency of degradation will depend upon the oxygen concentration, which determines the efficiency with

which the conduction band electrons are scavenged and (e^-/h^+) recombination is prevented (Haque and Muneer, 2007).

2.8 Photocatalytic degradation pathways and intermediates

The intermediate compounds during photocatalytic degradation and probable pathways for each pesticide have been identified by various researchers (Topalov *et al.*, 2000; Hequet *et al.*, 2001; Rafqah *et al.*, 2005; Sojic *et al.*, 2009; Aungpradit *et al.*, 2007; Han *et al.*, 2009; Muneer and Boxall, 2008; Lu *et al.*, 2009; Kaneco *et al.*; 2009, Wu *et al.*, 2010; Moctezuma *et al.*, 2007; Florencio *et al.*, 2004; Calza *et al.*, 2008; Aramendia *et al.*, 2005). Some intermediates belong to s-triazine pesticides, for example hexaconazole – the parent compound (Calza *et al.*, 2008). Intermediates from fenithion, diazinon, imidacloprid and dipyrone were found to be carboxylic acid (Mahmoohdi *et al.*, 2008; Mahmoodi *et al.*, 2007; Perez-Estrada *et al.*, 2007). Hydrochloric acid is one of the intermediate products discovered in dichloroacetic acid degradation (Zalazar *et al.*, 2008). Acetic acid is the product from glyphosate degradation in basic condition (Muneer and Boxall, 2008). Moreover, there are several stable intermediates, such as acetamide and formamide, which still remain at the end of removal of cymoxnil, methomyl, oxamyl, dimethoate, telone and pyrimethanil (Oller *et al.*, 2006). This means that investigation of the intermediate products is necessary for the treatment to obtain higher cleanliness of water. While comparing between the solar and the artificial irradiation source, imazquin degrades faster under solar light than under the artificial source (Garcia and Takashima, 2003); on the other hand, isoproturon

degrades better under the artificial source than under sunlight (Haque and Muneer, 2003). The Table below shows herbicides, divided by the chemical structures, the reaction pathways and the intermediate substances (Konstantinou and Albanis, 2003).

Herbicides	Reaction pathways	TPs
s-Triazines (s-Tr)		
Atrazine	Side alkyl chain oxidation	Amido and Dealkylated-(s-Tr)
Ametryne	Dealkylation	Hydroxy-(s-Tr)
Cyanazine	Decarboxylation	Ammeline
Irgarol	Deamination	Cyanouric acid
Propazine	Hydroxylation	
Prometryne		
Prometon		
Simazine		
Sulfonureas (Sus)		
Chlorsulfuron	Cleavage of sulfonyl-urea functional group s-Triazines reaction pathways	Hydroxy-Sus
Cinosulfuron		Dealkylated-Sus
Triasulfuron		Melamine
Thifensulfuron		Cyanouric acid
Thiocarbamates (ThCbs)		
Butylate	Scission of the amino group	Amine and carboxy-TPs
Cycloate	S-alkyl group oxidation	Keto and dealkylated-ThCbs
EPTC	Oxidation through peroxy radical formation	Sulfoxide and dealkylated-TPs
Eptam	S and O exchange of N(C)OS group	S-isomers of ThCbs
Molinate		
Thiocarbazil		
Thiobencarb		
Vernolate		
Vapam		

Amides, anilides		
3,4-Dichloropropioamide alachlor	Dechlorination	Hydroxy, aliphatic-TPs
Propachlor	Rupture of the amide group	Amine-TPs
Propanil	Oxidation through peroxy radical formation	Dechlorinated-TPs Dealkylated-TPs Cyclization-TPs
Phenylureas (PhUrs)		
Chlortoluron	Hydroxylation	Hydroxy-PhUrs
Diuron	Oxidation	Phenyl-hydroxyureas
Fenuron	Decarboxylation	Aniline derivatives
Isoproturon		
Monuron		
Metobromuron		
Phenoxy-acids		
MCPA	Hydroxylation	Hydroxy-phenoxy acids
Propoxur	Decarboxylation	Chlorophenols Quinonidal structures Carboxylic acids

Table 2.1 List of herbicides degradation by the TiO_2 photocatalysis, the main reaction pathways, the transformation products (TPs) (Konstantinou and Albanis, 2003)

2.9 Degradation pathways of isoproturon, simazine and propazine

For isoproturon, there are a lot of intermediates in the oxidation process. As illustrated in the pathway in Figure 2.2, it shows that the first are di and trihydroxylated intermediates. The next groups that will occur are aldehydes, ketones and organic acids. The final products from photocatalytic degradation of isoproturon are carbon dioxide, water, and nitric acid (Benitez *et al.*, 2006).

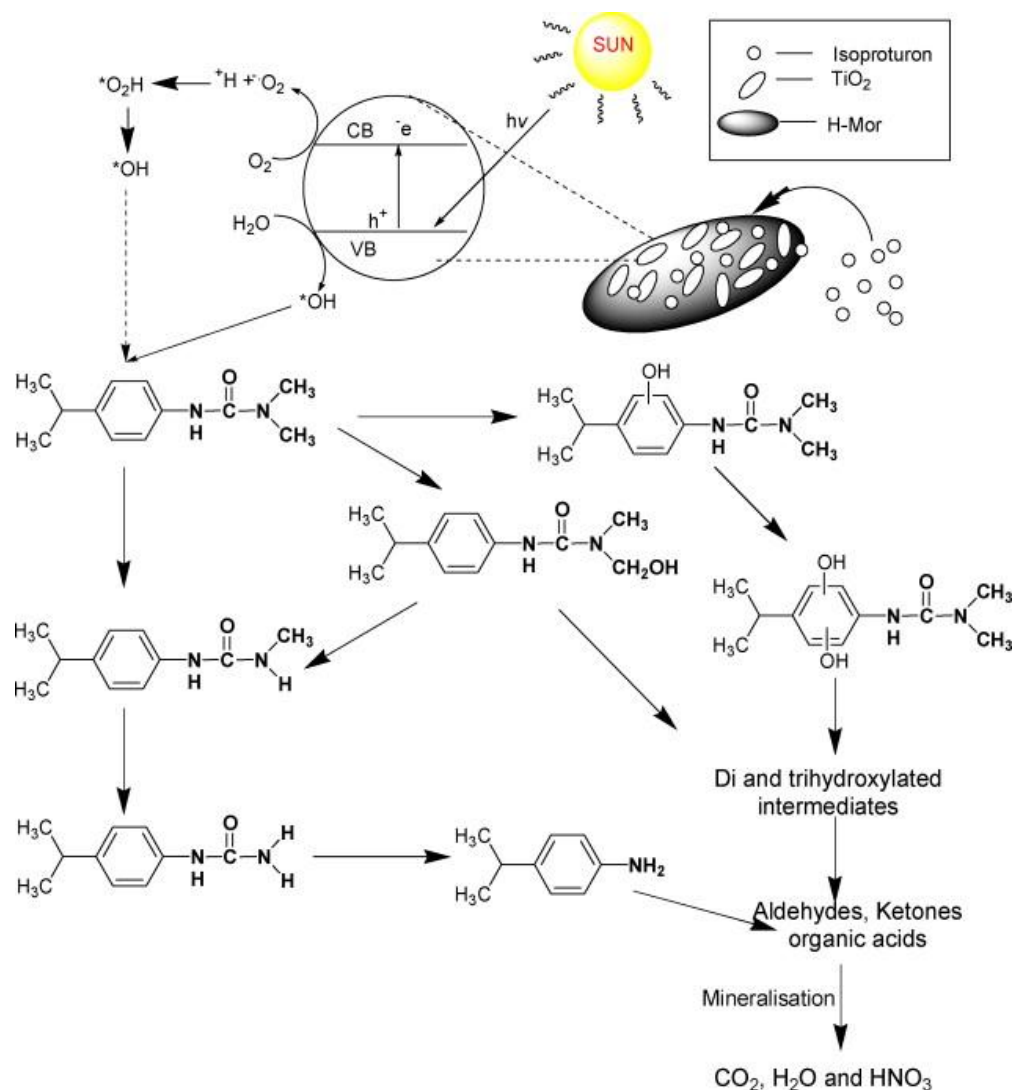


Figure 2.2 Degradation pathway of isoproturon in water (Benitez *et al.*, 2006)

In the case of simazine and propazine, there are two triazine metabolites, DEA and DIA, which were found to occur in water derived from parent triazine herbicides. DEA is derived from propazine and atrazine whereas DIA originated from atrazine and cyanazine. Trace amounts of DIA are contributed by simazine (Scribner *et al.*, 2000).

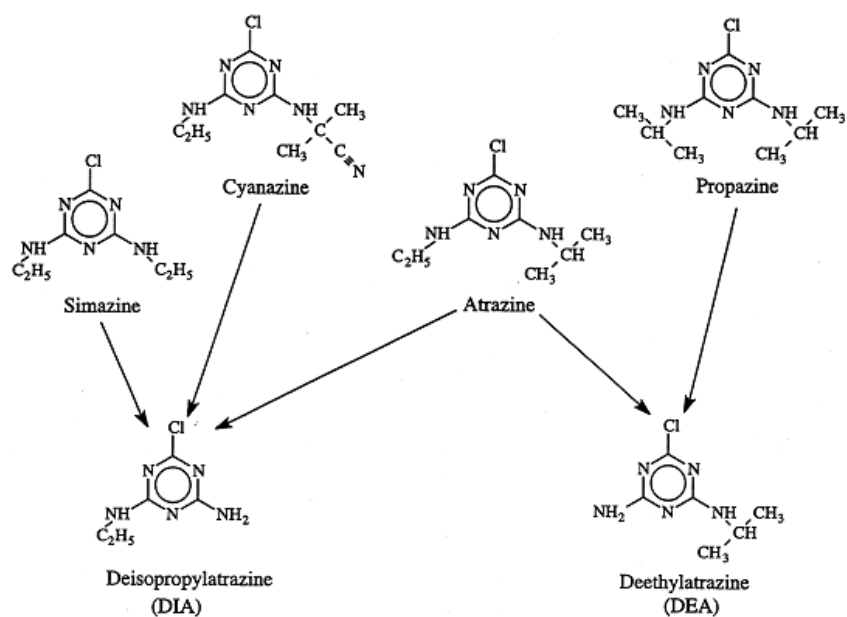


Figure 2.3 Degradation pathway of simazine, cyanazine, atrazine and propazine in water (Scribner et al., 2000)

Chemical name	Acronym
6-Amino-2-chloro-4-ethylamino-1,3,5-triazine	ACET
2-Chloro-4,6-diamino-1,3,5-triazine	CAAT
4,6-Diethylamino-2-hydroxy-1,3,5-triazine	EEOT
6-Amino-4-ethylamino-2-hydroxy-1,3,5-triazine	AEOT
2-Hydroxy-4,6-diamino-1,3,5-triazine (ammeline)	OAAT
2,4-Dihydroxy-6-amino-1,3,5-triazine (ammelide)	OOAT
2,4,6-Trihydroxy-1,3,5-triazine (cyanuric acid)	OOOT

Table 2.2 *main intermediates produced in the photocatalytic reaction of simazine (Lopez-Munoz et al., 2011)*

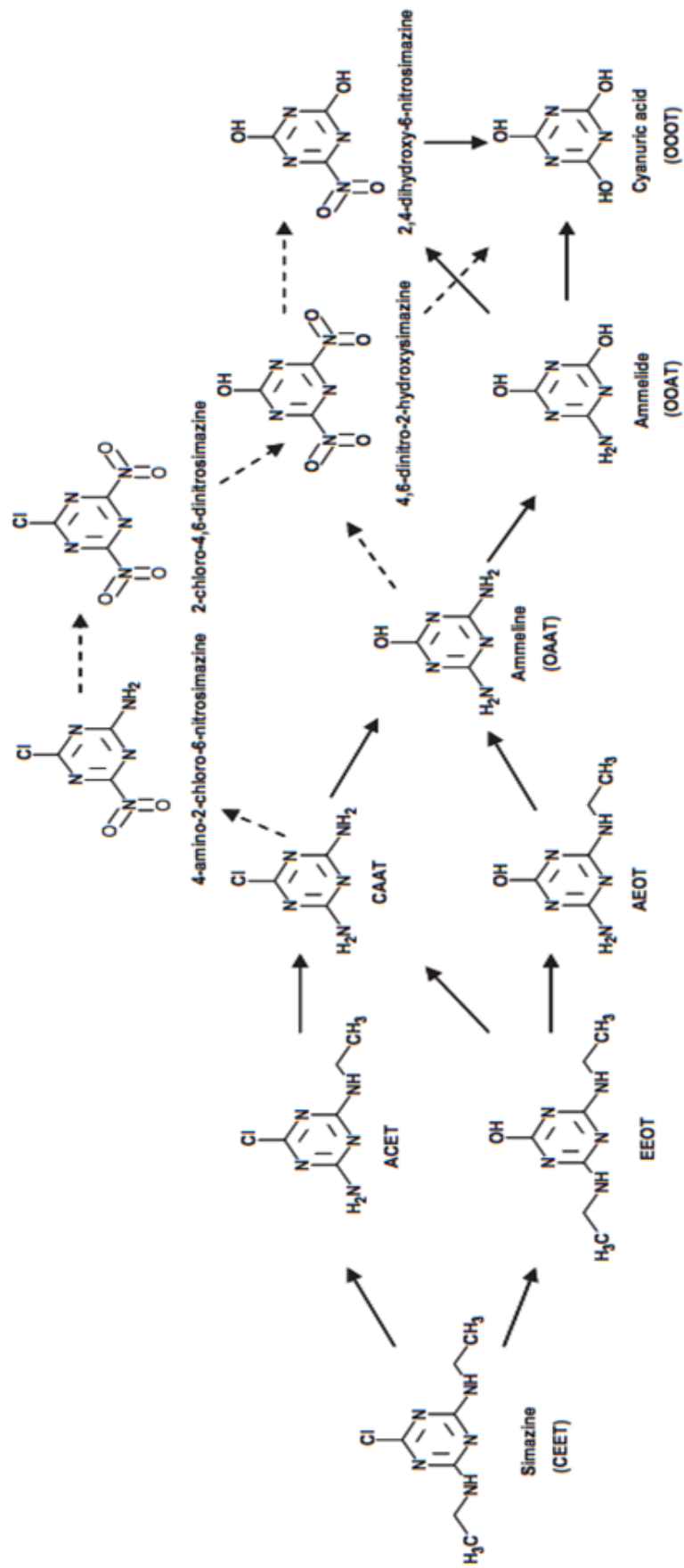


Figure 2.4 Scheme of proposed pathway for simazine photocatalytic degradation (Lopez-Munoz et al., 2011)

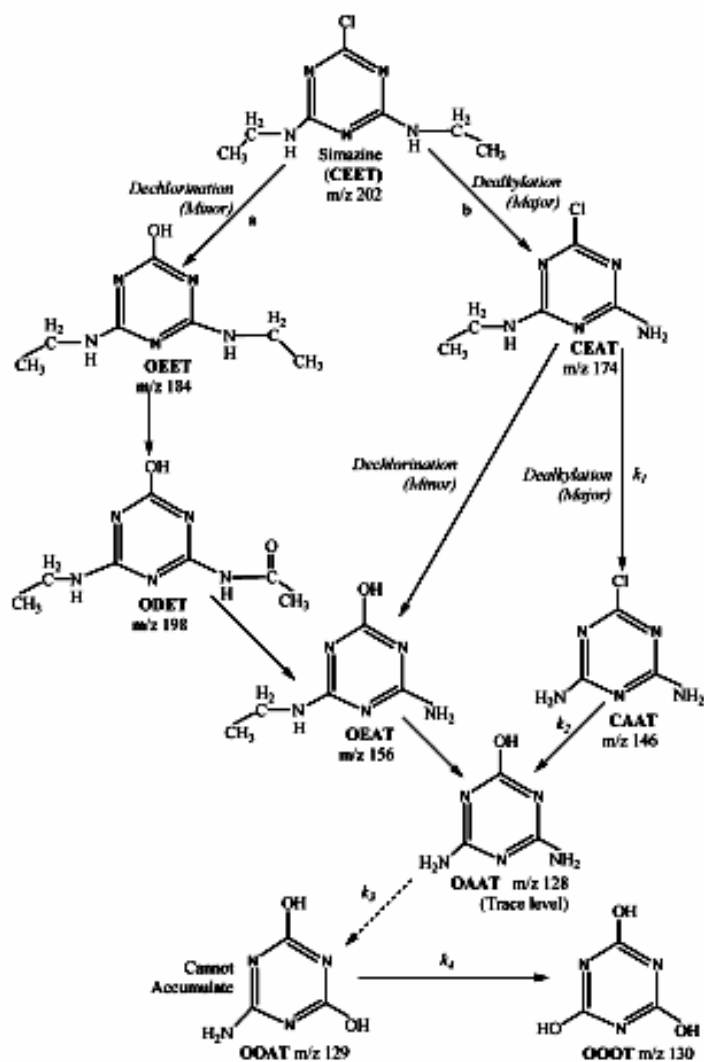


Figure 2.5 Proposed degradation pathway of simazine in UV/TiO₂ system. The dashed arrow indicates a possible pathway (Chu et al., 2009)

However, in 2009, Chu and co-workers proposed another photocatalytic degradation pathway which is different from that suggested by Lopez-Munoz and colleagues. However, the same final products, cyanuric acid (OOOT) and ammeline, were achieved which had a lower toxicity (Chu *et al.*, 2009).

The photodegradation pathway of propazine is shown in Figure 2.6 by Barcelo and co-workers (1993) The main photodegradation pathways correspond to dealkylation, hydroxylation and dehalogenation with the formation of deisopropylpropazine (deethyltriazine) (compound 2 in Figure 2.6), and hydroxypropazine (compound 4 in Figure 2.6). The final product is a hydroxyl-s-triazazine, compound 1.

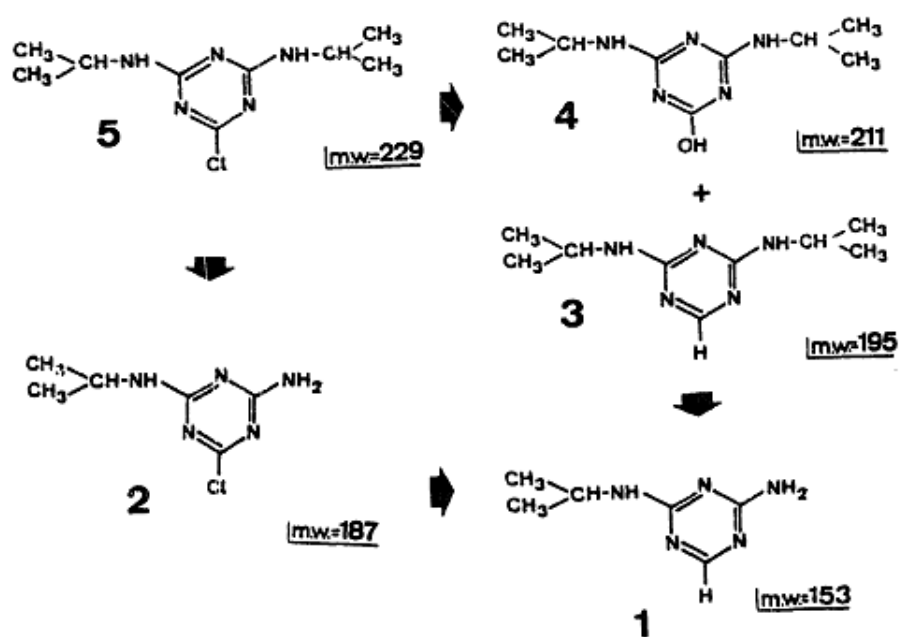


Figure 2.6 Tentative photodegradation pathway of propazine (compound 5, molecular weight = 229) in water containing 4% of methanol (Barcelo *et al.*, 1993)

2.10 The toxicity assessment of isoproturon, simazine and propazine

In 2011, Lopez-Munoz and co-workers analysed the toxicity of simazine and atrazine by withdrawing the samples along TiO₂ photocatalytic reactions and monitoring the changes in the natural emission of the luminescence bacteria *Vibrio fischeri*. The results are shown in Figure 2.7 which displays the percentage of the inhibition of the bacteria as a function of the irradiation time for atrazine and simazine degradation. After 15 min, the toxicity of atrazine was 82% and reached 31% at the end of inhibition; whereas, simazine was 73% and finally reduced to 46%. In case of ammeline, which is one of the intermediates of simazine degradation, the toxicity was reduced from 42% to 27%. However, the toxicity of ammelide, which lastly changed to cyanuric acid, significantly decreased from 33% to 1%.

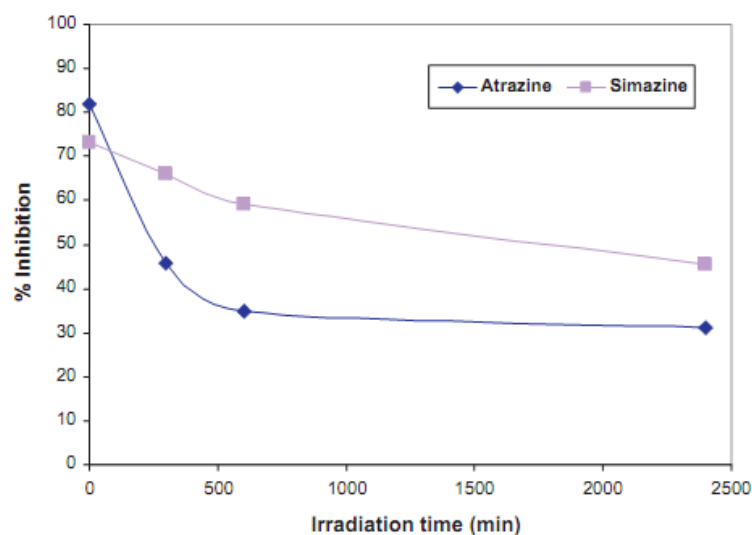


Figure 2.7 Results of toxicity in the triazine samples at condition simazine pH = 5.5, TiO₂ concentration = 0.25g/l, atrazine pH = 6, TiO₂ concentration = 1.8 g/l, immersion well photoreactor (Lopez-Munoz et al., 2011).

For isoproturon, the detoxification by the bacteria *Vibrio fischeri* was carried out by Hincapie and colleagues. They found that percentage inhibition of isoproturon decreased from 95 % to 60 % in first 50 min and reached 5 % at the end of TiO₂ photocatalytic degradation (300 min) (Hincapie *et al.*, 2005).

In the case of propazine, the *E. coli* bacterial biosensor was used to determine toxicity during the photocatalytic degradation, due to a higher sensitivity to the target pesticide than *Vibrio fischeri* (Strachan *et al.*, 2001). Strachan and co-workers recorded that the toxicity of propazine decreased to about half of the initial value at the end of the degradation. Their results showed the similar trend to that seen by Miquel *et al.*, 2012 which also occurred in the case of the TiO₂ photocatalytic degradation of other pesticides, including melamine and parathion (Kim *et al.*, 2006; Bozzi *et al.*, 2004).

2.11 Factors affecting the photocatalytic kinetics

Many researchers have studied the degradation kinetics under different conditions such as catalyst concentration, pH, substrate concentration, different types of TiO₂, light wavelength, light intensity, temperature, presence of electron acceptor such as H₂O₂, KBrO₃, (NH₄)₂S₂O₈ and operation mode of the photoreactor (Haque and Muneer, 2003; Rahman *et al.*, 2005; Shifu and Yunzhang, 2007; Qamar *et al.*, 2006; Qamar and Muneer, 2005; Muneer *et al.*, 2005; Singh *et al.*, 2007; Qamar and Muneer, 2009; Kaneco, 2009; Sojic *et al.*, 2009; Han *et al.*, 2009).

2.11.11 Crystal phase

Titanium dioxide has three different crystalline forms, depending on the synthesis method. The most common forms are the anatase and the rutile. In both forms, titanium (Ti^{4+}) atoms form TiO_6 octahedra by co-ordinating with six oxygen (O^{2-}) atoms. Figure 2.7 (a) shows the structure of the anatase forming (001) planes in a tetragonal structure by the corner (vertice) sharing octahedral. However, in the rutile phase, the octahedra shares edges at (001) planes to give a tetragonal structure, as seen in Figure 2.8 (b) (Pelaez *et al.*, 2012). Anatase is the most stable form by 8-12 KJ mol^{-1} and can be converted to the rutile by heating to 700 °C. The density of the rutile phase is greater at 4.26 g/ml, while anatase titania has a density of 3.9 g/ml (Radwan, 2005). Anatase has been reported to be more active as a photocatalyst than rutile (Hurum *et al.*, 2003; Qourzal *et al.*, 2008; Radwan, 2005; Pelaez *et al.*, 2012; Ahmed *et al.*, 2011).

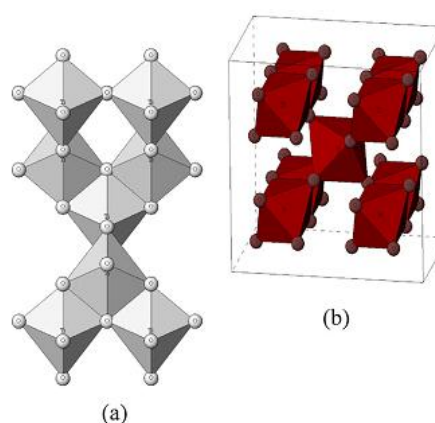


Figure 2.8 Crystalline structures of titanium dioxide (a) anatase, (b) rutile (Pelaez *et al.*, 2012)

There are 3 main types of commercial TiO₂ used in the literature: Degussa P-25 TiO₂, Millenium PC-500, and Hombikat UV-100 TiO₂. Hombikat UV-100 TiO₂ consists of the pure anatase modification. The majority of investigations have been performed using Degussa P-25 TiO₂. The efficiency of photocatalysts is shown to follow the order: P-25 > UV-100 > PC-500 for the degradation of pesticides derivatives, as shown in Table 2.3 (Bhatkhande *et al.*, 2001; Singh *et al.*, 2003; Singh *et al.*, 2007; Singh and Muneer 2004; Rahman and Muneer, 2005; Qamar and Muneer, 2005; Qourzal *et al.*, 2008; Qamar and Muneer., 2009; Singh *et al.*, 2007; Muneer *et al.*, 2005; Rafqah *et al.*, 2005). One of the examples related to the influence of TiO₂ types is shown in Table 2.3 which was the photocatalytic degradation of bromacil (Singh *et al.*, 2003). The commercial Degussa P-25 is composed of 75% anatase and 25% rutile (Singh and Muneer 2004; Singh *et al.*, 2007; Ahmed *et al.*, 2011). It has a BET surface area of 50 m² g⁻¹ and the diameters of its particles are between 20-30 nm. Hombikat UV-100 consists of 100% pure and smaller anatase with a BET surface area 186 m²g⁻¹ and particle size of 5 nm. In case of PC-500, it has a BET surface area 287 m²g⁻¹ with 100% anatase and particle size of 5-10 nm (Ahmed *et al.*, 2011). However, the difference in the photocatalytic activity also depends on a BET surface, the lattice mismatches, or the density of the hydroxyl groups on the catalysts surface. There are three reasons why the photoactivity of Degussa P-25 has been reported to be the superior: (1) The smaller band gap of the rutile extends the useful range of the photoactivity into the visible region. Then the electron transfer from the rutile

(conduction band) to the electron traps, in the anatase phase, takes place. (2) The recombination is inhibited by the stabilisation of the charge separation by the electron transfer from the rutile to the anatase. (3) The small size of the rutile crystallites facilitates this transfer, making the catalytic hot spots at the rutile/anatase interface. (Qourzal *et al.*, 2008; Hurum *et al.*, 2003).

Catalyst (1 g litre ⁻¹)	Rate/10 ⁻⁶ M min ⁻¹
P-25	1.116
UV-100	1.094
PC-500	0.755

Table 2.3 Photocatalytic degradation of bromacil in an aqueous suspensions under the different types of TiO₂ (Singh *et al.*, 2003)

In 2008, Yeredla and Xu investigated the nanostructured rutile and anatase plates with a view to improve the photo splitting of the water. They discovered the different photocatalytic performance of acetaldehyde decomposition due to the different phases: among mixed-phase P-25, anatase and rutile alone (Yeredla and Xu, 2008). As shown in Figure 2.9, Degussa P-25 TiO₂ and pure anatase show a very high activity for the photo-oxidation of acetaldehyde. In contrast, the rutile phase shows a moderate activity which is much less when compared to the anatase phase.

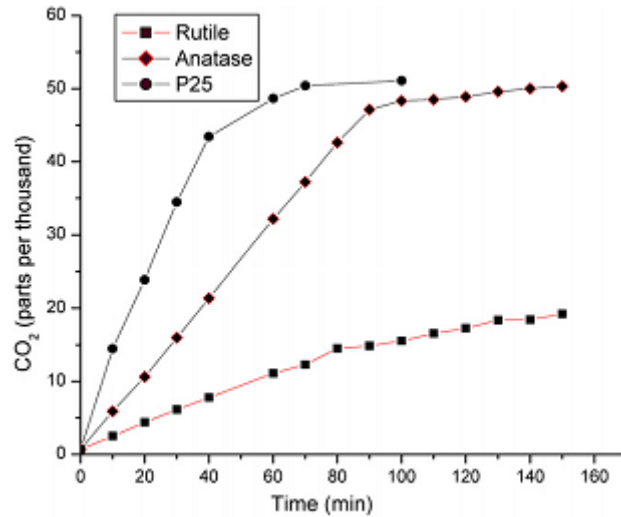


Figure 2.9 Photocatalytic oxidation of acetaldehyde with Degussa P-25 TiO₂, nanostructured anatase and rutile (Yeredla and Xu, 2008)

There was a theory that each TiO₂ phase has different rates of oxidation of H₂O molecules as an electron donor (electron transfer rate from H₂O to the holes on TiO₂ surface) and the reduction of molecular oxygen as an electron acceptor (electron transfer rate from TiO₂ surface to the molecular O₂) (Sato and Taya, 2006). The quantum yield for the generation of hydroxyl radicals in the anatase phase is limited by the oxidation reaction, whereas the rutile is limited by the reduction reaction to keep the electro-neutrality, as shown in Fig. 2.10 (a) and (b). However, in the case of the coexistence of both types of TiO₂, the close contact of the anatase and the rutile enables an exchange of the photo-excited electrons and the holes between the particles, leading to the balance in the acceleration of the oxidation and the reduction rates (Fig. 2.10 (c)).

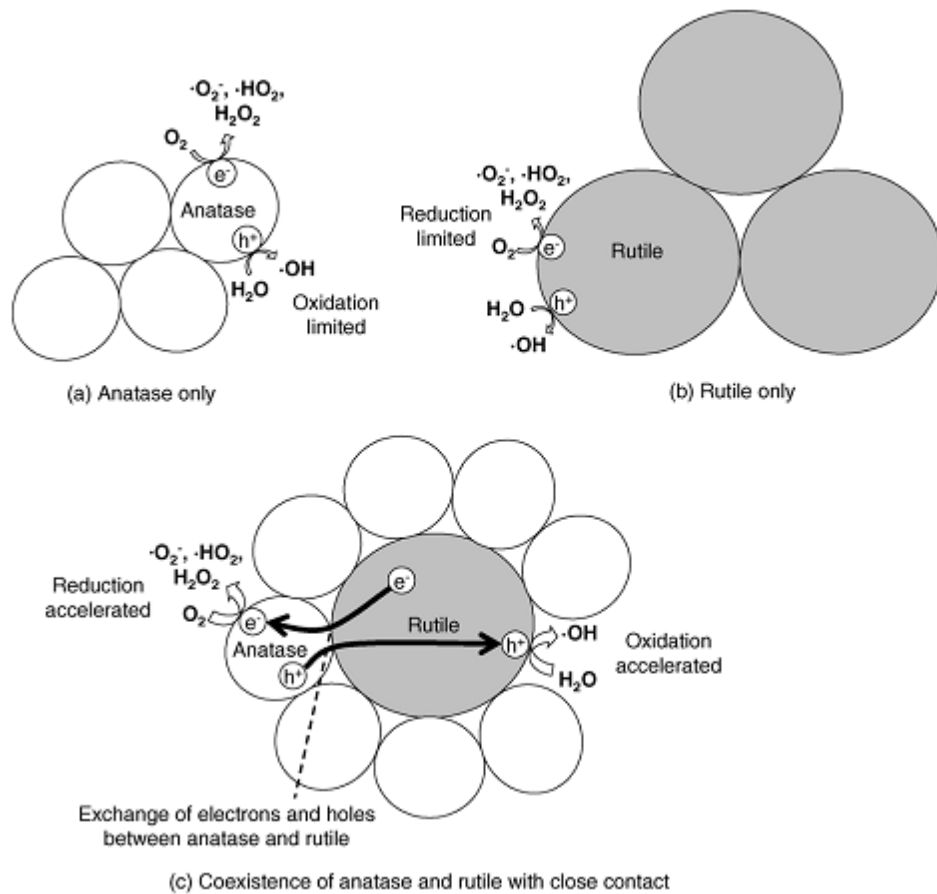


Figure 2.10 Possible mechanisms for enhancement of photocatalytic activity caused by contact between (a) anatase TiO_2 (b) rutile TiO_2 and (C) coexistence of anatase and rutile TiO_2 (Sato and Taya, 2006)

2.11.12 Organic pollutant concentration

The initial rate of the disappearance of the pollutant fits Langmuir-Hinshelwood (L-H) kinetics, which is the most commonly used kinetic expression to explain the kinetics of the heterogeneous catalytic processes. The Langmuir-Hinshelwood expression was given by Hoffmann *et al.*, 1995:

$$r_i = -d[C]_i/dt = \frac{k K[C]_i}{1 + K[C]_i} \quad (2.16)$$

The term r_i is represented in terms of the initial reaction rate of the disappearance of the pollutant. $[C]_i$ is the initial concentration of the pollutant C, K represent the Langmuir adsorption constant of the species C on the surface of TiO₂ and k is the proportional constant which provides a measure of the intrinsic reactivity of the photoactivated surface with the pollutant C.

The competition of a variety of pollutants was modelled as follows:

$$-r_j = \frac{k_j K_j C_j}{1 + \sum_{j=1}^n K_j C_{0j}} \quad \text{with } j = 1, 2, \dots, n \quad (2.17)$$

Where k_j (mol L⁻¹ s⁻¹) and K_j (L/mol) are the reaction kinetic constant and the binding constant of pollutant j respectively, C_j (L mol⁻¹) is the concentration of the pollutant in solution C_{0j} (L mol⁻¹) where the concentration of the pollutants at the initial time or in the reactor feed and n is the number of the pollutants in the solution (Li Puma *et al.*, 2007).

Note that the denominator in Equation (2.17) takes into account the effect of the Intermediate reaction products, since it assumes a stepwise reaction scheme with identical binding constants of the intermediates and the pollutant such that:

$$K_j C_j + (\sum K_i C_i) = K_j C_{0j} \quad (2.18)$$

where K_i ($L \text{ mol}^{-1}$) is the binding constant of the intermediate product adsorbed onto the surface of TiO_2 and C_i is the concentration of the intermediate in the solution (Li Puma *et al.*, 2007).

Many researchers have shown that, with an increase in the initial pollutant concentrations, the photocatalytic removal conversion of the pesticides decreases correspondingly. This is shown in Figure 2.11 (Gora *et al.*, 2006) and in Table 2.4 (Qamar and Muneer, 2005). The presumed reason is that when the pollutant concentration increases, the amount of the pesticide molecules adsorbed on the surface of TiO_2 also increases. The large amount of the adsorbed pesticide is thought to have an inhibiting effect on the reaction with the photogenerated holes or the hydroxyl radicals, due to the lack of the direct contact between them. Once the concentration of the pesticide reaches a critical level, the pesticide molecules adsorb all the light and the photons never reach the photocatalyst surface.

Moreover, increasing the initial concentration of pollutants results in higher concentrations of the intermediates, which adsorb on the surface of the catalyst. This, in turn, leads to a deactivation of the active sites of the photocatalyst. (Carp *et al.*, 2004; Pourata *et al.*, 2009; Garcia *et al.*, 2003; Rahmann and Muneer, 2005; Haque and Muneer, 2003; Qamar *et al.*, 2006; Singh *et al.*, 2007; Muneer *et al.*, 2005; Sojic *et al.*, 2009; Sharma *et al.*, 2008; Qamar and Muneer, 2009; Kaneco *et al.*, 2009; Han *et al.*, 2009).

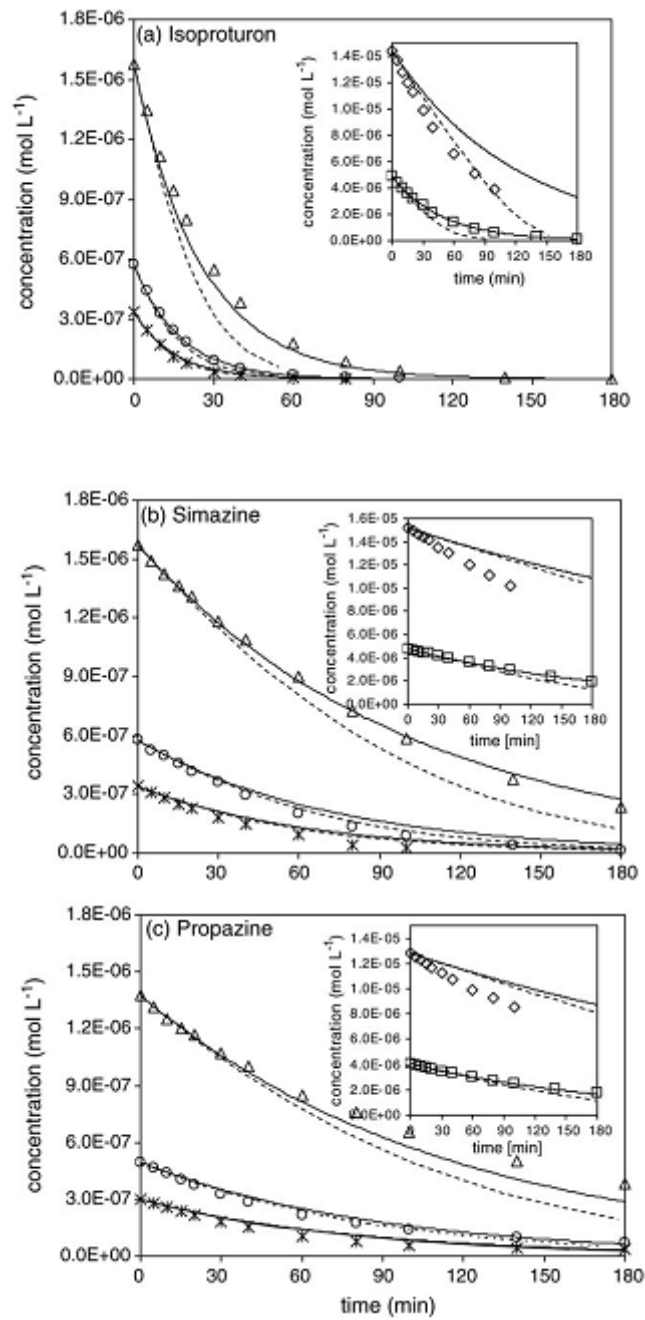


Figure 2.11 Initial rate of reaction calculated by L-H kinetics as a function of the initial concentration of isoproturon, simazine, and propazine. Symbols are experimental data at different initial herbicide concentrations. Solid lines are Langmuir–Hinshelwood model fitting (Gora et al., 2006)

IAA concentration (mM)	Degradation rate (10^{-3} mol/l min ⁻¹)
0.20	0.01260
0.30	0.01773
0.40	0.01361
0.60	0.00562

Table 2.4 Degradation rate of indole-3-acetic acid (IAA) in Degussa P-25 TiO₂ suspension at different indole-3-acetic acid (IAA) concentrations (Qamar and Muneer, 2005)

2.11.3 TiO₂ concentration

In any reactor system, the photocatalytic removal rate is found to be directly proportional to the photocatalyst concentration. However, when it reaches an optimum value, the efficiency decreases (Carp *et al.*, 2004; Konstantinou and Albanis, 2004; Cao *et al.*, 2005; Akpan and Hameed, 2009; Chong *et al.*, 2010). In slurry photoreactors, the optimal catalyst dosage reported lies in a wide range (from 0.15 to 8 g litre⁻¹) for different photoreactors (Carp *et al.*, 2004). The optimum concentration values for each reactor depends on the geometry of the reactor and working conditions where the surface reaction is initiated upon light photon absorption. This is because the light photon absorption coefficient decreases radially and light scattering increases (Chong *et al.*, 2010). At the high TiO₂ concentration, the excess TiO₂ particles start to agglomerate, so reducing surface area for the light absorption which leads to a drop in photocatalysis efficiency. Many studies revealed the non-uniformity of light intensity as a result of increased catalyst loadings beyond the optimum amount. (Wu *et al.*, 2010; Wu *et al.*, 2009; Pourata *et al.*, 2009; Chen and Liu,

2007; Qamar *et al.*, 2006; Sojic *et al.*, 2009; Sharma *et al.*, 2008; Qamar and Muneer, 2009; Kaneco *et al.*, 2009; Han *et al.*, 2009; Lu *et al.*, 2009).

In the research of Haque and colleagues (Haque, 2003), the optimum concentration of TiO₂ for isoproturon photocatalytic degradation using immersion well photoreactor was found to be 2 g litre⁻¹ as shown in Figure 2.12. The degradation rates scarcely increased beyond 2 g litre⁻¹.

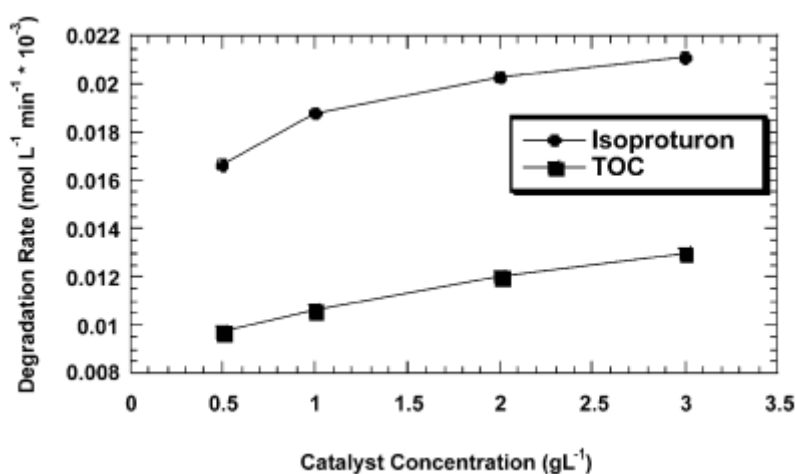


Figure 2.12 Influence of catalyst concentration on the photocatalytic degradation rate of isoproturon at UV=238 nm, 0.5 mM isoproturon, 250 ml, and P-25 (0.5, 1, 2 and 3 g litre⁻¹) (Haque *et al.*, 2003)

In 2004, Li Puma *et al.*, (2004) used the model simulation to validate the effect of TiO₂ concentration on the photocatalytic degradation of isoproturon in an annular photoreactor, as shown in Figure 2.13. They concluded that the optimum concentration of Degussa P-25 TiO₂ in an annular photoreactor was 0.4 kg m⁻³. Increasing the concentration beyond this value led to a decrease in the degradation rate.

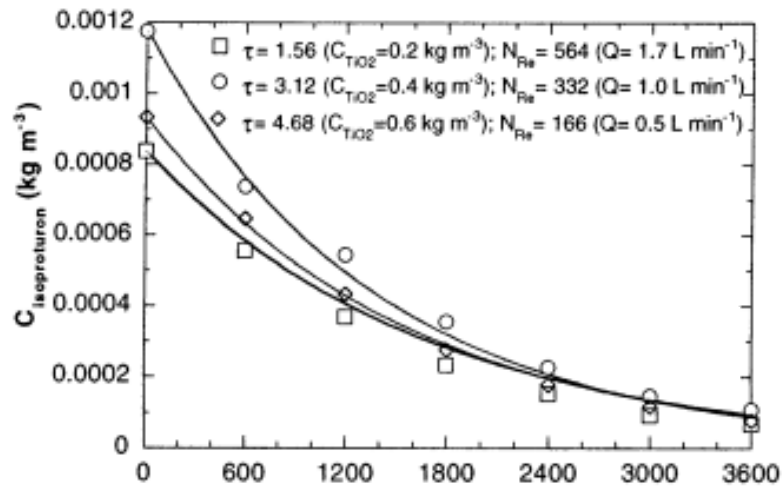


Figure 2.13 Effect of catalyst loading at $\text{pH} = 7$, radiation intensity = 185.2 W/m^2 , C_{TiO_2} = TiO_2 concentration (kg m^{-3}), τ = optical thickness, dimensionless, N_{Re} = Reynolds number, Q = volumetric flowrate ($\text{m}^3 \text{ s}^{-1}$) (Li Puma et al., 2004)

From Figure 2.14, the study of the photocatalytic degradation of glyphosate by TiO_2 was carried out in an annular photoreactor by Chen and Liu in 2007 (Chen and Liu, 2007). Their results showed that a further increase of the most favourable catalyst concentration equalled 6.0 g litre^{-1} since it led to a slight decrease in the degradation efficiency when the TiO_2 concentration exceeded that value. Results from 2009 showed a similar trend (Figure 2.15). As the concentration of TiO_2 increased from 2.0 to $12.0 \text{ g litre}^{-1}$, the photodegradation efficiency of methamidophos increased rapidly from 16.6% to 75.1% . Then, the efficiency slightly decreased when the amount of TiO_2 was above $12.0 \text{ g litre}^{-1}$.

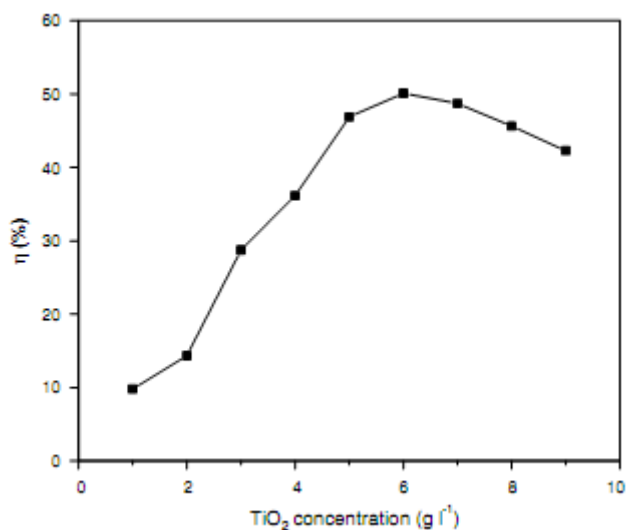


Figure 2.14 Effect of TiO₂ concentration on the photodegradation efficiency of glyphosate, $t = 1.0$ hr (Chen and Liu, 2007)

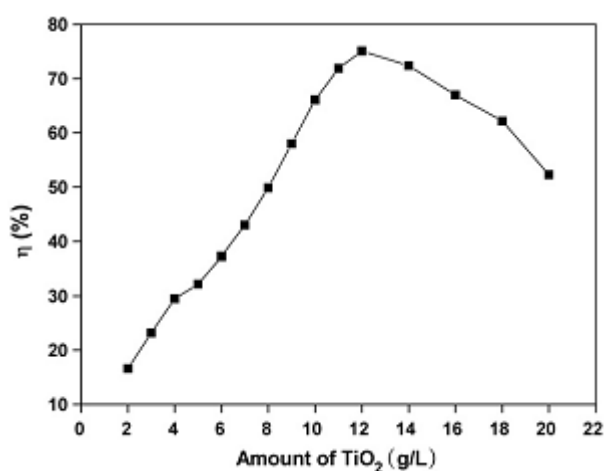


Figure 2.15 Effect of the amount of TiO₂ on the photodegradation efficiency of methamidophos, annular photoreactor, 375 W medium pressure mercury lamp, reaction temperature = 30 °C, illumination time = 30 min (Wei et al., 2009)

Table 2.5 shows the results from Muneer and co-workers who studied the photocatalysed reaction of tebuthiuron in an aqueous suspension of Degussa

P-25 TiO₂ in an immersion well photoreactor. The optimum TiO₂ concentration for tebuthiuron degradation was 5 g litre⁻¹, as shown in the table below (Muneer *et al.*, 2005).

TiO ₂ concentration (g litre ⁻¹)	Degradation rate (M min ⁻¹ x 10 ⁻³)
0.5	0.0085
1	0.0120
2	0.0140
5	0.0185
7.5	0.0180

Table 2.5 Photocatalytic degradation of tebuthiuron at different Degussa P-25 TiO₂ concentration (Muneer *et. al*, 2005)

2.11.4 O₂ initial concentration

The presence of oxygen assures the presence of sufficient electron scavengers, acts as an electron sink by trapping the excited conduction-band electron from the recombination, and enhances the decomposition of the organic compounds (Devipriya and Yesodharan, 2005; Chong *et al.*, 2009; Malato *et al.*, 2009; Chong *et al.*, 2010). The main role of the oxygen present during the reaction stage is to support the formation of the hydroxyl radicals and stabilise the intermediates. In 2001, Axelsson and Dunne studied the effect of the dissolved molecular oxygen on the mechanism of the photocatalytic oxidation of 3,4-dichlorophenol. They concluded that when it is

present, a simple hydroxyl addition to the dichlorophenol occurred (Axelsson and Dunne, 2001). Moreover, for a photoreactor, the delivered O₂ provides sufficient buoyancy force for the complete suspension of the TiO₂ particles. A linear dependence between the hydroxyl radical formation on TiO₂ and oxygen concentration was proven for 2-chlorobiphenyl, with an increase in degradation from 16% to 94% when the oxygen concentration increased from 0.5 to 186 kPa (Carp *et al.*, 2004). As illustrated in Figure 2.16, experimental results from Qamar and Muneer, investigating vanillin photocatalytic kinetics in an immersion well photoreactor, indicated that the degradation of vanillin was much higher in the presence of molecular oxygen in all types of photocatalysts (UV-100, ZnO and Degussa P-25) (Qamar and Muneer, 2009).

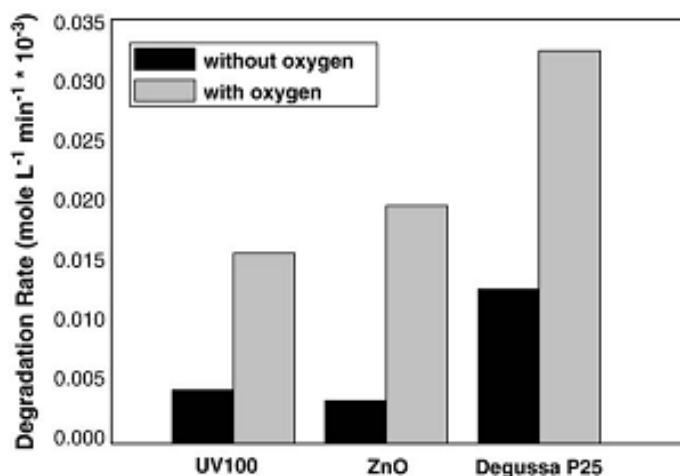


Figure 2.16 Effect of added molecular oxygen on the degradation rate of vanillin in the presence of Degussa P-25, UV-100 and ZnO. Experimental conditions: substrate concentration (0.5 mM), V = 250 mL, pH = 2 for TiO₂ samples and pH = 6 for ZnO, Degussa P-25, UV-100 and ZnO = 1g litre⁻¹, immersion well photoreactor, 125 W medium pressure Hg lamp, irradiation time = 45 min (Qamar and Muneer, 2009)

For the liquid phase reactions, the study of pressure and the influence of oxygen on degradation rates is difficult because the reaction is polyphasic. Therefore, it is generally assumed that the oxygen adsorbs TiO₂ from the liquid phase, following Henry's law. When the oxygen is continuously supplied, it can be assumed that the apparent integrated rate of its coverage at the surface of TiO₂ is as follows (Herrmann, 1999):



$$r_A = \frac{-d[A]}{dt} = k \Theta_A \Theta_{O_2} = k_{app} \Theta_A \quad (2.20)$$

Actually, the apparent rate constant is a function of the power flux (expressed in mW cm⁻²) and oxygen coverage.

2.11.5 pH

The effect of pH on the photocatalytic reaction is generally attributed to the surface charge of the photocatalyst and its relation to the ionic form of the organic compound (anionic or cationic). The point of zero charge (PZC) of TiO₂ is 6.25 (Saber *et al.*, 2011). At a pH value lower than 6.25 the catalyst

surface is positively charged and the positive holes are considered as major oxidation steps; whereas at higher pH values the catalyst surface is negatively charged and hydroxyl radicals are considered as the predominant species. Electrostatic attraction or repulsion between the catalyst's surface and the organic molecules are taking place, depending on the ionic form of the organic compound (anionic or cationic) and enhancing or inhibiting the photodegradation efficiency, respectively (Wu *et al.*, 2010; Wu *et al.*, 2009; Garcia *et al.*, 2003; Rahmann and Muneer, 2005; Haque and Muneer, 2003; Chen and Liu, 2007; Qamar and Muneer, 2005; Muneer *et al.*, 2005; Singh *et al.*, 2007; Sojic *et al.*, 2009; Sharma *et al.*, 2008; Qamar and Muneer, 2009; Kaneco *et al.*, 2009; Mahmoodi *et al.*, 2008). In the case of vanillin (Figure 2.18) (Qamar and Muneer, 2009), the degradation rate decreased with increasing pH. However, the photocatalytic degradation of trichlorfon preferred an alkaline condition, as shown in Figure 2.17 (Wei *et al.*, 2009). In the case of isoproturon and carbofuran, the optimum pH was 7, which is slightly higher than neutral pH, as shown in Table 2.6 (Sharma *et al.*, 2009; Saber *et al.*, 2011).

The ionisation state of the surface of the photocatalyst can be protonated and deprotonated under acidic and alkaline conditions respectively, as shown in the following equations (Malato *et al.*, 2009; Lu *et al.*, 2009):



Pollutant	Photocatalyst	optimum pH
Atrazine	TiO ₂	4-5
Diazinon	TiO ₂	5.2
Phorate	TiO ₂	8
Propachlor	TiO ₂	3
Dimethoate	TiO ₂	11.05
Isoproturon	TiO ₂	7
Turbophos	TiO ₂	8
Thiram	TiO ₂	8
Carbofuran	TiO ₂	7
Carbendazim	TiO ₂	9

Table 2.6 Influence of pH on the photocatalytic degradation of various pollutants (Saber et al., 2011; Sharma et al., 2009; Wu et al., 2009)

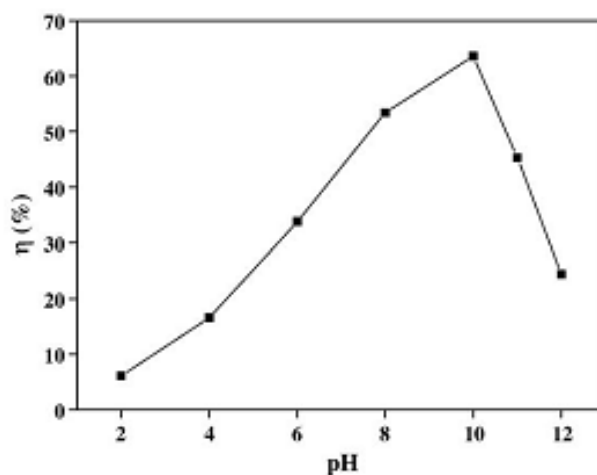


Figure 2.17 Effect of initial pH value on the photodegradation efficiency of trichlorfon using TiO_2 , annular photoreactor, 375 W medium pressure mercury lamp, illumination time = 30 min (Wei et al., 2009)

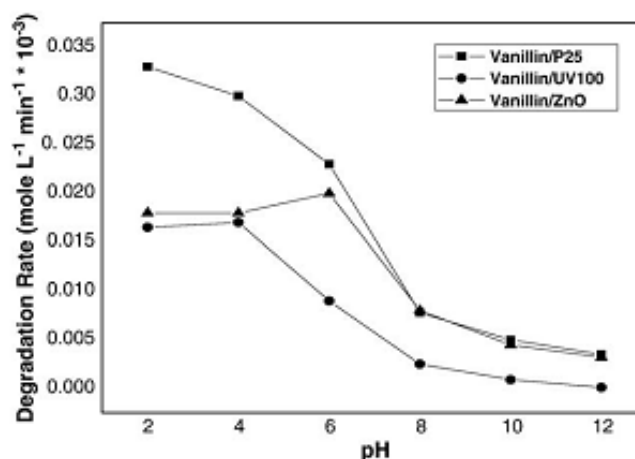


Figure 2.18 Influence of pH on the degradation rate of vanillin using Degussa P-25, UV-100 and ZnO = 1g/l. experimental conditions: substrate concentration (0.5 mM), V = 250 mL, immersion well photo-reactor, 125 W medium pressure Hg lamp, pH range (2, 4, 6, 8, 10 and 12), continuous O_2 purging and stirring, irradiation time = 45 min (Qamar and Muneer, 2009)

Adding anions or cations to increase or decrease pH has an effect on photocatalytic degradation rates. With industrial effluents, anions such as chloride, carbonate, and bicarbonate are commonly found. These ions have a significant effect on the adsorption of the degradation species; they decrease the rate by reaction with the hydroxyl radicals and absorption of UV light, especially chlorides. In Figure 2.19, Mahmoodi and coworkers studied the effect of the chloride, sulphates and nitrate ions on the photocatalytic degradation of Butachlor. Sulphate and nitrate also decrease the reaction rate

but have a smaller effect on the photo-oxidation (Mahmoodi *et al.*, 2007). However, in case of cations, conflicting results have been reported by many researchers (Bhatkhande *et al.*, 2001).

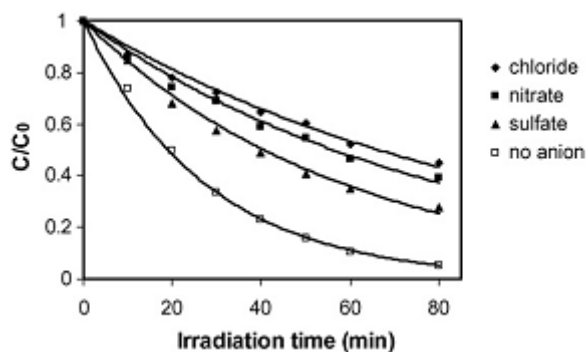


Figure 2.19 Effect of anions on the photocatalytic degradation rate constants of Butachlor (Mahmoodi *et al.*, 2007)

2.11.6 Reaction temperature

It is well known that the photocatalytic oxidation rate is not dependent on temperature. However, some researchers found that an increase of the photocatalytic reaction temperature (> 80 °C) promotes the recombination of the charge carriers and desorption of the organic compounds on the TiO₂ surface (Chong *et al.*, 2010). On the contrary, at temperatures below 80 °C, the adsorption mechanism is actually favorable. Consequently, the optimum reaction temperature for photocatalysis is reported to be in the range of 20-80 °C. In 2005, Cao and co-workers found that temperature had a slight effect on the degradation of chlorfenapyr, as shown in Figure 2.20.

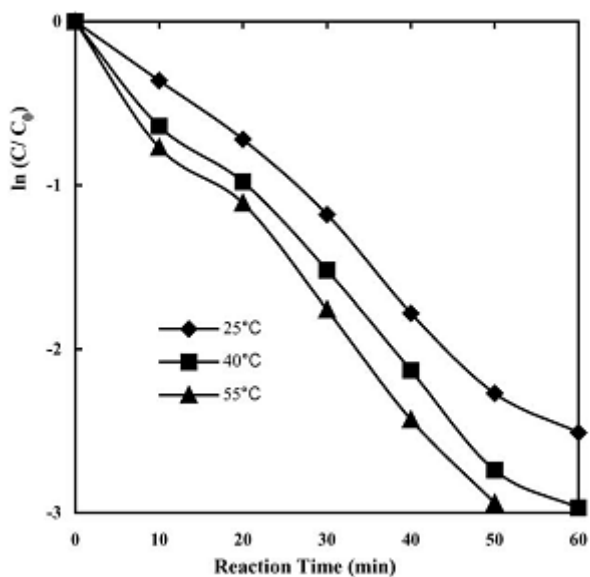


Figure 2.20 Comparison of the photocatalytic degradation of chlorfenapyr at 300 nm of UV at different temperature. The initial concentrations of chlorfenapyr and $TiO_2 = 800 \text{ mg litre}^{-1}$, $pH = 6$ (Cao *et al.*, 2005)

2.11.7 Irradiation wavelength

The different wavelength of an irradiation source has a profound effect on the photocatalytic reaction rate (Legrinl *et al.*, 1993). This discovery depends on the crystalline phase of photocatalyst, for example, anatase or rutile phase, elemental composition and photocatalyst doping. In the case of Degussa P-25 TiO_2 , which has a crystalline ratio of the anatase 75: 25, a light at wavelength lower than 380 nm is sufficient for photoactivation. The rutile TiO_2 has a smaller bandgap energy compared to the anatase TiO_2 . This dictates that rutile TiO_2 can be activated with a light wavelength up to 400 nm. For UV irradiation, it can be classified as UV-A, UV-B and UV-C, according to its emitting wavelength. The UVA wavelength ranges from 315 to 400 nm (3.10-3.94 eV), while UVB has a wavelength range from 280 to 315 nm (3.94-4.43

eV) and germicidal UVC ranges from 100 to 280 nm (4.43- 12.4 eV). There have been many studies that state that shorter wavelength radiations (254 nm) are considerably more effective for photocatalytic degradation, where the optimum rate can occur with a less catalyst than would be required at a higher wavelength (Bhatkhande *et al.*, 2001). The energy of a photon is related to its wavelength. The wavelength is inversely proportional to the energy; the higher the energy, the shorter the wavelength. The lower the energy the longer the wavelength, as explained in Planck's equation by the relationship between the wavelength and the energy of a photon (Equation (2.23)).

$$\text{The energy of photon} = E = h c / \lambda \quad (2.23)$$

Where λ is the wavelength of the light,

h is Planck's constant = 6.626×10^{-34} joule·s

c is the speed of light = 2.998×10^8 m/s

2.11.8 Light intensity

The rate of the photocatalytic reaction is strongly dependent on the intensity of the irradiation source. In order to achieve a high photocatalytic reaction rate, particularly in water treatment, a relatively high light intensity is required (Ahmed *et al.*, 2011; Cassano and Alfano, 2000). In the case of imazaquin, when the mercury lamp powers were changed from 125 to 250 W, the degradation rate increased by about 16% (Garcia and Takashima, 2003). The

overall energy input to a photocatalytic process is dependent on the light intensity. This corresponded to the concept of the quantum yield, which was used to describe the efficiency of the reaction under different intensities of light. The relationship between the quantum yield (Φ) and the quantity of photon in the system (N_a) was presented as follows:

$$\Phi = \Delta n / N_a \quad (2.24)$$

The quantity of photons from the lamp is related to the power of the lamp, P and energy per photon, E, as derived from Planck's equation (Equation (2.23)) as follows,

$$N_a = P E = \frac{P h c}{\lambda} = \frac{I A h c}{\lambda} \quad (2.25)$$

where I is the intensity of the visible light or the energy per unit area per unit time in units of W/m^2 and A is surface area.

Therefore, the rate of the photocatalytic removal increases at the higher irradiation intensities on the TiO_2 surface and hence more hydroxyl radicals are produced (Pourata *et al.*, 2009; Liu *et al.*, 2009; Faramazpour *et al.*, 2009; Kaneco *et al.*, 2009) However, at high light intensities, the reaction rate becomes independent of light intensity, because of the rate of flux and the increase in electron-hole recombination rates (Wong and Chu, 2003). Previous investigations have proved the relationship between the degradation rate and the light intensity, which is directly proportional to the square root of the light intensity (Herrmann, 1999; Garcia and Takashima, 2003).

2.11.9 Additional oxidants

(i) H₂O₂ (hydrogen peroxide)

Photo-assisted catalyst mediated degradation, in the combination with H₂O₂ has been found to be highly effective for the degradation of the water polluting pesticides such as simazine, propazine, terbutryn, alachlor, molinate, trifuralin, parathion, phorate, malathion, methamidophos, diazinon, isodrin, aldrin, and DDTs, as shown in Table 2.7 (Devipriya and Yesodharan, 2005; Wei *et al.*, 2009; Liu *et al.*, 2009; Miquel *et al.*, 2012). The reaction to generate the reactive species is written as follows (Radwan, 2005);



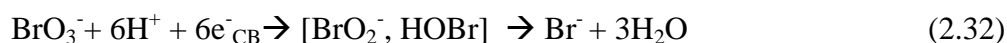
Group	Pesticide	Removal after TiO ₂ /radiation (%)	Removal after TiO ₂ /H ₂ O ₂ /radiation (%)
Triazines	Simazine	45	50
	Atrazine	35	40
	Propazine	35	40
	Terbutylazine	50	50
	Prometon	45	45
	Ametryn	55	55
	Prometryn	55	55
	Terbutryn	55	60
	Desethylatrazine	35	40
Organic phosphorated	Parathion methyl	90	90
	Parathion ethyl	55	55
	Chlorpyrifos	80	80
	Chlorfenvinfos	40	55
	Dimethoate	55	60
HCHs	α-HCH	20	20
	β-HCH	15	15
	γ-HCH	15	20
	δ-HCH	15	15
HCB	Hexachlorobenzene	35	35
Heptachlors	Heptachlor	50	50
	Heptachlor epoxide A	30	30
	Heptachlor epoxide B	30	30
Endosulphans	α-Endosulphan	90	100
	Endosulphan-sulphate	5	10
Drins	Endrin	50	50
	Dieldrin	30	30
	Isodrin	60	100
	Aldrin	55	95
DDTs	pp'-DDE	40	70
	pp'-DDD + op'-DDT	35	80
	pp'-DDT	20	70
Anilines	3,4-Dichloroaniline	100	100
	4-Isopropylaniline	100	100
Ureas	Isoproturon	85	85
	Diuron	75	75
Carbamate	Molinate	55	70
Nitroderivate	Trifluralin	55	70
Anilides	Alachlor	50	65
	Metholachlor	50	60
	Methoxychlor	55	75
Chlorophenols	Tetradiphon	40	40
	Dicofol	90	90
Chlorinated diphenyl	4,4'-Dichlorobenzophenone	5	30
	Average	48	57

Table 2.7 Comparing % removal of pesticides by photocatalytic treatments before adding H₂O₂ and after adding H₂O₂ (Miquel et al., 2012)

(ii) K₂S₂O₈ (potassium persulphate)



(iii) KBrO₃ (potassium bromate)



2.11.10 Mode of the catalyst application: the suspended or immobilised system

Photoreactors can be categorised into 2 main classes which rely on the mode of the catalyst application: the suspended and the immobilised system. These types will be explained more in Section 2.12. The suspended TiO₂ catalyst has superior photocatalytic efficiency compared to the same catalysts immobilised on substrate (Parra *et al.*, 2004; Pizarro *et al.*, 2005; Madani *et al.*, 2006; Lhomme *et al.*, 2008; Senthilnathan and Philip, 2009; Ahmed *et al.*, 2011). This can be explained by enhanced mass transfer in the suspended form. However, the need of the catalyst extraction seems to be the drawback of this system. The immobilised catalyst is slightly easier to handle, but the fouling and the deactivation of catalyst cause significant expenses because the activity of the catalyst drops after the reaction proceeds. The density of the hydroxyl groups on the catalyst surface decreases and strongly adsorbed intermediates occupy the active sites on the catalyst surface (Dutta and Ray, 2004).

2.12 Photocatalytic reactor

A literature review of reactor designs for photocatalytic oxidation was carried out in order to understand which designs are more optimal for continuous operation. Reactors can be classified into two types: reactors that use a catalyst in suspension and reactors that use an immobilised catalyst fixed on a film or other suspended material (Radwan, 2005).

2.12.1. Reactors using suspended solid photocatalysts

2.12.1.1 Annular reactor with horizontal flow

An annular reactor is composed of the vertical UV lamps centre inside a quartz tube surrounded by the polluted water, in which all the light is emitted reasonably uniformly along the tube's length (Figure 2.21) (Li Puma, 2005). The system includes a mechanically stirred tank with the air bubbling to supply the oxygen to the reaction (Bickley *et al.*, 2005).

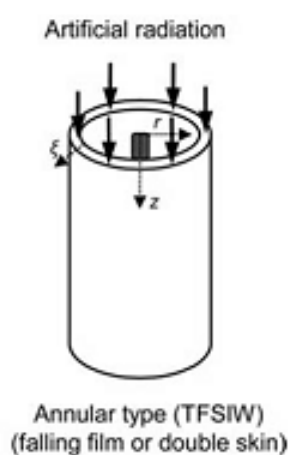


Figure 2.21 Geometry of annular photoreactor (Li Puma, 2005)

2.12.1.2 Thin-film slurry photocatalytic reactor (TFS)

TFS reactors can achieve a high light absorptivity for a TiO_2 slurry suspension and can operate at the high catalyst concentration. As a result of the high mass transfer rate of the reducing agent oxygen, this falling film reactor has a higher conversion rate than the annular type reactor. The illustration of a TFS is shown in Figure 2.22. One example of a thin-film, slurry, photocatalytic reactor is the Fountain photoreactor. The liquid film emerges from the nozzle in the shape of smooth, approximately horizontal and radially expanding water fountain, as shown in Figure 2.23. The radiation source is situated above the water fountain and can be either from solar radiation or artificial light sources. The photon collection efficiency of this new photoreactor can be higher than that of a flat-plate falling-film photoreactor (Li Puma and Yue, 2001). However, this reactor has the disadvantage that it requires catalyst separation post treatment.

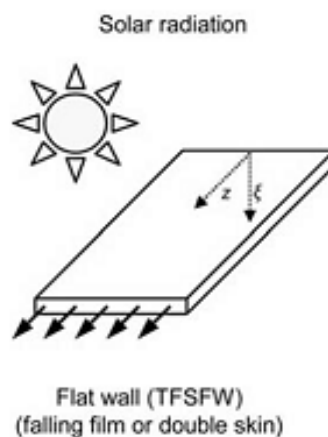


Figure 2.22 Geometry of TFS (Thin-film slurry photoreactor) (Li Puma, 2005)

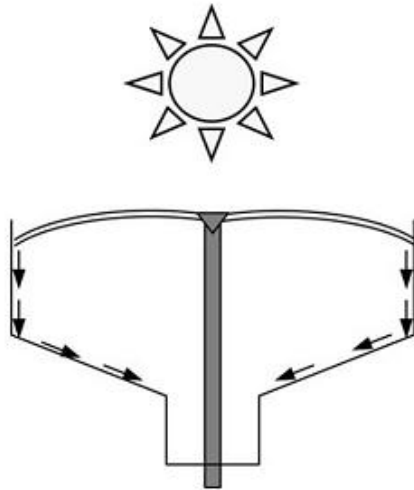


Figure 2.23 Geometry of water fountain photoreactor (Li Puma, 2005)

2.12.2 Fixed catalyst systems

2.12.2.1 Thin Film Fixed Bed Reactor (TFFBR)

Thin film fixed bed photocatalytic reactors (TFFBR) are one of the first solar reactors that do not require a light concentrating system and thus are able to utilise diffuse as well as direct portions of solar UVA irradiation during the photocatalytic process. The most important part of a TFFBR is the sloping plate coated with the photocatalyst which is brought into contact with the polluted water which is present as a thin film over the plate surface ($\sim 100 \mu\text{m}$). The flow rate is controlled by a cassette peristaltic pump and varies from 1 to 6.5 l/h. From Figure 2.24, this configuration benefits from a very large illuminated catalyst surface area per unit volume of the reactor and the minimal mass transfer limitation (Bahnemann, 2004). The catalyst particles are bonded to an immobilized surface to avoid the problem of catalyst

recovery (Zayani *et al.*, 2009; Feitz *et al.*, 2000). Pollutants have to be transported to the surface by convective motion and molecular diffusion. High intensities of irradiation are needed to enhance the rate of the degradation (Bickely *et al.*, 2005).

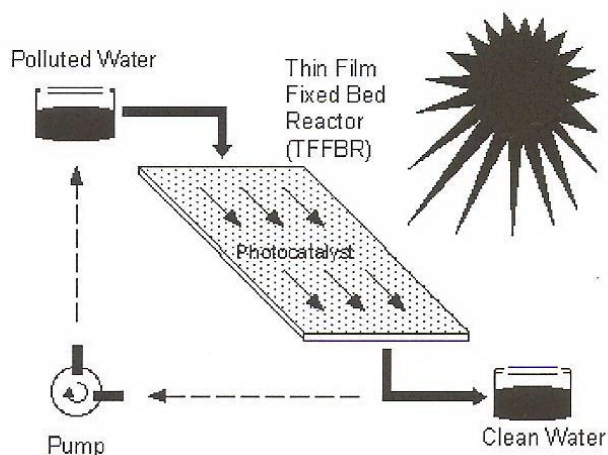


Figure 2.24 Flowchart of TFFBR (taken from Bahnemann, 2004)

2.12.2.2 Packed bed reactor (PBR), fixed-bed reactor and fluidised bed reactor

Photocatalyst particles are supported on larger particles for example, glass beads, sand, or other packing materials. This is advantageous because the catalyst is both fully suspended and supported, which gives very high photocatalyst surface areas and mass-transfer rates. At the same time, there is no need for a post-treatment separation process. Therefore, fluidised and fixed bed photoreactors have received significant attention, especially for gas-phase photoreactions, due to the high degree of interaction between the photocatalyst

particles and the reactant phase (Rowan and Andrew, 2009). It has been reported that titanium dioxide in a fluidised-bed reactor system has a higher activity compared to that of a fixed-bed (Alexander *et al.*, 2000).

2.12.2.3 Fibre Photoreactor (FP) and Optical Fibre Photoreactor (OFP)

In a fibre photoreactor, a photocatalyst is coated onto the fibres and immersed in the reactant fluid as shown in Figure 2.25. In the case of an optical fibre photoreactor (OFP), the parabolic dish is located in the centre, as shown in Figure 2.26, to act as the convex secondary reflector in order to concentrate the sunlight into a bundle of optical fibres. It has one advantage over other photoreactor designs in that it separates the light gathering and the photocatalytic components of the reactor. The light can be collected remotely and transmitted a great distance through the optical fibres to the vessel containing the reactant fluid and the photocatalyst. This allows this photoreactor design to be used within buildings, as long as the light gathering device and the connecting fibre optics are suitably placed (Rowan and Andrew, 2009).

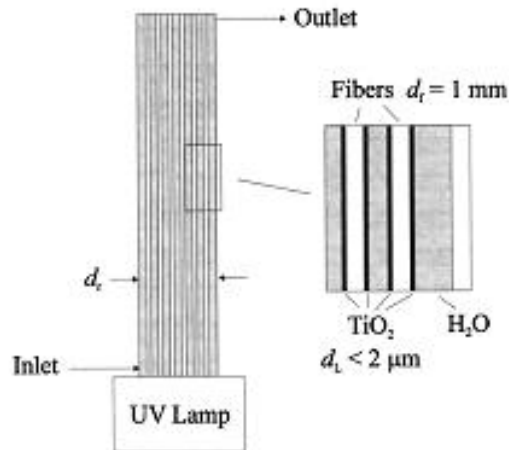


Figure 2.25 Illustration of Fibre Photoreactor (FP) (Dijkstra et al., 2003) TiO_2 is a thin film on the fibres (less than $1.3 \mu\text{m}$). The fibre has thickness = 1 mm. The length of the fibre is 0.7 m, which is equal to the illuminated length. The light is carried into the liquid by a large number of fibres. The reactant fluid is immerse at the inlet and flows pass on the fibre to the outlet.

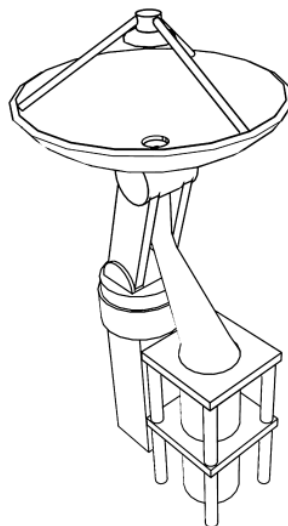


Figure 2.26 Layout for Optical Fibre Photoreactor (OFP) (Rowan and Andrew, 2009) An 24 inch parabolic dish with 3.5 inch convex secondary reflector to concentrate sunlight into bundle of 537 quartz optical fibres coated with a photocatalyst and immerse into the reactant fluid.

2.12.2.4 Rotating Disc Reactor (RDR)

A vertically orientated, radially rotating disk is half submerged in the reactant fluid with the photocatalyst supported on the disk, as illustrated in Figure 2.27. As a section of the surface of the disk emerges from the reactant fluid, it carries a thin film of the liquid. The exposed surface of the disk is illuminated using UV-lamps, with the thin film on the disk's surface allowing an efficient mass transfer between the reactant fluid and both the photocatalyst and the atmosphere (Dionysiou *et al.*, 2000; Rowan and Andrew, 2009). The limitation of this process could be the short residence times available for the oxidation process.

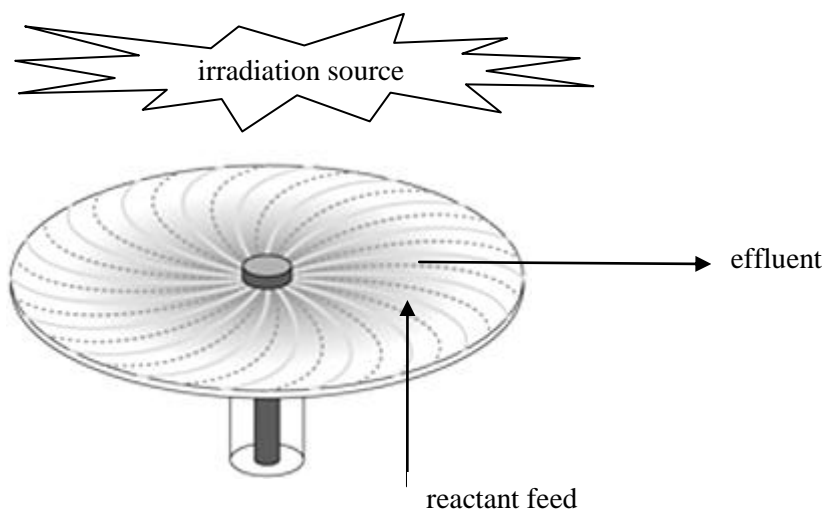


Figure 2.27 Horizontal RDR (Rowan and Andrew, 2009)

2.12.2.5 Photocatalytic Membrane Reactors (PMRs)

The photocatalytic membrane reactors (PMRs) constitute a hybrid photocatalytic membrane reactor system which uses the membrane filtration

unit to configure into the different positioning with the photocatalytic reactor, as shown in Figure 2.28. It can be either a slurry-type or deposit onto membrane that suspends in the water. In the system of an immobilised PM, the membrane module functions as the support for the photocatalyst particles and as the barrier against the different organic molecules in the reaction water. The membrane also helps in the resistance of the photocatalyst particles and organic molecules or the intermediate compounds not to be degraded in the slurry PMRs. The photocatalytic reaction takes place on the surface of the membrane or within its pores. It has been reported that the photo-oxidation efficiency of an immobilised PM was higher than in the case of the suspended catalyst. However, there will be severe membrane damage owing to the immobilising particles (Chong *et al.*, 2010).

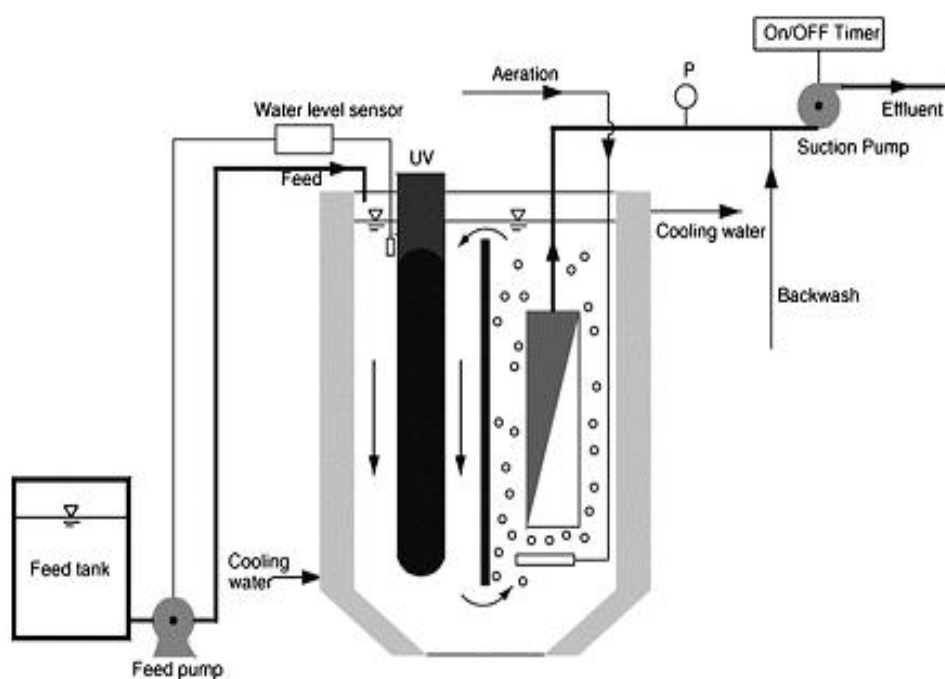


Figure 2.28 Schematic of submerged membrane photocatalytic reactor
(Chong *et al.*, 2010)

Suspended reactors	Immobilized reactors
<p>Advantages</p> <ul style="list-style-type: none"> (i) Fairly uniform catalyst distribution (ii) High photocatalytic area to reactor volume ratio (iii) High mass transfer (iv) Well mixed particles suspension (v) Low pressure drop through reactor (vi) Minimum catalyst fouling effects due to the continuous removal and catalyst replacement 	<p>Advantages</p> <ul style="list-style-type: none"> (i) Continuous process (ii) No need for additional removal catalyst process (iii) Improved removal of organic material from water phase while using a support with adsorption techniques
<p>Disadvantages</p> <ul style="list-style-type: none"> (i) Require post-separation 	<p>Disadvantages</p> <ul style="list-style-type: none"> (i) Low light utilization efficiency due to light scattering by immobilized photocatalyst (ii) Possible mass transfer limitation

Table 2.8 Comparing the advantages and drawbacks of suspended and immobilized photocatalytic system (Lasa et al., 2005)

2.13 Key elements elements of reactor design for photocatalytic reaction

A successful reactor design for the reduction of the organics pollution requires the following key factors:

2.13.1 High Mass Transfer

In a slurry system (non-fixed catalyst), mass transfer is increased by mixing of the pollutants through the turbulence and baffles. In the fixed-bed (or fixed catalyst) and fluidised-bed, mass transfer is controlled by the variation of the liquid and the gas flow rate.

2.13.2 Photocatalyst activation

Based on analysis of the literature, catalyst illumination is probably the most important factor. The UV-light penetration depth is limited due to the absorption by both catalyst particles and pollutants. Photocatalytic reactions occur on the catalyst surface and the catalyst can either be dispersed in the liquid or can be immobilised on the surfaces, but the contact between the catalyst and the contaminant is essential.

2.13.3 Oxygen content

The oxygen content in the water is defined by the solubility at saturation conditions and regarded to be relatively constant. However, oxygen or air is required to replace that used in the oxidation process. Without replenishment, the overall reaction rate could be limited by the reduction of dissolved oxygen. Low oxygen solubility in the water leads to a low rate of oxygen reduced by the controlled-band electrons; an accumulation of the electrons in a semiconductor would result. This accumulation enhances the rate of recombination of the photogenerated electrons and the holes (Sobczynski and Dobosz, 2001).

2.14 Supercritical water hydrothermal synthesis (ScWHS)

Continuous supercritical water synthesis is a relatively novel technique to produce the ultra fine particles of metal oxides (Poliakoff, 2001; Cabanas *et al.*, 2001; Cabanas *et al.*, 2007; Chudoba *et al.*, 2008; Matsui *et al.*, 2008; Atashfaraz *et al.*, 2007; Lester *et al.*, 2006; Edwards *et al.*, 2006; Sue *et al.*, 2004; Kawasaki *et al.*, 2009; Hobbs *et al.*, 2009; Lu *et al.*, 2012).

Supercritical water has been used as a solvent or antisolvent for particle formation because it offers the following advantages (Li, 2008; Aimable *et al.*, 2009)

- (i) Solvent properties that can be tuned by changing pressure or temperature
- (ii) Reduced viscosities and increased mass transfer
- (iii) Dramatic modification of the solvent strength by the dissolution of a dense gas
- (iv) Control of the super-saturation via the pressure, the temperature and the anti-solvent
- (v) Relatively low synthesis temperatures

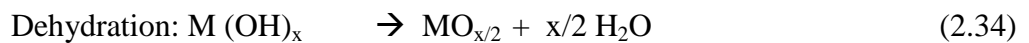
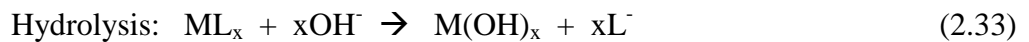
This method includes the chemical reactions to form the particles and adjust the direction of the crystal growth, the morphology, the particle size and the size distribution, because of the controllability of the thermodynamics and the transport properties by pressure and temperature.

The supercritical hydrothermal technique has an advantage in that it produces fine powders with high purity, controlled stoichiometry, high quality, narrow

particle size distribution, controlled morphology, uniformity, less defects, dense particles, high crystallinity, excellent reproducibility, controlled microstructure and high reactivity without sintering issues (Byrappa and Adschiri, 2007).

2.15 ScWHS Mechanisms

ScWHS involves the mixing of an aqueous metal salt stream with a supercritical water stream within a continuous reactor to produce the nano-sized metal oxide particles. When the water is heated to its critical point ($T_c = 374\text{ °C}$, $P_c = 22.1\text{ MPa}$), it changes from a polar liquid to a fluid with a low dielectric constant and low pH. The concentration of H^+ and OH^- increases. Under these conditions, a hydrolysis of the metal salts is immediately followed by a dehydration step



In Equation (2.33), a metal salt is first hydrolyzed to metal hydroxide, which is then dehydrated, according to Equation (2.34), forms metal oxide crystals with micro- or nano-size by precipitating from the solution. Therefore, supercritical water promotes a hydrolysis reaction (Equation (2.34)) and enhances a production of oxide particles.

2.16 Conclusion of background and review of literature

This chapter has reviewed the definition, kinetics, mechanisms, materials, parameters and reactor design of photocatalysis, and also briefly the technique for synthesising the nanoparticles by supercritical water. Photocatalytic treatment has been known for many years as a potential option for solving water pollution, especially that caused by pesticides. The most commonly used photocatalyst is Degussa P-25 TiO₂ due to the superior properties compared to other photocatalysts. The parameters which affect the photocatalytic reaction are the crystal phase of TiO₂, the pollutant concentration, the TiO₂ concentration, O₂ concentration, pH, the light wavelength, the light intensity, the additional oxidants and the operation mode of the reactor. The conclusion of the influence of each parameter on the degradation rate is shown in Figure 2.29 (Herrmenn, 1999).

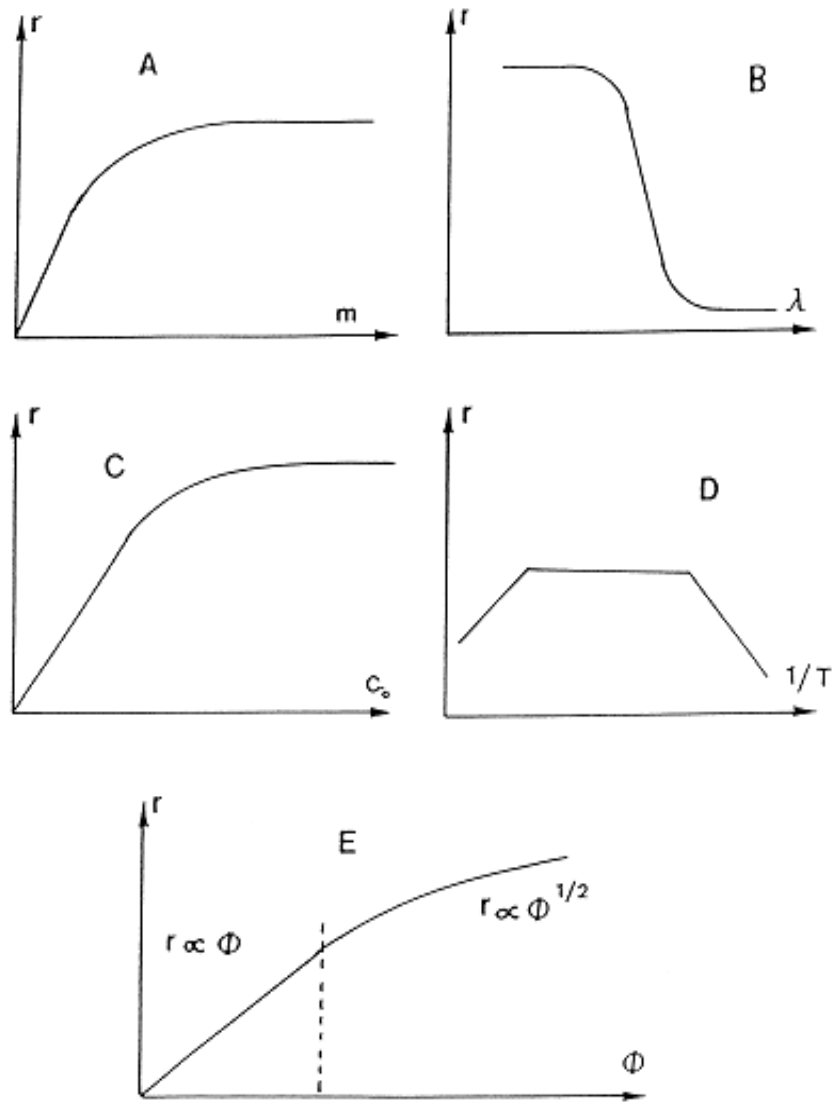


Figure 2.29 Influence of the different physical parameters which govern the reaction rate r (r is generally comprised between 1 and 0.1 mmol/h): (A) mass of catalyst; (B) wavelength; (C) initial concentration of reactant; (D) temperature; (E) radiant flux (Herrmann, 1999)

Photocatalytic reactor design can be categorised into 2 major types: the suspended and immobilised catalyst. The reactors which use an immobilised catalyst have the advantage in that there is no need to employ a separation

process after treatment. However, the efficiency of reactors using a suspension catalyst is still higher than an immobilised catalyst.

Chapter 3

EXPERIMENTAL

3.1 Introduction

This chapter describes the experimental procedures used in this thesis for carrying out photocatalytic oxidation treatment of three specific pesticides that pollute ground water. Stock solutions of each were made using de-ionised water. A laboratory scale stirred reactor, thin film fixed bed reactor, and fluidised bed photoreactor were constructed for these studies. Photographs and illustrations of these reactors are presented. Experimental reagents, procedures and all analytical techniques related to this study are also described. Calibration curves were established using high performance liquid chromatography (HPLC) in order to accurately quantify results from the peaks in the chromatography curve relating to the pesticides concentration.

3.2 Chemicals and materials

The materials were obtained from the following sources and were used as received: P-25 TiO₂ (Sigma-Aldrich, UK); Isoproturon, Simazine, and Propazine (Sigma-Aldrich, UK); Tibald (Titanium (IV) bis (ammonium lactato) dihydroxide solution 50 wt% in H₂O; Sigma-Aldrich, UK); Acetonitrile > 99% (Sigma-Aldrich, UK); DDSA (Dodecenyl Succinic

Anhydride; Fluka, UK); Toluene (Fisher Scientific, UK) Hydrogen peroxide > 30% (Fisher Chemical, UK); 0.45 µm nylon filters (Sartorius, UK).

3.3 Procedure for supercritical water synthesis of TiO₂

Precursor and reagent

0.2M of Tibald (Titanium (IV) bis (ammonium lactato) dihydroxide solution 50 wt% in H₂O; Sigma-Aldrich, UK) was used as a precursor in this synthesis. 0.005M of DDSA (Dodecanyl Succinic Anhydride; Fluka, UK) in Toluene (Fisher Scientific, UK) was used as a capping agent, which was introduced at the capping point as shown in Figure 3.1. Deionised water with 5% H₂O₂ (Hydrogen Peroxide; Fisher Scientific, UK) was used as a water stream feed.

Peroxide; Fisher Scientific, UK) was used as water stream feed.

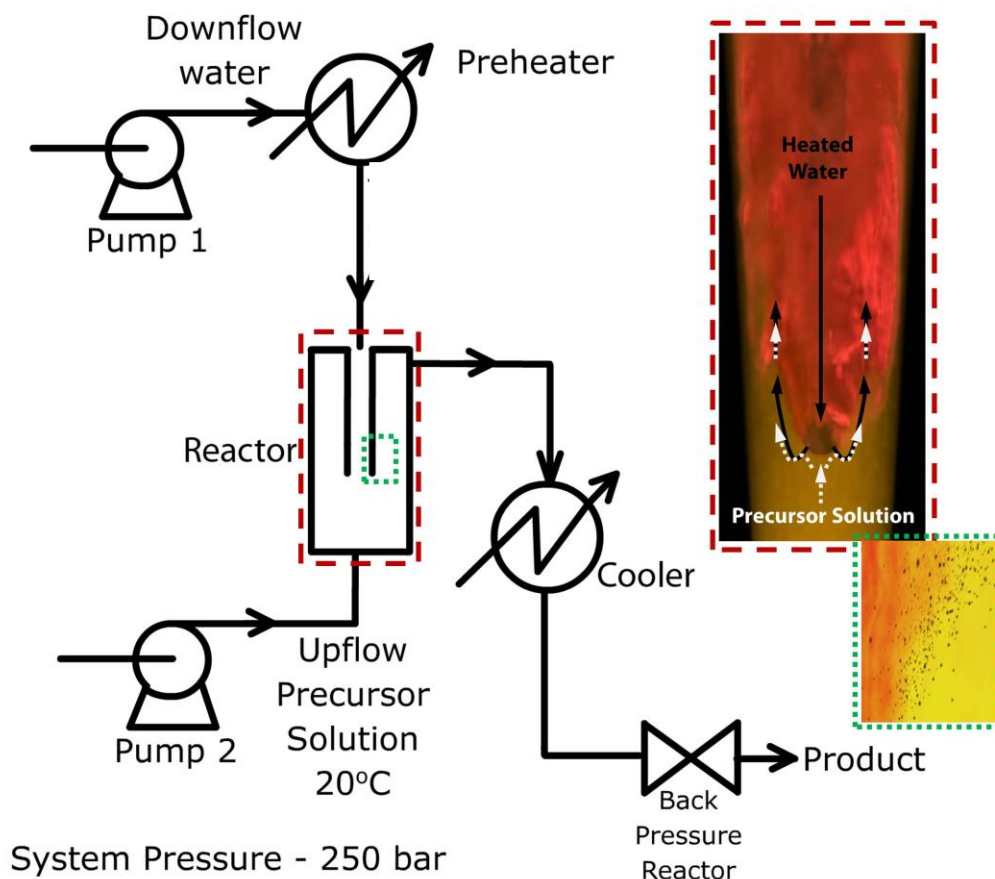


Figure 3.1 Supercritical hydrothermal synthesis rig. The Tibald is present in the upflow precursor solution.

1. Before starting

The fume cupboard was switched on and checked for correct operation. All the connections were checked by observation. The Back Pressure Regulator (BPR) was checked to be set to the minimum pressure. The de-ionised water supply was connected to the water pump, capping pump and salt pump 1.

2. Start-up

The main power and the computer were switched on in order to initialise the Picolog programme used for monitoring the temperature at each point of the system. The water pump, capping pump and salt pump 1 were switched on at the flow rate of 20 ml/min. The system pressure was increased using a spanner on the BPR. At this time, the pressure measured at the pressure transducer and the pressure gauge was monitored. The BPR was no longer adjusted once the pressure had reached 240 bars. The cooling water valves were opened to maximum flow. The water heater was switched on and set to 480 °C. The monitoring of the temperature and the pressure on a Picolog programme was started. When all parameters were stable, the water pump feed was changed to a 5% H₂O₂ solution. The salt pump 1 was then changed to feed Tibald and the capping pump was changed to feed DDSA in the toluene. The flow rate of the 5% H₂O₂ solution was 20 ml/min. The flow rate of the Tibald solution was 10 ml/min and the flow rate of DDSA in Toluene was 5 ml/min. The sample was taken when complete mixing of reagents and nanoparticles was observed after 3-5 minutes.

3. Shutdown procedure

The heater temperature was set to 0 °C. All the pumps were switched to a feed of de-ionised water. The pressure of the system was decreased slowly by loosening the BPR. During the depressuring process, the BPR inlet temperature was monitored until it had decreased to below 100 °C. The pumps were set to cool down the system. The cooling water valves were switched off when the temperature had dropped below 150 °C. The pumps, computer and the main power were then switched off.

3.4 Thin Film Fixed Bed Reactor System (TFFBR)

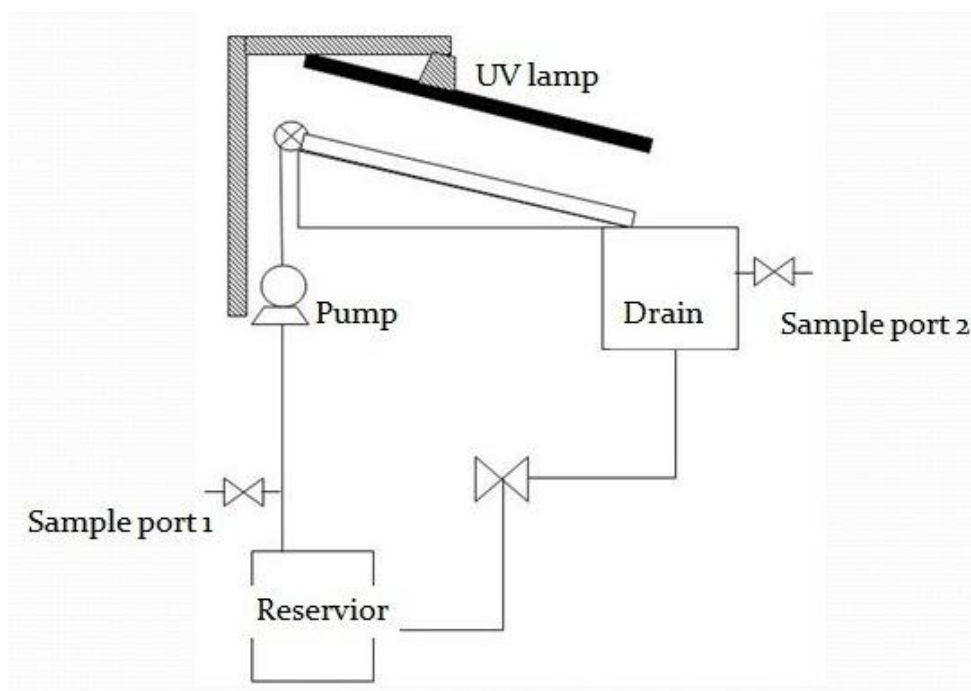


Figure 3.2 Schematic of TFFBR photocatalytic reactor

The reactor in Figure 3.2 was designed and constructed for this thesis. This reactor is based on the Thin Film Fixed Bed Reactor (TFFBR) concept which has the potential advantage of avoiding the need to separate the nanoparticles from the effluent. A stainless steel plate of 30.5 cm-long, 9 cm-width and 0.05 cm thickness was supported with two vertical parallel plates of 22.8 cm by 30.5 cm. Two 8 watt lamps of UVC (wavelength = 250 nm) and UVA (wavelength = 350 nm), 30 cm in length, were supported in the parallel direction, 10 cm above the surface. The TiO₂ was fixed on the surface of the plate to avoid the contamination of the effluent as described in the experimental procedures. Figures 3.3 and 3.4 show the reactor arrangement.

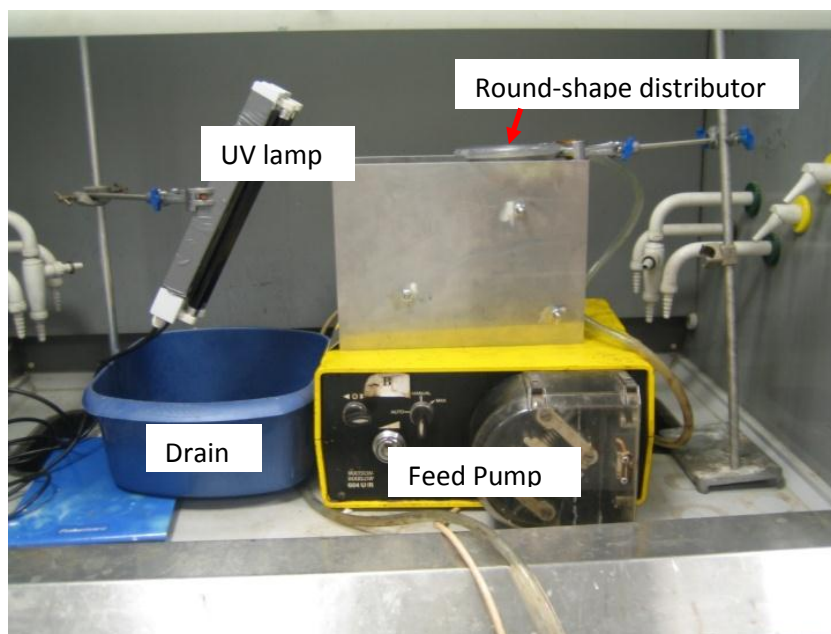


Figure 3.3 Photograph of the TFFBR photocatalytic reactor



Figure 3.4 Photograph of the reactive area and the water source

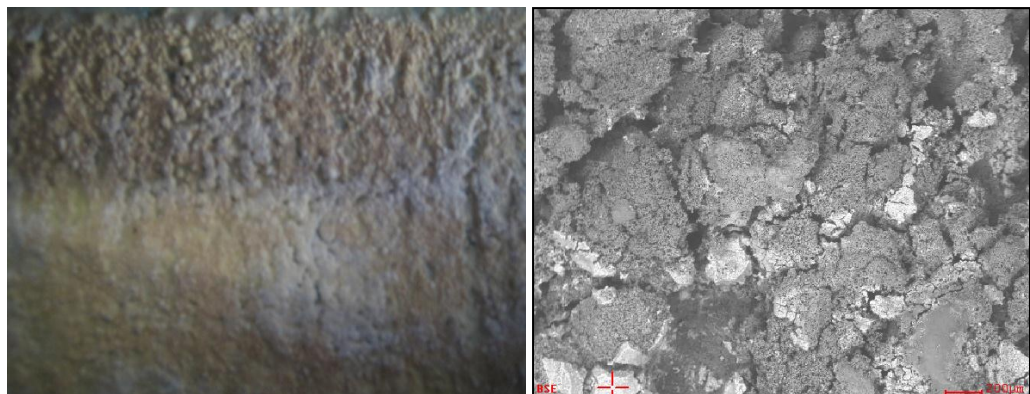


Figure 3.5 (a) Photograph of a P-25 TiO₂ coated surface on the stainless steel plate (b) SEM image of P-25 TiO₂ coated surface at a magnification 200 μm

3.4.1 Surface coating method

In this research, there were 2 stainless steel sheets. One was coated with 40% P-25 TiO₂ and the other was coated with 14% synthesised TiO₂.

Plate 1: 25 g of epoxy resin was mixed with 18 g of Degussa P-25 TiO₂ at 80 °C using a spatula in a fume cupboard. 3 g of hardener was then mixed and applied to the plate as a thin layer across the surface. A further 10 g of TiO₂ was spread on the polymer to increase the concentration of TiO₂ particles on the surface. Figure 3.5 shows the photograph and SEM image of P-25 surface on the metal sheet. The SEM image at high magnification shows a non homogeneous layer.

Plate 2: 2.6 g of synthesised TiO₂ from ScWHS was mixed with 18.6 g of epoxy using a spatula in a fume cupboard. As shown in the SEM image at high resolution in Figure 3.6, the synthesised TiO₂ is well distributed.

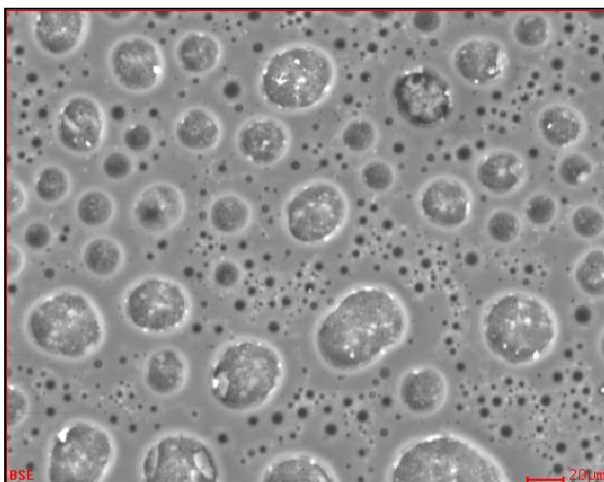


Figure 3.6 SEM image of synthesised TiO₂ coated surface with a scale bar of 20µm

3.4.2 Experimental procedures for the TFFBR

1. Before starting

All the connections were checked before conducting the experiments; the fittings of the tubing must be correctly connected before beginning the experiment. The position of the round-shaped distributor was checked to make sure that the water will distribute evenly on the stainless steel plate. The angle of the UV-lamp was checked by keeping the UV lamp parallel with the slope of the plate.

2. Start up

The amount of pesticide solution in the reservoir for each experiment was approximately 400 ml. The UV lamp was switched on 10 minutes prior to the experiment to allow the lamp to warm up. The feed pump was switched on to draw the water from the reservoir at either a high flow rate (100 ml/min), or a low flow rate (20 ml/min), as explained in the operating conditions. The first sample was taken from the sample port 1 at the time $t = 0$, shown in Figure 3.2. Then 50 ml of the 1st cycle sample was collect from the sample port 2 after the feed solution had been depleted and the concentration of pesticide in product was analysed. The by-product solution from the drain container was poured into the feed solution reservoir; the sample for the 2nd cycle was collected at sample port 2. Samples were collected in a similar way until the 5th cycle.

3. Shut down

After finishing the experiments, the surface of the reactor was cleaned by pumping 1000 ml water through. The UV lamps and pump were switched off.

3.4.3 Operating conditions

1. Polluted water feed at the high flow rate = 100 ml min^{-1} , at the low flow rate = 20 ml min^{-1}
2. Photolysis: without any photocatalyst, only under UV irradiation
3. Dark condition: with TiO_2 but without UV irradiation
4. At the high concentration of the pesticide solutions: isoproturon, simazine and propazine concentration = 20 ppm
5. At the low concentration of the pesticide solutions: isoproturon, simazine and propazine concentration = 2.5 ppm
6. The first cycle requires 25 minutes, then 15, 10, and 5, respectively for the remaining cycles
7. 2 UVA lamps (each equipped with a Phillips TL 8W BLB, length = 30 cm , wavelength = 350 nm, 8 watts)
8. 2 UVC lamps (each equipped with a Ultraviolet UV-C HG GBT5, length = 30 cm , wavelength = 250 nm, 8 watts)
9. The feed pump details : Watson Marlow 604 U/R, maximum speed: 165 rpm

3.5 Stirred Photoreactor

The photocatalytic degradation of isoproturon, simazine and propazine was studied through the small scale reactor. The initial TiO_2 concentration was 0.5

g litre⁻¹. The initial concentration of each pesticide is 2500 µg litre⁻¹ (2.5ppm). 200 ml of TiO₂ suspension with pesticides was put into the small container which was set on the stirrer at 900 rpm in the black box under 8 watt UVA lamp. 5 ml of samples were collected every 10 minutes and then filtered through nylon filters to remove the TiO₂ particles, to be promptly analysed by the Hewlett Packard 1050 series high performance liquid chromatography system fitted with a diode array detector and autosampler. The HPLC detection limits are 0.16 µg litre⁻¹ for isoproturon, 3.2 µg litre⁻¹ for simazine and 7.2 µg litre⁻¹ for propazine. The set-up of the system is shown in Figure 3.7.



Figure 3.7 *The set-up of stirred reactor*

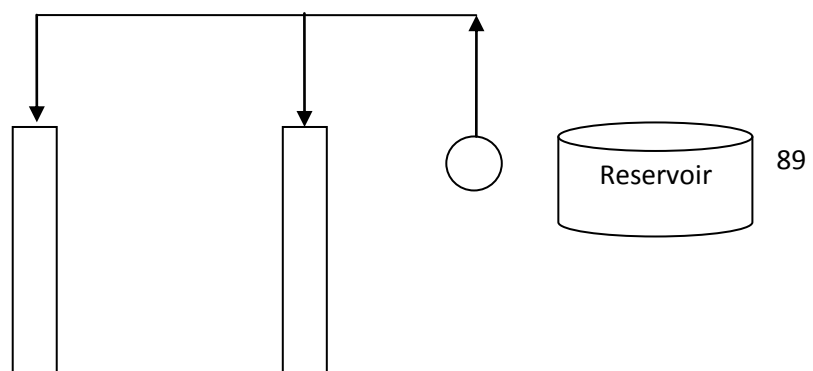
3.5.1 Operating conditions

1. ‘Dark’ conditions: 0.5 g litre⁻¹ P-25 TiO₂ added without any irradiation source
2. Photolysis: no photocatalyst, only under the UV light
3. At various concentrations of P-25 TiO₂: 0.25, 0.5, 1, 2.5, 5, 10 g litre⁻¹

4. UVA lamp (equipped with a Phillips TL 8W BLB, length = 30 cm., wavelength = 350 nm, 8 watts)
5. The magnetic stirrer details : KRET control-visc (Ika werke), maximum speed 1100 rpm

3.6 Fluidised bed photoreactor system

The fluidised bed photoreactor was designed for use with large scale experiments. It contains two 120 cm length of 1 inch-diameter quartz cylinder tubes circled with 2 UVA and 2 UVC lamps operated at 36 watts, as shown in Figure 3.8. The sintered TiO_2 was prepared by heating up 1.6 kg of the P-25 TiO_2 to 900 °C for 2 hours. Then, the sintered TiO_2 was carefully transferred into the photoreactor.



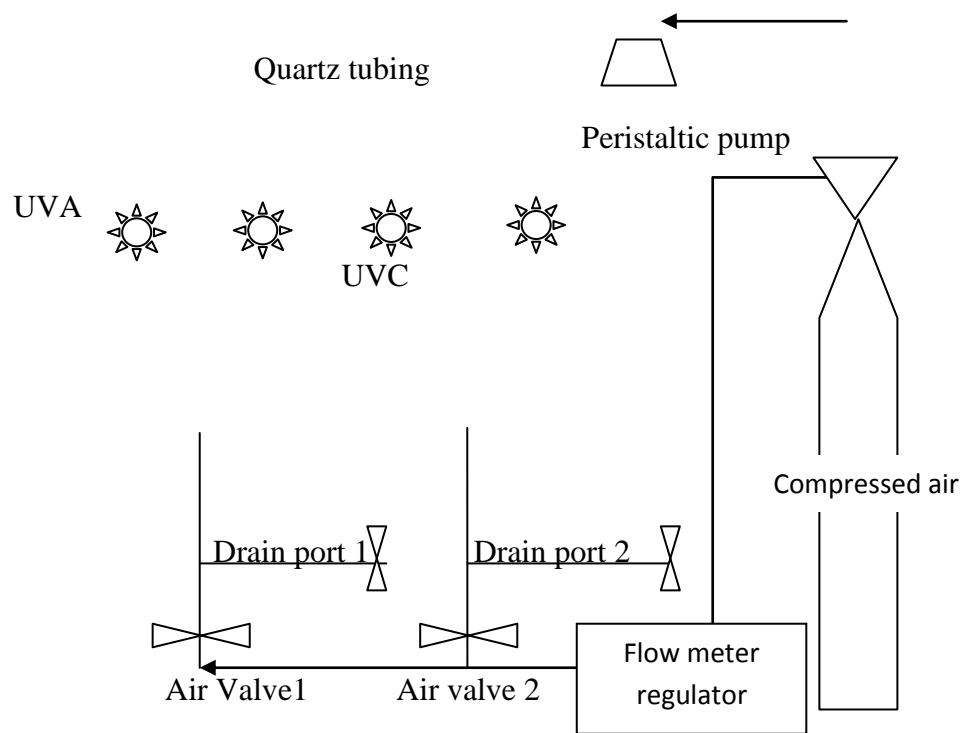


Figure 3.8 Schematic diagram of the fluidised bed photoreactor



Figure 3.9 Photograph of the fluidised bed photoreactor

In this reactor system, 2.5 ppm of one pesticide (isoproturon, simazine, propazine) was well-mixed with the de-ionized water in a fume cupboard. The reservoir tank was filled with the feed solution next to the peristaltic pump.

3.6.1 Experimental procedure for fluidised bed photoreactor

1. Before starting

All the connections were checked for leaks before doing the experiments and the air inlet valves 1 and 2 were in the closed position. The quartz tubing reactor was fixed in the rig and guaranteed that the discharge of the reactor was checked for any blockage as was the external ventilation.

2. Start-up

The pesticide solutions (isoproturon, simazine, propazine) were fed into the quartz tubing reactor by opening the stream water valve and switching on the peristaltic pump. The water level reached a steady state after waiting for approximately an hour. The compressed air cylinder was opened to let air pass upright from the bottom of the quartz tubing. Then, the sintered TiO₂ was applied. The outlet pressure from the gas cylinder was adjusted at the pressure regulator to introduce a small bubble into the tube. The tubing air inlet valve 1 and 2 were opened (Figure 3.8) and then the air flow meter was adjusted to ensure the air bubble was spread evenly (0.8 litre min⁻¹) and the sintered TiO₂ was suspended evenly in the tubing. The UV isolation shielding sheet was completely closed before switching on the UVA and UVC lamps. The samples

were taken from both drain ports 1 and 2 every 10 minutes for a period of 1.5 hours.

3. Shutdown Procedure

Both the UVA and UVC lamps were switched off. The air gas cylinder outlet valve was closed. The tubing air inlet valve 1 and 2 were then closed. The peristaltic pump was switched off and drain valves were opened to remove water from the reactor. The reactor was washed, and stored at the ambient temperature.

3.7 Analytical Techniques

3.7.1 High Performance Liquid Chromatography (HPLC)

HPLC is a chromatography method which is widely used for solution analysis. HPLC is a dynamic absorption process; it is a separation technique involving mass transfer between the stationary and mobile phase. The stationary phase is defined as the immobile packing material in the chromatography column, which can be a liquid or a solid phase. Firstly, the sample is dissolved in the mobile phase and then injected into a chromatography column under high pressure, as shown in Figure 3.10. The interaction between the solute and the mobile phase results in separation of the components which are detected by the UV absorption at the specific wavelength. The analytical software shows different absorption-peak heights and absorption-peak areas at the variable retention times. The concentration of each component can then be quantified by using a calibration curve from the set of the peak area data.

In this thesis, the samples were filtered through a 0.45 μm nylon filter, then injected and mixed with the mobile phase; the sample was then forced to flow through the chromatographic column under high pressure. The samples were promptly analysed using a Hewlett Packard 1050 series high performance liquid chromatography system fitted with a diode array detector and autosampler. The optimal separation and the sensitivity for isoprotruron, simazine, and propazine was achieved using a X-Terra RP 18 column of 3.0 mm x 150 mm (particle size 3.5 μm) for the stationary phase, and a mobile phase of 43% acetonitrile, 57 % water, at a flow rate of 0.7 ml/min, a column temperature 30 $^{\circ}\text{C}$, and a detector wavelength 254 nm. 3 injections were carried out for each sample. The response of the detector to each component was displayed on a chromatogram.

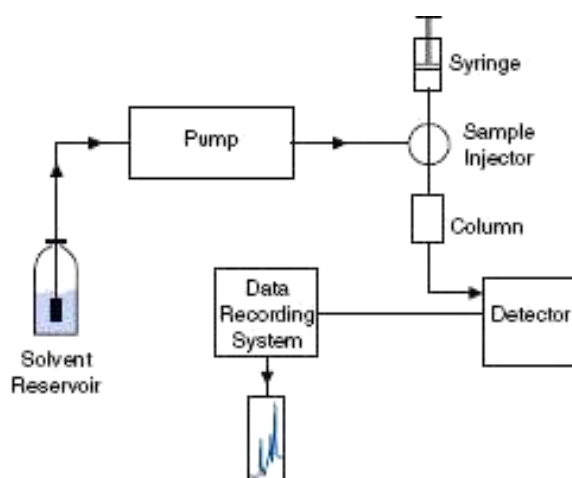


Figure 3.10 Schematic diagram of HPLC

3.7.2 Ultraviolet-visible Spectroscopy (UV-Vis)

Different molecules absorb radiation at different wavelengths. An absorption spectrum will show a number of absorption bands corresponding to the structural groups within the molecule.

This technique is based on Beer-Lambert's law:

$$A = \epsilon \ell c \quad (3.1)$$

where A is absorbance ($A = \log_{10} (I_0/I)$), where I_0 and I are the intensity (or power) of the incident light and the transmitted ϵ : molar absorptivity ($\text{L mol}^{-1} \text{cm}^{-1}$), ℓ : path length of the sample (cm), c : concentration (mol^{-1}).

A double-beam spectrophotometer works by sharing the light path to be directed through the sample and the reference cell, as shown in Figure 3.11.

In this thesis, spectrophotometric measurements were performed to measure the extinction coefficient of the supercritical water hydrothermal synthesised titanium (ScWHS TiO_2) and P-25 TiO_2 suspensions.

The photocatalyst was weighed and suspended in the ultrapure water. The suspension is maintained under the condition of permanent magnetic stirring during the course of the spectrophotometric measurement. After that, the sample is pipetted into quartz cell 2 mm and 10 mm optical path length. The measurement is taken immediately at the wavelength 310-380 nm. During the measurement, 2 separate readings are taken for each sample and compared. After the measurement, the cell was rinsed to eliminate traces of TiO_2 left from the previous run.

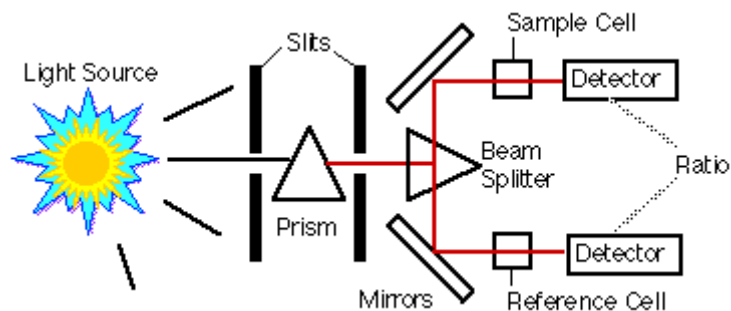


Figure 3.11 Double beam UV-Vis spectrophotometer

3.7.3 Scanning Electron Microscopy (SEM) and Energy Dispersive X-ray Spectroscopy (EDAX)

SEM is an analytical technique that uses a high energetic electron beam on a fine scale to examine the materials. In SEM, an electron beam from an electron source is focused by a fine probe that raster scans over the surface of the specimen under vacuum. Figure 3.12 shows the electron beam passes through the scan coils and the objective lens that deflect horizontally and vertically on the sample surface. As the electrons penetrate the surface, interactions occur that result in the emission of electrons or photons from or through the surface. Using a cathode ray tube (CRT), every point that the beam strikes on the sample is mapped directly onto a corresponding point on the screen.

Another application of the electron microscopy is to characterise the elements of a material by Energy Dispersive X-ray Spectroscopy or EDAX. The sample is bombarded with the electrons from the atoms on the surface of the specimens. This results in the electron vacancy which is then filled by another

electron from a higher shell. To balance the energy difference between the two electrons, an X-ray is emitted. The EDAX measures the number of emitted X-rays versus their energy, which is the characteristic of the element.

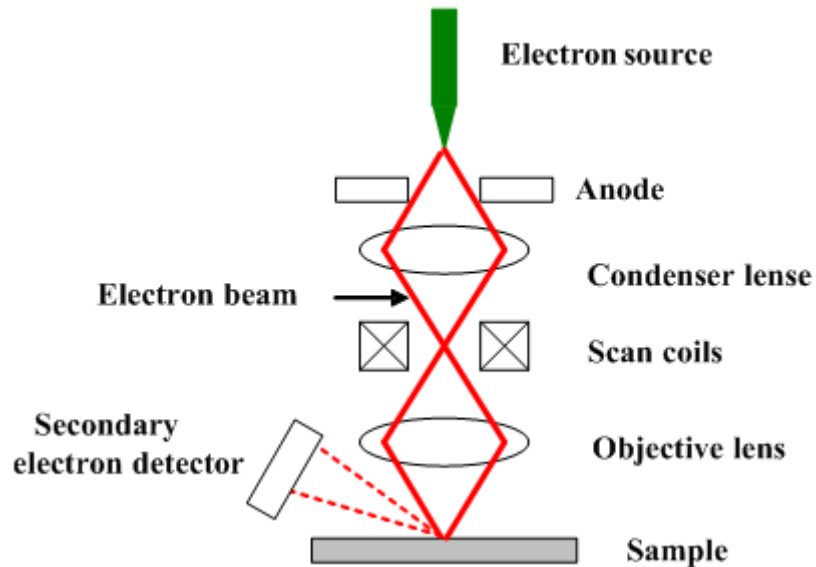


Figure 3.12 The basic layout of a scanning electron microscope

In this thesis, SEM was used to characterise the surface structure of TiO₂ (both ScWHS and P-25 TiO₂) coated the stainless steel plate of TFFBR system. EDAX was used to determine the possible composing elements.

3.7.4 Transmission Electron Microscope (TEM)

TEM is an analytical technique which uses an electron beam to interact and pass through a sample in the specimen. The configuration of the TEM system is shown in Figure 3.13. The electron beam is emitted from an electron source and is confined by the two condenser lenses. It then passes through the condenser aperture and hits the sample surface. Scattered electrons pass

through the objective lens and the objective apertures. The elastically scattered electrons are chosen by the objective aperture that will form the image of the microscope. Finally, the beam travels to the magnifying system. The formed image is shown either on a fluorescent screen or in a monitor or both and is printed on a photographic film.

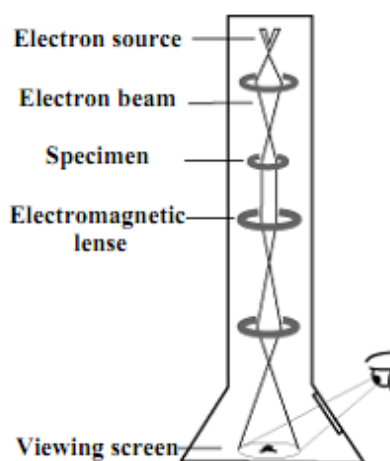


Figure 3.13 The basic layout of a transmission electron microscope (JEOL Transmission Electron Microscope, 2005)

In this thesis, the TEM was used for the characterisation and the size determining of ScWHS TiO_2 particle samples, compared to the P-25 TiO_2 sample. Samples were prepared in an aqueous solution phase before running the TEM.

3.7.5 X-Ray Diffraction (XRD)

XRD is a well-known analysis method for the characterisation of crystal structures. Diffraction effects are observed when an electromagnetic radiation impinges on the structure at the level of the radiation wavelength. XRD was developed from Bragg's law which is described as follows:

$$n\lambda = 2d \sin\theta \quad (3.1)$$

Although Bragg's law was used to explain the interference patterns of X-rays scattered by the crystals, the diffraction has been developed to study the structure of all the states of the matter with any beam; e.g. ion electrons, neutrons, and protons, with a wavelength similar to the distance between the atomic or the molecular structures of the interest. Because a pure substance has a unique diffraction pattern, the powder diffraction method is suitable for the characterisation and identification of the polycrystalline phases. The sample is pressed into a sample holder to create a smooth flat surface. When an X-ray beam hits an atom, the electrons around the atom start to oscillate with the same frequency as the incoming beam; this results in constructive or destructive interference, depending on the structure. Planes going through areas with high electron density will reflect strongly, planes with low electron density will give weak intensities. The schematic diagram of the XRD is shown in Figure 3.14.

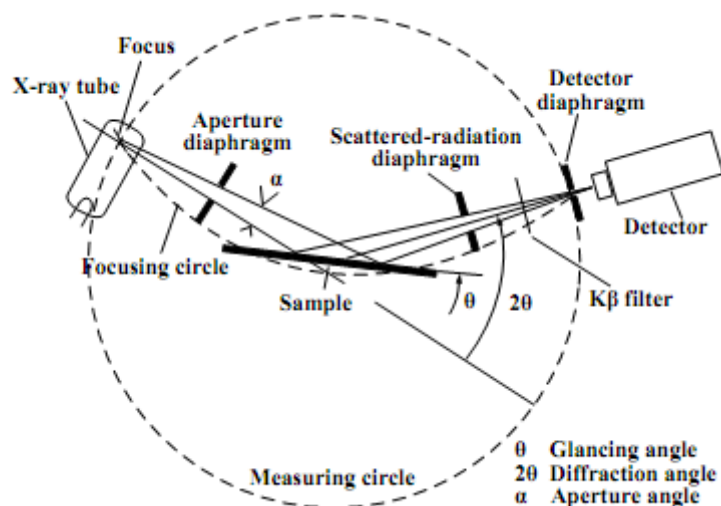


Figure 3.14 Schematic diagram of XRD (Connolly, 2007)

In this research, XRD was performed on the ScWHS TiO_2 at the different sintering temperatures, to see how the structure changes after increasing the sintering temperature. This information has a significant role in explaining the properties of ScWHS TiO_2 .

3.8 Calibration curves for pesticides quantification

High performance liquid chromatography (HPLC) is an analytical technique (as explained in Section 3.7.1) which is used to determine the concentration of chemical solutions by measurement of the area of the peak. The Y-axis represents the magnitude of the detector signal (mAU) and X-axis shows the retention time (min). The data was compiled by the diode array detector which is one part of the HPLC analysis shown in Figure 3.10. The system was operated using the Chemstation software and used for the sample analysis

during photocatalytic experiments. For isoproturon, simazine and propazine, HPLC was operating under the following conditions:

Column Type	X-Terra RP 18 column
Size of column	3.0 mm x 150 mm (particle size 3.5 μ m)
Mobile phase composition	43% acetonitrile, 57 % water
Flow rate	0.7 mL/min
Column temperature	30 °C
Detector wavelength	254 nm

In theory, HPLC was an instrument that separated the composition of a sample by the interaction of the solute with the mobile phase and the stationary phase. These interactions depend on the polarity, which is related to the functional groups, hydrophobic (dispersive), electronic charge such as dipole-dipole and ionic, and molecular size.

The area of the peak is proportional to the concentration of the pesticide. The height and width of the peak depend on how fast the pesticides move during injection. The attraction force of the solute with the mobile phase and the stationary phase determines how slow the solute comes out. If the shape of the peak is tall and thin, this means the separation process was speeded up.

The results are illustrated by the peaks of the chromatography, shown in Figure 3.15 for isoproturon, simazine and propazine. It can be claimed that simazine came out first and then isoproturon and finally propazine. The retention times of these three pesticides are different related to the molecular

weight and the polarity; the times also depend on the mobile phase, the type of column and the injection volume. For this X-Terra column with acetonitrile 43% and water 57% as mobile phase, the retention time was 6.27 min for isoproturon, 4.89 min for simazine, and 7.2 min for propazine, as shown in Figure 3.15. Simazine and propazine had similar structures, except the radical molecule was different (Trajkovska et al., 2004).

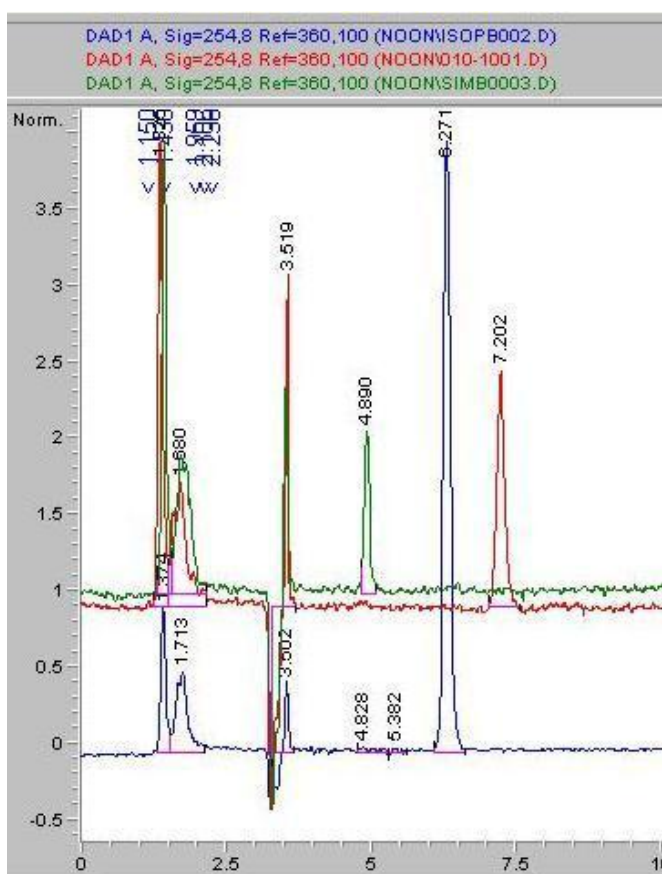
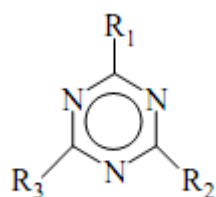


Figure 3.15 Overall chromatograph peak at concentration 5 ppm (5000 $\mu\text{g/L}$): blue line-isoproturon, green line-simazine, red line-propazine. The Y-axis show magnitude of detector signal (mAU) and X-axis show retention time (min)



Compound	R ₁	R ₂	R ₃
simazine	Cl	NH-C ₂ H ₅	NH-C ₂ H ₅
propazine	Cl	NH-CH(CH ₃) ₂	NH-CH(CH ₃) ₂

Figure 3.16 Structure of triazines (Trajkovska et al., 2004)

Compound	Molecular weight
isoproturon	206.3
simazine	201
propazine	229.71

Table 3.1 Comparing molecular weight of three chosen pesticides

From Figure 3.16 and Table 3.1, it can be seen that propazine has the highest molecular weight when compared to the other pesticides. In terms of the polarity, simazine has the smaller hydrophobic part as R₃ of simazine is shorter than R₃ of propazine (Figure 3.16). Then acetonitrile and water, a mobile phase, had a stronger attractive force to simazine than propazine. This meant that simazine emerged from the column first.

However, this retention time is quite different from that reported by others in 2006 (Gora et al., 2006), as shown in Figure 3.17, which used the different column and HPLC conditions. However, the orientation of the peak was still in the same order; first simazine then isoproturon and finally propazine.

In this HPLC analysis, the concentration of pesticide in the range of 2500-20,000 µg/litre was tested.

The calibration curves for these three pesticides were made by known concentration of isoproturon, simazine and propazine stock solutions which were related to the area under the chromatograph peaks, as illustrated in Figures 3.18, 3.19 and 3.20. For the same pesticide concentration, i.e. 2500-20,000 µg litre⁻¹, the resulting area was in the range of 100 for isoproturon, 12 for simazine, and 10 for propazine.

The response factor (RF) is the ratio between the signal produced by the solute and the quantity of solute which produces the signal. RF of each chemical is individual value. The response factor (RF) can be expressed on a molar, volume or mass basis:

$$RF_i = \frac{A_i}{A_{st}} RF_{std} \quad (3.2)$$

A is peak area and the subscript *i* indicates the sample and the subscript *st* indicates the standard. The RF value was used to calculate the concentration of sample when the peak area was known. RF can be found from the relationship between peak area (A) and concentration (C, µg/l or ppm), as follows:

$$A = RF * C \quad (3.3)$$

1) for isoproturon

From Figure 3.18, an equation from the calibration curve is

$$A = 4.5273 C$$

Therefore, RF = 4.5273

2) for simazine

From Figure 3.19, an equation from the calibration curve is

$$A = 0.3886 C$$

Therefore, RF = 0.3886

3) for propazine

From Figure 3.20, an equation from the calibration curve is

$$A = 0.4082 C$$

Therefore, RF = 0.4082

For these calibration curves, 3 injections per vial were carried out for each sample. The error bars in the graphs were calculated by the instrumentation error 5%.

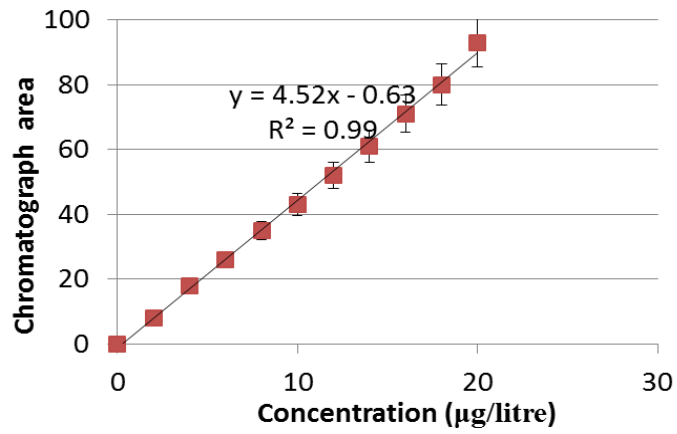


Figure 3.18 Isoproturon calibration curve

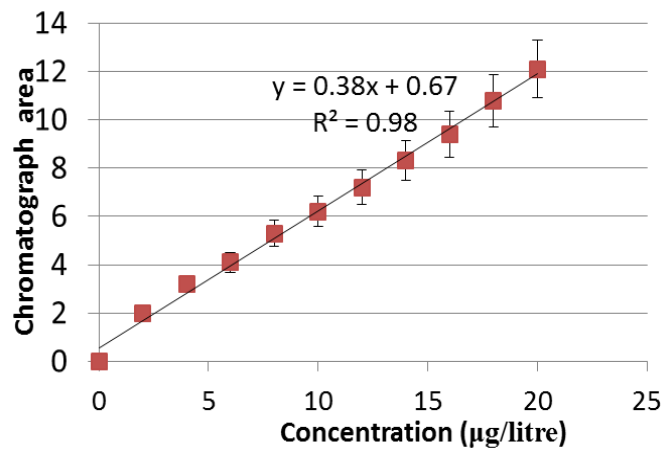


Figure 3.19 Simazine calibration curve

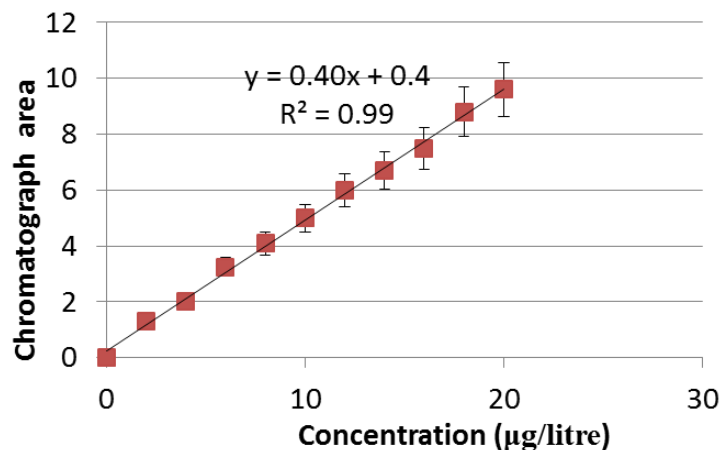


Figure 3.20 Propazine calibration curve

3.9 Conclusions of the Experimental Chapter

Three reactors: the TFFBR, the stirred reactor and the fluidised bed reactor were designed and used in this thesis to treat three pesticide solutions under different conditions. There were two types of photocatalyst material used in this research: the P-25 TiO₂ and the synthesised TiO₂ by the ScWHS method. In the case of the TFFBR, a coating procedure was necessary. However, the P-25 TiO₂ and the synthesised TiO₂ were used in the fluidised bed reactor after sintering at 900 °C for capped nanoparticles and for the separation process. HPLC was used for quantitative analysis of the remaining pesticides in the system. UV-Vis was used to determine the absorption wavelength. XRD, TEM, and SEM were used to detect the size and the morphology of the particles

Chapter 4

PHOTOCATALYTIC DEGRADATION OF PESTICIDES USING A THIN FILM FIXED BED REACTOR

4.1 Introduction to TFFBR results

This chapter discusses the results from the degradation of a range of pesticides (isoproturon, simazine, and propazine) using a thin film fixed bed reactor (TFFBR). Previous application of similar thin film reaction systems for the reduction of pesticides was discussed in Section 2.12. TFFBR is one type of immobilized catalyst reactor. In this reactor, the photocatalyst particles are bonded as the top layer of the bed, which is set as a sloping plate. The feed solution is controlled by a peristaltic pump and then covers the plate as a thin film. This system is attractive for application in the photocatalytic degradation of pesticides because such a technique does not require a light concentrating system and catalyst separation process after treatment. In the past, TFFBR has been used in many studies (Zayani *et al.*, 2009; Bahnemann *et al.*, 2004; Bickley *et al.*, 2005).

Details of the thin film reactor used in this study, how the catalysts were loaded onto the plates and the experimental conditions have been described in Section 3.4. A detailed description of the analytical techniques used to

quantify the degradation of the three pesticides studied was presented in Section 3.8. The research described in this chapter investigates and describes the performance of different catalysts (commercial P-25 TiO₂ and the synthesised TiO₂) and UV wavelengths on the three pesticides studied, in order to determine the effectiveness and optimal operation conditions for the TFFBR.

4.2. Aims and Objectives of TFFBR experiments

The objectives of this chapter are to determine and optimise the performance of the thin film fixed bed reactor (TFFBR) for the removal of pesticides from water. Experiments using the TFFBR were conducted by varying the experimental conditions to determine the optimum conditions for operation. Analysis of the treated pesticide solutions was conducted to determine the rate of reaction of the different pesticides. Full details of the experimental procedures used for the TFFBR and the analysis and quantification of the pesticides have been presented in Section 3.4. and Section 3.8, respectively.

- (i) Determination of the loss of pesticide from aqueous solution in the presence of catalyst, but absence of UV light.
- (ii) Determination of the photocatalytic rate of pesticide degradation in the presence of catalyst and UV irradiation.
- (iii) Evaluation of the influence of different feed flow rates and pesticide concentration on the rate of pesticide loss.

- (iv) Investigation of the pesticide removal performance of two different catalyst types on pesticides degradation.
- (v) Determination the effect of different UV wavelengths (UVA and UVC) on the rate of pesticide degradation.
- (vi) Comparison of the photocatalytic removal efficiency of each pesticide (isoproturon, simazine, and propazine).

4.3 Characterisation of the TiO₂ photocatalysts: Scanning Electron Microscope (SEM) image and Energy Dispersive X-ray Spectroscopy (EDAX) data

The SEM images of P-25 TiO₂ coated surface and the synthesised TiO₂ surface (Figures 3.5 and 3.6, respectively). It was observed at a magnification of 200 μm, particle size of the synthesised TiO₂ was much smaller than that of P-25 TiO₂ whereas there was a large agglomerate area in case of P-25 TiO₂. Figure 4.31 and Figure 4.32 show EDAX data and atomic composition of the P-25 surface and the synthesised surface, respectively. The data was collected after carrying out the experiments. This result proved that after photocatalytic reaction occurred, the structure of the surface of titania changed by reduction and oxidation reaction, based on photocatalytic reaction as a result of received photon energy from UVC. Ti²⁺ had been reduced to TiK as shown in Figure 4.1, the amount of TiK (Ti after losing electrons) was approximately 50 %.

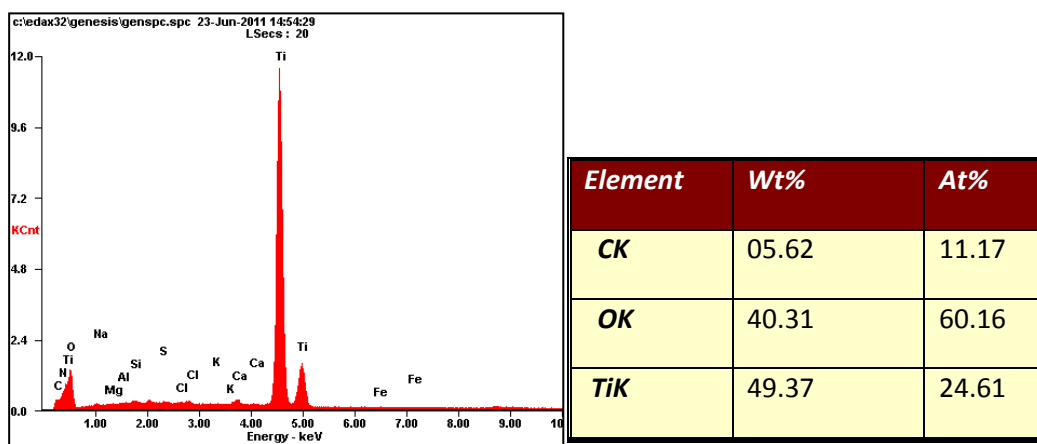


Figure 4.1 EDAX data of surface structure of 40 % wt of P-25 TiO₂ on TFFBR

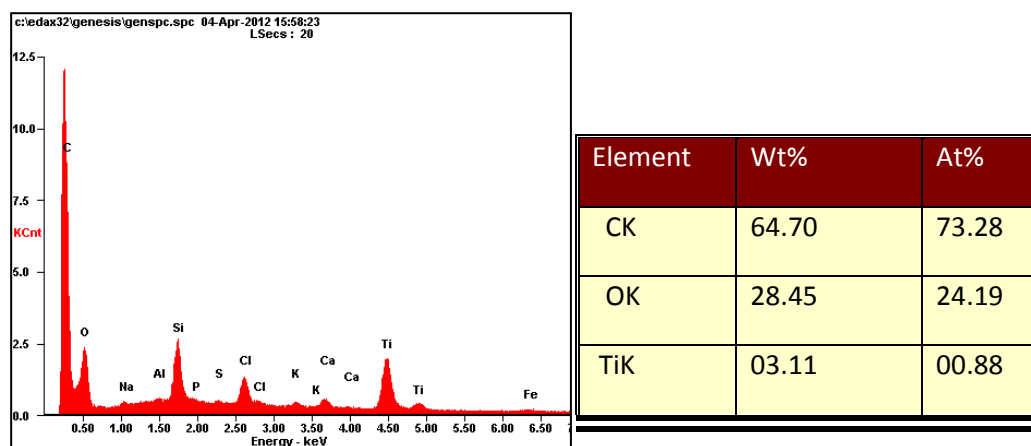


Figure 4.2 EDAX data of surface structure of 14 % wt of synthesised TiO₂ on TFFBR

In Figure 4.2, EDAX analysis shows the highest peak of the carbon atoms, as the impurities from DDSA molecules were added in the drying process, which led to TiK in the synthesised TiO₂ being drastically lower than the P-25 TiO₂ surface. The other reason why TiK was in lower amounts in the synthesised TiO₂ surface is due to the difference in the initial loading concentrations,

which was 40 % wt for P-25 TiO₂ coated on the stainless steel surface, whereas, there was only 14 % wt for the synthesised TiO₂ on the other plate.

4.4. Control experiments to determine the difference between photolysis and photocatalytic reaction

Prior to determining the influence of the different variables possible for the TFFBR, as described in the aims, it is important to conduct control experiments to determine the loss of any pesticides in the reactor by routes other than photocatalytic degradation by UV irradiation. An example would be losses from coating of the pesticide onto the surface of the catalyst and reactor. To determine these losses control experiments were conducted for the aqueous solutions at a concentration of 20 ppm of three selected pesticides; isoproturon, simazine, and propazine. The two different conditions used to determine the baseline rate of loss of the pesticides are as follows:

- (i) in the absence of UV or any light, but in the presence of TiO₂
- (ii) in the presence of UV, but in the absence of TiO₂

All the experiments were conducted separately but using the same TFFBR design (Chapter 3, Figure 3.2). All experiments were repeated 3 times to allow for the determination of standard errors which will determine the confidence level for comparison of the results between the different conditions. The error bars in the graphs were calculated by using the standard deviation and an average value of decreased concentration.

4.4.1 Determination of the rate of loss of pesticides in the absence of UV excitation but the presence of the presence of TiO₂

The control experiment was conducted without any UV irradiation. Solution of the three chosen pesticides (isoproturon, simazine, and propazine), with an initial concentration of 20 ppm at a flow rate of 20 ml min⁻¹, was fed on P-25 TiO₂ stainless steel plate. All experiments were conducted at room temperature over a total of 5 cycles; each cycle had a retention time of 1.35 min on the plate (Section 4.6).

Figure 4.3 shows the rate of loss of the three pesticides when flowing through the reactor in contact with P-25 TiO₂, but in the absence of UV light. Results are presented as a function of retention time versus concentration (in % of the original loading). The results show that the concentration of all pesticides decreased by approximately 10% after 7 minutes of contact with the TiO₂ surface. The rate of loss of the three pesticides appears to be similar and within the experimental error determined for each of the different molecules. It is proposed that, as these experiments were conducted in the absence of UV irradiation or any light source, these losses occurred as a result of absorption of the pesticides from the aqueous phase onto the surface of the TiO₂ catalyst. The significant loss of pesticide concentration (10 % of initial concentration) of the three pesticides (isoproturon, simazine, and propazine) through adsorption of the pesticide onto the surface of the catalyst is taken as the baseline for future experiments conducted in the presence of UV.

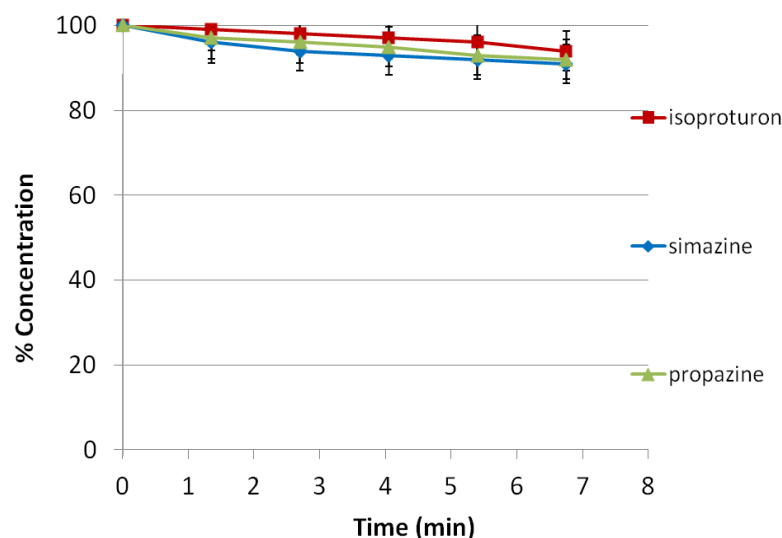


Figure 4.3 Remaining concentration (as a function of initial concentration), versus time plot for isoproturon, simazine and propazine over P-25 TiO₂ plate in the absence of UV irradiation (initial pesticide concentration = 20 ppm, flow rate = 20 ml min⁻¹)

4.4.2 Determination of the rate of loss of pesticides in the presence of UV irradiation without a TiO₂ catalyst.

It is also important to determine the influence of the catalyst on the rate of loss and degradation of the pesticides. This was achieved through a series of experiments conducted with UVA and UVC irradiation but without the presence of a catalyst. The results of these experiments are given in Figures 4.4, 4.5 and 4.6, which show the relative loss of isoproturon, simazine, and propazine over time when irradiated using UVA, as compared to UVC illumination. The rate of degradation of all pesticides is observed to be greater than for the experiments conducted with catalysts, but in the absence of any irradiation (Section 4.4.1). This indicates that UV irradiation results in the

degradation of the pesticides, even in the absence of a catalyst. This phenomenon has been reported previously and will be discussed in more detail later in this section. From the results it can be seen that the rate of pesticide degradation for all three pesticides studied, using UVC radiation, occurs at an apparently higher rate than with UVA. As in Section I.1 (Appendix I), the student T-test of UVA compared to UVC photolysis of isoproturon, simazine and propazine, showed that there was a significant difference of decreased concentration of three pesticides between UVA and UVC photolysis, since the probability for the two-tail test was higher than critical value (0.05). These results are consistent with previous findings (Legrinl *et al.*, 1993; Bhatkhande *et al.*, 2001; Hirahara *et al.*, 2001; Khor, 2004). Photolysis is generally triggered by the adsorption of light by the chemical compound; the most important factor affecting the UV photolysis is UV wavelength. This corresponds with the photon theory and can be explained by Planck's equation (Equation 2.23); the wavelength is inversely proportional to the energy. UVA wavelength is approximately 315-400 nm, whereas UVC wavelength is approximately 100-280 nm, as previously presented in Chapter 2, Section 2.11. Based on this theory, the shorter wavelength the higher the energy, resulting in more potential for increased activity and a higher probability of photocatalytic reaction. This theory is supported by a previous experimental study of photolysis and photocatalytic degradation of formaldehyde using silver titanium oxide in a cylindrical Pyrex reactor (Shei *et al.*, 2008). The proportion of formaldehyde degraded using UVC photolysis was approximately 60 % after 400 min, compared to 20% for UVA photolysis. Similar results were also reported for the photolysis of isoproturon, using an

annular photoreactor (Khor, 2004). This study reported that UVC photolysis reduced the isoproturon concentration by approximately 10% in an hour. In contrast, no isoproturon degradation was recorded when photolysis was conducted using UVA. A comparison of UVA photolysis and UVC photolysis and UVA-TiO₂ photocatalysis for the removal of 1, 4-dioxane and the natural (17 β -oestradiol, oestriol) and synthetic (17 α -ethynyloestradiol) oestrogens in water was carried out by Coleman *et al.*, (2007).

Results of this study demonstrated that degradation under UVC photolysis was far higher, equal to 100 % after 2 hours, which was significantly greater than UVA photolysis (30 % in 2 hours).

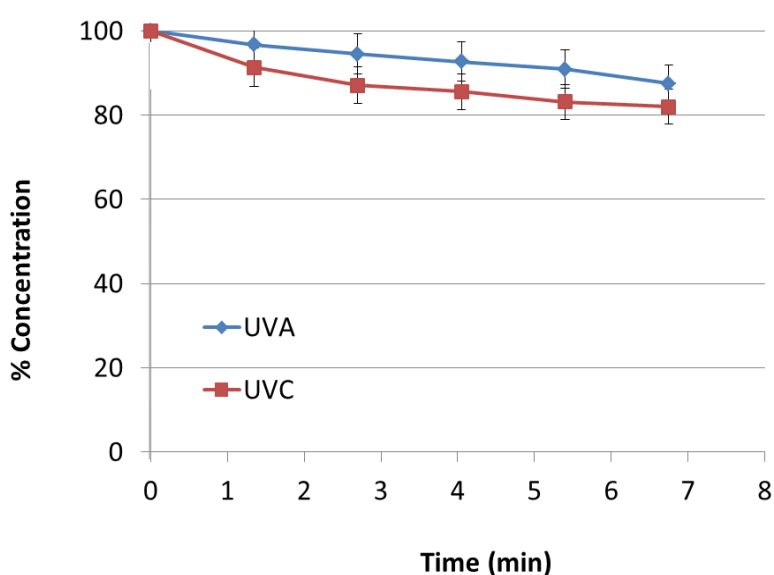


Figure 4.4 Remaining percentage after loss of isoproturon versus time: effect of light wavelength on the photolysis reaction (without catalyst), Initial concentration 20 ppm, flow rate = 20 ml min⁻¹

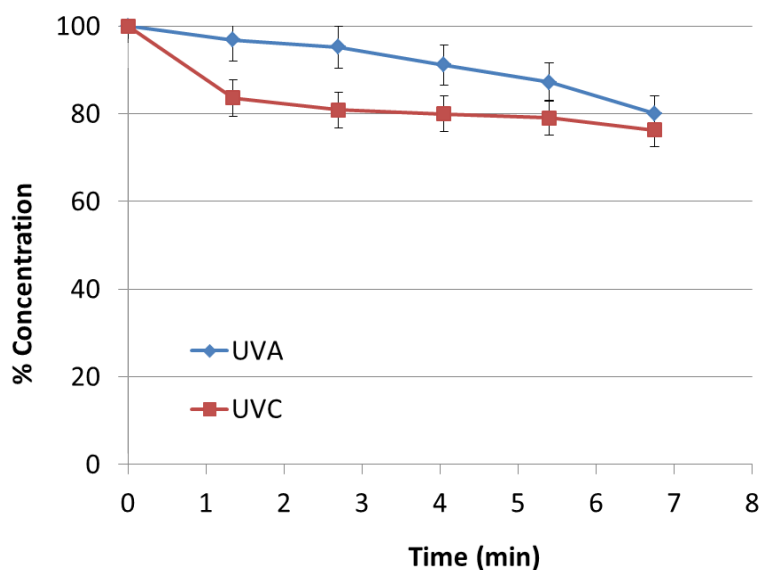


Figure 4.5 Remaining percentage after loss of simazine versus time: effect of light wavelength on the photolysis reaction of simazine (without catalyst). Initial concentration 20 ppm, flow rate = 20 ml min⁻¹

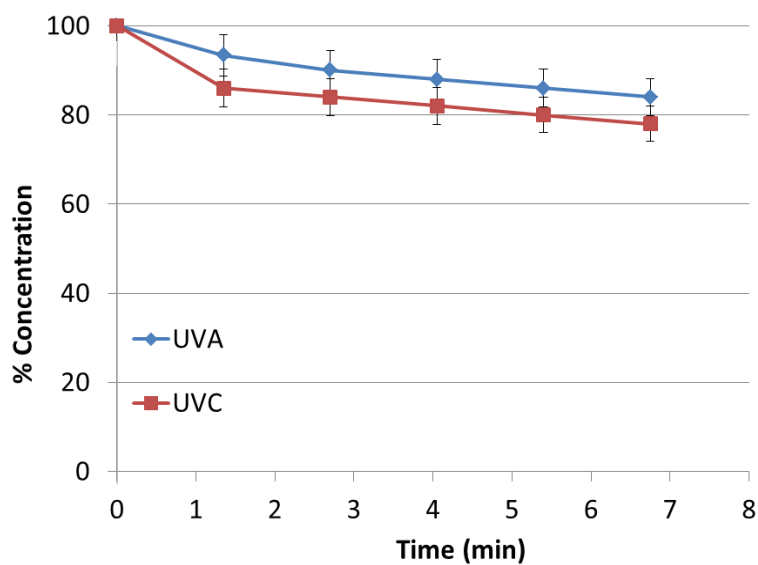


Figure 4.6 Remaining percentage after loss of propazine versus time: effect of light wavelength on the photolysis reaction of propazine (without catalyst). Initial concentration 20 ppm, flow rate = 20 ml min⁻¹

Amongst UVC photolysis of the three pesticides shown in Figure 4.7, the decreased concentrations of simazine and propazine due to photolysis were higher than isoproturon (approximately 20%). The set of average values and variance of data was shown in Section I.4-I.6 (Appendix I). From these results it can be assumed that photolysis of simazine and propazine was preferred when using TFFBR with UVC, which has a wavelength equal to 254 nm. Chu *et al.*, (2009) reported that the photolysis of simazine occurred at a faster rate when using UVC photolysis. The degradation concentration was approximately 90% in 5 minutes, which was higher than using TiO₂-photocatalytic, as shown in Figure 4.8. Also, there were the results obtained for simazine and atrazine by Comber (1999) that photolysis of simazine had been observed at approximately 300 nm or lower wavelengths. He found that even at natural sunlight, the intensity was sufficient to promote photolysis. That means some photolysis degradation of simazine and atrazine can occur under conditions of normal sunlight. In 2002 and 2004, the photolysis pathway of simazine was studied by many researchers (Evgenidou and Fytianos, 2002; Gunasekara, 2004). Photolysis affected molecule breakdown which leads to alkyl group loss and subsequent production of deisopropylatrazine (B) and diaminochlorotriazine (C), as shown in Figure 4.9.

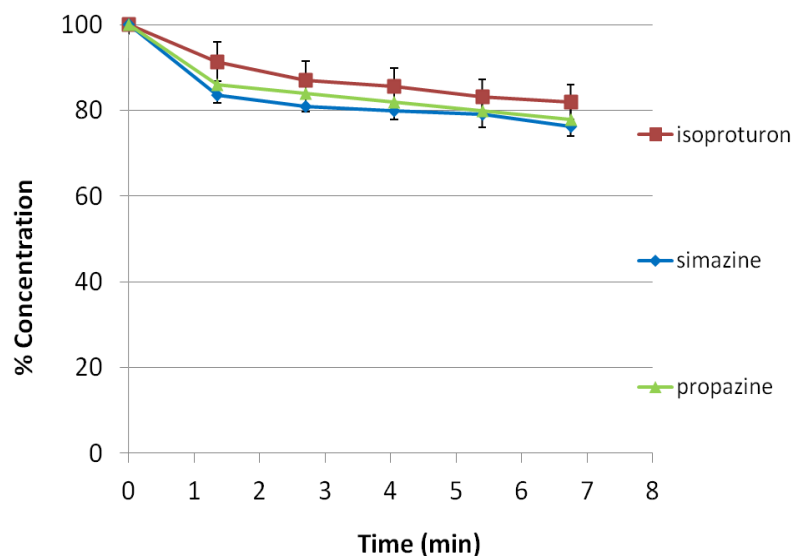


Figure 4.7 UVC photolysis on isoproturon, simazine, and propazine without any photocatalyst, initial concentration = 20 ppm, flow rate = 20 ml min⁻¹

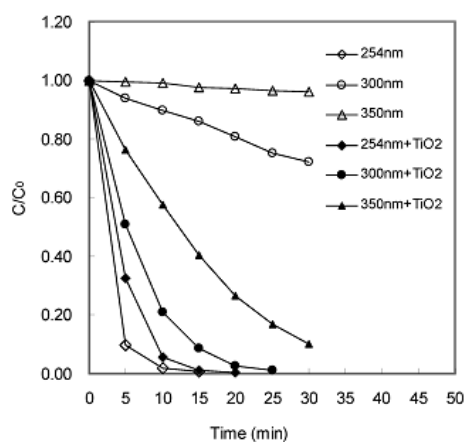


Figure 4.8 Simazine degradation by direct photolysis and photocatalysis. 8 UV lamps, initial simazine concentration was $2.5 \times 10^{-5} M$, TiO_2 dosage = 0.1 g litre⁻¹, and initial pH = 5.6. (Chu et al., 2009)

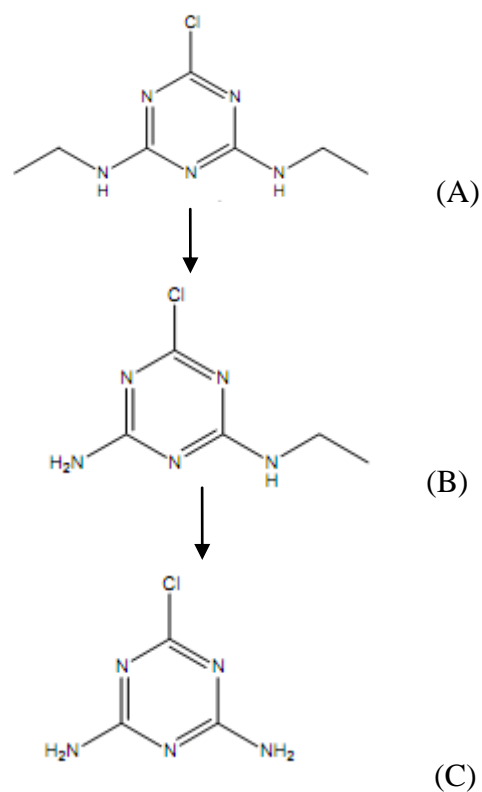


Figure 4.9 General degradation pathways of simazine (A) where (B) is deisopropyl atrazine and (C) is diamino chlorotriazine produced by photolytic loss of alkyl groups (Evgenidou and Fytianos, 2002, Gunasekara, 2004)

In summary, results from the control experiments show that

- (i) Experiments on the absence of light, but with a catalyst, result in a decrease in the concentration of all pesticides at a similar rate. This was proposed to be as a result of the pesticide coating on the surface of the catalyst. This loss should be considered in future experiments as the baseline against which photocatalytic degradation should be assessed.

(ii) Photolysis, reaction in the absence of a catalyst, occurs at a greater rate in UVC compared to UVA. Isoproturon was more stable compared to simazine and propazine. The reason why isoproturon has a different photolysis rate, when compared to simazine and propazine, was that it has a different functional group which is phenylurea, whereas simazine and propazine are triazine. The photolysis pathway of simazine and propazine are different from isoproturon. The main principle of photolysis of isoproturon is the hydroxylation of the aromatic ring in ortho and meta position of urea function, demethylation and methyl oxidation to obtain the formyl compound (Azizi *et al.*, 2013). However, in the case of simazine, photolysis affected molecule breakdown, which leads to alkyl group loss and subsequent production of deisopropyltriazine and diaminochlorotriazine. These results corresponding to the studies in the literature review (Comber, 1999; Chu *et al.*, 2009; Evgenidou and Fytianos, 2002; Gunasekara, 2004)

4.5 Photocatalytic degradation, effect of TiO₂ and the feed flow rate

In the previous sections, the rate of loss and degradation of the pesticides has been reported both with and without catalyst and UV light. Now that the baseline for these experiments with TFFBR has been established, it is possible to determine and compare the rate of degradation under photolysis and photocatalytic reaction conditions.

Figures 4.10 to 4.12 illustrate the rate of loss of isoproturon, simazine and propazine respectively under irradiation with UVA. Each of the figures

compare the rate of pesticide loss as a function of the presence of a catalyst (photolysis versus photocatalysis) and also the impact of flow rate of the pesticide solution. The influence of varying the feed flow rate from 100 ml min^{-1} to 20 ml min^{-1} was also compared in these experiments. Different results were observed for the different pesticides, with the loss of simazine (Figure 4.11) occurring at a faster rate than for the other two pesticides.

In most cases, the rate of loss of each pesticide was observed to occur at a faster rate in the presence of the TiO_2 catalyst. The influence of flow rate was observed to vary between pesticides. A similar rate of loss is observed for isoproturon (Figure 4.10) and propazine (Figure 4.12) for both the high and low flow rates. However, this trend again differed for simazine (Figure 4.11), where the high flow rate and reduced residence time reduced the amount of pesticide loss from the solution.

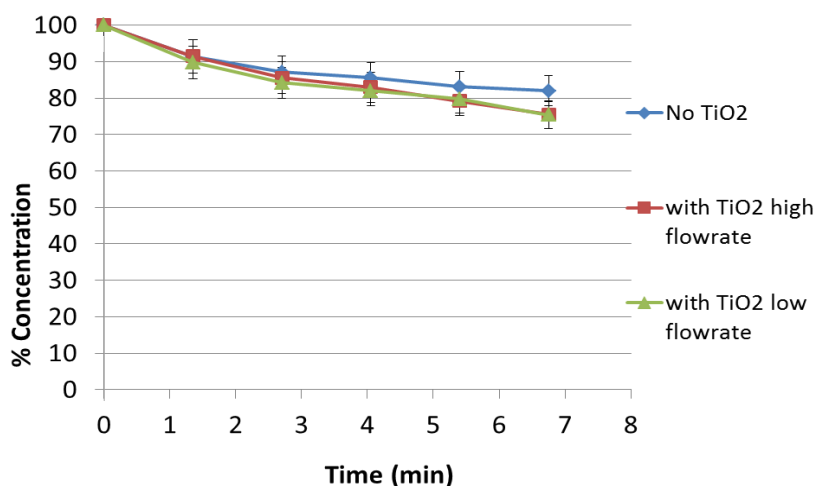


Figure 4.10 Degradation of isoproturon (initial concentration = 20 ppm) using P-25 TiO_2 under UVA with high and low flow rate (100 ml min^{-1} and 20 ml min^{-1} , respectively)

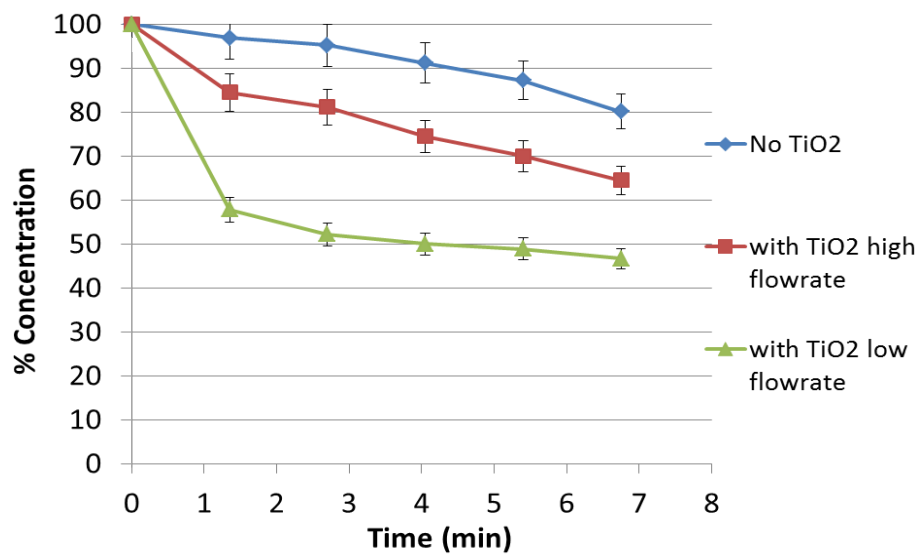


Figure 4.11 Degradation of simazine (initial concentration = 20 ppm) using P-25 TiO₂ under UVA with high and low flow rate (100 ml min⁻¹ and 20 ml min⁻¹, respectively)

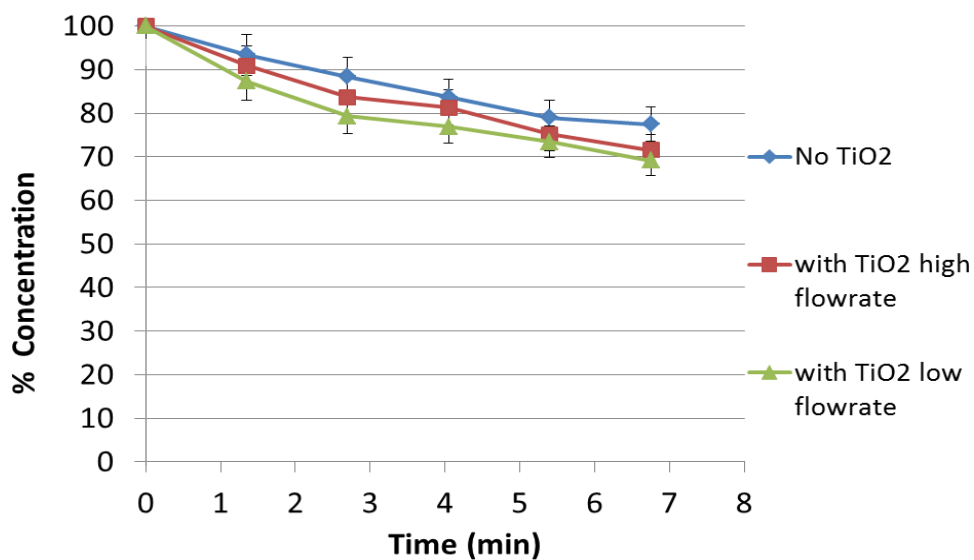


Figure 4.12 Degradation of propazine (initial concentration = 20 ppm) using P-25 TiO₂ under UVA with high and low flow rate (100 ml min⁻¹ and 20 ml min⁻¹, respectively)

The same experiments were conducted with irradiation by UVC (Figures 4.13 – 4.15). Similar trends were observed as for the UVA experiments as described previously, for example the greater degradation of simazine and the increase in reaction rate at decreased flow rate. Similarly to the photolysis experiments (Section 4.4.2) the rate of degradation of the pesticides is greater in the presence of UVC. These results and trends will be discussed in more detail in the following text.

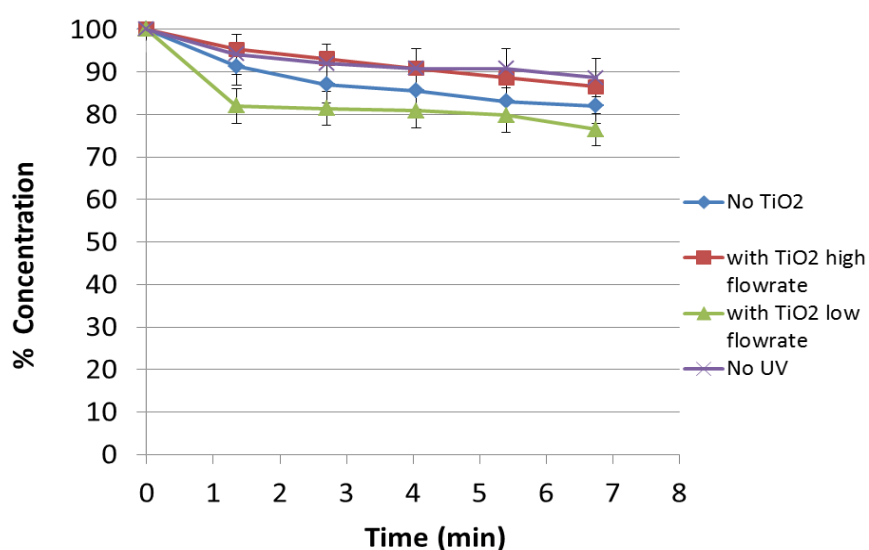


Figure 4.13 Remaining percentage after loss of isoproturon versus time (initial concentration = 20 ppm) using P-25 TiO₂ under UVC irradiation. High and low flow rate (100 ml min⁻¹ and 20 ml min⁻¹, respectively)

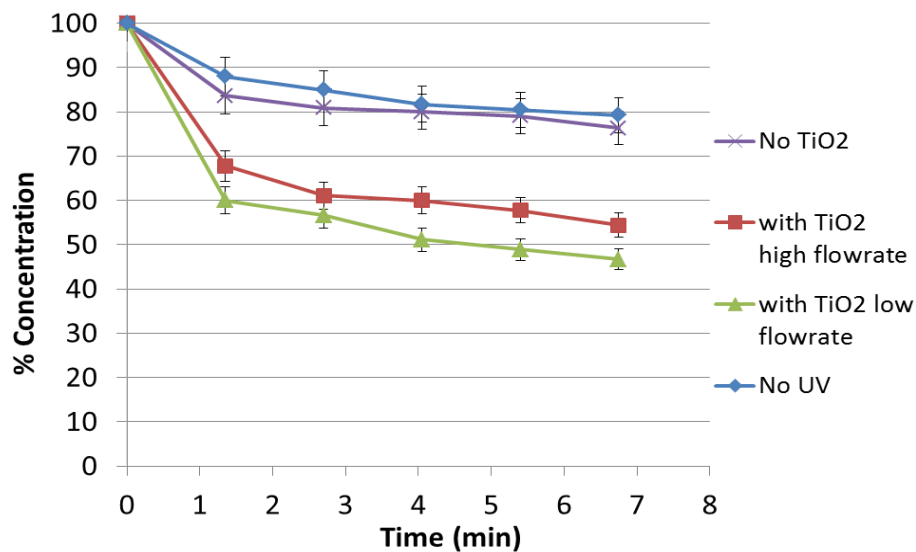


Figure 4.14 Remaining percentage after loss of simazine versus time (initial concentration = 20 ppm) using P-25 TiO₂ under UVC irradiation. High and low flow rate (100 ml min⁻¹ and 20 ml min⁻¹, respectively)

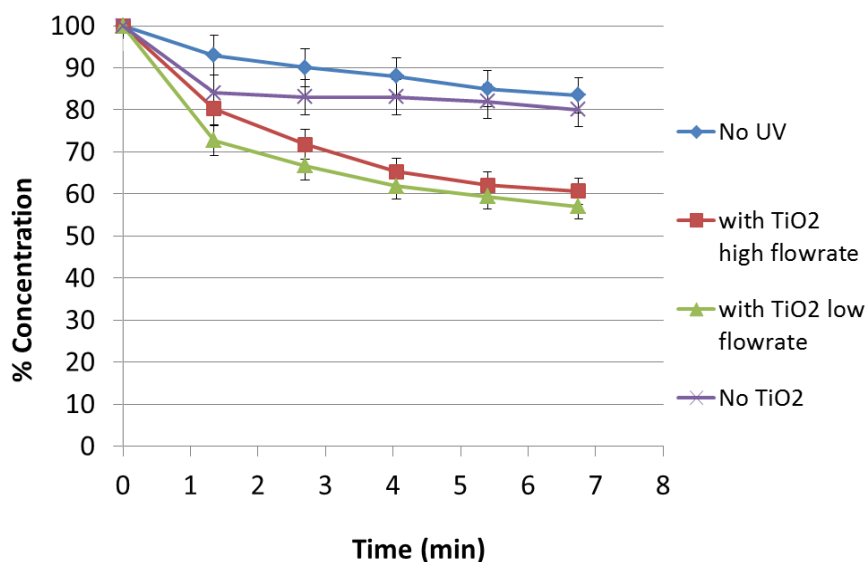


Figure 4.15 Remaining percentage after loss of propazine versus time (initial concentration = 20 ppm) using P-25 TiO₂ under UVC with high and low flow rate (100 ml min⁻¹ and 20 ml min⁻¹, respectively)

The flow rate of the pesticide solution was observed to influence the rate of degradation of most of the pesticides under both UVA and UVC. The student T-test for all sets of data was carried out and shown in Section I.10-I.15 (Appendix I). In general, degradation of the three pesticides occurred at a lower rate under a high feed flow, in comparison to a low feed flow rate. As the flow rate has a significant effect on the retention time of the pesticide on the catalyst bed, this is proposed to be the main cause of the difference in reactivity. The residence time can be calculated as follows:

Assume that layer of the solution = 0.1 cm

Dimension of the plate: length = 12 inch, width = 3.5 inch

Total volume of the solution on the top of plate

$$= 12 \times 2.54 \times 3.5 \times 2.54 \times 0.1 = 27 \text{ cm}^3$$

$$\text{Retention time per cycle} = \frac{\text{total volume}}{\text{flow rate}} = \frac{27 \text{ cm}^3}{20 \text{ ml/min}} = 1.35 \text{ min}$$

The shorter residence time on the bed at a high flow rate leads to a reduced probability of photocatalytic. This is an important consideration for the future design of photocatalytic bed reaction systems, in terms of optimising the bed size and flow rate to maximise the rate of pesticide degradation. A similar relationship between residence time and rate of degradation has been previously reported by Khan *et al.*, (2012) in a series of degradation experiments of the aquaculture pathogen, *aeromonas hydrophila*, using P-25

TiO₂ coated on a pilot scale TFFBR. The researchers varied 3 values of water flow rate (4.8 litre hr⁻¹, 8.4 litre hr⁻¹ and 16.8 litre hr⁻¹) under the sunlight intensity ranging from 300-1200 w m⁻². When comparing the low (4.8 litre hr⁻¹) and high (16.8 litre hr⁻¹) water flowrates, the highest photocatalytic activity was observed at the low flow rate, being twice that observed at the high flow rate. Li Puma (2003) proposed a thin-film slurry photocatalytic reactor to be affected by radiation scattering. It was proposed that, at the higher water flow rate, the falling film changed from laminar flow to turbulent flow. Therefore, in the case of a water falling film, laminar flow has a different flow configuration than that of the turbulent flow, resulting in a different film thickness. The Reynolds number is different at each position on the plate. Figure 4.16 is based on the assumptions that (i) water has constant physical properties (Newtonian fluid), (ii) catalyst particles were uniformly distributed on the surface (iii) the concentration of solids is not high enough to cause substantial changes in the rheological properties of water.

In this thesis, the TFFBR was used, which is different from the reactor used in Li Puma's research. However, this based on the assumptions above that consider as only fluid/water flow. When the flow rate is higher, the residence time is shorter (as per the calculation above). Flow regime will change from laminar to turbulent flow (as defined in Li Puma, 2003) when the Reynolds number is higher than 2000. This results in a complex direction leading to higher shear stress and pressure loss, as shown in Figure 4.17

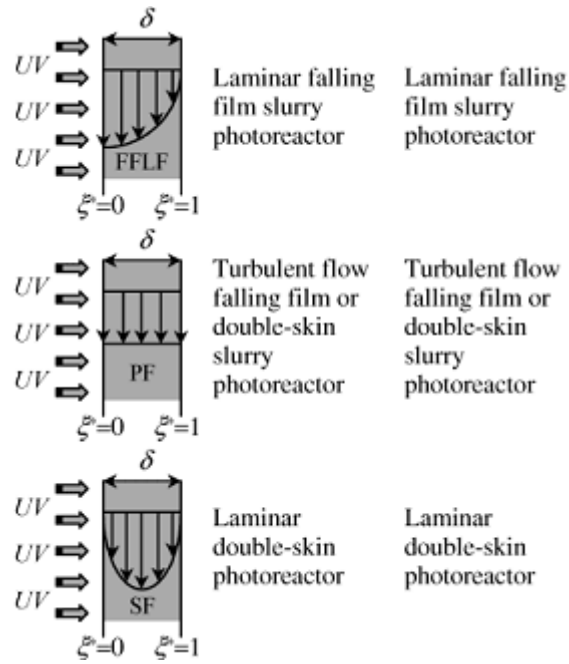


Figure 4.16 Different flow structure (a) FFLF is falling film laminar flow, (b)PF is plug flow, and (c) SF is slit flow (δ and ξ related to dimensionless Reynolds number, $\xi^* = \xi/\delta$) (Li Puma, 2003)

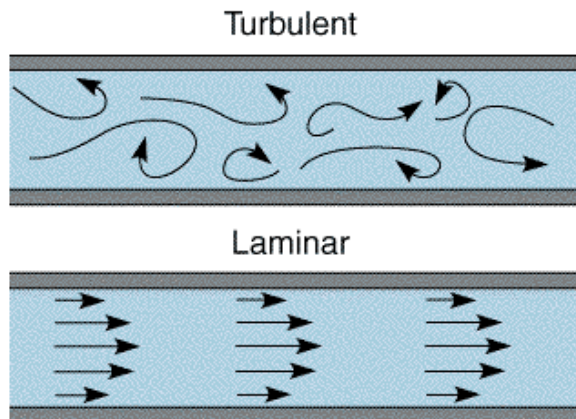


Figure 4.17 The difference between laminar flow and turbulent flow

Under both low and high flow rate conditions, isoproturon is seen to be the most stable molecule (Figures 4.18 and 4.19). Simazine and propazine are lost to a similar degree at high flow rates (Figure 4.18), whilst the loss of simazine is greater at low flow rates (Figure 4.19). The results obtained at high feed and low feed flow rate give a different order of reactivity for the three pesticides, in comparison to photocatalytic studies using a range of reactors (discussed later in Chapters 5 and 6). In the review of literature, the stability of the three pesticides were reported to decrease in the following order (as the remaining % of initial concentration after 15 minutes): isoproturon 50% < simazine 75% < propazine 90% (Gora *et al.*, 2006). In Figure 2.11, Gora and co-workers carried out the experiment of single pesticide component using annular photocatalytic system and discovered that the highest photocatalytic reaction rate belonged to isoproturon by L-H kinetics.

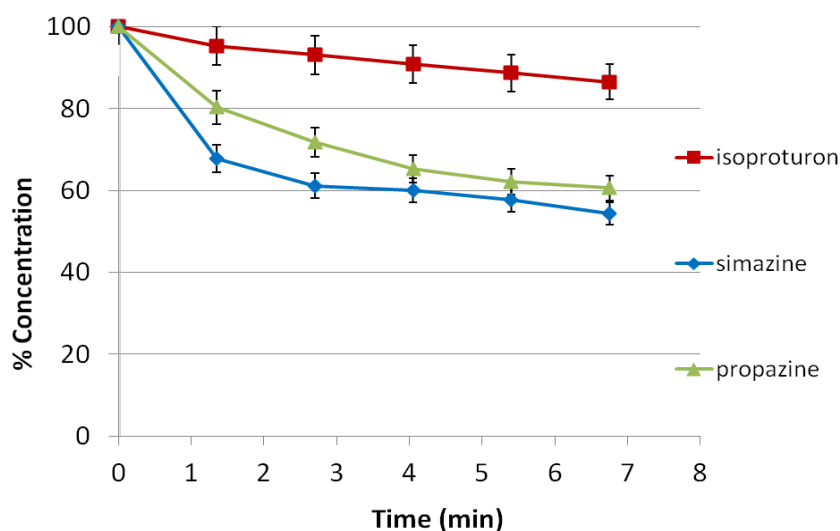


Figure 4.18 Comparison of photocatalytic degradation of three pesticides at high flow rate (initial concentration = 20 ppm) using P-25 TiO₂ under UV

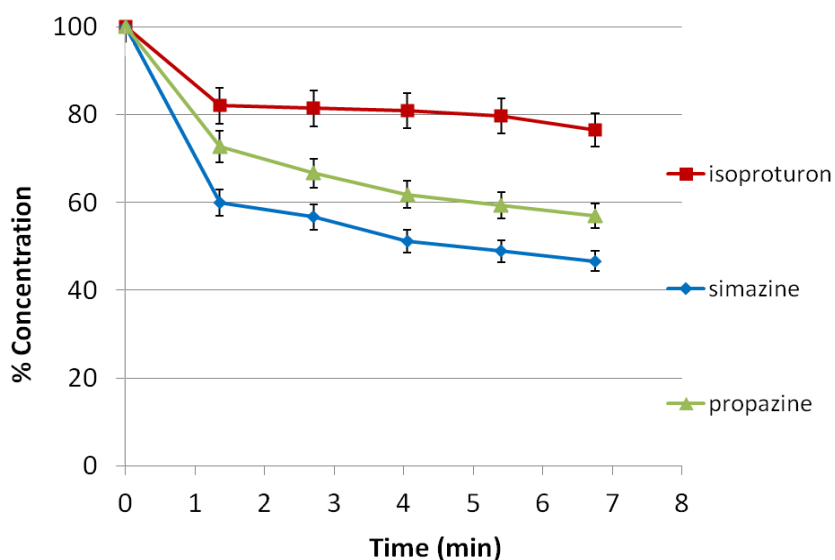


Figure 4.19 Comparison of photocatalytic degradation of three pesticides at low flowrate (initial concentration = 20 ppm) using P-25 TiO₂ under UVC

4.6 Influence of the initial pesticides concentration

A further variable to explore is the effect of the initial concentration of the pesticide in solution entering the reactor. To achieve this a series of experiments was conducted with isoproturon, and propazine at low concentration of 2.5 ppm over the same P-25 TiO₂ coated stainless steel plate with UVC illumination. With P-25 TiO₂ under UVC at low concentration of pesticides (2.5 ppm), there were substantial decreases in isoproturon and propazine concentrations of about 50 % after 7 minutes, as shown in Figure 4.18 and Figure 4.21. For non-UV and without TiO₂ experiments, the decrease of the concentrations at low initial pesticide concentration appeared to be only 20 % of the initial pesticide concentration and showed a similar trend as at high (20 ppm) pesticide concentration.

Figure 4.20 and Figure 4.21, show the results when the initial concentration of both isoproturon and propazine are lower. As compared to the data in Figure 4.13 and 4.15, the photocatalytic degradation of isoproturon and propazine under UVC, at 2.5 ppm initial concentration, was higher than 20 ppm initial concentration. The table of average, variance and T-test was shown in Section I.16-I.17 (Appendix I). These results are in agreement with the theory explained by Langmuir-Hinshelwood (L-H) kinetics, presented in Section 2.11. It is proposed that there is an optimum initial concentration of a compound to maximise the photocatalytic rate. It has previously been reported that, for isoproturon, simazine and propazine, the rate of degradation does not improve with the excess initial concentration (Figure 2.10, Gora *et al.*, 2006). Khor (2004) studied the effect of the initial isoproturon concentration on the TiO₂ photocatalytic rate, over a range of 1-8 ppm. This study showed a linear relationship between the photocatalytic rate and initial isoproturon concentration. However, when employing a 20 ppm initial concentration, the intermediates concentration is also significantly high and influences the rate of reaction. Therefore, Equation (2.17) will be changed as follows:

$$-r = \frac{kKC}{1 + KC + \sum_{i=1}^n K_i C_i} \quad \text{with } i = 1, 2, \dots, n \quad (4.1)$$

where *i* is the number of intermediates formed during degradation.

When more intermediates are formed at higher initial pesticide concentration, a competitive adsorption on the surface of the catalyst occurred, which leads

to a decrease of reaction rate, as described by Equation 4.1 (Khor, 2004, Li Puma *et al.*, 2007, Toepfer *et al.*, 2006).

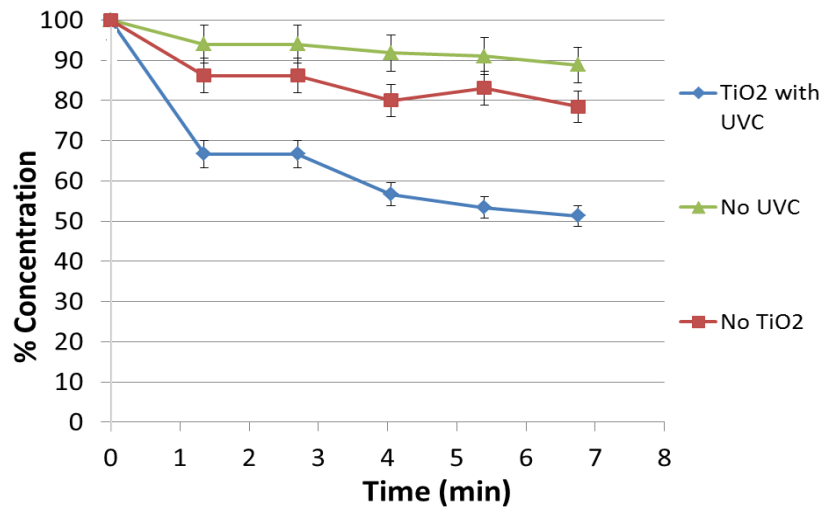


Figure 4.20 Remaining percentage after loss of isoproturon versus time (initial concentration = 2.5 ppm) using P-25 TiO₂ under UVC with low flow rate

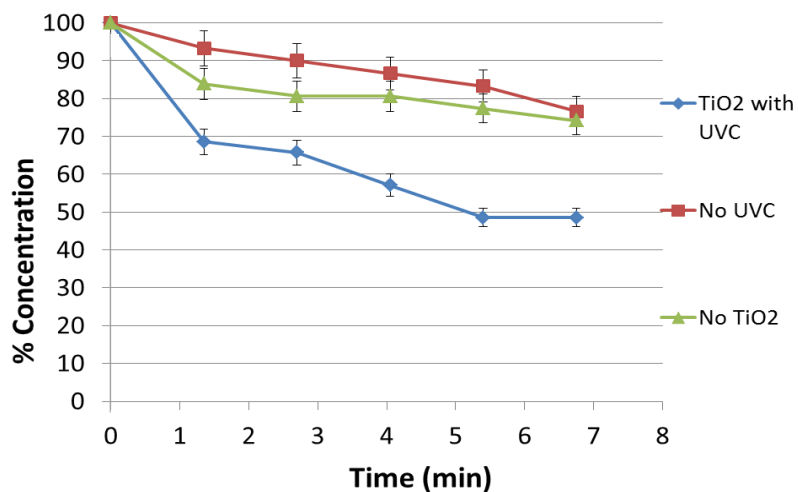


Figure 4.21 Remaining percentage after loss of propazine versus time (initial concentration = 2.5 ppm) using P-25 TiO₂ under UVC with low flow rate

4.7 Influence of photocatalyst type, comparison of commercial P-25 with TiO₂ synthesised in supercritical water

In this section, the performance of the synthesised TiO₂ coated plate was analysed in comparison to the plate coated with commercially available P-25 TiO₂. Comparison between the performance of the commercial P-25 catalyst and TiO₂, synthesised using supercritical water hydrothermal synthesis (ScWHS) (Section 3.3), was achieved by performing experiments under identical conditions. The synthesised TiO₂ was coated on the stainless steel plate using the same process as previously (Section 3.4.1). The first plate was loaded with P-25 TiO₂ at approximately 40 % wt on the stainless steel plate. However, the loading amount of synthesised TiO₂ on the second plate was lower, equal to 14 %. Experiments were conducted with two initial pesticide concentrations, 20 ppm (high concentration) and 2.5 ppm (low concentration). Photocatalytic degradation was performed under both UVA and UVC irradiation with a feed flow rate at 20 ml min⁻¹.

The performance of the two different catalysts studied varied between different pesticides and their initial concentration in the aqueous solution. The remaining concentration of the pesticides, after using the synthesised TiO₂, was calculated per gram of photocatalyst and plotted to compare the photocatalytic efficiency with P-25.

The degradation of isoproturon was observed to be similar for both catalysts under the conditions studied (Figures 4.22 – 4.25). Taking into account the experimental errors and uncertainty for the different conditions explored (concentration, UVA or UVC), the performance of the catalyst can be

assumed to be similar for the duration of the experiments studied. Isoproturon was shown to be the most resistant to photocatalytic degradation for this reactor (see Section 4.5). Given the low rate of loss of this pesticide during both photolysis and photocatalytic experiments, the difference in performance of the catalyst are not that surprising.

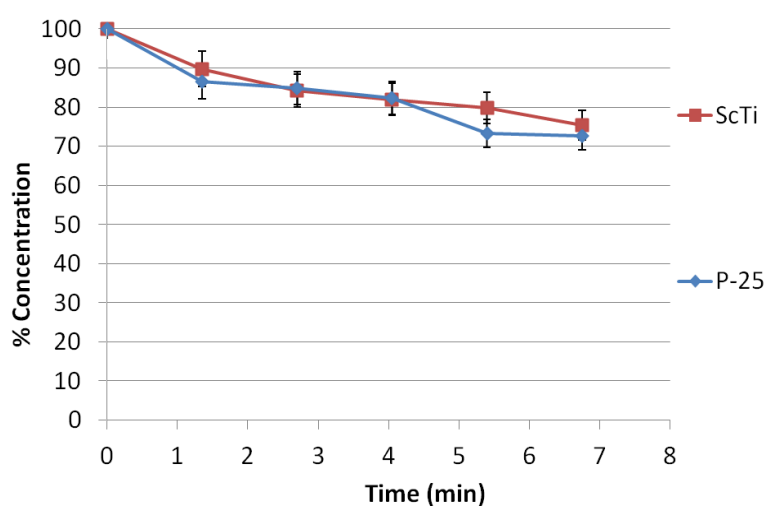


Figure 4.22 Remaining percentage (per gram of catalyst) after loss of isoproturon versus time (initial concentration = 20 ppm) under UVA using P-25 TiO_2 comparing to synthesised TiO_2

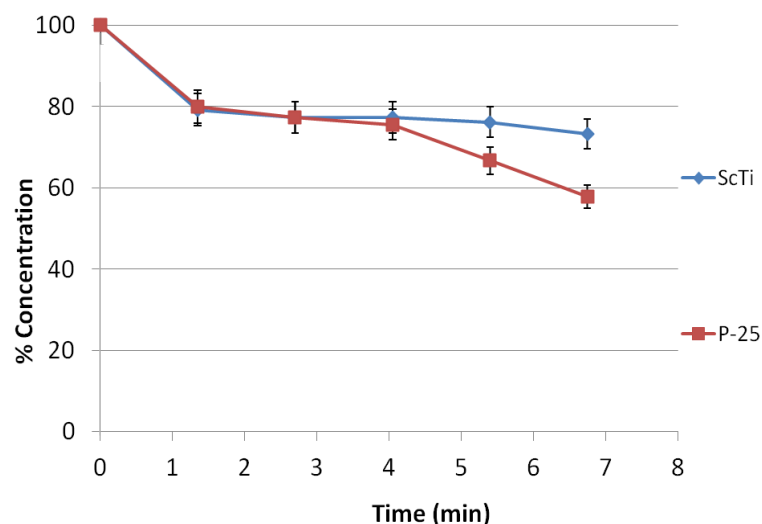


Figure 4.23 Remaining percentage (per gram of catalyst) after loss of isoproturon versus time (initial concentration = 2.5 ppm) under UVA using P-25 TiO₂ comparing to synthesised TiO₂

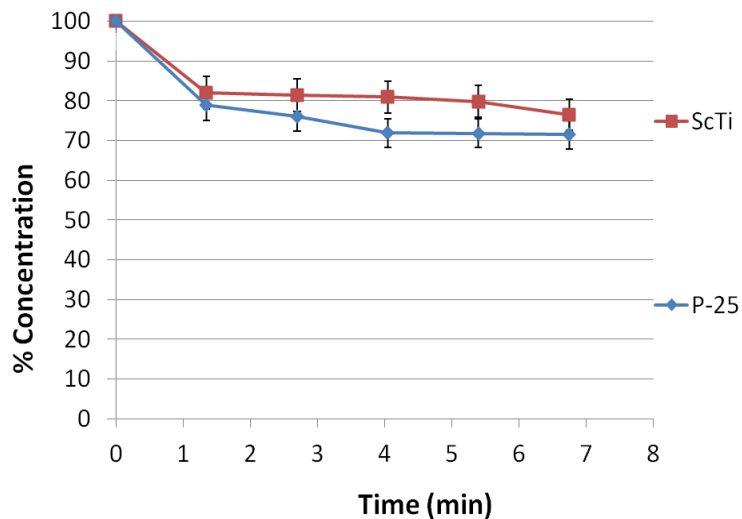


Figure 4.24 Remaining percentage (per gram of catalyst) after loss of isoproturon versus time (initial concentration = 20 ppm) under UVC using P-25 TiO₂ comparing to synthesised TiO₂

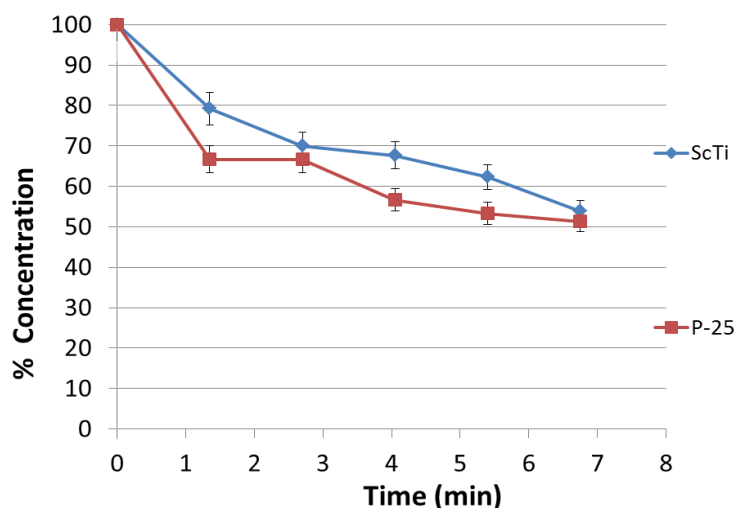


Figure 4.25 Remaining percentage (per gram of catalyst) after loss of isoproturon versus time (initial concentration = 2.5 ppm) under UVC using P-25 TiO₂ comparing to synthesised TiO₂

For TFFBR, simazine was found to be more reactive under photocatalytic conditions when compared to isoproturon. Under UVA or UVC illumination, the supercritical water synthesised TiO₂ had lower photocatalytic efficiency when compared to P-25 for degrading the pesticide (Figure 4.26 and 4.27). The largest difference in performance was recorded for the high (20 ppm) concentration of simazine under UVC conditions, where P-25 resulted in significantly greater degradation of the pesticide (approx. 50%) when compared to the synthesised catalyst (20%, Figure 4.26). The decrease in the concentration of simazine was no greater than observed for the photolytic degradation of the pesticide under UVC (Figure 4.5). These results suggest that over the duration of the experiments conducted, synthesised TiO₂ catalyst

has little activity. This effect was less pronounced in the case of a low concentration (2.5 ppm) of simazine

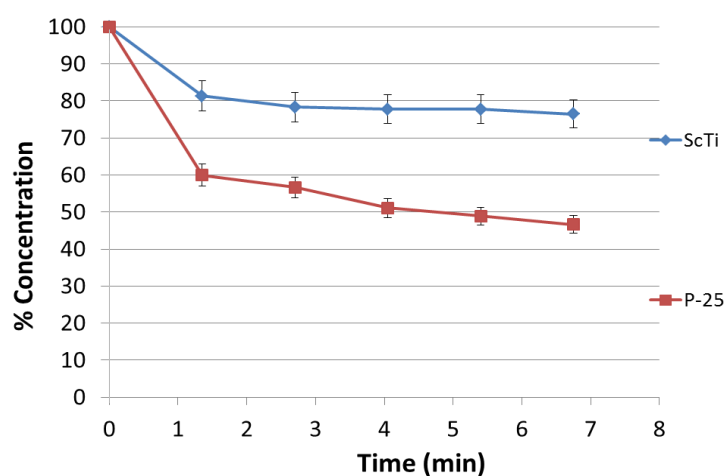


Figure 4.26 Remaining percentage (per gram of catalyst) after loss of simazine versus time (initial concentration = 20 ppm) under UVC using P-25 TiO_2 comparing to synthesised TiO_2

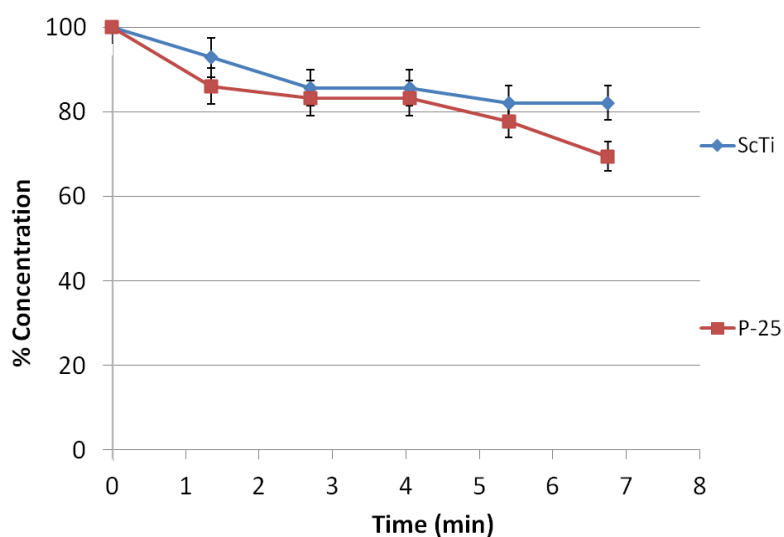


Figure 4.27 Remaining percentage (per gram of catalyst) after loss of simazine versus time (initial concentration = 2.5 ppm) under UVC using P-25 TiO_2 comparing to synthesised TiO_2

Figures 4.28 to 4.31 show photocatalytic degradation of propazine under different conditions, after using the synthesised TiO₂ as compared with P-25 TiO₂. In the case of propazine, the results differed from those of simazine and isoproturon degradation under UVC and UVA. The assumption was made why the decrease of the concentration of propazine, after using the synthesised TiO₂, was higher than after using P-25 TiO₂. In the case of the synthesised TiO₂ plate, dodecanyl succinic anhydride (DDSA), a curing epoxy agent, was added onto the stainless steel plate during drying process before experiments. The structure of DDSA can be defined as surfactant (composed of non-ionic and anionic part) which was a hydrophilic copolymer. As shown in Figure 4.32, the non-ionic part composed of nonpolar hydrocarbon chain, which has the number of carbon atoms nearly equal to that of propazine. Therefore, the polarity of DDSA and propazine are compatible, leads to London dispersion force (intermolecular attraction of nonpolar molecules) between DDSA and propazine. This can be confirmed by research conducted by Matveeva *et al.*, (1997) who studied the reverse micelle system, n-octane containing reverse micelles of sodium bis (2-ethyl-hexyl) sulfosuccinate in binding with hydrophobic pesticide propazine. They found that the removal concentration of propazine, by using reverse micelles of sodium bis (2-ethyl-hexyl) sulfosuccinate, was up to 42 %. This study proves that there is the possibility of using nonpolar organic solvents to extract propazine. Therefore, this discovery confirms that the reason why high concentration loss occurred in propazine experiments using the synthesised TiO₂-coated plate could be due to high removal of propazine by DDSA molecules, a main polymer in the curing agent.

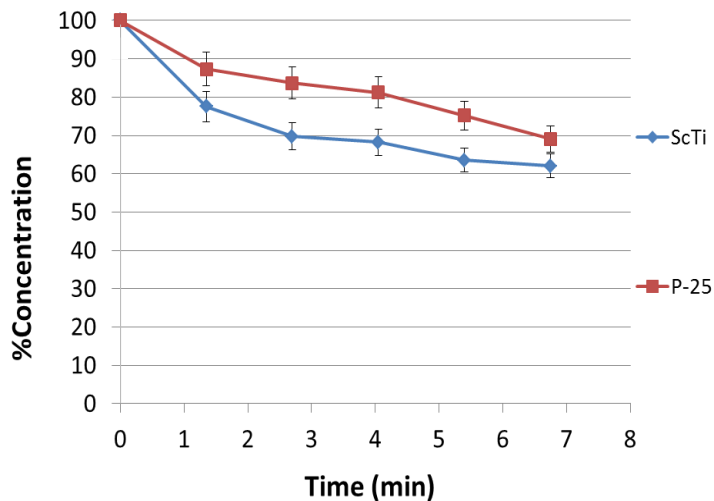


Figure 4.28 Remaining percentage (per gram of catalyst) after loss of propazine versus time (initial concentration = 20 ppm) under UVA using P-25 TiO₂ comparing to synthesised TiO₂

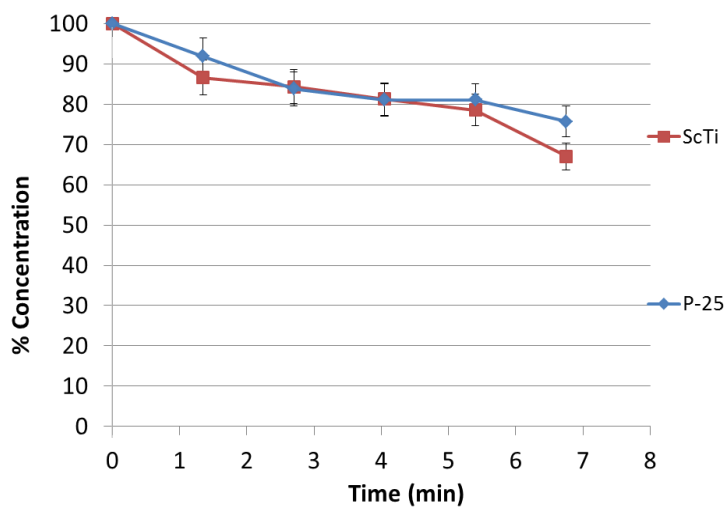


Figure 4.29 Remaining percentage (per gram of catalyst) after loss of propazine versus time (initial concentration = 2.5 ppm) under UVA using P-25 TiO₂ comparing to synthesised TiO₂

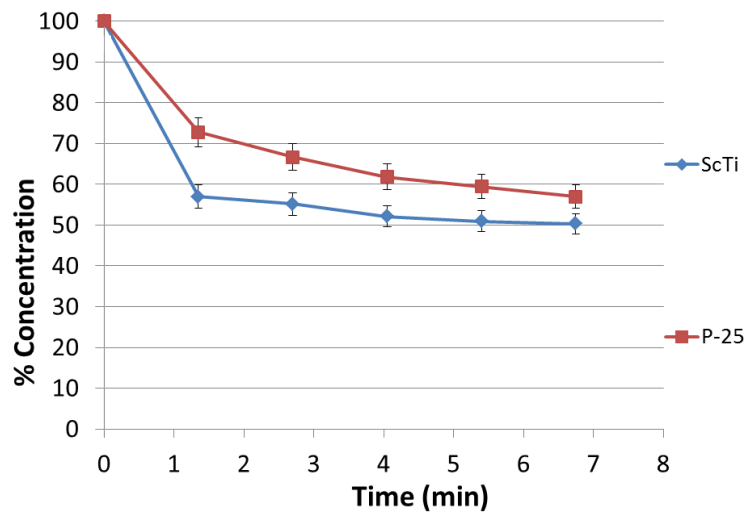


Figure 4.30 Remaining percentage (per gram of catalyst) after loss of propazine versus time (initial concentration = 20 ppm) under UVC using P-25 TiO_2 comparing to synthesised TiO_2

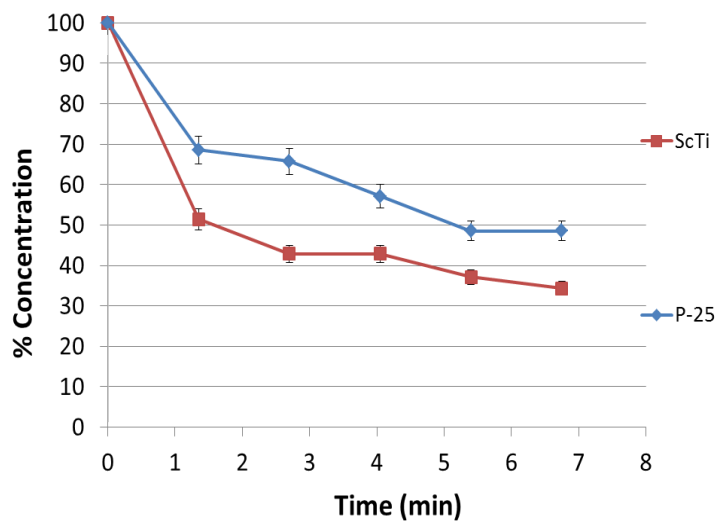


Figure 4.31 Remaining percentage (per gram of catalyst) after loss of propazine versus time (initial concentration = 2.5 ppm) under UVC using P-25 TiO_2 comparing to synthesised TiO_2

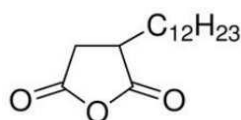


Figure 4.32 Structure of dodecyl succinic anhydride (DDSA)

4.8 Conclusions of TFFBR experiments

All the results from TFFBR were discussed in this chapter. The experiments were carried out under controlled conditions, in the presence of TiO_2 but absence of UV. There was an overall loss of 10% of pesticide concentration (isoproturon, simazine and propazine) due to adsorption onto the TiO_2 surface. However, when adding TiO_2 under UV illumination, the photocatalytic reaction appeared and showed a higher degradation rate than in the case of only UV photolysis (without TiO_2). It can be concluded that TiO_2 was one of the main factors exerting a significant effect on the photocatalytic rate. The other factors are feed flow rate, pesticide concentration, type of catalyst and UV wavelength. At low feed flow rate (20 ml min^{-1}), the degradation concentration was higher due to a longer residence time for photocatalytic reaction. According to the L-H model, the high initial concentration of pesticides between 1-8 ppm (in this thesis, the initial concentration of pesticides = 2.5 ppm) leads to a higher photocatalytic reaction rate. However, in excess of the initial concentration, at 20 ppm, the photocatalytic reaction rate is lower due to high amounts of intermediate competitive adsorption on the TiO_2 surface. The synthesised TiO_2 from supercritical water hydrothermal synthesis (ScWHS) had no potential in photocatalytic treatment, as compared

to the commercial TiO₂, since the results with or without the synthesised catalyst were similar. The possible reason for this similarity was then addressed in the EDAX analysis, indicating that the synthesised TiO₂ had considerably high impurities, as compared to P-25 TiO₂. UVC showed higher photolysis and photocatalytic rates than UVA, since UVC has a shorter wavelength (254 nm) when compared to UVA (365 nm). TiO₂ absorbs light at lower wavelength better than at higher wavelength; this fact also related to Planck's Equation that the shorter wavelength corresponds to higher photon energy. For this reactor, amongst the three pesticides, simazine degraded the most as was seen in both the photolysis and photocatalytic degradation results, under UVA and UVC, using a P-25 TiO₂ plate.

Chapter 5

PHOTOCATALYTIC DEGRADATION OF PESTICIDES USING A STIRRED PHOTOREACTOR

5.1 Introduction to stirred photoreactor results

This chapter discusses all the results of pesticide degradation experiments carried out in the stirred reactor, a small-scale reactor which works under UV irradiation, as previously described in Section 3.5. The stirred reactor is suitable for small scale experiments, in order to study the photocatalytic reaction and the influencing parameters, prior to designing a pilot plant or large scale reactor. Although the volume size of sample, per experiment, is a small amount compared to other systems, the efficiency is sufficient to understand the photocatalytic reaction under difference conditions. It has full UV irradiation as lamp alignment is in the middle and the container is made of quartz and placed under an 8 watt UV lamp, as shown in Figure 3.7. The container held 200 ml of isoproturon, simazine and propazine solution. TiO₂ photocatalyst was used at different types and at different concentrations (0.5, 1, 2.5, 5, 10 g litre⁻¹). The magnetic stirrer at 900 rpm was used in this system

to achieve good mixing, leading to a high contacting area between catalyst molecules and pesticides.

This chapter is divided into 4 parts and investigates: the effect of catalyst concentration on the photocatalytic degradation, effect of catalyst types on the photocatalytic degradation, and adsorption of isoproturon, simazine and propazine onto P-25 TiO₂ surface under the absence of UV.

The experimental technique used with the stirred reactor was performed as a simple batch system with the commercial P-25 TiO₂ and the synthesised TiO₂. A detailed description of the experimental set-up was provided in Section 3.5. For comparison, an in-house synthesised TiO₂ was prepared by using supercritical water hydrothermal synthesis (ScWHS) (Section 3.2 and Section 3.3). The decreased concentration of isoproturon, simazine and propazine were then evaluated using high performance liquid chromatography (HPLC) (Section 3.7.1 and Section 3.8).

5.2 Aims and Objectives

The stirred reactor was used in this chapter to study the effects of various operation parameters on the photocatalytic reaction. The principal aim of this chapter is to understand the rate of the photocatalytic reaction and investigate the degradation mechanism. The other aims of this chapter are to find the most appropriate concentration of P-25 TiO₂ and to investigate the photocatalytic performance of the synthesised TiO₂.

The main objectives of this chapter are as follows:

- (i) Determination of the influence of P-25 TiO₂ concentration on the photocatalytic degradation and optimisation of the most appropriate P-25 TiO₂ concentration.
- (ii) Determination of the influence of catalyst types on photocatalytic degradation (commercial P-25 TiO₂ and the synthesised TiO₂).
- (iii) Evaluation of the pesticide concentration adsorbed on TiO₂, under the absence of UV.
- (iv) Explain the photocatalytic reaction and mechanism in terms of the reaction law and relate the results to the Langmuir–Hinshelwood (L–H) theory (Section 2.11).

5.3 Control experiments to determination the rate of pesticide loss in the absence of UV but the presence of TiO₂

To determine if loss of the pesticides occurred within the reactor as a result of coating of the surfaces of the catalyst or reactor, a series of experiments were conducted in the reactor in the presence of the P-25 TiO₂ catalyst, but without UV irradiation. All three pesticides, isoproturon, simazine, and propazine, were analysed in order to determine whether the adsorption of the pesticide onto the catalyst plays any role in the rate of pesticide loss. Figure 5.1 shows the amount of loss of the three pesticides in the reactor. In all cases, there was an apparent decrease of 5-10 % in the concentration of the pesticide in solution. There was no statistical difference in the loss concentration among the three pesticides, as shown in student T-test in Appendix II. This decrease

suggests that there is some adsorption of the pesticides onto the surface of the P-25 TiO₂ catalyst. This observation agrees with previous studies of isoproturon in a stirred photoreactor containing 0.4 g litre⁻¹ of the TiO₂ in suspension (Khor, 2004). A similar amount of isoproturon was adsorbed onto the catalyst, as shown in Figure 5.2. This led to the loss of approximately 0.15% of the initial pesticide concentration for an initial concentration of isoproturon equal to 3 ppm. In the experiments here presented, when using P-25 TiO₂ at the highest concentration of 5 g litre⁻¹ with an initial concentration of isoproturon 2.5 ppm, the adsorption was lower than 10 %. There was a study carried out by Gora and co-workers (Gora *et al.*, 2006) that investigated the dark adsorption (in the absence of UV but the presence of P-25 TiO₂) of isoproturon onto TiO₂. They explained that in the initial concentration range of up to approximately 3 mg litre⁻¹, isoproturon molecules were adsorbed to be a mono layer, a result which fitted with Langmuir's model, Equation (5.1). When the concentration increased, there was a multilayer adsorption allowing a larger coverage onto TiO₂.

$$\frac{C_{eq}}{q} = \frac{1}{q_{max}} + \frac{C_{eq}}{K_{dark} q_{max}} \quad (5.1)$$

q = number of moles of herbicide adsorbed per gram of TiO₂ (mol g⁻¹)

C_{eq} = herbicide equilibrium concentration (mol litre⁻¹)

q_{max} = the maximum number of herbicide molecules that can be adsorbed as a monolayer onto a gram of TiO₂ (mol g⁻¹)

K_{dark} = the binding constant observed under dark adsorption (litre mol^{-1})

In future experiments, it is important to consider that approximately 5% loss of each of the pesticides will occur as a result of adsorption of the pesticide onto the catalyst.

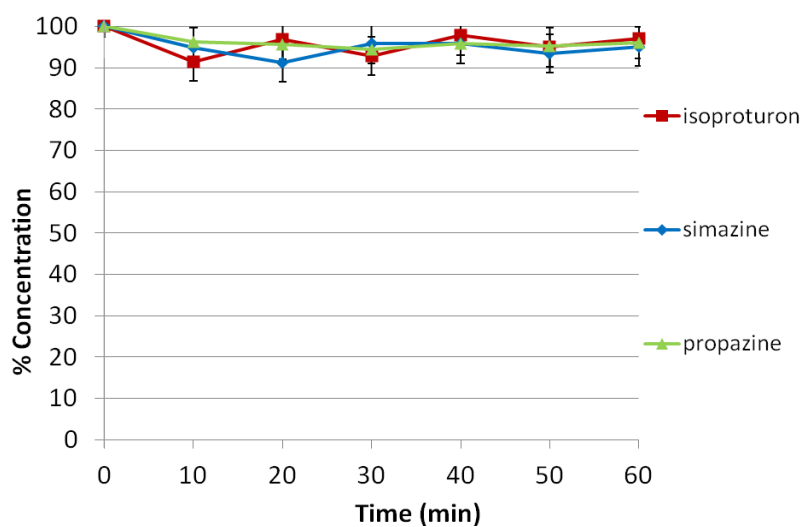


Figure 5.1 Degradation rate of pesticides in the absence of UV but the presence of $P-25 \text{ TiO}_2 = 5 \text{ g litre}^{-1}$

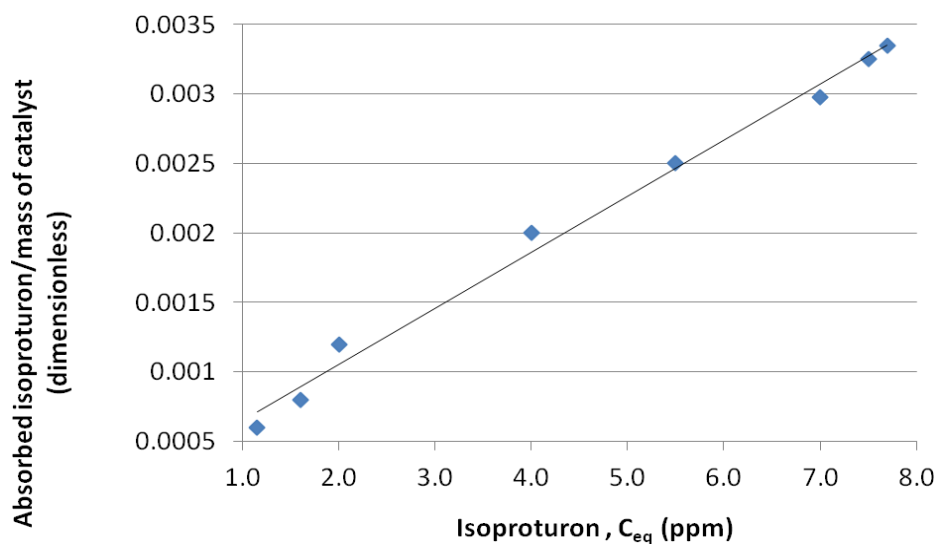


Figure 5.2 Adsorbed concentration of isoproturon in the absence of UV onto TiO_2 at different isoproturon concentration. TiO_2 concentration = 0.4 g litre^{-1} and isoproturon concentration = 1-8 ppm (Khor, 2004)

5.4 Determination of the effect of P-25 TiO_2 concentration on photocatalytic degradation

The loading of catalyst into the stirred reactor is an important variable in the design and operation of the reactor. In this section, the effect of P-25 TiO_2 loadings on the rate of degradation of the pesticides was studied to determine the optimum catalyst loading for the stirred reactor.

A series of experiments was conducted using UVA irradiation with various concentrations of P-25 TiO_2 of 0.5, 1, 2.5, 5, and 10 g litre^{-1} for an initial concentration of pesticides equal to 2.5 ppm at $25 \text{ }^\circ\text{C}$ and 900 rpm. The results are shown in Figure 5.3, 5.4 and 5.5 for the photocatalytic degradation of isoproturon, simazine, and propazine, respectively. The experiments were carried out over 60 minutes and each sample was taken out every 10 minutes.

The rate of degradation of the three pesticides is presented in Figures 5.3, 5.4, 5.5. All of the three pesticides studies are observed to degrade significantly on irradiation with UV, in all cases decreasing from an initial concentration of $2500 \text{ mg litre}^{-1}$ to less than $500 \text{ mg litre}^{-1}$. There is clearly a far greater loss of the three pesticides compared to the control experiments conducted in the absence of UV irradiation (Section 5.3). It is proposed that this loss is as a result of the photocatalytic degradation of the pesticides.

It is clear that the rate at which the concentration of isoproturon, simazine and propazine decreases is a function of the catalyst concentration. The rate of degradation is observed to increase up to a catalyst concentration of 5 g litre⁻¹. However, above this concentration, the amount of pesticide degraded over the duration of the experiment decreases. This trend clearly demonstrates that there is a trade off between catalyst concentration and the rate of photocatalytic reaction.

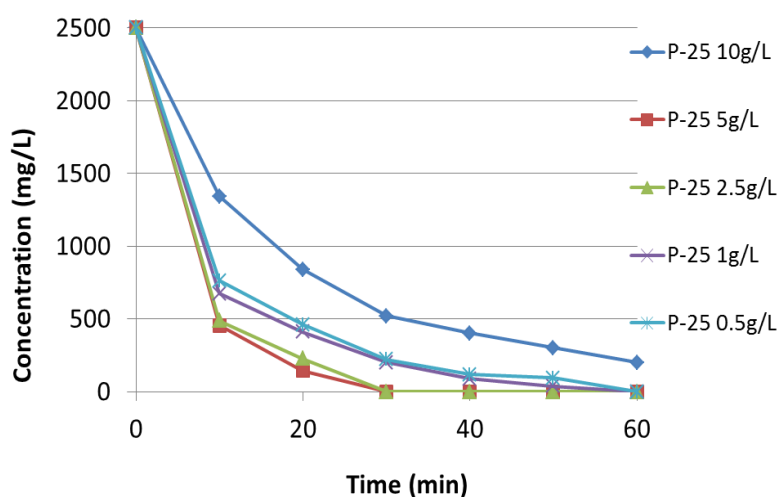


Figure 5.3 Effect of P-25 TiO₂ loadings on the degradation of isoproturon versus time under UVA irradiation

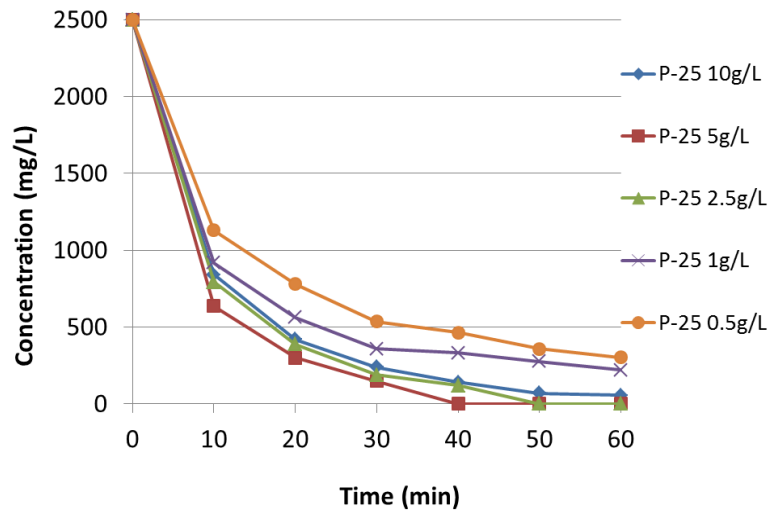


Figure 5.4 Effect of P-25 TiO₂ loadings on the degradation of simazine under versus time UVA irradiation

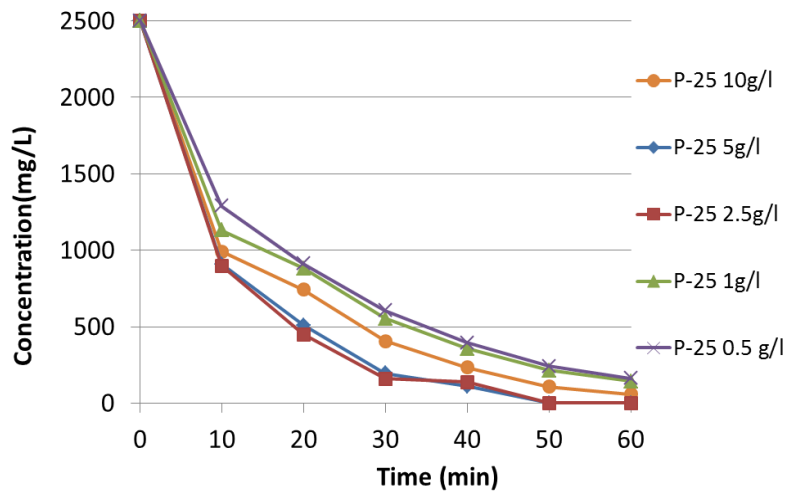


Figure 5.5 Effect of P-25 TiO₂ loadings on the degradation of propazine versus time under UVA irradiation

The results of using the stirred reactor can be explained as a simple batch system. The batch recirculation system was successfully modelled using an approximation of the Langmuir–Hinshelwood (L–H) theory, as proposed by

Toepfer (2006) as explained in Equation (2.16). For a case with a low pesticide concentration of less than 12 ppm, with only a single pesticide in solution, Equation (2.16) can be simply rewritten as follows:

$$\text{Rate} = k [C_R] \quad (5.1)$$

where $k = k_r K$, and $1 + KC_R \approx 1$

k_r = proportional constant which provides a measure of the intrinsic reactivity of the photoactivated surface with the pesticide

K = Langmuir adsorption constant of pesticide on TiO_2 surface

C_R = concentration of the pesticide

The rate reaction, involving materials A,B,....,D, can be approximated by the concentration of the chemicals: where a,b,....,d are not necessarily related to the stoichiometric coefficients. Thus, the reaction is ath order with respect to A, bth order with respect to B, nth order overall (Levenspiel, 1999)

$$-r_A = k C_A^a C_B^b \dots C_D^d, \quad a + b + \dots + d = n \quad (5.2)$$

For brevity, elementary reactions are often represented by the equation



for this would imply that the rate expression is

$$-r_A = r_R = k_1 C_A \quad (5.4)$$

The photocatalytic reaction was the first order reaction, as shown in Figure 5.6

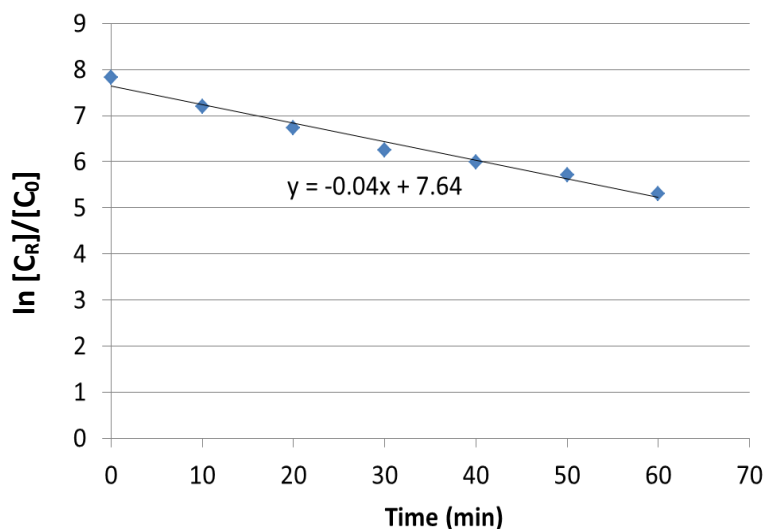


Figure 5.6 $\ln [C_R]/[C_0]$ (Remaining concentration divide by initial concentration of isoproturon when using 10 g litre^{-1} of P-25 TiO_2) versus time which related to slope as reaction rate constant or k , for this figure $k = 0.04 \text{ min}^{-1}$

Figure 5.7 shows that reaction rate constant (k) as a function of catalyst loading. The overall trend is the same for all three pesticides studied, with simazine having similar rate constants to propazine, whilst the rate constant for isoproturon is higher in all cases. Generally, the rate constant and the rate of degradation increase with the catalyst loading. This is proposed to be as a result of the higher surface area of the catalyst available for adsorption and degradation of the pesticide in solution. However, the photocatalytic degradation rate of isoproturon, simazine and propazine decreased when TiO_2 concentration exceeded 5 g litre^{-1} . When the concentration of TiO_2 is extremely high, a screening effect is caused by the TiO_2 particles. This results in the degradation rates of the three pesticides decreasing as a result of the

excessive opacity of the solutions, which prevents the catalyst from receiving light. This results in a higher the amount of UV being reflected from the mixture, resulting in a decrease in the UV absorption intensity onto the catalyst surface.

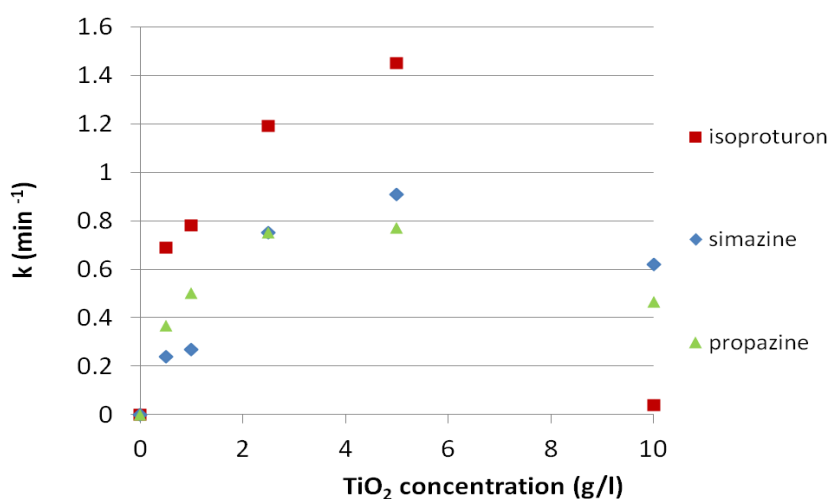


Figure 5.7 Optimum P-25 TiO₂ loading of the stirred reactor under UVA, *k* value was calculated from Figure 5.1, Figure 5.2, and Figure 5.3

This result agrees with previous research for which the same catalyst loading phenomenon was observed, as discussed in Section 2.11. There have been many studies in the past that have investigated the issue of establishing an optimum catalyst concentration for each system (Carp *et al.*, 2004; Konstantinou and Albanis, 2004; Cao *et al.*, 2005; Akpan and Hameed, 2009; Chong *et al.*, 2010). When the catalyst concentration exceeded the optimum value, the light scattering increased. This led to non-uniformity of light intensity and lower photocatalytic efficiency. Each catalyst has an optimum concentration, depending on which type it is. Overall optimum concentration

of the catalysts in each reported research lies in a wide range (from 0.15 to 8 g litre⁻¹), which can be a result of a number of factors, such as different systems, operational parameters, chemical compounds, and the reactor design (Carp *et al.*, 2004). Haque and Muneer, (2003) reported the optimum concentration for the photocatalytic degradation of isoproturon using the P-25 TiO₂ in an immersion well reactor to be approximately 3 g litre⁻¹, a similar value to that found in this study. Reddy *et al.*, (2010) using C, N, S doped TiO₂, reported that a lower optimum catalyst concentration was 1 g litre⁻¹ at neutral pH for efficient degradation of isoproturon in a small stirred reactor. A more recent study (Lopez-Munoz *et al.*, 2013) discovered the optimum concentration of P-25 TiO₂ was 1.95 g litre⁻¹ at pH 3.8 for the photocatalytic degradation of 5 mg litre⁻¹ of isoproturon in a Pyrex batch reactor. Due to different conditions, the optimum P-25 TiO₂ concentration in this reaction system was equal to 5 g litre⁻¹, at neutral pH in a stirred reactor. The screening effect can be explained with a six-flux absorption-scattering model (SFM) (Khor, 2004; Li Puma *et al.*, 2004; Li Puma 2005; Toepfer *et al.*, 2006). The model has many assumptions as follows:

- (i) large spaced particles
- (ii) particles randomly distribution inside the space considered
- (iii) the fluid is transparent to the UV irradiation
- (iv) there is no emission by the heterogeneous system
- (v) when a photon hits a particle only scattering or absorption occurs

(vi) the scattering can only occur along six directions of the Cartesian coordinates, as shown in Figure 5.5

(vii) for symmetry considerations, the probability of scattering along any of four directions of the plane normal to the incoming direction is the same

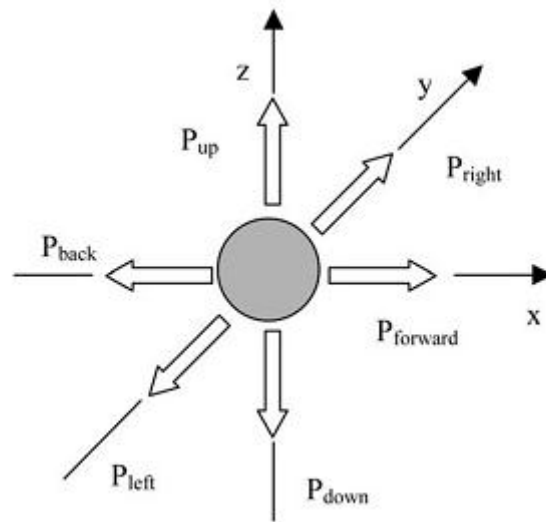


Figure 5.8 The six principal directions of photons scattering in the six-flux model (SFM) and the scattering probabilities (Li Puma, 2005)

Based on this theory, above the optimal catalyst loading, the increased particles present in the volume of the reactor cause more scattering and absorption of the light. However, as the scattering can occur in only six directions, this results in a high possibility for the particles close to the light source adsorbing the light onto the catalyst surface but not fully scattering the light to other catalyst particles. Therefore, the efficiency of the reactor

becomes limited by the opacity, which reduces the number of particles being exposed to the light penetration.

5.5 Influence of catalyst type on the photocatalytic degradation (P-25 TiO₂ VS synthesised TiO₂)

A comparison was made between the photocatalytic degradation of the pesticides using two different catalysts, a commercially available P-25 catalyst and TiO₂ nanoparticles that were synthesised using the supercritical water hydrothermal synthesis (ScWHS) rig at the University of Nottingham (Section 3.3). The efficiency of the synthesised TiO₂ in the photocatalytic reaction was studied with isoproturon, simazine, and propazine. The synthesised TiO₂ or ScWHS TiO₂ was used for treatment of pesticide solutions by adding nanoparticles into the stirred reactor under UVA or the UVC irradiation. The photolysis experiment, without the synthesised TiO₂, was also carried out to compare the amount of the pesticides' degradation.

Figure 5.9 shows the photodegradation results of propazine with the fresh synthesised TiO₂, compared with P-25 TiO₂ and at a mixing ratio of 50:50 (P-25 TiO₂: the synthesised TiO₂) by % weight under the UVA at TiO₂ concentration = 0.5 g litre⁻¹. The results show that P-25 TiO₂ is more active as a photocatalyst than the synthesised TiO₂. The photocatalytic degradation of propazine using P-25 TiO₂ results in nearly 100 % loss of the compound after an hour, which is far greater than the reaction under identical conditions using the synthesised TiO₂ (ScWHS TiO₂) where only 40 % loss was recorded over

the same time period. The mixture of P-25 TiO₂ and the synthesised TiO₂ resulted in an intermediate rate of photocatalytic degradation in comparison to the use of the two catalysts in isolation.

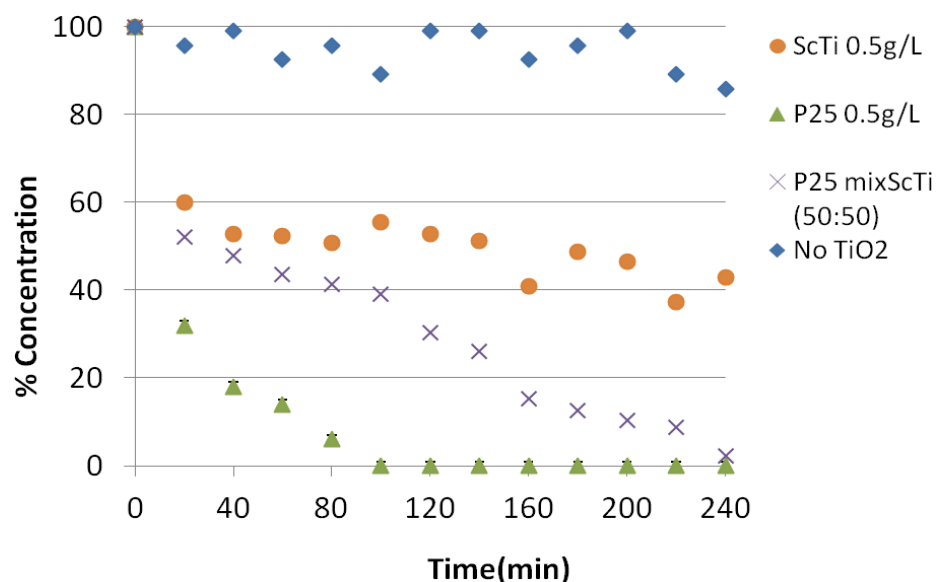


Figure 5.9 Degradation of propazine (initial concentration = 2.5 ppm) using P-25 TiO₂ and synthesised TiO₂ under UVA

The phase of the catalyst has previously been reported to significantly influence the photocatalytic activity of that catalyst (Section 2.11). P-25 TiO₂ phase contains both anatase and some amount of rutile phase, which has an impact on the photocatalytic efficiency of P-25 TiO₂. As the rutile acted as an electron trap, the exchange of electrons and holes between rutile and anatase easily occurs. The mixture between anatase and rutile reduced the oxidation and reduction limit when compared to the case of anatase or rutile only, as shown in Figure 2.10. The presence of the rutile phase in the photocatalysts

results in photocatalytic performance at a rate higher than when only pure anatase phase is present (Sato and Taya, 2006; Yeredla and Xu, 2008; Qourzal *et al.*, 2008; Hurum *et al.*, 2003). It is for this reason that P-25 has the highest photocatalytic efficiency when compared to other commercial TiO₂ catalysts (Bhatkhande *et al.*, 2001; Singh *et al.*, 2003; Singh *et al.*, 2007; Singh and Muneer 2004; Rahman and Muneer, 2005; Qamar and Muneer, 2005; Qourzal *et al.*, 2008; Qamar and Muneer., 2009; Singh *et al.*, 2007; Muneer *et al.*, 2005; Rafqah *et al.*, 2005). The sintering temperature affects the structural stability as discovered by Wang and co-workers (Wang *et al.*, 2005). They studied the effect of the sintering temperature on the oxidization of ethylene in a gas-phase medium. They found that when the catalyst calcined at 350 °C, it possessed a macro/mesoporous structure and showed photocatalytic reactivity about 60% higher than that of commercial P-25 TiO₂ due to its larger surface area. Therefore, the assumption was then made with the case of the synthesised TiO₂ to find out the photocatalytic efficiency after high temperature sintering.

To determine if the performance of the synthesised TiO₂ catalyst from supercritical water hydrothermal synthesis (ScWHS) could be improved, it was sintered at 900 °C, above the 700 °C temperature at which the rutile phase of TiO₂ has been reported to occur (Rath *et al.*, 2009). To test this hypothesis a series of experiments was conducted using the hydrothermal synthesised TiO₂, dried at 80 °C for two days and sintered at 900 °C for an hour.

As in Figure 5.10 after sintering at 900 °C, the particles developed to more agglomeration which led to larger grain size. However, the agglomerates

were hand milled using mortar and pestle to smaller than 5 mm-particles before starting the experiments.



Figure 5.10 Photograph of synthesised TiO₂ after sintering at 900 °C for an hour

It should be noted there was no phase transition at temperatures from 30-1000 ° C, as shown in XRD results in Section 5.6. Figure 5.11 to Figure 5.13 compare the rate of loss of isoproturon, simazine and propazine containing the sintered TiO₂ with UVA irradiation, compared to UVA photolysis of the solution (UVA only). The same results are reported for the three pesticides, with the loss of the pesticides occurring at the same rate with or without the catalyst present.

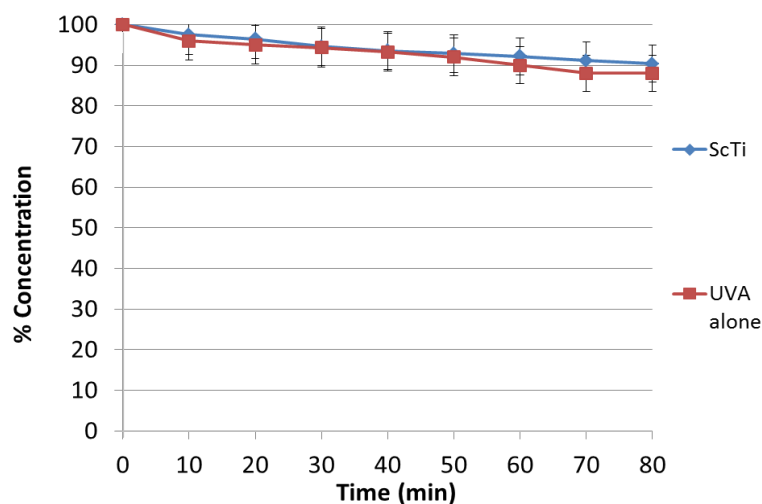


Figure 5.11 Degradation of isoproturon (initial concentration = 2.5ppm) using the synthesised TiO_2 under UVA, $[TiO_2] = 5 \text{ g litre}^{-1}$ after drying at 80 °C and sintering at 900 °C

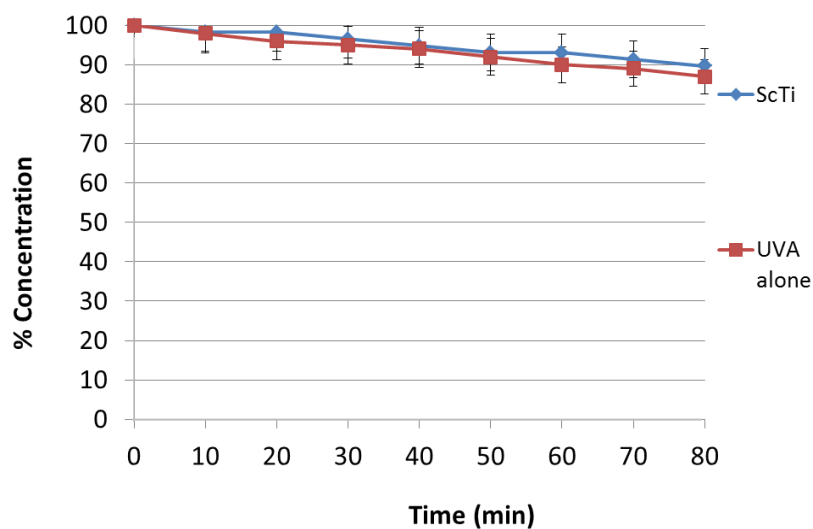


Figure 5.12 Degradation of simazine (initial concentration = 2.5ppm) using the synthesised TiO_2 under UVA, $[TiO_2] = 5 \text{ g litre}^{-1}$ after drying at 80 °C and sintering at 900 °C

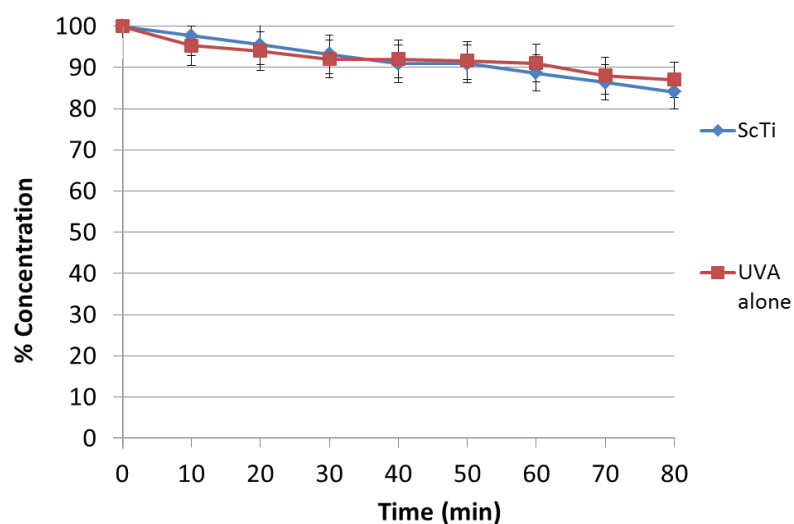


Figure 5.13 Degradation of propazine (initial concentration = 2.5ppm) using the synthesised TiO_2 under UVA, $[TiO_2] = 5 \text{ g litre}^{-1}$ after drying at $80 \text{ }^\circ\text{C}$ and sintering at $900 \text{ }^\circ\text{C}$

The same trend is observed for the irradiation of the pesticides under UVC irradiation (Figure 5.14 to Figure 5.16 for isoproturon, simazine and propazine, respectively). Overall, there is no difference between the rate of degradation with or without a catalyst present. Therefore, over the time studied in these experiments, it can be concluded that the synthesised TiO_2 (after sintering) has no activity in the stirred reactor system. It is clear that the rate of degradation with UVC irradiation occurs at a faster rate than in UVA for all three pesticides.

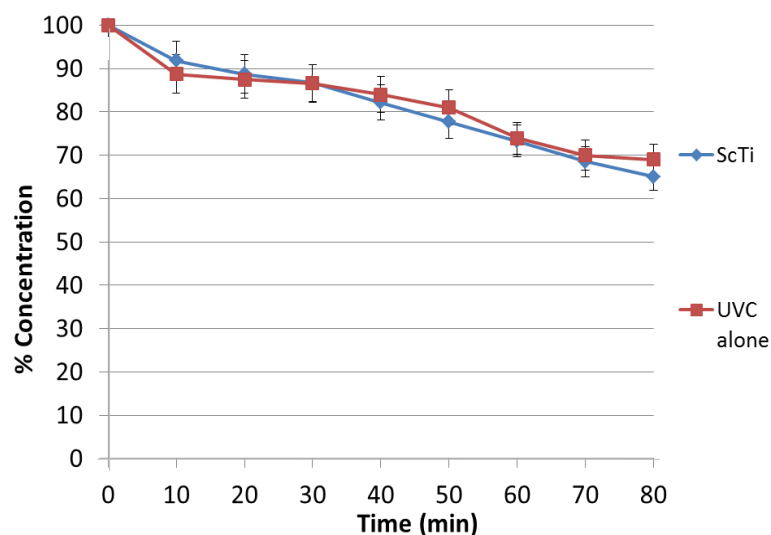


Figure 5.14 Degradation of isoproturon (initial concentration = 2.5ppm) using the synthesised TiO_2 under UVC, $[TiO_2] = 5 \text{ g litre}^{-1}$ after drying at 80 °C and sintering at 900 °C

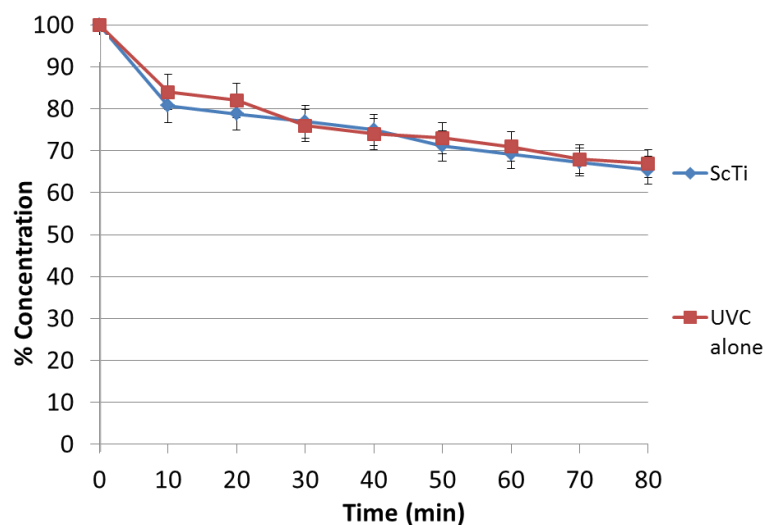


Figure 5.15 Degradation of simazine (initial concentration = 2.5ppm) using the synthesised TiO_2 under UVC, $[TiO_2] = 5 \text{ g litre}^{-1}$ after drying at 80 °C and sintering at 900 °C

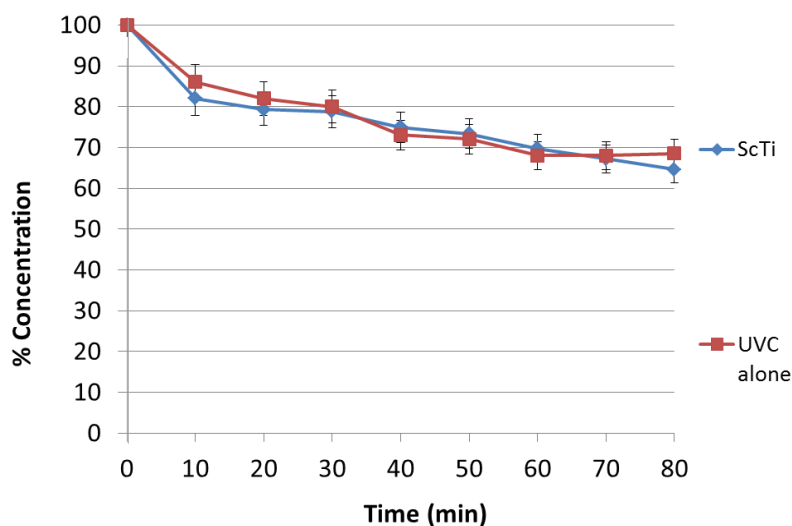


Figure 5.16 Degradation of propazine (initial concentration = 2.5ppm) using the synthesised TiO_2 under UVC, $[\text{TiO}_2] = 5 \text{ g litre}^{-1}$ after drying at $80 \text{ }^\circ\text{C}$ and sintering at $900 \text{ }^\circ\text{C}$

Figure 5.17 illustrates that the rate of pesticide degradation in the synthesised TiO_2 after sintering seems to have lower photocatalytic efficiency than the catalyst without sintering. This result conflicts with the assumption that photocatalytic degradation will occur at a higher rate after sintering and increase in the concentration of the rutile phase. To determine the reason for the loss of performance of the catalyst, further analysis of the catalyst before and after sintering was conducted and is discussed in the following section.

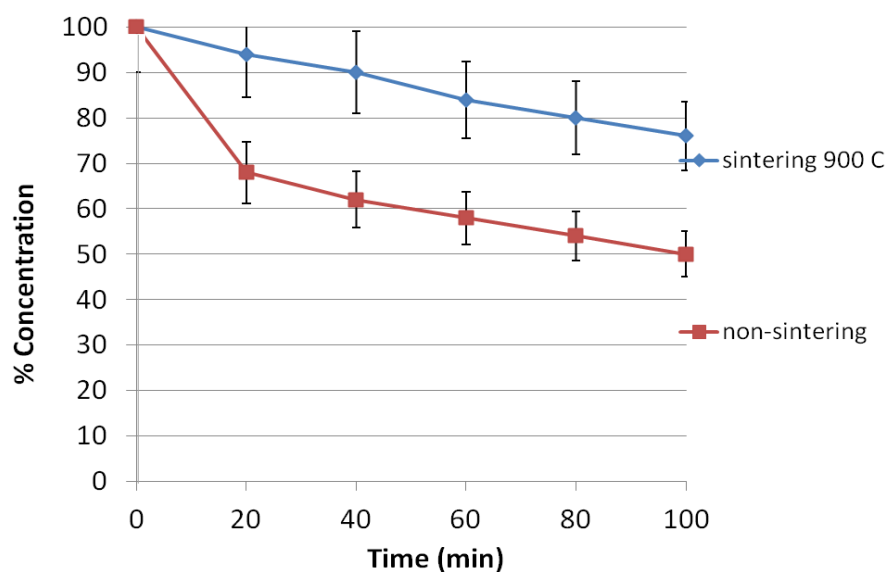


Figure 5.17 Degradation of propazine using the synthesised TiO_2 under UVA [TiO_2] = 5 g litre⁻¹ after drying at 80 °C and sintering at 900 °C compared with the non-sintering synthesised TiO_2

5.6 X-ray Diffraction (XRD) results at different sintering temperature

XRD analysis of the different catalyst (Figure 5.18) can be used to explain why the synthesised TiO_2 has a lower photocatalytic efficiency compared to P-25 TiO_2 . Contrary to previous studies (Rath *et al.*, 2009) no rutile phase has developed in the catalyst after sintering of the hydrothermally synthesised TiO_2 at temperatures of between 30-1000 °C). Despite heat treatment and sintering over a range of temperatures up to 1000 °C, the synthesised TiO_2 remains predominantly composed of anatase. However, commercial P-25 TiO_2 is composed of both the active rutile as well as the anatase phase. These phases had already been proved to have co-operative performance in photocatalytic reaction (Qourzal *et al.*, 2008; Hurum *et al.*, 2003; Yeredla and

Xu, 2008). Yeredla and Xu (2008) reported that the mixed phase P-25 TiO₂ exhibited higher activity for the photo-oxidation of acetaldehyde than anatase and rutile alone. The pure rutile phase has lowest activity as the decomposed acetaldehyde was approximately 30% when using the mixed phase TiO₂ (P-25 TiO₂). However the result of the pure anatase sample was lower than the mixed phase for 10%. There was a basic explanation that, as P-25 TiO₂ is composed of small nano-crystallites of rutile dispersed within an anatase matrix, the smaller band gap of rutile catches the photons generating electron/hole pairs. The electron then transfers from rutile (conduction band) which acted as electron traps, to anatase phase (Qourzal *et al.*, 2008). Hurum (2003) explained the enhanced photocatalytic activity of P-25 TiO₂ using electron paramagnetic resonance (EPR) spectroscopy. They proposed that the increased activity of P-25 TiO₂ is due to a rutile sink, preventing anatase recombination and allowing an anatase-originating hole to move to the surface. Sato and Taya (2006) carried out research using various anatase to rutile ratios in the catalyst (0 %, 30 %, 50 %, 70%, and 100% anatase). They discovered that the highest photocatalytic activity occurred for materials containing 70% anatase (30% rutile), with the lowest activity reported for the 0% anatase (100% rutile) catalyst. Therefore, the synthesised TiO₂ had lower efficiency compared to P-25 TiO₂ because it did not have any rutile phase.

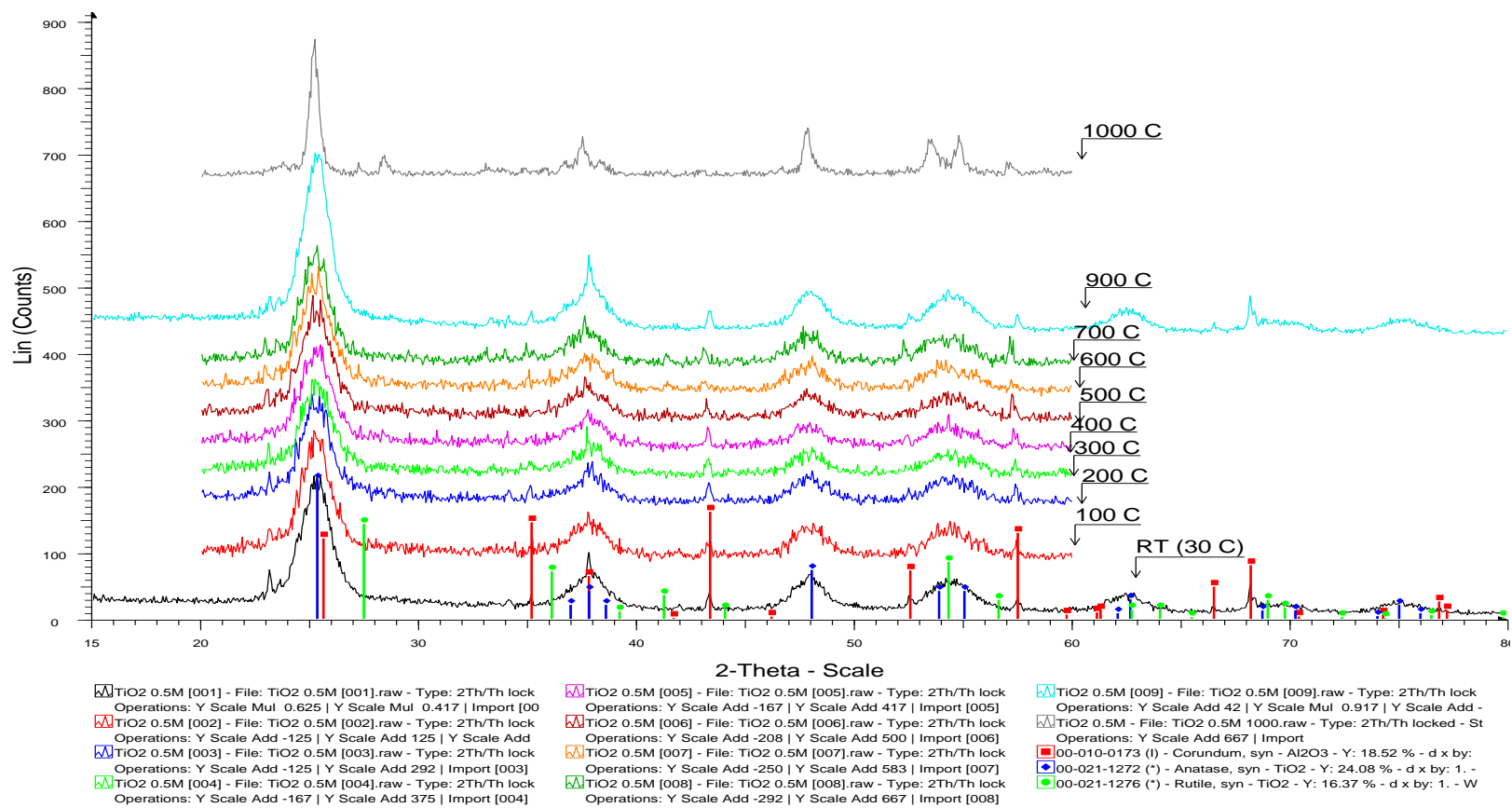


Figure 5.18 Results of XRD analysis of synthesised TiO₂ sintered at different temperatures (30-1000 °C)

In 2007, Gemelli and Camargo studied the XRD results of pure commercial titanium oxidation in the temperature range 400 – 800 °C, Figure 5.19. Above 718 °C, phase transition from anatase to rutile occurred, which indicated that anatase is no longer stable, converting to rutile, which is the only stable phase.

However, in case of the synthesised TiO₂ that has been used in this thesis, XRD showed only anatase from room temperature until 900 °C and still with dominant peaks of anatase at 1000 °C. However, there were some small amounts of rutile that started to nucleate at 1000 °C (at $2\theta = 54^\circ$ and 57°). Therefore, there is probability for phase transition of the synthesised TiO₂, when the sintering temperature was higher than 1000 °C. The suspicious point in this discovery leads to future study and further experiments.

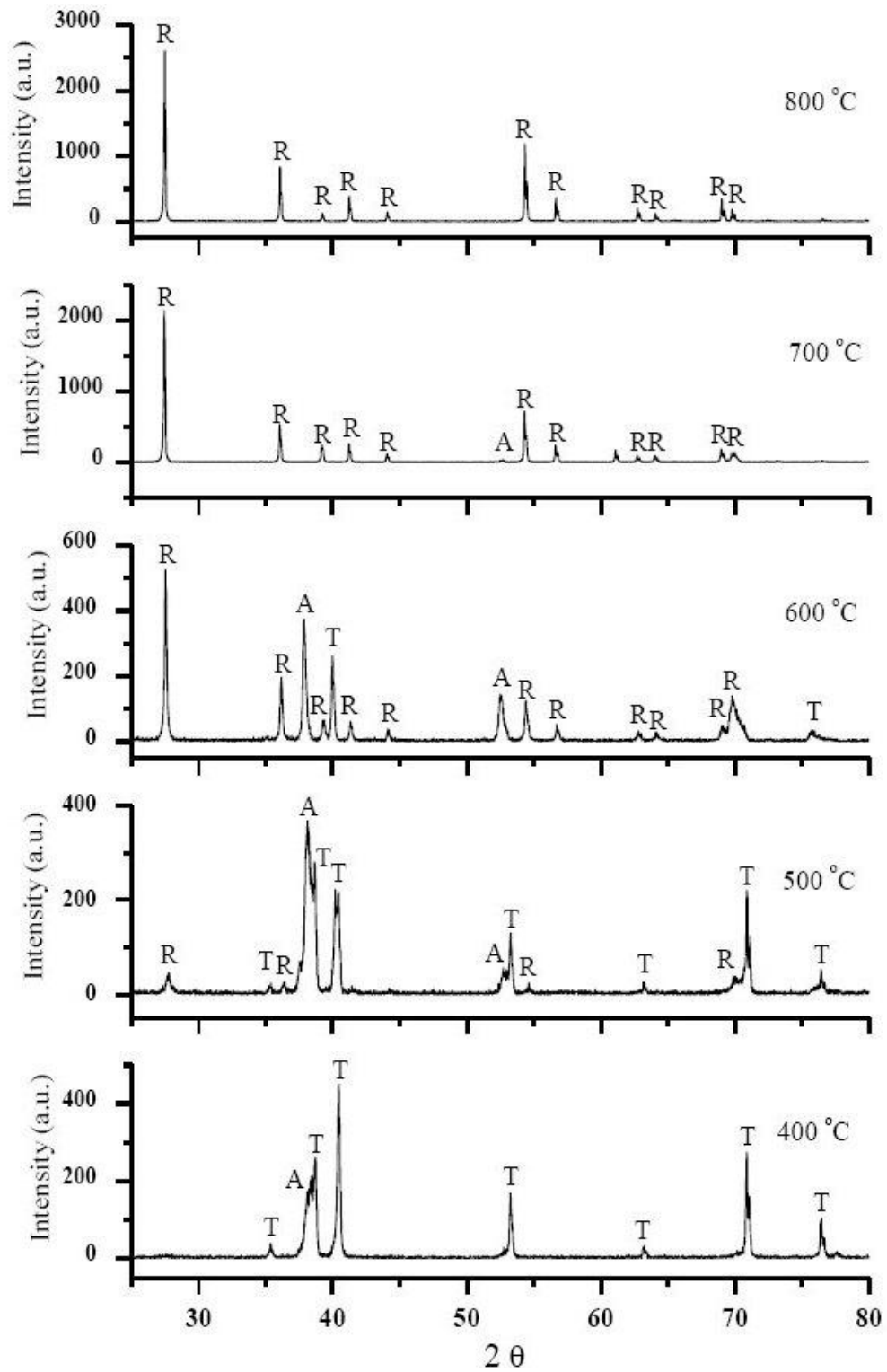


Figure 5.19 XRD of pure titanium when oxidation in the temperature range 400 – 800 °C (Gemelli and Camargo, 2007) A: Anatase, R: Rutile and T: Titanium

5.7 Conclusions of stirred photoreactor experiments

In this chapter, the experimental results carried out with stirring batch system were discussed. The influence of photocatalyst was studied at different concentrations of P-25 TiO₂ under UVA. The optimum concentration of P-25 TiO₂ for use with the stirring reactor was found to be 5 g litre⁻¹. The experiments with synthesised TiO₂ (after sintering and non-sintering) were carried out to compare the photocatalytic performance with the commercial TiO₂. The sintering sample had a lower photocatalytic efficiency than expected and than the non-sintering case due to no phase transition occurring. After using the sintered, synthesised TiO₂ treatment with polluted-water, there was rarely difference in the degradation concentration of the three pesticides from UVA or UVC photolysis (UVA or UVC only). It can be concluded that the sintered, synthesised TiO₂ was barely active as a photocatalyst in this system, which is different from the case of P-25 TiO₂. In the absence of UV experiments, there was no significant difference of the degradation concentration amongst the three pesticides. The concentration loss was equal to 10%, which corresponds with TFFBR (Chapter 4). The photocatalytic reaction rates of the three pesticides under UVA illumination was defined as first order reaction and followed the L-H (Langmuir–Hinshelwood) theory.

Chapter 6

PHOTOCATALYTIC DEGRADATION OF PESTICIDES USING A FLUIDISED BED PHOTOREACTOR

6.1 Introduction to fluidised bed photoreactor results

This chapter presents the results from the degradation of the three pesticides used in this study using a fluidised bed photoreactor. A fluidised bed photoreactor has previously been demonstrated to have good potential as a reactor that uses immobilized photocatalysts (Section 2.12, Alexander *et al.*, 2000, Rowan and Andrew, 2009). The reactor is constructed to allow counter-current mixing of air introduced at the bottom of the reactor and TiO₂, so creating a high contact, well mixed contact area between oxygen molecules, contaminated solution and catalyst surfaces. Therefore, in this thesis, the photocatalytic experiments with a fluidised bed photoreactor are the major priority, which was observed after using both P-25 TiO₂ and the TiO₂ catalyst synthesised in a supercritical water reactor.

The details of the experiments and the reactor design were previously described in Section 3.6.

A series of experiments have been conducted and will be described in this chapter, to establish the performance of the reactor. Initial control experiments

were conducted on solutions of isoproturon, simazine, and propazine in the presence of the P-25 TiO₂ catalyst at a concentration of 5 g litre⁻¹ but in the absence of UV irradiation. A comparison will also be drawn between the degradation results of the pesticides under UVA and UVC photolysis, compared to photocatalytic degradation in the presence of P-25 TiO₂ at a range of concentrations. Finally the effect of different catalyst types, and the results of various characterisations are also presented, including Transmission Electron Microscopy (TEM), X-ray Diffraction (XRD), and Ultraviolet-visible Spectroscopy (UV-Vis), (analytical techniques which were previously described in Section 3.7).

The performance of the supercritical water synthesised TiO₂ (Section 3.3) in the fluidised bed photoreactor is also studied and compared to the commercial TiO₂.

6.2 Aims and Objectives

The principal aim of this chapter is to develop the fluidised bed photoreactor, and, through conducting a series of experiments under a range of experimental conditions, to determine and optimise the performance of the photocatalytic treatment. More detailed objectives of this chapter are as follows:

- (i) Determine the pesticide concentration adsorbed onto the TiO₂ surface under absence of UV

- (ii) Determine the rate of pesticide degradation using UV photolysis (in the absence of a catalyst) to allow comparison with a photocatalytic reaction using P-25 TiO₂
- (iii) Determine the influence of UV wavelength in the photocatalytic reaction and comparison with previous results using a thin film fixed bed reactor (Chapter 4)
- (iv) Optimization of the appropriate TiO₂ concentration to achieve the highest reactor performance as compared with the results using the stirred reactor (Chapter 5)
- (v) Determine the photocatalytic mechanism occurring during pesticide degradation using the fluidised bed photoreactor and determine the reaction rate law and relate the results to the Langmuir–Hinshelwood (L–H) theory (Section 2.11).
- (vi) Determine the performance of the synthesised TiO₂ after sintering and compare performance with the commercial P-25 TiO₂
- (vii) Characterization of the synthesised TiO₂ from the ScWHS technique using Transmission Electron Microscopy (TEM), X-ray Diffraction (XRD), and Ultraviolet-visible Spectroscopy (UV-Vis)

6.3 Control experiments, determination of the rate of loss of pesticides in the absence of UV but in the presence of TiO₂

A series of control experiments were conducted using the fluidised bed reactor for the three pesticides (isoproturon, simazine, and propazine) in the presence of the P-25 TiO₂ catalyst but in the absence of UV irradiation. An initial set of experiments was conducted to confirm that the amount of adsorption of the pesticide onto the catalyst to determine a baseline for the photolysis and photocatalytic experiments. P-25 TiO₂ was added at a concentration of 5 g litre⁻¹ for all of the experiments without the UV illumination.

The rate of loss from solutions of isoproturon, simazine, and propazine are shown in Figure 6.1. In all cases there is a small initial decrease in the concentration of the pesticides in the solution. Overall a decrease of approximately 10% - 15% of the pesticide is observed (The standard deviation for isoproturon, simazine and propazine data were 3.44, 2.17, 4.63 % of initial pesticide concentration, respectively). These results are in the same direction as the results from TFFBR (Chapter 4) and stirred photoreactor (Chapter 5), though the loss amount was higher due to higher TiO₂ concentration (5 g litre⁻¹). Taking into account the uncertainty in the loss of the pesticides as a result of analytical experimental errors, it is assumed that the rate of loss of the different pesticides is equal. It is proposed that this is as a result of the adsorption of the pesticides onto the surface of the P-25 TiO₂ catalyst surface. It is possible that volatiles loss of the pesticide could account for this decrease in concentration. However, this is predicted to be minimal as the pesticide solutions are in liquid phase and rapidly transfer to the reactor. There is also a

low surface area for evaporation to occur from the top of the column, due to the column dimension that has a high length-width ratio (48:1). This decrease in the concentration of the pesticides under the control experiments, in the absence of UV irradiation, is equivalent to that observed for all of the different reactors used in this study (Section 4.3.1, and Section 5.3).

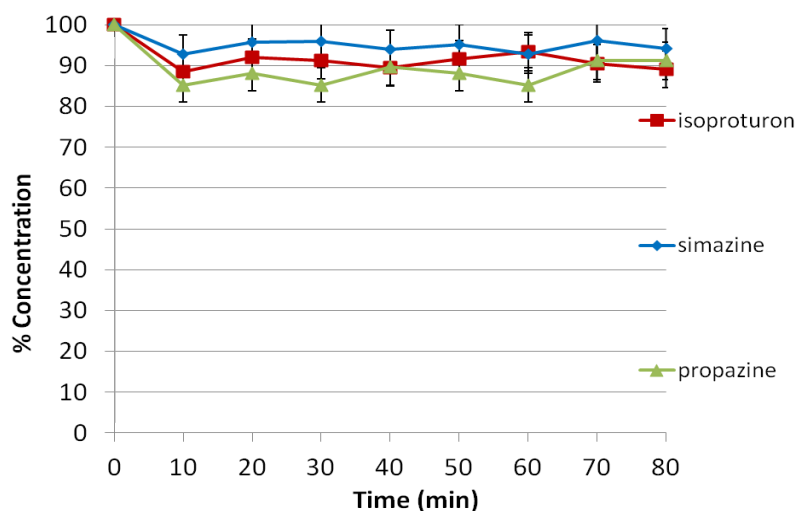


Figure 6.1 Decrease in the concentration of pesticides in the absence of UV irradiation but in the presence of P-25 TiO_2 (5 g litre^{-1})

6.4 UVA and UVC photolysis

To determine the rate of loss of the three pesticides in the absence of UV irradiation, a number of experiments were conducted with UVA and UVC in the absence of a catalyst. The efficiency of UVA and UVC photolysis of the three pesticides was also compared. Figure 6.2 shows the results of UVA photolysis in the fluidised bed photoreactor, without adding any photocatalyst. UVA photolysis leads to a 20-30 % decrease in the concentration of the pesticides in solution. The rate of degradation varied for the three pesticides

studied, with the initial rate and total degradation of simazine after 80 minutes of treatment being the greatest (Figure 6.2). The statistical values of the remaining pesticide concentration were shown in Section III.4-III.6 (Appendix III). The results are consistent with those from the thin film fixed bed reactor in Section 4.4.

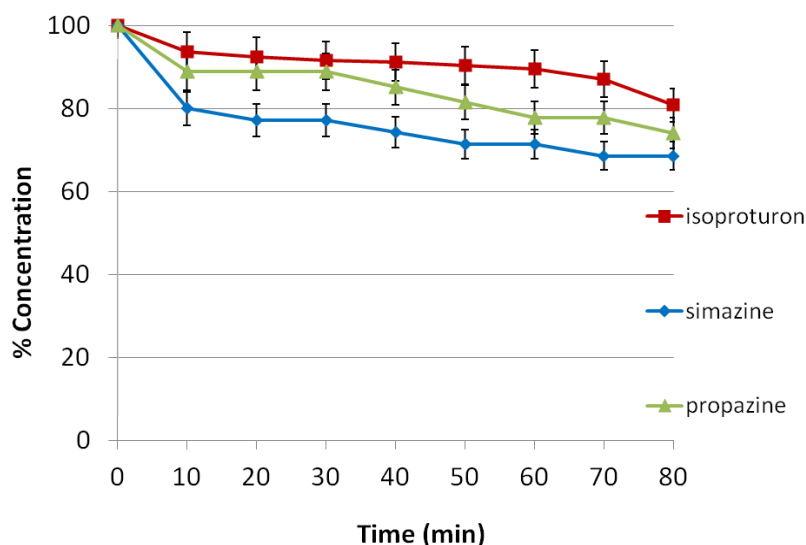


Figure 6.2 UVA photolysis of isoproturon, simazine, and propazine without any catalyst

The rate of loss for all three pesticides under UVC irradiation was seen to be greater than that of UVA (Figure 6.3). For all of the three pesticides studied, a decrease in concentration of approximately 80 % was observed after 50 minutes (Figure 6.3). This relates to the theory that the light wavelength did have influence on the photolysis, as previously described in Section 4.4. UVC has a shorter wavelength (100-280 nm), which resulted in the higher energy of the photon emission compared to the UVA, which has a longer wavelength

(315-400 nm) (Section 2.11). These results are consistent with the study of Liang *et al.*, (2010) on the photolysis and TiO₂-photocatalytic reduction of diphenamid. They found that photolysis by UVC alone was highly efficient, resulting in up to 100% degradation of diphenamid after 360 minutes. In comparison, the heterogeneous photocatalytic reduction of the same compound with TiO₂ and UVA showed a lower rate of degradation, resulting in a residual concentration of 51% after the same treatment time.

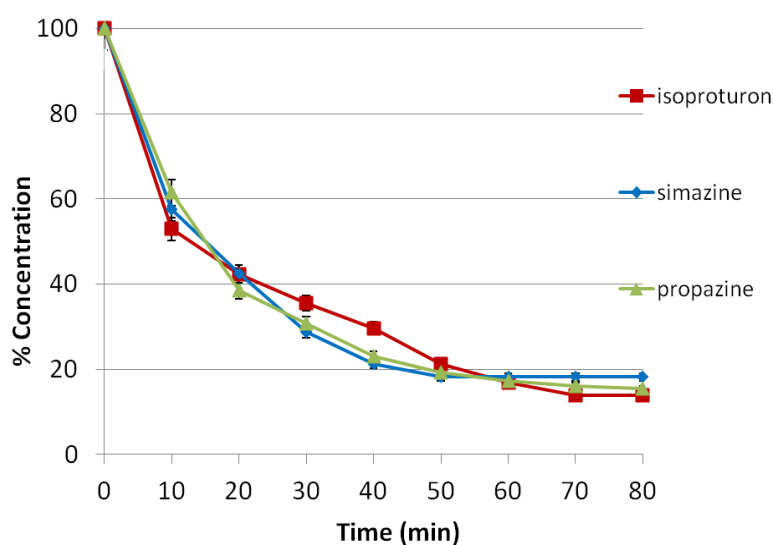


Figure 6.3 UVC photolysis of isoproturon, simazine, and propazine without any catalyst

6.5 Photocatalytic degradation of pesticides

Figure 6.4, Figure 6.5 and Figure 6.6 show the results of four different experimental conditions on the degradation of isoproturon, simazine and propazine (initial concentration of pesticides = 2.5 ppm), respectively, which are:

- (i) the UVA photolysis reaction
- (ii) the UVC photolysis reaction
- (iii) the photocatalytic reaction with P-25 TiO₂ at a concentration of 5 g litre⁻¹ under the UVA
- (iv) the photocatalytic reaction with P-25 TiO₂ at a concentration of 5 g litre⁻¹ under the UVC

The higher rate of pesticide degradation was observed when the reaction was conducted in the presence of P-25 TiO₂ under UVC irradiation. In all cases, nearly complete degradation of all three pesticides was observed after 80 minutes. Over the first ten minutes of the experiments, significant differences are reported in the rate of degradation of the three compounds in the following order: isoproturon > propazine > simazine.

The results clearly demonstrate that both photolysis and photocatalytic reaction occur at a significantly higher rate in UVC compared to UVA. Whilst the addition of the catalyst under UVA irradiation provided a higher photocatalytic degradation rate than only UVA, this approach for all three pesticides was less effective at degrading the compounds than UVC irradiation alone. These results are in accordance with the observation in the previous chapter (Section 4.3) where photocatalytic reaction occurred when adding P-25 TiO₂, which had higher degradation rates than UV photolysis. Photocatalytic reaction is different from photolysis reaction, since there is a photocatalyst involved in the reaction. In photolysis, the reaction is mainly affected by light intensity and light wavelength. However, in photocatalytic reaction, the

photocatalysts play a main role to oxidise the substrate activated by light illumination. The oxidation rate of a photocatalytic reaction depends on hydroxyl radicals, which are formed by reaction between TiO_2 , water, and oxygen molecules (Section 2.7 and Figure 2.1) These results agree with a large number of studies for a range of pesticides (isoproturon: Khor, 2004; alachlor: Wong 2003; malathion, isomalathion and malaoxon: Kralj *et al.*, 2007) which demonstrate that the degradation rate of pesticides or organic compounds due to photocatalytic oxidation was significantly higher than photolysis alone (only UV). In this thesis, the photocatalytic rate under UVC of isoproturon was twice as much as the UVC photolysis rate referred to in Figure 6.4.

It can also be observed from Figures 6.5 that the photocatalytic rate reaction of isoproturon, simazine and propazine improves under UVC at a greater rate than under UVA. The activity of the photocatalyst depends strongly on the light-illumination (energy per unit area) or the photon flux on the surface of the catalyst. For photocatalytic reaction, the efficient photon has to be considered as a reactant. The photon energy can be explained as Planck's equation (Section 2.11.7). In this theory, it depended on the light wavelength; the shorter the light wavelength, the higher the photon energy.

However, there are other possible reasons explained by Khor (2004) that the appropriate absorption wavelength of TiO_2 is near 254 nm (UVC) which therefore provides enough energy to overcome the energy band gap.

(i) The penetration distance of photons into particles is shorter when under the shorter wavelength. Therefore, TiO₂ particles absorbed the shorter wavelength more strongly than the longer wavelength.

(ii) Photoelectrons and holes are formed closer to the surface of the catalyst particles, which reduces the possibilities of the electron-hole recombination.

Previous studies have reported high rates of organic compound degradation in fluidised photocatalytic reactors. The degradation efficiency of three pesticides using a fluidised bed photoreactor is high. The efficient degradation of similar compounds has been demonstrated in previous studies (Nam *et al.*, 2002; Lee *et al.*, 2004; Kanki *et al.*, 2005). Nam *et al.* (2002) carried out photocatalytic treatment of methyl orange in a fluidised bed photoreactor, using TiO₂ as the photocatalyst. They reported the decomposition results of 100 % after 1.5 hr passed (at TiO₂ concentration = 0.2 g litre⁻¹, air flow rate = 1.5 litre min⁻¹). In 2004, photocatalytic oxidation of microcystin-LR in a fluidised bed reactor using TiO₂-coated activated carbon was carried out by Lee and colleagues. This compound is a cyclic heptapeptide containing 3-amino -9- methoxy -2, 6 ,8- trimethyl -10- phenyldeca -4, 6-dienoic acid, with leucine (L) and arginine (R). They succeeded in achieving high photocatalytic activity as 100 % degradation of microcystin-LR within 20 minutes. In 2005, Kanki and co-workers used a fluidised bed for bisphenol A treatment with TiO₂-coated ceramic particles. Their results showed that 10 mg dm⁻³ in 2 litre water of bisphenol A can be decomposed almost 100% in about 200 min.

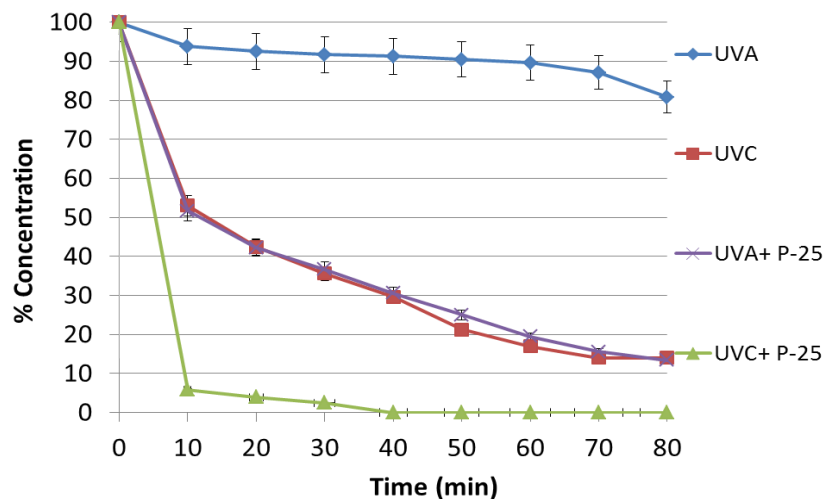


Figure 6.4 Effect of light wavelength on the photocatalytic oxidation rate of isoproturon, $[TiO_2] = 5 \text{ g litre}^{-1}$, initial concentration of isoproturon = 2.5 ppm, P-25 TiO_2 sintered at $900 \text{ }^\circ\text{C}$ for an hour

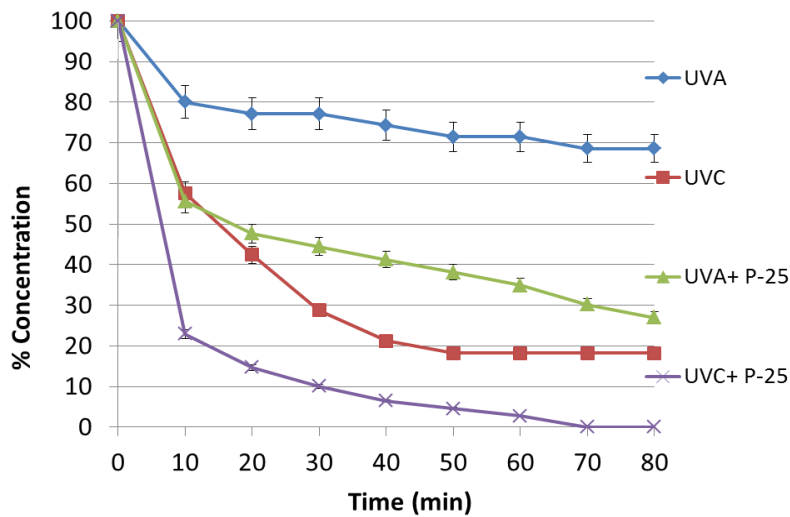


Figure 6.5 Effect of light wavelength on the photocatalytic oxidation rate of simazine, $[TiO_2] = 5 \text{ g litre}^{-1}$, initial concentration of simazine = 2.5 ppm, P-25 TiO_2 sintered at $900 \text{ }^\circ\text{C}$ for an hour

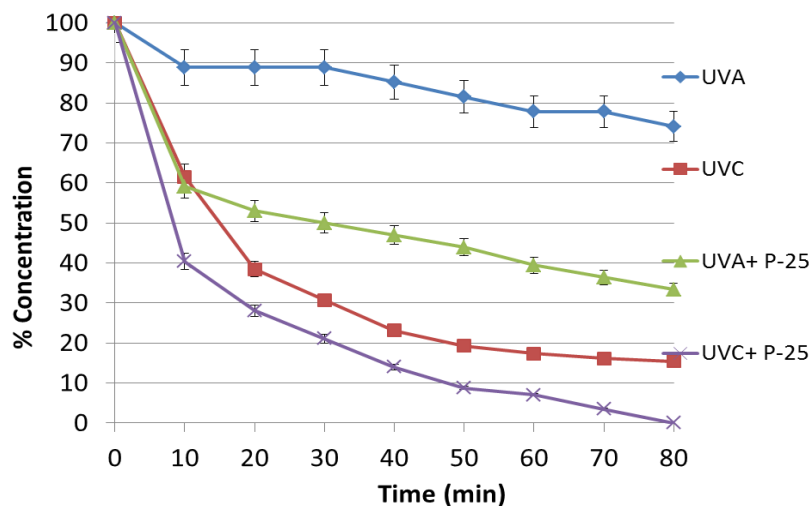


Figure 6.6 Effect of light wavelength on the photocatalytic oxidation rate of propazine, UVA $[TiO_2] = 5 \text{ g litre}^{-1}$, UVC $[TiO_2] = 5 \text{ g litre}^{-1}$, initial concentration of simazine = 2.5 ppm, P-25 TiO_2 sintered at 900 °C for an hour

The fluidised bed photoreactor has the highest efficiency compared to the other two reactors, the thin film reactor (Chapter 4) and the stirred photoreactor (Chapter 5). As shown from Section III.10-III.21 (Appendix III) the average value of % remaining concentration of the three pesticides from UVA and UVC photolysis, using a fluidised bed photoreactor were lower than using other reactors. A number of explanations are possible for the difference in performance.

Light intensity can play a significant role in the rate of degradation of organic compounds under both photolysis and photocatalytic conditions. The fluidised bed photoreactor has two parallel 36 watt-UV lamps which are located in parallel and close to the column (Section 3.6). The column has dimensions of

120 cm length and 1 inch diameter, which is an extreme length-width ratio (fluidised bed = 48:1, whereas stirred photoreactor = 5:3). This results in an increased illuminated area for the UV photolysis. The distance between the light source and the column also important. The closer the light source, the higher the light intensity. As previously described in Section 2.11, light intensity has a great influence on photocatalytic reactions (Ahmed *et al.*, 2011; Cassano and Alfano, 2000). The relationship between the rate of the photocatalytic removal and light intensity has previously been reported for TiO₂ photocatalytic systems. Greater surface irradiation leads to more hydroxyl radicals being present, which play an important role in the photocatalytic mechanism (Pourata *et al.*, 2009; Liu *et al.*, 2009; Faramazpour *et al.*, 2009; Kaneco *et al.*, 2009).

The introduction and mixing of oxygen into the reactor is also another important variable between the different reactor types. The fluidised bed photoreactor has a continuous stream of air introduced at the base, whilst there was no continuous source of oxygen flow in both the stirred reactor and the thin film fixed bed reactor (TFFBR). Hence, due to the low concentration of oxygen, the potential for the photocatalytic reaction in these two models is predicted to be lower than in the fluidised bed reactor. In the case of the fluidised bed photoreactor, an air supply was fed from the bottom of the column at a flow rate of 0.8 ml min⁻¹. During the experimental period of 90 minutes, the volume of oxygen can be calculated as follows,

The total volume of oxygen = 0.8 x 90 = 72 ml

When the dimension of the column,

radius of the column = $R = 0.5 \text{ inch} = 1.27 \text{ cm}$,

the height of the column = $h = 120 \text{ cm}$;

$$\begin{aligned} \text{The volume of column} &= \pi R^2 h \\ &= \pi (1.27)^2 \times 120 = 608.04 \text{ ml} \end{aligned}$$

The volume of solution equal to $\frac{3}{4}$ of total reactor volume = $608.04 \times 0.75 = 456 \text{ ml}$

$$\text{oxygen ratio per total volume} = \frac{72}{456} = 0.158 = 15.8 \% \text{ by volume}$$

From the calculation above, the volume ratio of the oxygen compared to the total volume was equal to 15.8 %. The oxygen concentration was higher than in the stirred reactor and the thin film fixed bed reactor (TFFBR), which had no oxygen source.

Previous studies of fluidised bed reactors have shown that the oxygen flowrate has a significant impact on photocatalytic activity. The higher the oxygen flowrate, the higher the photocatalytic activity (Nam *et al.*, 2002; Dong *et al.*, 2008) Nam *et al.*, (2002) studied 4 values of oxygen flowrate (0.5, 1, 1.5, 2 litre min^{-1}). They discovered that the highest decomposition rate of methyl orange occurred at 1.5 litre min^{-1} (75% decreased concentration in an hour). Gong *et al.*, (2008) and co-workers carried out research using a fluidised bed photoreactor with titanium dioxide immobilised onto activated carbon for phenol degradation. They found that there was the optimum limit of the oxygen flowrate in photocatalytic reaction, as shown in Figure 6.7. In this

graph, at oxygen flowrate equal to 5 litre min⁻¹, the degradation fraction of phenol was lower than at 3 litre min⁻¹ oxygen flow rate by approximately 10 - 15 %.

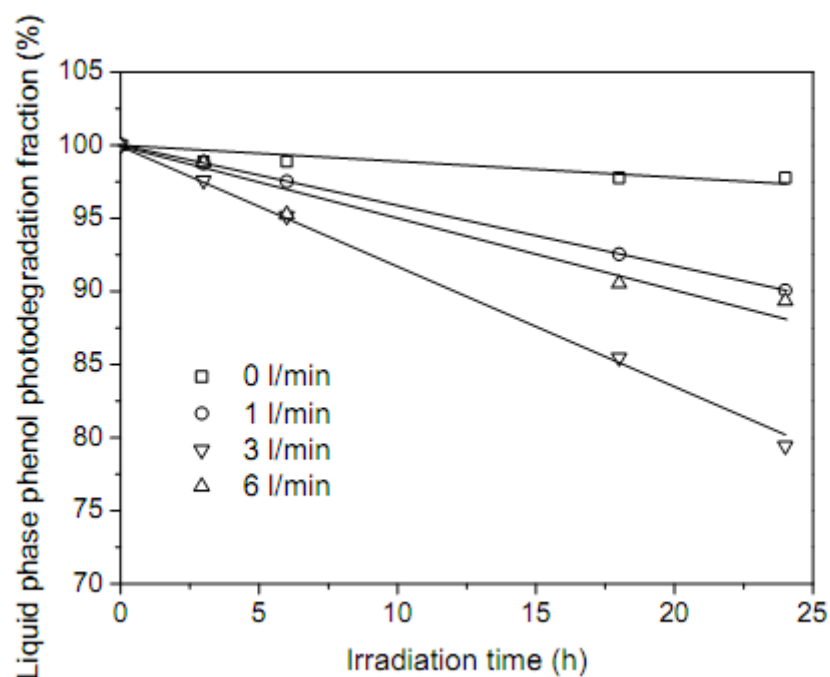


Figure 6.7 Effect of air flow rate on liquid phase phenol degradation fraction
(Gong et al., 2008)

6.6 Effect of P-25 TiO₂ concentration on the photocatalytic degradation

The concentration of the catalyst is another important variable in the operation of the fluidised bed reactor. In this section, P-25 TiO₂ was sintered at 900 °C for an hour to increase the particle size before being added to the reactor in order to stop clogging of particles in the bottom of reactor. Experiments were conducted as follows to determine the influence of catalyst concentration under a range of different conditions:

- (i) The photocatalytic effect was compared under UVA for the degradation of isoproturon and simazine, as shown in Figure 6.8 and 6.9, respectively.
- (ii) Comparison of the photocatalytic degradation of isoproturon, simazine, and propazine with P-25 TiO₂ under UVC irradiation or a range of catalyst loadings.

Comparison of the different catalyst loadings under UVA at three different concentrations (2.5, 5, 7.5 g litre⁻¹) shows that there is not a linear relationship between the rate of polymer degradation and the concentration of the catalyst. In the case of isoproturon degradation (Figure 6.8), the rate of loss of the pesticide is seen to increase up to 5 g litre⁻¹, but decrease as the catalyst concentration is raised above this point. The same trend is also seen with simazine in Figure 6.9 at the two different concentrations (5, and 7.5 g litre⁻¹) of P-25 TiO₂. The photocatalytic degradation of isoproturon and simazine, using different P-25 TiO₂ concentrations are compared with the blank sample (UVA photolysis or UVA only).

The most appropriate amount of P-25 TiO₂ for photocatalytic treatment of pesticides in a fluidised bed photoreactor is 5 g litre⁻¹ as shown in both graphs (Figure 6.8 and 6.9) since the decreased concentration of isoproturon and simazine were the highest when using P-25 TiO₂ at 5 g litre⁻¹. This result corresponds to the result using the stirred reactor, that 5 g litre⁻¹ is the optimum P-25 TiO₂ concentration (Section 5.3).

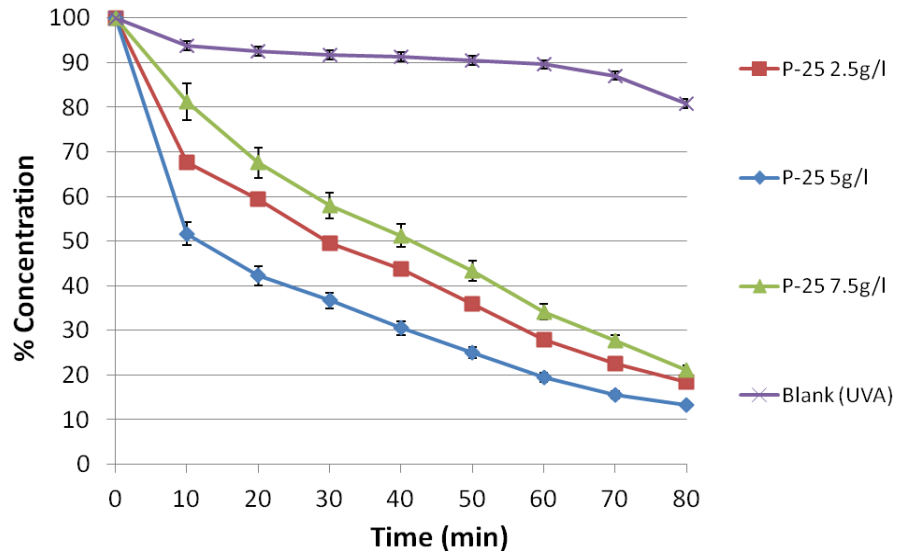


Figure 6.8 Photocatalytic degradation of isoproturon using fluidised bed reactor under UVA with P-25 TiO₂ concentration 2.5, 5 and 7.5 g litre⁻¹

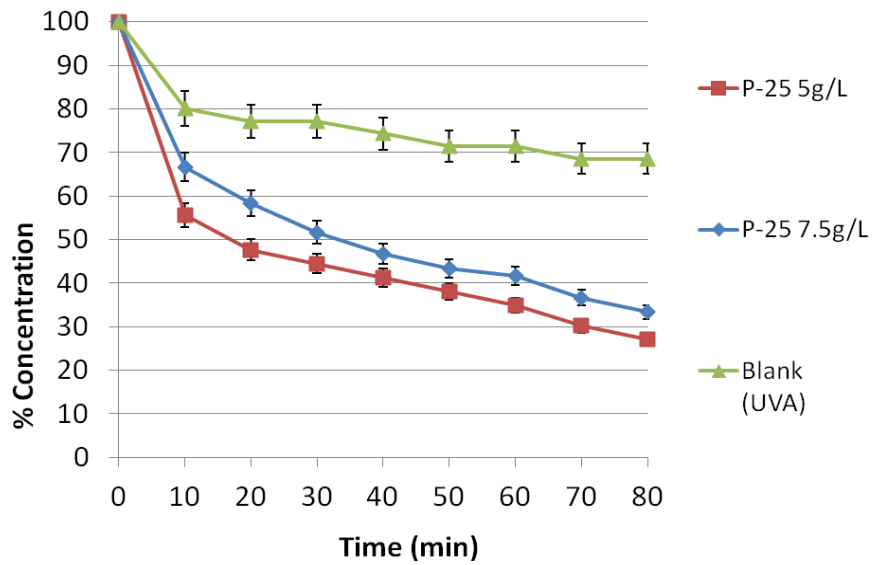


Figure 6.9 Photocatalytic degradation of simazine using fluidised bed reactor under UVA with P-25 TiO₂ concentration 5 and 7.5 g litre⁻¹

From the results in Figure 6.10 and Figure 6.12, amongst three pesticides, the degradation of isoproturon using P-25 TiO₂ was the highest under both UVA and UVC irradiation for the fluidised bed photoreactor. The reaction rates for isoproturon, simazine and propazine were calculated from the first 10 minutes to compare under both UVA and UVC irradiation, as shown in Table 6.1. It can be assumed that P-25 TiO₂ accelerated the most in the photocatalytic reaction of isoproturon, when compared to other pesticides, since the degradation rate was the highest for both the UVA and UVC conditions.

Pesticides	Photocatalytic reaction rate dC/dt (µg l ⁻¹ min ⁻¹)	
	UVA	UVC
Isoproturon	120.83	235.43
Simazine	111.11	192.66
Propazine	102.27	149.12

Table 6.1 Photocatalytic reaction rate of isoproturon, simazine, and propazine using P-25 TiO₂ under UVA and UVC (reaction rate constant at the first 10 minutes)

From Table 6.1 and Figure 6.10, isoproturon has the highest photocatalytic reaction rate among the three pesticides. This result corresponded to the earlier research carried out by Gora *et al.*, (2006) and also the research of Toepfer *et al.*, (2006) which studied the photocatalytic degradation of isoproturon, simazine and propazine in a multi-component system. The order of the photocatalytic rate was isoproturon, simazine and propazine, respectively,

which is the same as in the review of literature, explained in Section 2.11 and Section 4.5. Therefore, it can be concluded that isoproturon has the lowest stability when compared to the other two chemicals. The reason for this lack of stability is due to different structure or functional groups (Scribner *et al.*, 2000; Konstantinou and Albanis 2003; Benitez *et al.*, 2006; Lopez-Munoz *et al.*, 2011). Isoproturon is the phenylurea, whereas simazine and propazine are s-triazine (Section 1.1.5). Therefore, the degradation pathways are different, resulting in different degradation rates and different intermediates or by-products (Section 2.9). In the case of isoproturon, phenylurea herbicides, the structure breaks up due to (i) the attack of hydroxy radicals on the aromatic ring and (ii) abstraction of hydrogen atoms of the methyl group, followed by the addition of oxygen and decarboxylation. However, in the case of simazine and propazine (s-triazines), the degradation pathway start from displacement of the substituent at the position 2, side alkyl chain oxidation appears, followed by dealkylation and deamination. S-triazine is a group of pesticides which has highest tolerant against photocatalytic oxidation. However, the cyanouric acid, which is a by-product, exhibits very low toxicity.

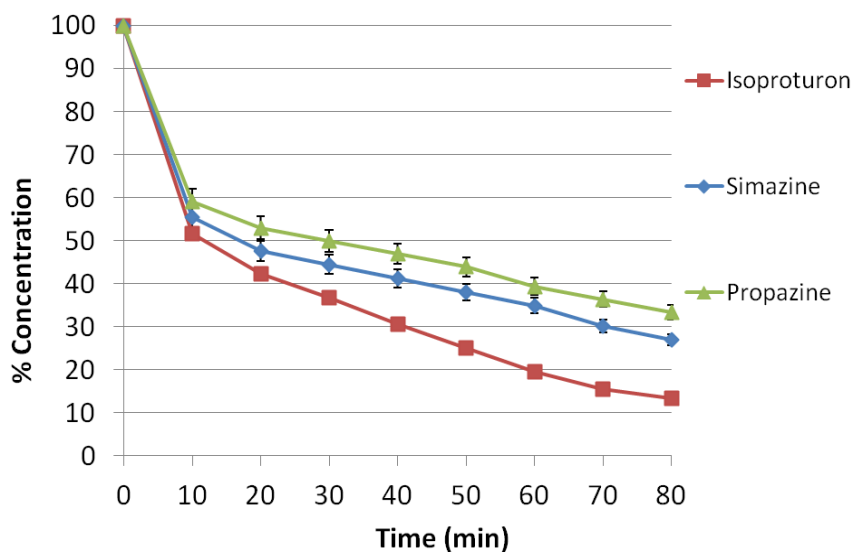


Figure 6.10 Photocatalytic degradation of isoproturon, simazine and propazine using fluidised bed reactor under UVA with P-25 TiO₂ concentration 5 g litre⁻¹

The effect of different catalyst loadings seems to differ for irradiation with UVC compared to UVA. As shown in Figure 6.11, the degradation concentrations of isoproturon using different P-25 TiO₂ concentrations under UVC were the same within the experimental error. For all three concentrations of UVC, the amount of catalyst has no influence on the degradation rate, since all samples had a decreased concentration equal to 90 % of the initial concentration in the first 10 minutes. In all cases, the photocatalytic rate of degradation is significantly greater than results when a catalyst is not present.

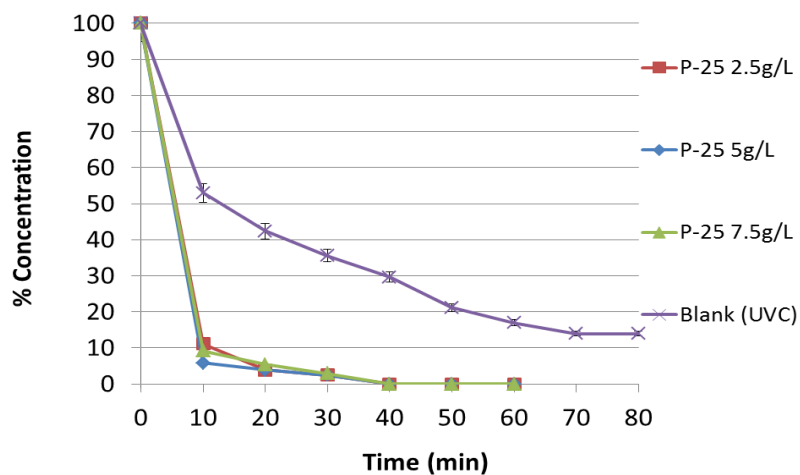


Figure 6.11 Photocatalytic degradation of isoproturon using fluidised bed reactor under UVC with P-25 TiO_2 concentration 2.5, 5 and 7.5 g litre^{-1}

From the results in Figure 6.12, the degradation rate of the three pesticides under UVC is in the order of isoproturon, simazine and propazine, respectively. This shows the same trend as the photocatalytic degradation under UVA, as illustrated in Figure 6.10. Therefore, isoproturon has the lowest stability amongst three pesticides when using a fluidised bed reactor.

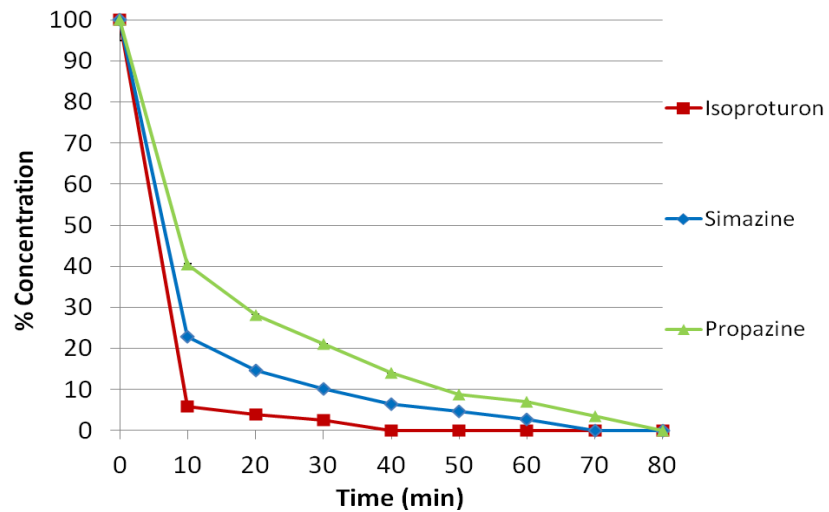


Figure 6.12 Photocatalytic degradation of isoproturon, simazine and propazine using fluidised bed reactor under UVC with P-25 TiO₂ concentration 5 g litre⁻¹

From the reaction law in Section 5.2, the photocatalytic reaction in the fluidised bed when using UVA was a first order reaction since there was a linear relationship between $\ln [C_R]/[C_0]$ and time, as shown in Figure 6.13. In Figure 6.14, the plot of $\ln [C_R]/[C_0]$ versus time was non-linear, when $C_R =$ concentration of pesticides.

$$\text{Rate} = dC/dt = k [C_R], \quad k = \text{min}^{-1} \quad (6.1)$$

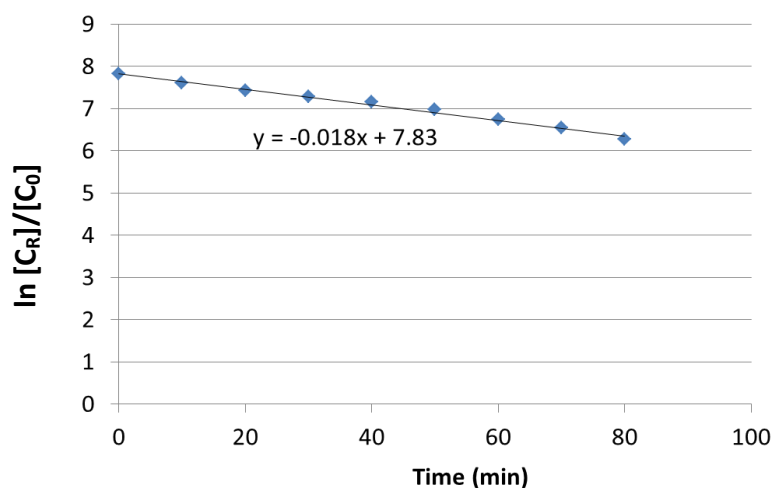


Figure 6.13 The linear relationship between $\ln [C_R]/[C_0]$ (remaining concentration divide by the initial concentration of isotroturon using P-25 7.5 g litre⁻¹ under UVA) and time, in this graph $k = 0.018 \text{ min}^{-1}$

The optimum curves relating to under UVA and UVC photocatalysis were plotted between the reaction rate constant of isotroturon and variable concentration of P-25 TiO₂, as shown in Figure 6.14. The data confirms that the optimum concentration of P-25 TiO₂ was equal to 5 g litre⁻¹, the same value as in the stirred system reported in Chapter 5. It can be seen from Figure 6.14 that beyond the optimum P-25 TiO₂ concentration, the reaction rate constant of isotroturon drastically decreased in the case of UVA and remained almost constant in the case of UVC.

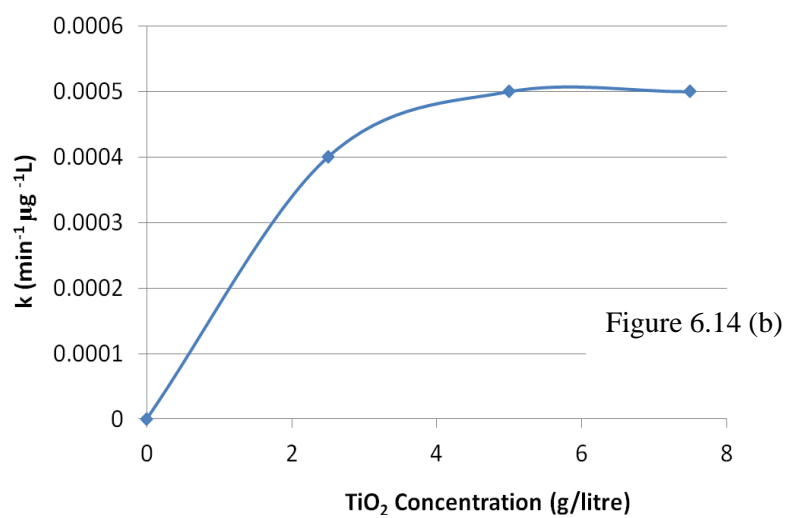
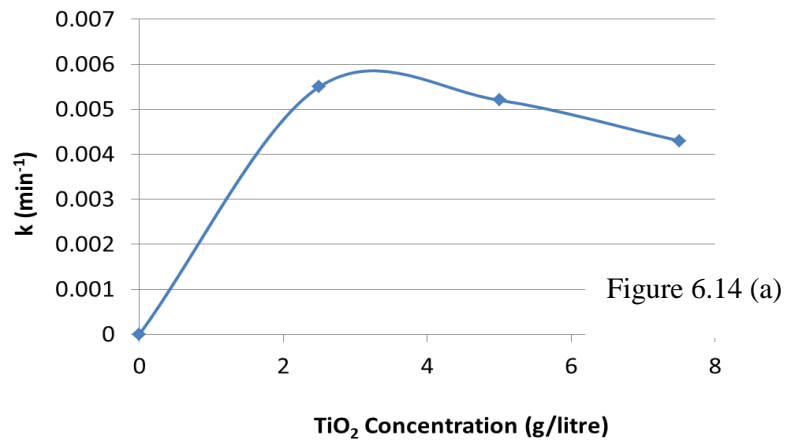


Figure 6.14 Optimum P-25 TiO₂ loading of the fluidised bed photoreactor under UVA (a), and UVC (b) irradiation for photocatalytic degradation of isoproturon, *k* value was calculated from Figure 6.8, and Figure 6.12 of isoproturon degradation

6.7 Influence of catalyst type (P-25 TiO₂ VS synthesised TiO₂)

In this section, degradation of the pesticides was conducted using the synthesised TiO₂ from ScWHS (Section 3.3) to compare the photocatalytic efficiency with P-25 TiO₂ under the same conditions. The TiO₂ synthesised

by ScWHS was further modified by drying at 80 °C for two days, followed by sintered at 900 °C for an hour. Both sets of experiments with the two TiO₂ catalysts were studied at a concentration of 5 g litre⁻¹. The P-25 TiO₂ catalyst was also sintered at the same temperature.

The results under UVA and UVC of the degradation of isoproturon are shown in Figures 6.15 and 6.16. The results of the degradation of the three pesticides photolysis using this fluidised bed photoreactor without any catalyst were also plotted in every graph to provide a baseline against which to measure the effectiveness of the catalyst. Both Figure 6.15 and Figure 6.16 clearly show that there was no difference in the rate of degradation of the pesticide in the presence of the synthesised TiO₂ as compared to the UVA and UVC photolysis of isoproturon.

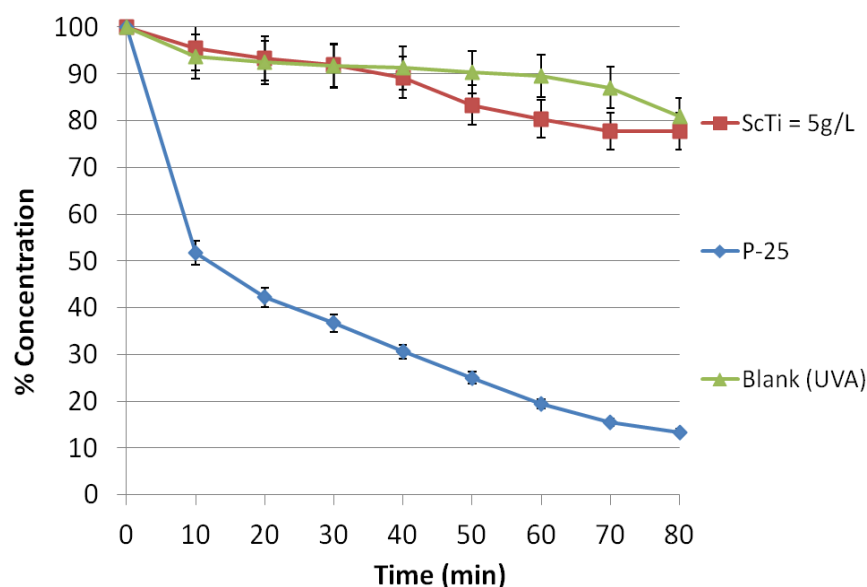


Figure 6.15 Photocatalytic degradation of isoproturon under UVA using synthesised TiO₂ 5 g litre⁻¹ compared with using P-25 TiO₂ 5 g litre⁻¹

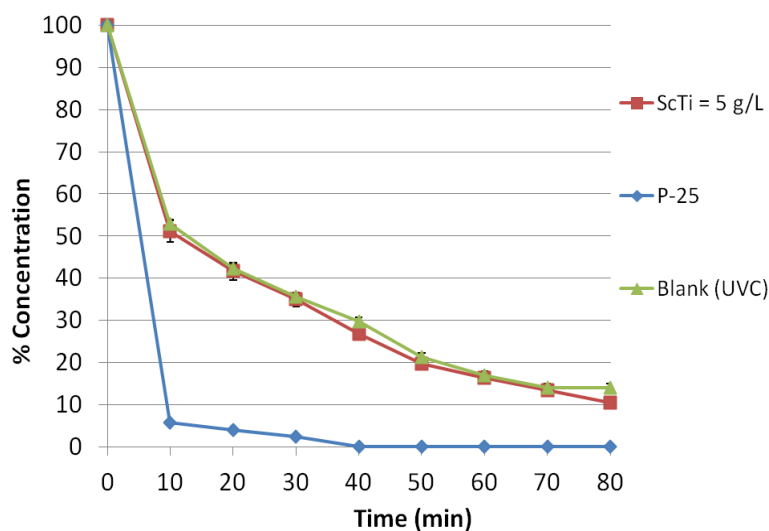


Figure 6.16 Photocatalytic degradation of isoproturon under UVC using synthesised TiO_2 5g litre^{-1} compared with using P-25 TiO_2 5g litre^{-1}

The results under UVA and UVC of the degradation of simazine using the synthesised TiO_2 after sintering at 900°C are compared with the sintered P-25 TiO_2 in Figure 6.17 and Figure 6.18. With simazine, the synthesised TiO_2 has a lower photocatalytic performance than P-25 TiO_2 after using both UVA and UVC.

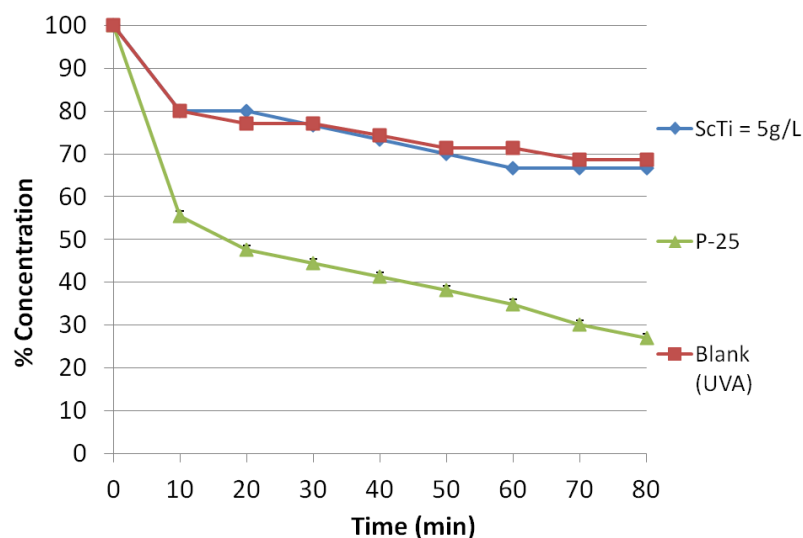


Figure 6.17 Photocatalytic degradation of simazine under UVA using synthesised TiO_2 5 g litre⁻¹ compared with using P-25 TiO_2 5 g litre⁻¹

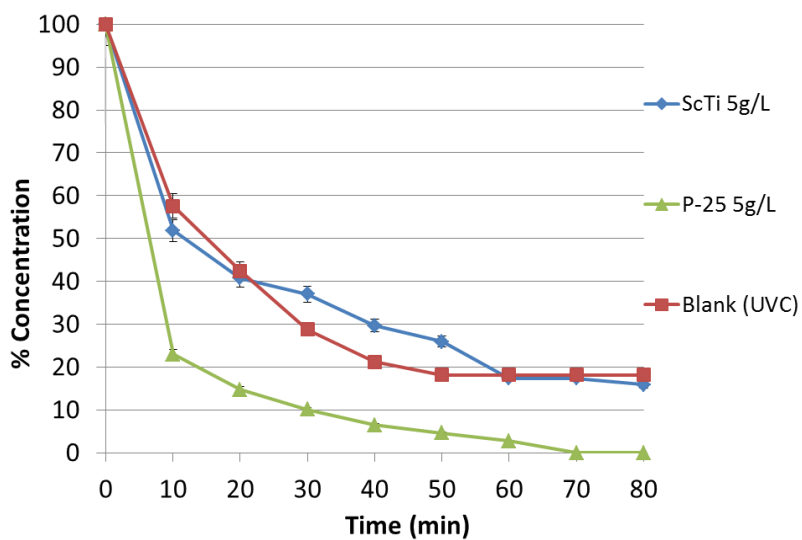


Figure 6.18 Photocatalytic degradation of simazine under UVC using synthesised TiO_2 5 g litre⁻¹ compared with using P-25 TiO_2 5 g litre⁻¹

The degradation results of propazine using the synthesised TiO_2 after sintering at 900°C compared with those of using the sintered P-25 TiO_2 for both under UVA and UVC irradiation are presented in Figure 6.19 and Figure 6.20.

From Figure 6.15 to Figure 6.20, it can be concluded that the synthesised TiO_2 had no effect on degradation and was not active in the photocatalytic reaction, since there was no difference between the results after adding the synthesised TiO_2 and blank samples (UVA or UVC only). The possible reason for this lack of activity can be explained using some characterisation techniques to prove the structure, phase, and size of the synthesised TiO_2 particles using transmission electron microscopy (TEM) and x-ray diffraction (XRD). Moreover, UV absorption ability was tested using ultraviolet-visible spectroscopy (UV-Vis).

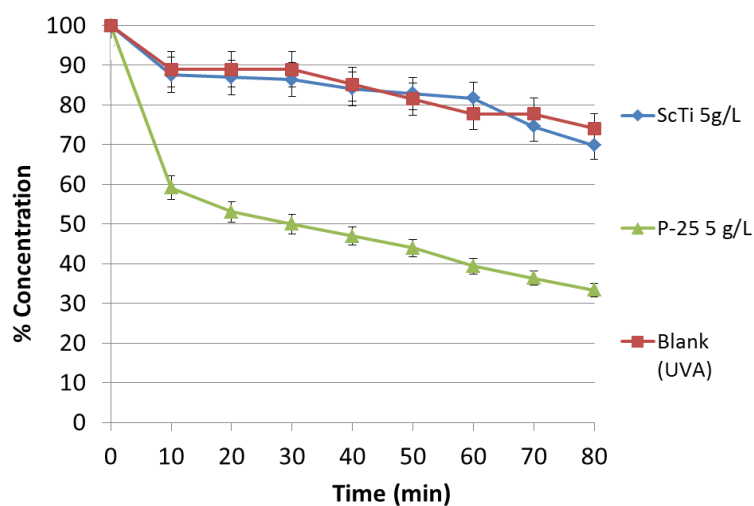


Figure 6.19 Photocatalytic degradation of propazine under UVA using synthesised TiO_2 5 g litre^{-1} compared with using P-25 TiO_2 5 g litre^{-1}

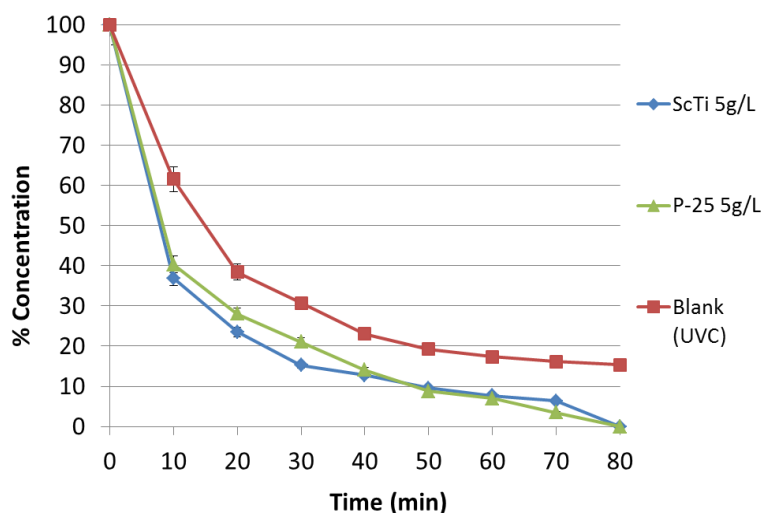


Figure 6.20 Photocatalytic degradation of propazine under UVC using synthesised TiO_2 5 g litre^{-1} compared with using P-25 TiO_2 5 g litre^{-1}

6.7 Transmission Electron Microscopy (TEM) results

TEM characterisations of both commercial P-25 TiO_2 and the synthesised TiO_2 were carried out to compare the particle size, as shown in Figure 6.21 and Figure 6.22 for P-25 TiO_2 and the synthesised TiO_2 , respectively. As seen in Figure 6.21, the particle size of P-25 TiO_2 is varied from 25-50 nm. The size of the synthesised TiO_2 was smaller than P-25 TiO_2 , which was 10-15 nm. However, the high surface area of the synthesised TiO_2 leads to the agglomeration of particles, as can be seen in Figure 6.27 (b). This agglomeration is one of the reasons why the synthesised TiO_2 had lower photocatalytic efficiency compared to P-25 TiO_2 . In addition, the synthesised TiO_2 was not as active as the commercial P-25 TiO_2 , since the data showed the same trend as the blank.

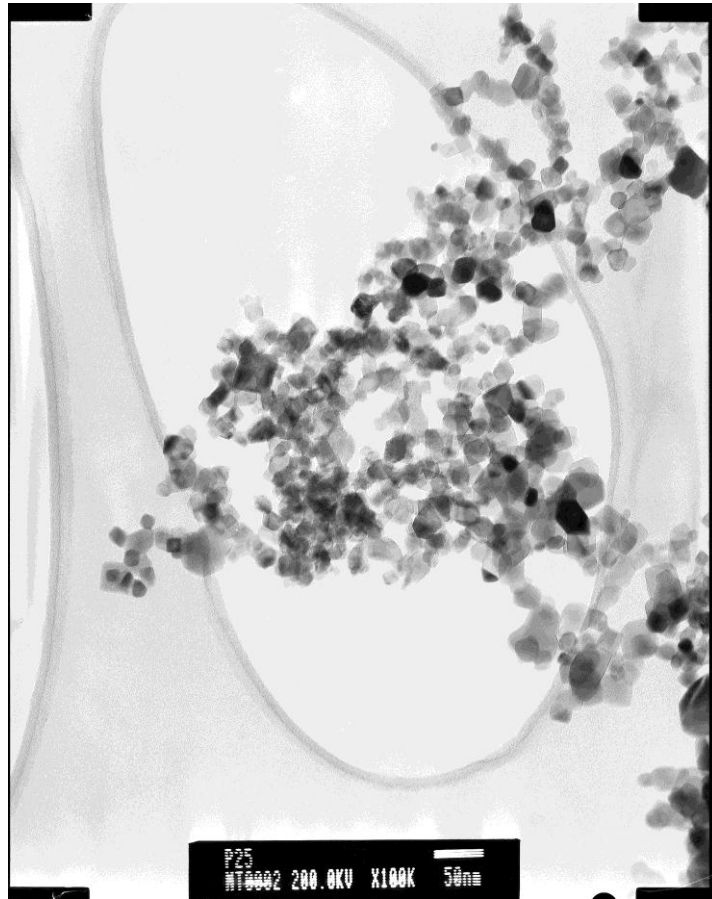


Figure 6.21 TEM photograph of P-25 TiO₂ in aqueous suspension

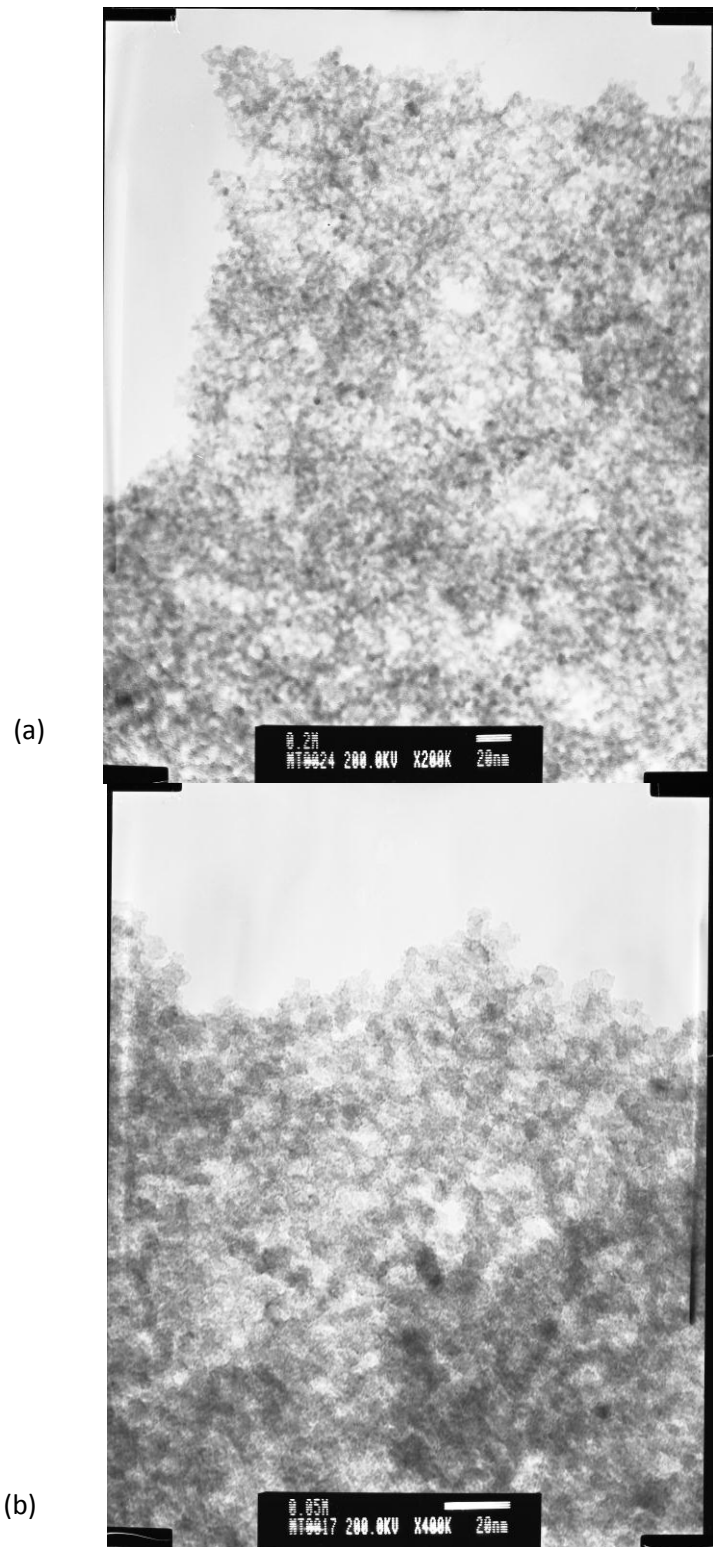


Figure 6.22 TEM photograph of synthesised TiO_2 in aqueous suspension (a) fine particles with the size of 10-15 nm (b) start to agglomerate due to high surface area

6.8 X-Ray Diffraction (XRD) results

Bulk TiO₂ in anatase phase underwent the transition to rutile phase when heated to a temperature above 700 °C, as described in Section 2.11 (Radwan, 2005; Pelaez *et al.*, 2012; Ahmed *et al.*, 2011). For the synthesised TiO₂ from the supercritical water hydrothermal synthesis (ScWHS), the phase remains anatase even at temperatures as high as 1000 °C, as shown in the XRD results in Chapter 5, Figure 5.19. This is the other reason why this TiO₂ had lower photocatalytic performance than P-25 TiO₂ at any temperature. From the review of the literature in Chapter 2, P-25 TiO₂ composed of 75 % anatase phase and 25 % rutile (Singh and Muneer 2004; Singh *et al.*, 2007; Ahmed *et al.*, 2011) which suggests a co-operative performance in photocatalytic reaction, as proposed by many researchers (Qourzal *et al.*, 2008; Hurum *et al.*, 2003; Yeredla and Xu, 2008).

6.9 Ultraviolet-visible Spectroscopy (UV-Vis) results

The UV-Vis characterisation of the synthesised TiO₂, compared with the commercial P-25 TiO₂, was performed in this section. The result of UV-Vis absorption on both types of TiO₂ is shown in Figure 6.25. The synthesised TiO₂ had higher absorptivity at low wavelength (at 200 nm to 350 nm) when compared to the P-25 TiO₂. From Figure 6.23, the commercial P-25 TiO₂ has better UV absorption than the synthesised variety. The cut-off wavelength, the wavelength that has lowest UV absorptivity, of P-25 TiO₂ was equal to 410.57 nm. In the case of the synthesised TiO₂, the cut-off wavelength was equal to

380 nm, which was a lower wavelength than P-25 TiO₂. From Planck's Equation (Equation 2.23), the energy band gap of P-25 TiO₂ and the synthesised TiO₂ can be calculated from the UV-Vis results as follows,

$$E = hc / \lambda \quad (2.23)$$

$$h = \text{Planck's constant} = 6.626 \times 10^{-34} \text{ J s}$$

$$C = \text{speed of light} = 3 \times 10^8 \text{ m/s}$$

$$\lambda = \text{cut-off wavelength}$$

(i) For P-25 TiO₂,

$$E = \frac{(6.626 \times 10^{-34} \text{ J s}) \times (3 \times 10^8 \text{ m/s})}{410.57 \times 10^{-9} \text{ m}}$$

$$E = 4.84 \times 10^{-19} \text{ J}$$

$$= 3.02 \text{ eV (where } 1 \text{ eV} = 1.6 \times 10^{-19} \text{ J, conversion factor)}$$

(ii) For the synthesised TiO₂ from ScWHS

$$E = \frac{(6.626 \times 10^{-34} \text{ J s}) \times (3 \times 10^8 \text{ m/s})}{380 \times 10^{-9} \text{ m}}$$

$$E = 5.23 \times 10^{-19} \text{ J}$$

$$= 3.27 \text{ eV}$$

From the calculation above, it can be seen that P-25 TiO₂ had a lower energy bandgap (3.02 eV) than the synthesised TiO₂ (3.27 eV). This energy bandgap is the required energy of photons used in photoactivation of the photocatalytic

reaction. If the photocatalyst has a low energy bandgap, the required energy for photocatalytic reaction is also low. This means there is a high possibility of a photocatalytic reaction occurring even at low photon energy levels; the lower the bandgap, the higher the efficiency of the photocatalyst. Therefore, the synthesised TiO₂ had inferior photocatalytic efficiency when compared to P-25 TiO₂.

The synthesised TiO₂ has pure anatase phase which can absorb only the lower wavelength, whereas the commercial P-25 TiO₂ has 25 wt% rutile, which can absorb at the longer wavelength up to 400 nm, as explained in Section 2.11.

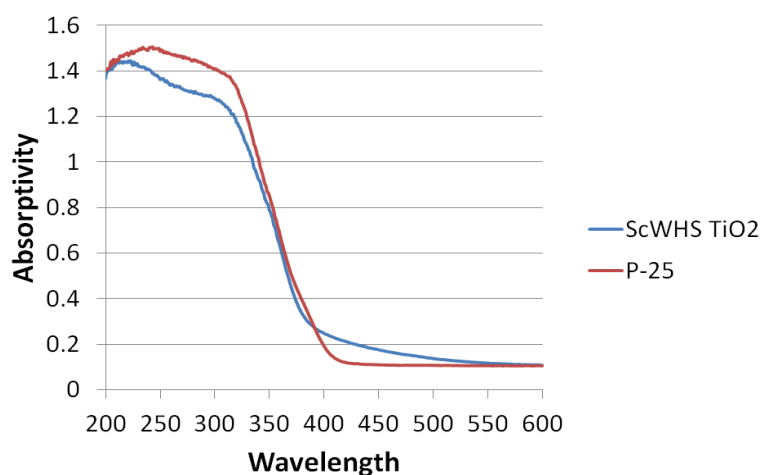


Figure 6.23 UV-Vis spectroscopy of the P-25 TiO₂ comparing with the synthesised TiO₂

6.10 Conclusions of fluidised bed photoreactor experiments

In this chapter, several experiments were carried out using a fluidised bed photoreactor. The pesticide concentration adsorbed on TiO₂ particles was

between 10-15%, due to high concentration of TiO_2 . There was almost no difference between the concentration loss of isoproturon, simazine, and propazine. In photolysis and photocatalytic reaction, UVC showed higher performance than UVA, which is in accordance with the results using other types of reactor (Chapter 4: TFFBR and Chapter 5: stirred photoreactor). Amongst the three reactors studied, the fluidised bed showed the highest photodegradation efficiency, yielding the highest degradation concentration of the three pesticides from both UVA and UVC photolysis and photocatalytic. The fluidised bed photoreactor has counter-current mixing of air bubbling from the bottom of the column, while the sintered TiO_2 was introduced from the top, and dropped to the bottom of the column by gravity. This increases the contact area and contact time between oxygen molecules and the TiO_2 surface. Moreover, the UV intensity is another reason, since there is high surface for UV illumination in the length dimension of the column. The influence of different photocatalyst loading on the pesticide degradation was performed and resulted in the optimal TiO_2 concentration = 5 g litre^{-1} , which was similar to the case of the stirred photoreactor (Chapter 5). The photocatalytic mechanism of UVC illumination was different from UVA. In the case of UVA, the reaction rate was defined as the first order, whereas for UVC it was defined as the second order. For the fluidised bed reactor, isoproturon has the lowest stability amongst the three chosen pesticides. Photolysis and photocatalytic of pesticide solutions under the UVA and the UVC irradiation were studied and compared, using the P-25 TiO_2 and the synthesised TiO_2 . The P-25 TiO_2 had extremely performance in photocatalytic activity. However, the (sintered) synthesised TiO_2 showed inferior photocatalytic

efficiency. This result corresponds with the results from the other two reactors (Chapter 4: TFFBR, Chapter 5: stirred photoreactor). The various characterisations of TiO₂, which was synthesised by the super critical water hydrothermal synthesis process (ScWHS) were also carried out. In TEM images, the particle size of the synthesised TiO₂ was approximately 10-15 nm, which was smaller than P-25 TiO₂ (25-50 nm). However, an agglomeration was clearly shown, which may be one reason why the synthesised TiO₂ had low efficiency. The results from XRD at different sintering temperatures also supported this discovery, by showing no phase transition appear at any temperature from 30-1000 °C. In addition, UV-Vis results disclosed that the commercial TiO₂ absorb at the visible wavelength better than the synthesised one.

Chapter 7

CONCLUSIONS AND RECOMMENDATIONS

7.1 Overview of results and experimental work

This chapter concludes the main achievements of work presented in this thesis and suggests recommendations for future work.

The main objectives of this study are reiterated:

- (i) To use TiO₂ nanoparticles synthesised by the supercritical water in the waste water treatment
- (ii) To characterise TiO₂ produced via hydrothermal synthesis using Scanning Electron Microscopy (SEM), Transmission Electron Microscopy (TEM), Ultraviolet-Visible absorption spectroscopy (UV-Vis) and X-Ray Diffraction (XRD)
- (iii) To design, construct and develop three different types of reactors (thin film fixed bed reactor, stirred reactor and fluidised bed photoreactor) for the treatment of the water polluted by three pesticides
- (iv) To evaluate the effectiveness of commercial P-25 TiO₂ compared with ScWHS synthesised TiO₂ when applied to the photocatalytic degradation of the aqueous solutions of three selected pesticides (isoproturon, simazine and propazine)

(v) To study the effect of the operating parameters such as catalyst concentration, pesticide concentration, and the wavelength of light on the photocatalytic degradation of the pesticides

7.2 Conclusions

(i) The adsorption mechanism of pesticide solutions onto TiO_2 has no influence on the photocatalytic degradation of isoproturon, simazine and propazine. The results suggested that the decreases of the three pesticide concentrations, under darkness, were only 10% of the initial concentration.

(ii) UVC has more effect on both photolysis and photocatalytic reaction when compared to UVA. Under UVC illumination, the decrease of the concentrations of isoproturon, simazine, and propazine was higher than under UVA, after 90 minutes. This corresponds to Planck's equation, a relationship between photon energy and light wavelength.

(iii) The commercial TiO_2 (P-25 TiO_2) has high performance and is the important part of the photocatalytic reaction, since photolysis showed lower pesticide degradation than in the case of a photocatalytic (adding TiO_2). The optimum concentration of P-25 TiO_2 was found to be equivalent to 5 g/litre while using the fluidised bed photoreactor and stirred reactor.

(iv) The efficiency of the synthesised TiO_2 from ScWHS techniques is lower than that of P-25 TiO_2 . It can be referred to many results in

Chapter 5 and 6 that degradation of isoproturon, simazine and propazine was nearly the same amount as without any photocatalyst (UV alone or photolysis reaction). In addition, P-25 TiO₂ has superior photocatalytic performance, since degradation levels of the concentration of isoproturon, simazine and propazine, after using P-25 TiO₂, were significantly higher than after using the synthesised TiO₂.

(v) The fluidised bed photoreactor presented the highest performance among the three types of reactor, because there was a counter-current flow of water and oxygen, initiating a thorough mixing process which helps oxygen molecules to attach themselves onto photocatalyst surfaces. Moreover, the design of the fluidised bed photoreactor had the advantage that two UV lamps were set up nearby and covered almost all the surface area of the reactor (quartz tube).

(vi) Amongst the three selected pesticides, photocatalytic degradation of isoproturon was the highest. However, in case of photolysis, the decrease of simazine concentration was higher than isoproturon and propazine.

(vii) There was an assumption that there was some effect from dodecyl succinic anhydride (DDSA) on adsorption of propazine on the synthesised TiO₂ surface, due to its polarity. DDSA is an additional surfactant in the drying process for coating synthesised TiO₂ on stainless steel plate of the Thin Film Fixed Bed Reactor (TFFBR) in Chapter 4.

(viii) The synthesised TiO_2 on the surface of the TFFBR has small particles, as shown by SEM images in Chapter 4, when compared to the TiO_2 surface. EDAX data proposed that the surface of synthesised TiO_2 contained high quantities of carbon molecules, which came from DDSA and reduced photocatalytic efficiency.

(ix) The characterisation results of synthesised TiO_2 in Chapter 6 showed that UV absorption slightly shifts to a visible wavelength from Ultraviolet-visible Spectroscopy (UV-Vis) for P-25 TiO_2 , when compared to the synthesised TiO_2 . However, there was a higher grain size due to agglomeration of fine particles as shown in Transmission Spectroscopy Microscope (TEM). Also, after sintering at $900\text{ }^\circ\text{C}$, the phase of synthesised TiO_2 was still anatase, having not changed to the rutile, as seen from X-Ray Diffraction (XRD) results at different temperatures. This led to inferior photocatalytic performance, when compared to P-25 TiO_2 .

7.3 Recommendations for future work

More characterisation techniques of synthesised TiO_2 (by ScWHS) might be advantage to explain in depth-detail for this study. A study of photocatalytic kinetics over a wide concentration range of initial pesticides (0.5, 1, 2, 3, 4, 5, 6, 7, 8, 9, 10 ppm), using a stirred reactor and a fluidised bed photoreactor, would be carried out to investigate the influence of pesticide concentration on photocatalytic reaction rate and also optimise the most efficient initial

concentration that would achieve the highest degradation. Moreover, the studies of other operation parameters, such as oxygen flowrate, H_2O_2 or using different light intensities should be included. Further development of synthesised TiO_2 by the supercritical water hydrothermal method, or other techniques, would be beneficial for the photocatalytic treatment of water. Adding some metals or chemical compounds into the nanoparticles synthesis process would also be interesting to investigate; particularly whether they help improve the ability of UV absorption and assist the photocatalytic reaction. In addition, the impact of using supercritical water on oxidation would also be valuable to study, as a challenging option for water treatment.

The main recommendations for future work are then related to the synthesis of immobilised photocatalysts by coating TiO_2 on ceramics, polymers, or activated carbon to improve fluidised bed efficiency, working on the pilot plant scale, doing simulation and evaluating the cost of the fluidised bed as it has high performance in photocatalytic reaction compared to other reactor.

APPENDICES

These appendices (I, II, III) show the average remaining concentration (in % of initial concentration of pesticide), variance, and the probability from two-tail T-tests comparing two sets of data, as an analysis database, to find out whether there are significant differences.

- (i) When the probability value of the T-test is higher than 0.05 (critical value): there is no significant difference between two sets of data
- (ii) When the probability value of the T-test is lower than or equal to 0.05 (critical value): there is a significant difference between two sets of data

Appendix I: Student T-test for TFFBR results

Appendix II: Student T-test for stirred photoreactor results

Appendix III: Student T-test for fluidised bed photoreactor

APPENDIX I

Student T-test for

Thin film fixed bed results

I.1. UVA/UVC photolysis of isoproturon

<i>Statistical value</i>	<i>UVA</i>	<i>UVC</i>
Mean	88.138	81.7
Variance	6.192	2.48
Observations	3	3
P(T<=t) two-tail	0.032	
t Critical two-tail	3.182	

I.2 UVA/UVC photolysis of simazine

<i>Statistical value</i>	<i>UVA</i>	<i>UVC</i>
Mean	80.208	76.33
Variance	0.567	0.33
Observations	3	3
P(T<=t) two-tail	0.002	
t Critical two-tail	2.776	

I. 3 UVA/UVC photolysis of propazine

<i>Statistical value</i>	<i>UVA</i>	<i>UVC</i>
Mean	85	79
Variance	1	1
Observations	3	3
P(T<=t) two-tail	0.002	
t Critical two-tail	2.77	

I.4 UVC photolysis of isoproturon VS simazine

<i>Statistical value</i>	<i>Isoproturon</i>	<i>Simazine</i>
Mean	82.268	76.454
Variance	0.062	0.26
Observations	3	3
P(T<=t) two-tail	0	
t Critical two-tail	3.182	

I.5 UVC photolysis of simazine VS propazine

<i>Statistical value</i>	<i>Simazine</i>	<i>Propazine</i>
Mean	76.454	78
Variance	0.256	1
Observations	3	3
P(T<=t) two-tail	0.011	
t Critical two-tail	3.182	

I.6 UVC photolysis of isoproturon VS propazine

<i>Statistical value</i>	<i>Isoproturon</i>	<i>Propazine</i>
Mean	82.26	78
Variance	0.062	1
Observations	3	3
P(T<=t) two-tail	0	
t Critical two-tail	2.776	

I.7 UVA photolysis of isoproturon VS simazine

<i>Statistical value</i>	<i>Isoproturon</i>	<i>Simazine</i>
Mean	87.5	79.04
Variance	0.25	0.043
Observations	3	3
P(T<=t) two-tail	0	
t Critical two-tail	3.182	

I.8 UVA photolysis of simazine VS propazine

<i>Statistical value</i>	<i>Simazine</i>	<i>Propazine</i>
Mean	79.04	83.6
Variance	0.043	0.28
Observations	3	3
P(T<=t) two-tail	0.002	
t Critical two-tail	3.182	

I.9 UVA photolysis of isoproturon VS propazine

<i>Statistical value</i>	<i>Isoproturon</i>	<i>Propazine</i>
Mean	87.5	83.6
Variance	0.25	0.28
Observations	3	3
P(T<=t) two-tail	0	
t Critical two-tail	2.776	

I.10 UVA photocatalytic of isoproturon at high flow rate (100 ml min⁻¹) VS low flow rate (20 ml min⁻¹)

<i>Statistical value</i>	<i>High flow</i>	<i>Low flow</i>
Mean	75.17	73.6
Variance	1.088	2.325
Observations	3	3
P(T<=t) two-tail	0.219	
t Critical two-tail	2.776	

I.11 UVA photocatalytic of simazine at high flow rate (100 ml min⁻¹) VS low flow rate (20 ml min⁻¹)

<i>Statistical value</i>	<i>High flow</i>	<i>Low flow</i>
Mean	63.814	46.85
Variance	2.547	3.8
Observations	3	3
P(T<=t) two-tail	0	
t Critical two-tail	2.776	

I.12 UVA photocatalytic of propazine at high flow rate (100 ml min⁻¹)VS low flow rate (20 ml min⁻¹)

<i>Statistical value</i>	<i>High flow</i>	<i>Low flow</i>
Mean	71.178	68.7
Variance	4.095	2.37
Observations	3	3
P(T<=t) two-tail	0.167	
t Critical two-tail	2.776	

I.13 UVC photocatalytic of isoproturon at high flow rate (100 ml min⁻¹)VS low flow rate (20 ml min⁻¹)

<i>Statistical value</i>	<i>High flow</i>	<i>Low flow</i>
Mean	86.18	76.154
Variance	1.1	1.07
Observations	3	3
P(T<=t) two-tail	0	
t Critical two-tail	2.776	

I.14 UVC photocatalytic of simazine at high flow rate (100 ml min⁻¹) VS low flow rate (20 ml min⁻¹)

<i>Statistical value</i>	<i>High flow</i>	<i>Low flow</i>
Mean	54.148	46.2
Variance	1.065	1.148
Observations	3	3
P(T<=t) two-tail	0	
t Critical two-tail	2.776	

I.15 UVC photocatalytic of propazine at high flow rate (100 ml min⁻¹) VS low flow rate (20 ml min⁻¹)

<i>Statistical value</i>	<i>High flow</i>	<i>Low flow</i>
Mean	60.2	55.328
Variance	4.129	2.309
Observations	3	3
P(T<=t) two-tail	0.029	
t Critical two-tail	2.776	

I.16 UVC photocatalytic of isoproturon at low initial concentration (2.5 ppm)
VS high initial concentration (20 ppm)

<i>Statistical value</i>	<i>2.5 ppm</i>	<i>20ppm</i>
Mean	51.44	77.154
Variance	0.26	0.607
Observations	3	3
P(T<=t) two-tail	0	
t Critical two-tail	3.18	

I.17 UVC photocatalytic of propazine at low initial concentration (2.5 ppm)
VS high initial concentration (20 ppm)

<i>Statistical value</i>	<i>2.5 ppm</i>	<i>20 ppm</i>
Mean	48.69	56.895
Variance	0.073	0.128
Observations	3	3
P(T<=t) two-tail	0	
t Critical two-tail	2.776	

APPENDIX II

Student T-test for

Stirred photoreactor results

II.1 Adsorption concentration of isoproturon VS simazine in the absence of

UV

<i>Statistical value</i>	<i>Isoproturon</i>	<i>Simazine</i>
Mean	95.883	95.561
Variance	8.317	6.414
Observations	3	3
P(T<=t) two-tail	0.804	
t Critical two-tail	2.120	

II.2 Adsorption concentration of simazine VS propazine in the absence of UV

<i>Statistical value</i>	<i>Simazine</i>	<i>Propazine</i>
Mean	95.561	96.325
Variance	6.414	2.446
Observations	3	3
P(T<=t) two-tail	0.455	
t Critical two-tail	2.160	

II.3 Adsorption concentration of isoproturon VS propazine in the absence of

UV

<i>Statistical value</i>	<i>Isoproturon</i>	<i>Propazine</i>
Mean	95.883	96.325
Variance	8.317	2.446
Observations	3	3
P(T<=t) two-tail	0.693	
t Critical two-tail	2.179	

APPENDIX III

Student T-test for

Fluidised bed photoreactor results

III.1 Adsorption concentration of isoproturon VS simazine in the absence of

UV

<i>Statistical value</i>	<i>Isoproturon</i>	<i>Simazine</i>
Mean	91.764	95.238
Variance	11.86	4.75
Observations	3	3
P(T<=t) two-tail	0.023	
t Critical two-tail	2.145	

III.2 Adsorption concentration of simazine VS propazine in the absence of UV

<i>Statistical value</i>	<i>Simazine</i>	<i>Propazine</i>
Mean	95.238	89.379
Variance	4.75	21.5
Observations	3	3
P(T<=t) two-tail	0.006	
t Critical two-tail	2.201	

III.3 Adsorption concentration of isoproturon VS propazine in the absence of UV

<i>Statistical value</i>	<i>Isoproturon</i>	<i>Propazine</i>
Mean	91.764	89.379
Variance	11.86	21.5
Observations	3	3
P(T<=t) two-tail	0.235	
t Critical two-tail	2.131	

III.4 UVA photolysis of isoproturon VS simazine

<i>Statistical value</i>	<i>Isoproturon</i>	<i>simazine</i>
Mean	76	68.57
Variance	1	0
Observations	3	3
P(T<=t) two-tail	0.005	
t Critical two-tail	4.3	

III.5 UVA photolysis of simazine VS propazine

<i>Statistical value</i>	<i>Simazine</i>	<i>Propazine</i>
Mean	68.5	74.183
Variance	0.01	0.015
Observations	3	3
P(T<=t) two-tail	0	
t Critical two-tail	2.77	

III.6 UVA photolysis of isoproturon VS propazine

<i>Statistical value</i>	<i>Isoproturon</i>	<i>Propazine</i>
Mean	76	74.183
Variance	1	0.015
Observations	3	3
P(T<=t) two-tail	0.089	
t Critical two-tail	4.3	

III.7 UVC photolysis of isoproturon VS simazine

<i>Statistical value</i>	<i>Isoproturon</i>	<i>Simazine</i>
Mean	13.8	18.13
Variance	0.01	0.023
Observations	3	3
P(T<=t) two-tail	0	
t Critical two-tail	3.18	

III.8 UVC photolysis of simazine VS propazine

<i>Statistical value</i>	<i>Simazine</i>	<i>Propazine</i>
Mean	18.13	15.36
Variance	0.023	0.003
Observations	3	3
P(T<=t) two-tail	0.001	
t Critical two-tail	4.3	

III.9 UVC photolysis of isoproturon VS propazine

<i>Statistical value</i>	<i>Isoproturon</i>	<i>Propazine</i>
Mean	13.8	15.36
Variance	0.01	0.003
Observations	3	3
P(T<=t) two-tail	0	
t Critical two-tail	3.18	

III.10 UVA photolysis of isoproturon using fluidised bed VS stirred photoreactor

<i>Statistical value</i>	<i>Fluidised bed</i>	<i>Stirred reactor</i>
Mean	76	87.33
Variance	1	1.33
Observations	3	3
P(T<=t) two-tail	0	
t Critical two-tail	2.776	

III.11 UVA photolysis of isoproturon using fluidised bed VS TFFBR

<i>Statistical value</i>	<i>Fluidised bed</i>	<i>TFFBR</i>
Mean	76	87.17
Variance	1	0.08
Observations	3	3
P(T<=t) two-tail	0.003	
t Critical two-tail	4.3	

III.12 UVA photolysis of simazine using fluidised bed VS stirred photoreactor

<i>Statistical value</i>	<i>Fluidised bed</i>	<i>Stirred reactor</i>
Mean	68.5	85
Variance	0.01	0.25
Observations	3	3
P(T<=t) two-tail	0	
t Critical two-tail	4.3	

III.13 UVA photolysis of simazine using fluidised bed VS TFFBR

<i>Statistical value</i>	<i>Fluidised bed</i>	<i>TFFBR</i>
Mean	68.5	79.04
Variance	0.01	0.043
Observations	3	3
P(T<=t) two-tail	0.003	
t Critical two-tail	4.3	

III.14 UVA photolysis of propazine using fluidised bed VS stirred photoreactor

<i>Statistical value</i>	<i>Fluidised bed</i>	<i>Stirred reactor</i>
Mean	74.18	87
Variance	0.016	0
Observations	3	3
P(T<=t) two-tail	0	
t Critical two-tail	4.3	

III.15 UVA photolysis of propazine using fluidised bed VS TFFBR

<i>Statistical value</i>	<i>Fluidised bed</i>	<i>TFFBR</i>
Mean	74.18	83.6
Variance	0.015	0.28
Observations	3	3
P(T<=t) two-tail	0	
t Critical two-tail	3.182446305	

III.16 UVC photolysis of isoproturon using fluidised bed VS stirred

photoreactor

<i>Statistical value</i>	<i>Fluidised bed</i>	<i>Stirred reactor</i>
Mean	13.8	65.5
Variance	0.01	0.25
Observations	3	3
P(T<=t) two-tail	0	
t Critical two-tail	4.3	

III.17 UVC photolysis of isoproturon using fluidised bed VS TFFBR

<i>Statistical value</i>	<i>Fluidised bed</i>	<i>TFFBR</i>
Mean	13.8	82.268
Variance	0.01	0.062
Observations	3	3
P(T<=t) two-tail	0	
t Critical two-tail	4.3	

III.18 UVC photolysis of simazine using fluidised bed VS stirred photoreactor

<i>Statistical value</i>	<i>Fluidised bed</i>	<i>Stirred reactor</i>
Mean	18.13	67
Variance	0.023	0
Observations	3	3
P(T<=t) two-tail	0	
t Critical two-tail	4.3	

III.19 UVC photolysis of simazine using fluidised bed VS TFFBR

<i>Statistical value</i>	<i>Fluidised bed</i>	<i>TFFBR</i>
Mean	18.13	76.454
Variance	0.023	0.26
Observations	3	3
P(T<=t) two-tail	0	
t Critical two-tail	3.18	

III.20 UVC photolysis of propazine using fluidised bed VS stirred

photoreactor

<i>Statistical value</i>	<i>Fluidised bed</i>	<i>Stirred reactor</i>
Mean	15.36	68
Variance	0.003	0
Observations	3	3
P(T<=t) two-tail	0	
t Critical two-tail	4.30	

III.21 UVC photolysis of propazine using fluidised bed VS TFFBR

<i>Statistical value</i>	<i>Fluidised bed</i>	<i>TFFBR</i>
Mean	15.36	78
Variance	0.003	1
Observations	3	3
P(T<=t) two-tail	0	
t Critical two-tail	4.3	

III.22 UVA photocatalytic of isoproturon using fluidised bed VS stirred

photoreactor

<i>Statistical value</i>	<i>Fluidised bed</i>	<i>Stirred reactor</i>
Mean	11.58	0
Variance	0.453	0
Observations	3	3
P(T<=t) two-tail	0.001	
t Critical two-tail	4.3	

III.23 UVA photocatalytic of simazine using fluidised bed VS stirred

photoreactor

<i>Statistical value</i>	<i>Fluidised bed</i>	<i>Stirred reactor</i>
Mean	23.456	0
Variance	0.134	0
Observations	3	3
P(T<=t) two-tail	0	
t Critical two-tail	4.3	

III. 24 UVA photocatalytic of propazine using fluidised bed VS stirred

photoreactor

<i>Statistical value</i>	<i>Fluidised bed</i>	<i>Stirred reactor</i>
Mean	28.29	0
Variance	0.24	0
Observations	3	3
P(T<=t) two-tail	0	
t Critical two-tail	4.3	

BIBIOGRAPHY

Abramovic B. F., Anderluh V. B., Topalov A. S. and Gaal F. F., Titanium dioxide mediated photocatalytic degradation of 3-amino-2-chloropyridine *App. Cat. B: Environ.* 48 (2004) 213-221.

Ahmed S., Rasul M.G., Brown R., Hashib M.A. Influence of parameters on the heterogeneous photocatalytic degradation of pesticides and phenolic contaminants in wastewater: A short review. *J. Env. Man.* 92 (2011) 311-330.

Aimable A., Muhr H., Gentric C., Bernard F., Le Cras F., Aymes D. Continuous hydrothermal synthesis of inorganic nanopowders in supercritical water: Towards a better control of the process *Powd. Tech.* 190(1-2)(2009) 99-106.

Akpan U.G. and Hameed B.H. Parameters affecting the photocatalytic degradation of dyes using TiO₂-based photocatalysts: A review *J. Haz. Mat.* 170 (2009) 520–529.

Alexander V. V., Evgueni N. S. and Panagiotis G. S., Vibrofluidized- and fixed-bed photocatalytic reactors: case of gaseous acetone photooxidation *Chem. Eng. Sci.* 55(21) (2000) 5089-5098.

Aungpradit T., Sutthivaiyakit P., Martens D., Sutthivaiyakit S., Kettrup A. A. F. Photocatalytic degradation of triazophos in aqueous titanium dioxide suspension: Identification of intermediates and degradation pathways *J. Hazard. Mat.* 146 (2007) 204-213.

Aramendia M. A., Marinas A., Marinas J. M., Moreno J. M., Urbano F. Photocatalytic degradation of herbicide fluoroxypyr in aqueous suspensions of TiO₂ *Cat. Today* 101 (2005) 187-193.

Atashfaraz, M., M. Shariaty-Niassar, et al. Effect of titanium dioxide solubility on the formation of BaTiO₃ nanoparticles in supercritical water *Fluid Phase Equ.* 257(2) (2007) 233-237.

Axelsson A.K. and Dunne L.J. Mechanism of photocatalytic oxidation of 3, 4-dichlorophenol on TiO₂ semiconductor surfaces *J. Photochem. Photobio. A: Chem.* 144(2-3) (2001) 205-213.

Azizi S., Sehili T., Djebbar K., Comparative Study of Phototransformation of Isoproturon Aqueous Solution by UV/H₂O₂ Treatment, Fenton's Reagent, Photo-Fenton and Photocatalytic Processes *J. Env. Eng. Tech.* 2 (1) (2013) 17-24.

Barcelo D., Durand G., Bertrand N., Albaiges J. Determination of aquatic photodegradation products of selected pesticides by gas chromatography-mass

spectrometry and liquid chromatography-mass spectrometry *Sci. Total Env.* 132 (2–3) (1993), 283–296.

Bahnemann D., Photocatalytic water treatment: solar energy applications. *Solar Energy* 77 (2004) 445-459.

Bambang V. and Jae-Duck K. Supercritical water oxidation for the destruction of toxic organic wastewaters: A review. *J. Env. Sci.* 19 (2007): 513-522.

Benitez J., Real F. J., Acero J. L., Garcia C. Photochemical oxidation processes for the elimination of phenyl-urea herbicides in waters *J. Hazard. Mat. B* 138 (2006) 278–287

Bermejo M. D. and Cocero M.J. Supercritical water oxidation: a technical review *AIChE J.* 52 (11) (2006) 3933-3951

Bickley, R. I., M. J. Slater, et al. Operating experience and performance evaluation of a photocatalytic Reactor *Proc. Safety Env. Prot.* 83 (3) (2005) 217-223.

Bickley R. I., Slater M. J., Wang W. J., Engineering development of a photocatalytic reactor for waste water treatment *Proc. Safety Env. Prot.* 83 (B3) (2005) 205-216.

Bigda, R. Consider Fenton's chemistry for wastewater treatment. *Chem. Eng. Prog.* 91 (12) (1995) 62-66.

Bhatkhande, D. S., Pangarkar, V.G., Beenackers, AA. CM., Photocatalytic degradation for environmental applications:a review *J. Chem. Tech. Bio.* 77 (2011) 102-116.

Bozzi A., Dhananjeyan M., Guasaquillo I., Parra S., Pulgarin C., Weins C., and Kiwi J. Evolution of toxicity during melamine photocatalysis with TiO₂ suspensions, *J. Photochem. Photobio. A* 162(1) (2004) 179–185.

Braham R. J. and Harris A. T., Review of major design and scale-up considerations for solar photocatalytic reactors *Ind. Eng. Chem. Res.* 48 (2009) 8890-8905.

Byrappa K. and Adschiri T. Hydrothermal technology for nanotechnology *Prog. Cryst. Growth Char. Mat.* 53(2) (2007) 117-166.

Cabanas A., Li J., Blood P., Chudoba T., Lojkowski W., Poliakoff M., Lester E. Synthesis of nanoparticulate yttrium aluminum garnet in supercritical water-ethanol mixtures *J. Supercritical Fluids* 40(2) (2007) 284-292.

Cabanas A., Darr J. A., Lester E., Poliakoff M., *J. Mat. Chem.* 11 (2) (2001) 561-568.

- Cabanas A. and Poliakoff M. Continuous hydrothermal synthesis of inorganic materials in a near-critical water flow reactor; the one-step synthesis of nanoparticulate $Ce_{1-x}Zr_xO_2$ ($x=0-1$) solid solutions *J. Mat. Chem.* 11 (2001) 1408-1416.
- Calza P., Massolino C., Pelizzetti E., Light induced transformations of selected organophosphorus pesticides on titanium dioxide: pathways and by-products evaluation using LC-MS technique *J. Photochem. Photobio. A: Chem.* 199 (2008) 42-49.
- Calza P., Sakkas V. A., Villioti A., Massolino C., Boti V., Pelizzetti E., Albanis T., Multivariate experimental design for the photocatalytic degradation of imipramine: determination of the reaction pathway and identification of intermediate product *App. Cat. B: Environ.* 84 (2008) 379-388.
- Calza P., Massolino C., Pelizzetti E., Photo-induced transformation of hexaconazole and dimethomorph over TiO_2 suspension *J. Photochem. Photobio. A: Chem.* 200 (2008) 356-363.
- Carp O., Huisman C. L., and Reller A. Photoinduced reactivity of titanium dioxide *Prog. Solid State Chem.* 32 (2004) 33-177.
- Cassano A. E., and Alfano O. M., Reaction engineering of suspended solid heterogeneous photocatalytic reactors, *Cat. Today* 58 (2000) 167-197.
- Chong, M.N., Lei, S., Jin, B., Saint, C., Chow, C.W.K. Optimisation of an annular photoreactor process for degradation of Congo red using a newly synthesized titania impregnated kaolinite nano-photocatalyst. *Sep. Purif. Tech.* 67 (2009) 355-363.
- Chong, M. N., B. Jin, et al., Recent developments in photocatalytic water treatment technology: a review *Water Res.* 44 (10) (2010) 2997-3027.
- Chu W., Rao Y., Hui W. Y. Removal of simazine in a UV/ TiO_2 heterogeneous system *J. Agric. Food Chem* 57 (2009) 6944-6949.
- Chudoba T., Lester E., Lojkowski W., Poliakoff M., Li J., Grzanka E., Presz A. Synthesis of nano-sized yttrium-aluminum garnet in a continuous-flow reactor in supercritical fluids *J. Chem. Sci.* 63 (6) (2008) 756-764.
- Comber S. DW., Abiotic persistence of atrazine and simazine in water *Pestic. Sci.* 55 (1999) 696-702.
- Comninellis C., Kapalka A., Malato S., Parsons S. A., Poulouis I., Mantzavinos D., Perspective advanced oxidation processes for water treatment: advances and trends for R&D *J. Chem. Tech. Biotech.* 83 (2008) 769-776.

Coleman H.M., Vimonses V., Leslie G. and Amal R. Removal of contaminants of concern in water using advanced oxidation techniques *Water Sci. Tech.* 55 (12) (2007) 301–306.

Colina-Marquez J., Machuca-Martinez F. and Li Puma G., Photocatalytic mineralization of commercial herbicides in a pilot-scale solar CPC reactor: photoreactor modeling and reaction kinetics constants independent of radiation field *Env. Sci. Tech.* 43 (2009) 8953-8960.

Croll, B. T., Pesticides in surface waters and groundwaters *J. Insti Water and Env. man.* 5 (4) (1991) 389-395.

Devipriya S. and Yesodharan S., Photocatalytic degradation of pesticide contaminants in water *Solar Energy Mat. Solar Cells* 86 (2005) 309-348.

Dijkstra M. F. J., Koerts E. C. B., Beenackers A. A. C. M., Wesselingh J. A., Performance of immobilized photocatalytic reactors in continuous mode *AIChE J.* (2003) 734-744.

Diosyniou D. D., Barasubramanian G., Suidan M.T., Khoddadoust A.P., Baudin I. and Laine J.-M. Rotating disk photocatalytic reactor: development, characterization, and evaluation for destruction of organic pollutants in water *Wat. Res.* 34 (11) (2000) 2927-2940.

Dong S., Zhou D., Bi X. T. Effects of liquid and gas flow rates on the performance of a fluidized bed photocatalytic reactor *Int. J. Chem. Reactor Eng.* 6 (2008) Article A100 1-15.

Echavia G. R. M., Matzusawa F., Negishi N., Photocatalytic degradation of organophosphate and phosphonoglycine pesticides using TiO₂ immobilized on silica gel *Chemosphere* 76 (2009) 595-600.

Edwards H. K., Evans E., McCaldin S., Blood P., Gregory D. H., Poliakoff M., Lester E., Walker G. S., Brown P. D., Hydrothermally synthesised Fe₂O₃ nanoparticles as catalyst precursors for the CVD production of graphitic nanofibres *EMAG-NANO 2005: Imaging, Analysis and Fabrication on the Nanoscale* 26 (2006) 195-198.

Evgenidou, E., and Fytianos, K. Photodegradation of trazine herbicides in aqueous solutions and natural waters. *J. Agric. Food Chem.* 50(2002) 6423-6427.

Fang, Z. Rapid production of micro- and nano-particles using supercritical water *Eng. Mat.* 30(2011) 11-27.

Faramazpour M., Vossough M., Borghei M., Photocatalytic degradation of furfural by titania nanoparticles in a floating-bed photoreactor *Chem. Eng. J.* 146 (2009) 79-85.

Feitz A.J., Boyden B.H and Waite T.D., Evaluation of two solar pilot scale fixed-bed photocatalytic reactors *Water Res.* 34 (2000) (16) 3927.

Florencio M. H., Pires D.E., Castro A. L., Nunes M. R., Borges C., Costa F. M., Photodegradation of diquat and paraquat in aqueous solutions by titanium dioxide: evolution of degradation reactions and characterization of intermediates *Chemosphere* 55 (2004) 345-355.

Fox, M. A., Dulay, M.T. Heterogeneous photocatalysis *Chem. Rev.* 93 (1993) 341-357.

Fujishima, A., Honda, K., Electrochemical photolysis of water at a semiconductor electrode *Nature* 238 (1972) 37-38.

Galvez J.B. and Rodriguez S.M. *Solar detoxification.*
(<http://unesdoc.unesco.org/images/0012/001287/128772e.pdf>)

Garcia J. C., Takashima K., Photocatalytic degradation of imazaquin in an aqueous suspension of titanium dioxide *J. Photochem. Photobio. A: Chem.* 155 (2003) 215-222.

Garcia, A. M. A., A. Arques ,R. Sanchis ,W. Gernjak,M. I. Maldonado, I. Oller, S. Malato, Detoxification of aqueous solutions of the pesticide “SevnoI” by solar photocatalysis *Env. Chem. Lett.* 3 (2006)169-172.

Gemelli, E. and Camargo, N.H.A. Oxidation kinetics of commercially pure titanium *Revista Matéria* 12(3) (2007) 525 – 531.
<http://www.materia.coppe.ufrj.br/sarra/artigos/artigo10919>

Gora A., Toepfer B., Puddu V., Li Puma G., Photocatalytic oxidation of herbicides in single-component and multicomponent systems: Reaction kinetics analysis *App. Cat. B: Env.* 65 (2006) 1-10.

Gunasekara A.S., *Environmental fate of simazine*, 2004
(www.cdpr.ca.gov/docs/emon/pubs/fatememo/simazine.pdf)

Hamilton D. J., Ambrus A., Dieterle R.M., Felsot A.S., Harris, C.A., Holland P.T., Katayama A., Kurihara N., Linders J., Unsworth J. and Wong S.S., Regulatory limits for pesticide residues in water (IUPAC technical report) *Pure Appl. Chem.* 75 (8) (2003) 1123–1155.

Han S., Li J., Xi H., Xu D., Zuo Y., Zhang J., Photocatalytic decomposition of acephate in irradiated TiO₂ suspensions *J. Hazard. Mat.* 163 (2009) 1165-1172.

Hatakeda K., Ikushima Y., Sato O., Aizawa T., and Saito N. Supercritical water oxidation of polychlorinated biphenyls using hydrogen peroxide *Chem. Eng. Sci.* 54 (1999) 3079.

Haque M. M., and Muneer M., Photodegradation of norfloxacin in aqueous suspensions of titanium dioxide *J. Hazard. Mat.* 145 (2007) 51-57.

Haque M. M. and Muneer M., Heterogeneous photocatalysed degradation of a herbicide derivative, isoproturon in aqueous suspension of titanium dioxide *J. Env. Man.* 69 (2003) 169-176.

Hequet V., Gonzalez C., Le Cloirec P., Photochemical processes for atrazine degradation: methodological approach *Water Res.* 35 (18) (2001) 4253-4260.

Herrmann, J.M. Heterogeneous photocatalysis: fundamentals and applications to the removal of various types of aqueous pollutants *Cat. Today* 53 (1999) 115-129.

Hirahara Y., Ueno H., and Nakamuro K., Comparative photodegradation study of fenthion and disulfoton under irradiation of different light sources in liquid- and solid-phases *J. Health Sci.* 47(2) (2001) 129-135.

Hincapie M., Maldonado M.I., Oller I., Gernjak W., Sanchez-Perez J.A., Ballesteros M.M., Malato S. Solar photocatalytic degradation and detoxification of EU priority substances *Cat. Today* 101 (2005) 203–210.

Hobbs H., Briddon S., Lester E. The synthesis and fluorescent properties of nanoparticulate ZrO₂ doped with Eu using continuous hydrothermal synthesis *Green Chem.* 11(4) (2009) 484-491.

Hoffmann M.R., Martin S.T., Choi W., and Bahnemann D.W. Environmental applications of semiconductor photocatalysis *Chem. Rev.* 95 (1995) 69-96.

Horikoshi S., Hidaka H. Non-degradable triazine substrates of atrazine and cyanuric acid hydrothermally and in supercritical water under the UV-illuminated photocatalytic cooperation *Chemosphere* 51 (2003) 139-142.

Hurum D. C., Agrios A. G., Gray K.A., Rajh T. and Thurnauer M. C. Explaining the enhanced photocatalytic activity of Degussa P-25 mixed-phase TiO₂ using EPR *J. Phys. Chem. B* 107 (2003) 4545-4549.

Igor M. S. and Andriy P. Supercritical water oxidation of o-dichlorobenzene: degradation studies and simulation insights *J. Supercritical Fluids* 37(2006): 94-101.

Kaneco S., Li N., Itoh K., Katsumata H., Suzuki T., Ohta K., Titanium dioxide mediated solar photocatalytic degradation of thiram in aqueous solution: kinetics and mineralization *Chem. Eng. J.* 148 (2009) 50-56.

Kanki T., Hamasaki S., Sano N., Toyoda A., Hirano K. Water purification in a fluidized bed photocatalytic reactor using TiO₂-coated ceramic particles *Chem. Eng. J.* 108 (1–2) (2005) 155–160.

Kawasaki S-I., Xiuyi Y., Sue K., Hakuta Y., Suzuki A., Arai K. Continuous supercritical hydrothermal synthesis of controlled size and highly crystalline anatase TiO₂ nanoparticles *J. Supercritical Fluids* 50 (3) (2009) 276-282.

Khor J. N. *Oxidation of pesticides in photocatalytic reactors* (2004) PhD. Thesis, School of chemical and environmental engineering, University of Nottingham

Kim T.S., Kim J.K, Choi K., Stenstrom M.K., and Zoh K.D. Degradation mechanism and the toxicity assessment in TiO₂ photocatalysis and photolysis of parathion *Chemosphere* 62 (6) (2006) 926–933.

Kitsiou V., Filippidis N., Mantzavinos D., Poullos I., Heterogeneous and homogeneous photocatalytic degradation of the insecticide imidacloprid in aqueous solutions *App. Cat. B: Env.* 86 (2009) 27-35.

Konstantinou I. K., and Albanis T. A., Photocatalytic transformation of pesticides in aqueous titanium dioxide suspensions using artificial and solar light: intermediates and degradation pathways. *Applied Cat. B : Env.* 42 (2003) 319-335.

Konstantinou.K. and Albanis T.A., TiO₂-assisted photocatalytic degradation of azo dyes in aqueous solution: kinetic and mechanistic investigations: A review *Appl. Catal. B: Env.* 49 (2004) 1-14.

Kumar K. V., Porkodi K., Rocha F., Langmuir-Hinshelwood kinetics-a theoretical study *Cat. Comm.*, 9 (1) (2008) 82-84.

Lasa H., Serrano B., Salices M. *Photocatalytic Reaction Engineering* (2005) 19-21.

Lee D. K., Kim S. C., Cho I. C., Kim J. S., Kim S. W. Photocatalytic oxidation of microcystin-LR in a fluidized bed reactor having TiO₂-coated activated carbon *Sep. and Purifica. Tech.* 34 (1–3) (2004) 59–66.

Legrini O., O. E., Braun, A.M., Photochemical process for water treatment *Chem. Rev.* 93 (1993) 671-698.

Lester E., Blood P., Denyer J., Giddings D., Azzopardi B., Poliakoff M., Reaction engineering: The supercritical water hydrothermal synthesis of nanoparticles *J. Supercritical Fluids* 37 (2006) 209-214.

Levenspiel O., *Chemical reaction engineering* (1999) 15-17.

Lhomme L., Brosillon S., Wolbert, D. Photocatalytic degradation of pesticides in pure water and a commercial agricultural solution on TiO₂ coated media *Chemosphere* 70 (2008) 381-386.

Li Puma G., Modeling of thin-film slurry photocatalytic reactors affected by radiation scattering *Env. Sci. Tech.*, 37 (24) (2003) 5783–5791.

Li Puma G., Khor J. N., Brucato A., Modeling of an annular photocatalytic reactor for water purification: oxidation of pesticides *Env. Sci. Tech.* 38 (2004) 3737-3745.

Li Puma G., Dimensionless analysis of photocatalytic reactors using suspended solid photocatalysts, *Chem. Eng. Res. Des.* 83 (A7) (2005) 820-826

Li Puma G., Toepfer B., Gora A., Photocatalytic oxidation of multicomponent systems of herbicides: scale-up of laboratory kinetics rate data to plant scale *Cat. Today* 124 (2007) 124-132.

Li Puma G., Yue P.L., The modeling of a fountain photocatalytic reactor with a parabolic profile *Chem. Eng. Sci.* 56 (2001) 721-726.

Li Puma G., Yue P.L., A novel fountain photocatalytic reactor: model development and experimental validation *Chem. Eng. Sci.* 56 (2001) 2733-2744.

Li D. and Qu J., The progress of catalytic technologies in water purification: a review *J. Env. Sci.* 21 (2009) 713-719.

Liang H.C., Li X. Z., Yang Y. H., Sze K. H., Comparison of the degradations of diphenamid by homogeneous photolysis and heterogeneous photocatalysis in aqueous solution *Chemosphere* 80 (4) (2010) 366-374.

Linsebigler A. L., Lu G. and Yates J. T., Photocatalysis on TiO₂ surfaces: principles, mechanisms, and selected results *Chem. Rev.* 95 (1995) 735-758.

Liu W., Chen S., Zhao W., Zhang S., Study on the photocatalytic degradation of trichlorfon in suspension of titanium dioxide *Desalination* 249 (2009) 1288-1293.

Lopez-Munoz M. J., Aguado J., Revilla A. Photocatalytic removal of s-triazines: evaluation of operational parameters *Cat. Today* 161 (2011) 153-162

Lopez-Munoz M. J., Aguado J., Revilla A. Heterogeneous photocatalytic degradation of isoproturon in aqueous solution: experimental design and intermediate products analysis *Cat. Today* (2013) In press, corrected-proof

Lu C., Chen C., Mai F., Li H., Identification of the degradation pathways of alkanolamines with TiO₂ photocatalysis *J. Hazard. Mat.* 165 (2009) 306-316.

Lu J., Minami K. , Takami S., Shibata M., Kaneko Y, Adschiri T. Supercritical hydrothermal synthesis and in situ organic modification of indium tin oxide nanoparticles using continuous-flow reaction system. *Appl. Mater. Interfaces* 4 (1) (2012) 351–354.

Madani M.E., Guillard C., Perol N., Chovelon J.M., El Azzouzi M., Zrineh A., Herrmann J. M. Photocatalytic degradation of diuron in aqueous solution in presence of two industrial titania catalyst, either as suspended powders or a deposit on flexible industrial photoresistant papers. *App. Cat. B: Env.* 65 (2006) 70-76.

Mahmoodi N., Arami M., Limaee N., Gharanjig K., Photocatalytic degradation of agricultural *N*-heterocyclic organic pollutants using immobilized nanoparticles of titania. *J. Hazard. Mat.* 145 (2007) 65-71.

Mahmoodi N. M., Arami M., Gharanjig K., Nourmohammadian F., Bidokhti A.Y., Purification of water containing agricultural organophosphorus pollutant using titania nanophotocatalysis: laboratory studies and numerical modeling. *Desalination* 230 (2008) 183-192.

Mahmoodi N. M., Arami M., Limaee N. Y., Gharanjig K., Nourmohammadian F. Nanophotocatalysis using immobilized titanium dioxide nanoparticle: degradation and mineralization of water containing organic pollutant: case study of Butachlor *Mat. Res. Bull.* 42 (5) (2007) 797-806.

Malato S., Blanco J., Alarcon D.C., Maldonado M. I., Fernandez-Ibanez P., Gernjak W., Photocatalytic decontamination and disinfection of water with solar collectors *Cat. Today* 122 (2007) 137-149.

Malato S., Blanco J., Caceres J., Fernandez-Alba A. R., Aguera A., Rodriguez A., Photocatalytic treatment of water-soluble pesticides by photo-Fenton and TiO₂ using solar energy *Cat. Today* 76 (2002) 209-220.

Malato S., Blanco J., Richter C., Fernandez P., Maldonado M. I, Solar photocatalytic mineralization of commercial pesticides: oxamyl *Solar Energy Mat. & Solar Cells* 64 (2000) 1-14.

Malato S., Blanco J., Alarcon D. C., Maldonado M. I., Fernandez-Ibanez P., Gernjak W., Photocatalytic treatment of diuron by solar photocatalysis: evaluation of main intermediates and toxicity *Solar Energy* 75 (2003) 329-336.

Malato S., Fernandez-Ibanez P., Maldonado M. I., Blanco J., Gernjak W., Decontamination and disinfection of water by solar photocatalysis: recent overview and trends *Cat. Today*, 147 (2009) 1-59.

Malato S., Blanco J., Vidal A., Richter C. , Photocatalysis with solar energy at a pilot-plant scale: an overview *App. Cat. B: Env.* 37 (2002) 1-15.

Matveeva, E. G., Samsonova, J. V., Eremin, S. A. A quenching fluoroimmunoassay for analysis of the pesticide propazine in an apolar organic solvent, reverse micelles of AOT in octane: effect of the micellar matrix and labeled antigen structure *J. Fluorescence* 7 (3) (1997) 211 - 216.

Matsui K., Noguchi T., Islam N.M., Hakuta Y., Hayashi H. Rapid synthesis of BaTiO₃ nanoparticles in supercritical water by continuous hydrothermal flow reaction system *J. Cryst. Growth* 310(10)(2008) 2584-2589.

Mills, A., LeHunte, S., An overview of semiconductor photocatalysis *J. Photochem. Photobiol. A: Chem.* 108 (1997) 1-35.

Mills, A., Davies, R.H., Worsley, D., Water purification by semiconductor photocatalysis. *Chem. Soc. Rev.* 22 (1993) 417-425.

Miguel N., Ormad M.P., Mosteo R., and Ovelleiro J. Photocatalytic degradation of pesticides in natural water: effect of hydrogen peroxide *Int. J. Photoenergy*, Article ID 371714 (2012) 1-11.

Muller P., Glossary of terms used in physical organic chemistry (IUPAC recommendation 1994), *Pure Appl. Chem.* 66(5) (1994) 1077-1184.

Muneer M., Qamar M., Saquib M., Bahnemann D. W., Heterogeneous photocatalysed reaction of three selected pesticide derivatives, prothion, propachlor and tebuthiuron in aqueous suspensions of titanium dioxide *Chemosphere* 61 (2005) 457-468.

Moctezuma E., Leyva E., Palestino G., De Lasa H., Photocatalytic degradation of methyl parathion: reaction pathways and intermediate reaction products *J. Photochem. Photobiol. A: Chem.* 186 (2007) 71-84.

Mohapatra S. P., Michell A., *Drinking water quality standards in Ontario-are they tough?* (2003) 8.

Muneer M., Qamar M., Saquib M., Bahnemann D. W. Heterogeneous photocatalysed reaction of three selected pesticide derivatives, prothion, propachlor and tebuthiuron in aqueous suspensions of titanium dioxide *Chemosphere* 61 (2005) 457-468.

Muneer M. and Boxall C., Photocatalyzed degradation of a pesticide derivative glyphosate in aqueous suspensions of titanium dioxide *Int. J. Photoenergy* 2008 (2008) 1-7.

Nam W., Kim J., Han G. Photocatalytic oxidation of methyl orange in a three-phase fluidized bed reactor *Chemosphere* 47 (9) (2002) 1019–1024.

Oancea P., and Oncescu T. The photocatalytic degradation of dichlorvos under solar irradiation *J. Photochem. Photobio. A: Chem.* 199 (2008) 8-13.

Oller I., Gernjak W., Maldonado M. I., Perez-Estrada L. A., Sanchez-Perez J. A., Malato S. Solar photocatalytic degradation of some hazardous water-soluble pesticides at pilot-plant scale *J. Hazard. Mat. B* 138 (2006) 507-517.

Paritam K. Dutta, A. K. R. Experimental investigation of Taylor vortex photocatalytic reactor for water purification *Chem. Eng. Sci.* 59 (2004) 5249-5259.

Parra S., Stanca S. E., Guasaquillo I., Thampi K. R. Photocatalytic degradation of atrazine using suspended and supported TiO₂ *App. Cat. B: Env.* 51 (2004) 107-116.

Perez-Estrada L. A., Malato S., Aguera A., Fernandez-Alba A. R., Degradation of dipyrone and its main intermediates by solar AOPs identification of intermediate products and toxicity assessment *Cat. Today* 129 (2007) 207-214.

Pelaeza M., N. T. Nolanb, Pillai S.C., Seeryc M.K., Falarasd P., Kontosd A.G., Dunlope P. S. M., Hamiltone J.W.J., Byrne J.A., O'Sheaf K., Entezari M.H., Dionysiou D. D. A review on the visible light active titanium dioxide photocatalysts for environmental applications *App. Cat. B: Env.* 125 (2012) 331– 349.

Pizarro P., Guillard C., Perol N., Herrmann J. M. Photocatalytic degradation of imazapyr in water: comparison of activities of different supported and unsupported TiO₂-based catalysts. *Cat. Today* 101 (2005) 211-218.

Pirkanniemi, K., Sillanpaa, M. Heterogeneous water phase catalysis as an environmental application: a review *Chemosphere* 48 (2002) 1047-1060.

Pourata R., Khataee A.R., Aber S., Daneshvar N., Removal of the herbicide Bentazon from contaminated water in the presence of synthesized nanocrystalline TiO₂ powders under irradiation of UV-C light *Desalination* 249 (2009) 301-307.

Qamar M., and Muneer M. Comparative photocatalytic study of two selected pesticide derivatives, indole-3-acetic acid and indole-3-butyric acid in aqueous suspensions of titanium dioxide *J. Hazard. Mat. B* 120 (2005) 219-227.

Qamar M., Muneer M., Bahnemann D. Heterogeneous photocatalysed degradation of two selected pesticide derivatives, triclopyr and daminozid in aqueous suspensions of titanium dioxide *J. Env. Man.* 80 (2006) 99-106.

Qamar M. and Muneer M. A comparative photocatalytic activity of titanium dioxide and zinc oxide by investigating the degradation of vanillin *Desalination* 249 (2009) 535-540.

Qamar M., Saquib M., Muneer M. Photocatalytic degradation of two selected dye derivatives, chromotrope 2B and amido black 10B, in aqueous suspensions of titanium dioxide. *Dyes and Pigments* 65 (2005) 1-9.

Qourzal S., Barka N., Tamimi M., Assabbane A., Ait-Ichou Y., Photodegradation of 2-naphthol in water by artificial light illumination using TiO₂ photocatalyst: identification of intermediates and the reaction pathway *App. Cat. A: Gen.* 334 (2008) 386-393.

Radwan A. A-R. *Water Treatment by Heterogeneous Photocatalysis: an Overview*. SWCC acquired experience symposium (2005).

Rafqah S., Wong-Wah-Chung P., Aamili A., Sarakha M. Degradation of metsulfuron methyl by heterogeneous photocatalysis on TiO₂ in aqueous suspensions: kinetic and analytical studies. *J. Mol. Cat. A: Chem.* 237 (2005) 50-59.

Rahman M. A. and Muneer M. Photocatalysed degradation of two selected pesticides derivatives, dichlorvos and phosphamidon in aqueous suspension of titanium dioxide *Desalination* 181 (2005) 161-172.

Rath H., Anand S., Mohapatra M., Dash P., Som T., Singh U. P. , Mishra N. C., Effect of thermal annealing on the structure and microstructure of TiO₂ thin films *Indian J. Phys.* 83 (4) (2009) 559-565.

Reddy P. A. K., Reddy P. V. L., Sharma V. M., Srinivas B., Kumari V.D., Subrahmanyam M. Photocatalytic degradation of isoproturon pesticide on C, N and S doped TiO₂ *J. Water Res. and Protec.*(2010) 2, 235-24.

Rowan J. B. and Andrew T. H. Review of major design and scale-up considerations for solar photocatalytic reactors. *Ind. Eng. Chem. Res.* 48 (2009), 8890–8905.

Sanches S., Crespo M. T. B., Pereira V. J. Drinking water treatment of priority pesticides using low pressure UV photolysis and advanced oxidation processes. *Water Res.* 44, (2010) 1809-1818.

Sato T. and Taya M. Enhancement of phage inactivation using photocatalytic titanium dioxide particles with different crystalline structures *Biochem. Eng. J.* 28 (2006) 303–308.

Schwarz P. F., Turro N. J., Bossmann S. H., Braun A. M., Abdel Wahab A.-M. A., Duerr H. A new method to determine the generation of hydroxyl radicals in illuminated TiO₂ suspensions. *J. Phys. Chem. B* 101 (1997) 7127-7134.

- Scribner E. A., Thurman E. M., Zimmerman L. R. Analysis of selected herbicide metabolites in surface and ground water of the United States. *Sci. Total Env.* 248 (2000) 157-167.
- Senthilnathan J., Philip L. Removal of mixed pesticides from drinking water system by photodegradation using suspended and immobilized TiO₂. *J. Env. Sci. and Health: B* 44 (2009) 262-270.
- Serpone N. and Emeline A.V. *Fundamentals in Metal-oxide Heterogeneous Photocatalysis*, (2004), 275-391.
- Shie J. L., Lee C. H., Chiou C. S., Chang C.T., Chang C.C., Chang C.Y. Photodegradation kinetics of formaldehyde using light sources of UVA, UVC, and UVLED in the presence of composed silver titanium oxide photocatalyst. *J. Hazard. Mat.* 155 (2008) 164-172.
- Shifu C. and Yunzhang L. Study on the photocatalytic degradation of glyphosate by TiO₂ photocatalyst. *Chemosphere* 67 (2007) 1010-1017.
- Shukla S. S., Dorris K. L., Chikkaveeraiah B. V. Photocatalytic degradation of 2,4- dinitrophenol. *J. Hazard. Mat.* 164 (2009) 310-314.
- Sharma M.V.P., Sadanandam G., Ratnamala A., Kumari V., Subrahmanyam M. An efficient and novel porous nanosilica supported TiO₂ photocatalyst for pesticide degradation using solar light. *J. Hazard. Mat.* 171 (2009) 626-633.
- Singh H. K., Muneer M., and Bahnemann D. Photocatalysed degradation of a herbicide derivative, bromacil, in aqueous suspensions of titanium dioxide *Photochem. Photobiol. Sci.* 2 (2003) 151–156.
- Singh H. K., Saquib M., Haque M. M., Muneer M. Heterogeneous photocatalyzed degradation of uracil and 5-bromouracil in aqueous suspensions of titanium dioxide. *J. Hazard. Mat.* 142(2007) 425-430.
- Sirtori C., Zapata A., Malato S., Gernjal W., Fernandez-Alba A. R. and Aguera A. Solar photocatalytic treatment of quinolones: intermediates and toxicity evaluation. *Photochem. Photobio. Sci.* 8 (2009), 644-651.
- Sobczyński A., Dobosz A. Water purification by photocatalysis on semiconductors. *Polish J. Env. Studies* 10(4) (2001), 195-205
- Sojic D. V., Anderluh V. B., Orcic D.A., Abramovic B. F. Photodegradation of clopyralid in TiO₂ suspensions: identification of intermediates and reaction pathways. *J. Hazard. Mat.* 168 (2009) 94-101.
- Stapleton D. R., Konstantinou I. K., Mantazavinos D., Hela D., Papadaki M. On the kinetics and mechanisms of photolytic/TiO₂-photocatalytic degradation of substituted pyridines in aqueous solutions. *App. Cat. B: Env.* 95 (2010) 100-109.

Sue K., Kimura K., Murata K., Arai K. Effect of cations and anions on properties of zinc oxide particles synthesized in supercritical water. *J. Supercritical Fluids* 30(3) (2004) 325-331.

Tariq M. A., Faisal M., Muneer M., Bahnemann D., Photochemical reactions of few selected pesticide derivatives and other priority organic pollutants in aqueous suspensions of titanium dioxide. *J. Mol. Cat. A: Chem.* 265 (2007) 231-236.

Toepfer B., Gora A., Li Puma G. Photocatalytic oxidation of multicomponent solutions of herbicides: Reaction kinetics analysis with explicit photon absorption effects *App. Cat. B: Env.* 68 (2006) 171-180.

Topalov A., Molnar-Gabor D., Kosanic M., Abramovic B., Photomineralization of the herbicide mecoprop dissolved in water sensitized by TiO₂ *Water Res.* 34(5) (2000) 1473-1478.

Trajkovska V., Petrovska-Jovanovi S., Pavlova V. Separation of simazine, atrazine and propazine using reversed-phase high-performance liquid chromatography *Proceeding book in 4th AACD Congress 29 Sept - 3 Oct 2004, Turkey* (2004), 85-87.

Turner L., *Simazine analysis of risks to endangered and threaten salmon and steelhead* (2003), 3-5.

Wang X., Yu J. C., Ho C., Hou Y., Fu X., Photocatalytic activity of a hierarchically macro/mesoporous titania *Langmuir* 21 (2005) 2552-2559.

Wang Y, Hong C-S. TiO₂ mediated photomineralization of 2- chlorobiphenyl: the role of O₂. *Water Res.* 34 (2000) 2791-2797.

Ward N., Clark J., Lowe P., Seymour S. *Water pollution from agricultural pesticides.* (1993) 1-83.

Wei L., Shifu C., Wei Z., Sujuan Z., Titanium dioxide mediated photocatalytic degradation of methamidophos in aqueous phase *J. Hazard. Mat.* 164 (1) (2009) 154-160.

Wei L., Shifu C., Wei Z., Sujuan Z., Study on the photocatalytic degradation of trichlorfon in suspension of titanium dioxide. *J. Hazard. Mat.* 164 (2009) 154-160.

Wong C.C., The direct photolysis and photocatalytic degradation of alachlor at different TiO₂ and UV sources. *Chemosphere* 50 (2003) 981-987.

Wu R., Chen C., Chen M., Lu C., Titanium dioxide-mediated heterogeneous photocatalytic degradation of terbufos: parameter study and reaction pathways. *J. Hazard. Mat.* 162 (2009) 945-953.

Wu R., Chen C., Lu C., Hsu P., Chen M. Phorate degradation by TiO₂ photocatalysis: parameter and reaction pathway investigations. *Desalination* 250 (2010) 869-875.

Vora J.J., Chauhan S.K., Parmar K.C., Vasava S.B., Sharma S., and Bhutadiya L.S. Kinetic study of application of ZnO as a photocatalyst in heterogeneous medium. *E-J. Chem.* 6(2) (2009) 531-536.

Voutou B. and Stefanaki E-C., Electron Microscopy: the basics. *Phys. Adv. Mat. Winter Sch.* (2008) 1-11.

Vrielynck L., Dupuy N., Kister J., and Nowogrocki G. Molecular structure and vibrational spectroscopy of isoproturon. *J. Mol. Struct.* 788 (2006) 232-237.

Yeredla R. R. and Xu H. An investigation of nanostructured rutile and anatase plates for improving the photosplitting of water *Nanotech.* 19 (2008) 055706.

Zalazar C. S., Satuf M. L., Alfano O. M., Cassano A. E., Comparison of H₂O₂/UV and heterogeneous photocatalytic processes for the degradation of dichloroacetic acid in water. *Env. Sci. Tech.* 42 (2008) 6198-6204.

Zayani G., Bousselmi L., Mhenni F., Ghrabi A., Solar photocatalytic degradation of commercial textile azo dyes: performance of pilot plant scale thin film fixed-bed reactor. *Desalination* 246 (1-3) (2009), 344-352.

Zhou Q., Xiao J., Ding Y., Sensitive determination of fungicides and prometryn in environmental water samples using multiwalled carbon nanotubes solid-phase extraction cartridge. *Analytica Chimica Acta*, 602 (2) (2007) 223-228.

The Food and Environment Research Agency

(<http://pusstats.csl.gov.uk/myindex.cfm>)

EPA: United states Environmental Protection Agency

(<http://water.epa.gov/type/rs1/monitoring/vms52.cfm>)